Anti-*c-myc* cholesterol-based lipoplexes: Development, characterisation and evaluation as onconanotherapeutic agents *in vitro*

Saffiya Habib
(206507144)

Submitted in fulfilment of the academic requirements for the degree of
Doctor of Philosophy
in the
Discipline of Biochemistry
School of Life Sciences
College of Agriculture, Engineering and Science
University of KwaZulu-Natal
Westville

June 2018

As the candidate's supervisor I have approved this dissertation for submission.

Supervisor: Prof M. Singh Signed: _____ Date: _____

The financial assistance of the National Research Foundation (NRF) towards this research is hereby acknowledged. Opinions expressed and conclusions arrived at, are those of the author and are not necessarily to be attributed to the NRF.

ABSTRACT

Strategies aimed at inhibiting the expression of the *c-myc* oncogene could provide the basis for alternative cancer treatment. In this regard, silencing *c-myc* expression using small interfering RNA (siRNA) is an attractive option. However, the development of a clinically viable, siRNA-based, *c-myc* silencing system is largely dependent upon the design of an appropriate siRNA carrier that can be easily prepared. Nanostructures formed by the electrostatic association of siRNA and cationic lipid vesicles represent uncomplicated, well-recognised siRNA delivery systems. Therefore, this study has focused on traditional cationic liposomes as the foundation for the development of a simple, but effective anti-*c-myc* onconanotherapeutic agent.

Novel liposome formulations contained equimolar quantities of the cytofectin, *N*,*N*-dimethylaminopropylamidosuccinylcholesterylformylhydrazide (MS09), and cholesterol (Chol); with or without 2 mol % pegylation. Liposomes which contained dioleoylphosphatidylethanolamine (DOPE) as the co-lipid were included for comparative purposes. Pegylated and non-pegylated MS09/Chol (1:1) suspensions were reproducibly prepared by lipid film hydration to give unilamellar vesicles that were stable for at least 10 months at 4 ˚C.

Liposomes successfully bound siRNA to form lipoplexes of less than 200 nm in size, with zeta potentials between -16 and -44 mV. These assumed globular and bilamellar structures in which siRNA was partially protected. Although all formulations were well tolerated at ≤14 nM siRNA, pegylation severely inhibited siRNA delivery in cancer cell lines, MCF-7 and HT-29, which overexpress *c-myc*.

The non-pegylated MS09/Chol (1:1) lipoplex, at the MS09:siRNA ($^{w}/_{w}$) ratio of 16:1, was most effectively taken up by MCF-7 and HT-29 cells, with negligible effect in non-transformed cells when applied at 12 nM siRNA. Lipoplexes directed against the *c-myc* transcript (anti-*c-myc* siRNA), mediated a dramatic reduction in *c-myc* mRNA and protein levels. This was accompanied by a loss of migratory potential and apoptotic cell death. Moreover, oncogene knockdown and anti-cancer effects were superior to that of a commercially available transfection reagent, Lipofectamine™ 3000. Although the DOPE-containing counterpart performed with

comparable efficacy under standard *in vitro* conditions, it was incapable of siRNA delivery at physiological serum concentration. Hence, the anti-*c-myc* MS09/Chol (1:1) lipoplex reported exemplifies a straightforward anti-cancer agent that warrants further investigation *in vivo*.

PREFACE

The experimental work described in this dissertation was carried out in the Discipline of Biochemistry, School of Life Sciences, University of KwaZulu-Natal, Westville from March 2013 to March 2018, under the supervision of Prof Moganavelli Singh, and co-supervision of Prof Mario Ariatti.

These studies represent original work by the author and have not otherwise been submitted in any form for any degree or diploma to any tertiary institution. Where use has been made of the work of others it is duly acknowledged in the text.

COLLEGE OF AGRICULTURE, ENGINEERING AND SCIENCE

DECLARATION I – PLAGIARISM

I, Saffiya Habib, declare that

1. The research reported in this thesis, except where otherwise indicated, is my original research.

2. This thesis has not been submitted for any degree or examination at any other university.

3. This thesis does not contain other persons' data, pictures, graphs or other information, unless specifically acknowledged as being sourced from other persons.

4. This thesis does not contain other persons' writing unless specifically acknowledged as being sourced from other researchers. Where other written sources have been quoted then:

    a. Their words have been re-written but the general information attributed to them has been referenced.
    b. Where their exact words have been used, then their writing has been placed in italics and inside quotation marks, and referenced.

5. This thesis does not contain text, graphics or tables copied and pasted from the Internet, unless specifically acknowledged, and the source being detailed in the thesis and in the References sections.

Signed: _____

DECLARATION II – PUBLICATIONS

DETAILS OF CONTRIBUTION TO PUBLICATIONS that form part and/or include research presented in this thesis (include publications in preparation, submitted, *in press* and published and give details of the contribution of each author to the experimental work and writing of each publication).

Published abstract (Appendix A)

Habib, S., Ariatti, M. & Singh, M. 2016. Novel cholesterol based siRNA lipoplexes with and without PEG-modification: Characterization and in vitro cytotoxicity studies. *Journal of Pharmaceutical Care and Health Systems*, 3(2), 72.

Signed: _____

RESEARCH PRESENTATIONS

The following presentations were made from data obtained during the study.

- Habib, S., Ariatti, M., Singh, M. Novel cholesterol based liposomes: characterisation and evaluation as siRNA carriers in vitro. **University of KwaZulu-Natal, School of Life Sciences Research Day 2016**, Pietermaritzburg, South Africa, 20 May 2016. Oral presentation.

- Saffiya Habib, Mario Ariatti and Moganavelli Singh. Novel cholesterol based siRNA lipoplexes with and without PEG-modification: Characterization and *in vitro* cytotoxicity studies. **4th African Pharma Congress**, Cape Town, South Africa, 20-22 June 2016. E-Poster presentation. http://african.pharmaceuticalconferences.com/eposter-presentation.php (accessed as at 20/06/16)

- Habib, S., Ariatti, M., Singh, M. Novel cholesterol based liposomes: characterisation and evaluation as siRNA carriers in vitro. **25th SASBMB Congress**, East London, South Africa, 10-13 July 2016. Poster presentation.

- Habib, S., Ariatti, M., Singh, M. MS09/Chol/PEG liposomes: characterisation and potential for siRNA delivery in vitro. **University of KwaZulu-Natal, School of Life Sciences Research Day 2017**, Westville, South Africa, 23 May 2017. Oral presentation.

- Habib, S., Ariatti, M., Singh, M. Anti-cancer potential of novel c-myc-specific lipoplexes: An in vitro study. **University of KwaZulu-Natal, School of Life Sciences Research Day 2018**, Pietermaritzburg, South Africa, 22 May 2018. Oral presentation.

ACKNOWLEDGEMENTS

I wish to express my gratitude to the following individuals and organisations:

- My supervisor, Prof M. Singh, for her invaluable assistance with cell culture.
- My co-supervisor, Prof M. Ariatti, for his assistance with the synthesis of MS09 and the preparation of liposomes.
- Mr Phillip Christopher of the Microscopy and Microanalysis Unit (UKZN, Westville) for his assistance with cryo-transmission electron microscopy and for supplying formvar coated grids and staining solutions.
- Dr B. Masola and Mr A. Mukundwa (both of the Discipline of Biochemistry, UKZN, Westville) for assisting with the densitometric analysis of agarose gels.
- Dr O.J. Pooe and Dr A.N. Daniels (both of the Discipline of Biochemistry, UKZN, Westville) for their assistance and advice with respect to the gene expression assays.
- Prof A.O. Olaniran of the Discipline of Microbiology (UKZN, Westville) for use of the NanoDrop spectrophotometer.
- Prof B. Pillay and Mr T. Chiliza (both of the Discipline of Microbiology, UKZN, Westville) for use of the real-time PCR detection system.
- The National Research Foundation (NRF), for providing financial support from 2013 to 2016 (reference no. SFH12082810951 and AEMD150723129783).
- The University of KwaZulu-Natal (UKZN) for contributing towards part of the running costs incurred in this study.
- The staff of the Discipline of Biochemistry and post-graduate students of the Non-viral Gene and Drug Delivery and Mammalian Tissue Culture Laboratory (UKZN, Westville) for providing a pleasant work environment.

TABLE OF CONTENTS

List of figures

List of tables

Abbreviations

AB	alamarBlue®
Ago	Argonaute
Ago2	Argonaute2
ANOVA	analysis of variance
AO	acridine orange
APC	adenomatous polyposis coli
ASOs	antisense oligonucleotides
BCA	bicinchoninic acid
BET	bromodomain and extra-terminal
BIRC5	baculoviral IAP repeat-containing 5 (gene)
BSA	bovine serum albumin
Caco-2	human colorectal adenocarcinoma cell line
CAMKIIγ	Ca^{2+}/calmodulin-dependent protein kinase II γ
CBP	cAMP response element binding protein
CCND1	cyclin D1 (gene)
CD47	cluster of differentiation 47
cDNA	complementary DNA
Chol	cholesterol
CFO	clamp-forming oligonucleotide

CRD-BP	coding region determinant-binding protein
Cryo-TEM	cryogenic transmission electron microscopy
C_q	quantification cycle
CTD	carboxy-terminal domain
DC-Chol	3β[*N*-(*N′*, *N′*-dimethylaminoethane)-carbamoyl] cholesterol
DMSO	dimethylsulphoxide
DNA	deoxyribonucleic acid
DNase	deoxyribonuclease
dNTPs	deoxyribonucleoside triphosphates
DOPC	dioleoylphosphatidylcholine
DOPE	dioleoylphosphatidylethanolamine
DOTAP	1,2-dioleoyl-3-trimethylammonium-propane
DsiRNA	dicer-substrate siRNA
DSPE	distearoylphosphatidylethanolamine
DSPE-PEG	distearoylphosphatidylethanolamine-poly(ethylene glycol)
$DSPE\text{-}PEG_{2000}$	1,2-distearoyl-s*n*-glycero-3-phosphoethanolamine-*N*-[methoxy (polyethylene glycol)-2000]
dsRNA	double-stranded RNA
dT	deoxythymidine
E-box	enhancer box
EDTA	ethylenediaminetetra acetic acid

ELISA	enzyme-linked immunosorbent assay
EMEM	Eagle’s Minimum Essential Medium
EMT	epithelial-to-mesenchymal transition
EPR	enhanced permeability and retention
ER	oestrogen receptor
EtBr	ethidium bromide
FAM46C	family with sequence similarity 46, member C (gene)
FBS	foetal bovine serum
FITC	fluorescein isothiocyanate
GCN5	general control of amino acid synthesis protein-5
gDNA	genomic DNA
HBS	HEPES buffered saline
HCF-1	host cell factor-1
HEK293	human embryonic kidney 293
HEPA	high efficiency particulate air
HEPES	2-[-(2-hydroxyethyl)-piperazinyl]-ethanesulphonic acid
HLH	helix-loop-helix
HN1	haematological and neurological expressed 1
HPV 18	human papilloma virus 18
HRP	horseradish peroxidase
HT-29	human colorectal adenocarcinoma cell line

hTERT	human telomerase reverse transcriptase
Ig	immunoglobulin
Inr	initiator element
KRAS	Kirsten rat sarcoma viral oncogene homologue
LCP	lipid calcium phosphate
LF3K	Lipofectamine™ 3000
LPD	liposome-polycation-DNA
LZ	leucine zipper
Max	Myc-associated factor X
MB0	Myc box 0
MBI	Myc box 1
MBII	Myc box II
MBIIIa	Myc box IIIa
MBIIIb	Myc box IIIb
MBIV	Myc box IV
MCF-7	Michigan Cancer Foundation 7
MDM2	Mouse double minute 2 homologue (gene)
miRNA	microRNA
Miz-1	Myc-interacting zinc finger protein-1
mRNA	messenger RNA
MS08	cholesterylformylhydrazide hemisuccinate

MS09	*N*,*N*-dimethylaminopropylamidosuccinylcholesterylformylhydrazide
MTT	3-(4,5-dimethylthiazol-2-yl)-2,5-diphenyltetrazolium bromide
NELFE	negative elongation factor E
NHE	nuclease hypersensitivity element
NLS	nuclear localisation signal
NTA	Nanoparticle Tracking Analysis
NTD	amino-terminal domain
Oligo	oligomer
ORC1	origin recognition complex-1
PAZ	Piwi/Argonaute/Zwille
PBS	phosphate buffered saline
PCR	polymerase chain reaction
PD-L1	programmed death-ligand 1
pDNA	plasmid DNA
PEG	poly(ethylene glycol)
PEG_{2000}	poly(ethylene glycol) (molecular weight of 2000)
PMO	phosphorodiamidate morpholino oligomer
PNA	peptide nucleic acid
pol	polymerase
PS	phosphorothioate
PS-ASO	phosphorothioate antisense oligonucleotide

PSME3	proteasome activator subunit 3
qPCR	quantitative real-time PCR
RdTS	siRNA-directed transcriptional silencing
RFU	relative fluorescence units
RIPA	radioimmunoprecipitation assay
RISC	RNA-induced silencing complex
RNA	ribonucleic acid
RNAi	RNA interference
RNA pol II	RNA polymerase II
RNase	ribonuclease
rpm	revolutions per minute
rRNA	ribosomal RNA
RT	reverse transcription
RT-qPCR	reverse transcription quantitative real-time PCR
sCMOS	scalable complementary metal-oxide semi-conductor
SD	standard deviation
SDS	sodium dodecylsulphate
shRNA	short hairpin RNA
siRNA	small interfering RNA
Skp2	S-phase kinase-associated protein 2
SPOP	speckle-type POZ protein

SREBP1	sterol regulatory element-binding protein 1
TAD	transactivation domain
TAR	transactivating response
TBP	TATA-binding protein
TBS	tris-buffered saline
TBST	TBS containing 0.1 % Tween 20
TCF	T-cell factor
TEM	transmission electron microscopy
TFO	triplex-forming oligonucleotide
TGFβ	transforming growth factor-β
TMB	3,3′,5,5′-Tetramethylbenzidine
TPE	Tris-phosphate-EDTA
TRBP	TAR RNA-binding protein
TRD	transcriptional regulatory domain
Tris-HCl	tris(hydroxymethyl)-aminomethane hydrochloride
TRRAP	transformation/transcription domain-associated protein
USP22	ubiquitin-specific protease 22
VEGF	vascular endothelial growth factor
XBP1	X-box binding protein 1 (gene)
ZNF746	zinc finger protein 746
Z-NTA	Zeta Potential Nanoparticle Tracking Analysis

CHAPTER 1 - INTRODUCTION

1.1 Background to the study

The *c-myc* gene encodes a nuclear phosphoprotein that is widely recognised for its role as a transcription factor. The c-Myc protein is believed to participate in the regulation of 10 – 15 % of all genes (Zeller *et al*., 2006). These include genes involved in cell cycle progression (Berns *et al*., 1997, Hermeking *et al*., 2000), metabolism (Kim *et al*., 2004), cell growth (Liu *et al*., 2008b, Schuhmacher *et al*., 1999, Van Riggelen *et al*., 2010), differentiation (Wilson *et al*., 2004), adhesion (Gebhardt *et al*., 2006), and apoptosis (Morrish *et al*., 2003). Due to its function in regulating essential cellular functions, expression of the *c-myc* gene and activity of the c-Myc protein is, under normal circumstances, tightly controlled. However, abnormal *c-myc* expression can occur due to genetic events which include translocations (Battey *et al*., 1983), rearrangements (Dalla-Favera *et al*., 1983) and amplification (Treszl *et al*., 2004), as well as flaws in pathways implicated in regulation of this gene or the protein that it encodes (Smith *et al*., 1993).

Research carried out in the 1980s showed an association between the deregulated expression of *c-myc* and tumourigenesis (Adams *et al*., 1985, Leder *et al*., 1986). Further work showed that abnormal *c-myc* expression causes neoplastic changes by eliminating check-points in the cell cycle (Li and Dang, 1999, Gil *et al*., 2005), prompting genomic instability (Kuzyk and Mai, 2014) and through association with other oncogenes (Vaux *et al*., 1988, Wang *et al*., 2011). In fact, tumour cells often rely on *c-myc* expression for the maintenance of the cancerous state. This phenomenon, known as oncogene addiction, was emphasised by studies which show that *c-myc* inactivation caused tumour regression in transgenic mice (Arvanitis and Felsher, 2006) by inhibiting cellular proliferation, and inducing senescence or apoptosis and differentiation (Felsher, 2010). Moreover, the effects of systemic *c-myc* inhibition were found to be mild in normal tissues, and were well tolerated over time (Soucek *et al*., 2008). These findings, together with an estimation that *c-myc* is deregulated in up to 70 % of human cancers (Dang, 2012), motivate strongly for the therapeutic value of inhibiting oncogenic *c-myc*.

In theory, the oncogenic activity of *c-myc* can be eliminated by inhibiting expression of the activated gene, inhibiting inter-protein associations that are critical for c-Myc function, or by

disrupting pathways that support *c-myc* deregulation in cancer cells; and this has provided a basis for the design and evaluation of several potential anti-cancer strategies. The antisense oligonucleotides have featured in some of the earliest reports of *c-myc* inhibition (Holt *et al*., 1988, Loke *et al*., 1988, Wickstrom *et al*., 1988). These short, single-stranded DNA molecules hybridise to complementary regions of *c-myc* messenger RNA (mRNA), and prevent its translation either by acting as a physical impediment or by engaging ribonuclease (RNase) H activity (Dias and Stein, 2002). The application of antisense technology to c-Myc inhibition has expanded with nucleotide modifications designed to confer greater stability and specificity (Cutrona *et al*., 2003, Hudziak *et al*., 2000). However, Nobel Prize-winning work which described an endogenous gene silencing mechanism, known as RNA interference (RNAi), (Fire *et al*., 1998) presented further possibilities.

Short RNA duplexes, known as small interfering RNA (siRNA), associate with a network of cytoplasmic proteins to form the RNA-induced silencing complex (RISC), through which they guide the degradation of mRNA bearing a complementary sequence (Elbashir *et al*., 2001). In theory, effective silencing of *c-myc*, or any oncogene, may be achieved using endogenous cellular machinery, provided that the appropriately designed siRNA molecule is successfully introduced. However several factors militate against the success of naked siRNA molecules *in vivo*. Naked siRNA molecules are highly susceptible to serum nucleases (Cao and Ji, 2009) and are rapidly cleared by the kidneys (Huang *et al*., 2011). Furthermore, the size (approximately 14 kDa) and net negative charge of the siRNA prevent its passage across biological membranes (Akhtar and Benter, 2007). Therefore, an appropriate carrier is required to protect the siRNA molecules from damage and elimination as well as to disguise its negative charge.

The fact that nucleic acids can electrostatically associate with positively charged agents led to the investigation of a wide variety of cationic molecules as potential carrier vehicles. These include cationic cell-penetrating peptides (Eguchi *et al*., 2009), polymers (Urban-Klein *et al*., 2005), dendrimers (Taratula *et al*., 2009), and lipids (Zheng *et al*., 2014). Among them the cationic lipids have received the most attention, both in laboratory-scale experiments and clinical trials (Hope, 2014, Leung *et al*., 2014, Singh *et al*., 2015). The earliest cationic lipid-based delivery system is the cationic liposome, that is formed from the self-assembly of cationic and neutral or helper lipids (Felgner *et al*., 1987). These form nanostructures, known as lipoplexes, when

associated with siRNA. More recently cationic lipids have served as the nucleation centres or outer coatings of more elaborate lipid nanoparticles in which siRNA is encapsulated (Chen *et al*., 2010, Morrissey *et al*., 2005, Zhang *et al*., 2013). However, traditional siRNA lipoplexes are arguably easier and less time-consuming to prepare. Other favourable characteristics which include safety, biocompatibility, and, importantly, amenability to modification have sustained the interest in the field of cationic liposomal-siRNA delivery (Shim *et al*., 2013).

In a recent review of siRNA delivery systems for cancer treatment, Xu and Wang (2015) outline the properties of the ideal siRNA carrier. The vector system must have low toxicity, afford stability in the presence of serum, avoid recognition by the immune system, avoid renal clearance, reach and successfully enter the diseased cells to deliver its contents to the RNAi machinery. Although numerous studies documenting novel liposomal-siRNA systems have shown promise, none have resulted in a commercially available treatment (Singh *et al*., 2015). Major barriers to the application of cationic liposomal systems as nanomedicines include poor stability in the bloodstream and early recognition by the immune system. The net positive charge of lipoplexes encourages association with anionic serum proteins such as albumin and lipoproteins. The effect of these interactions is two-fold. Firstly, opsonisation by serum components can cause destabilisation of the lipoplex structure, and consequently, damage to the nucleic acid cargo before it reaches the diseased cells. Secondly, lipoplexes often aggregate to form large particles that accumulate in the lung and are rapidly cleared by the reticuloendothelial system. This reduces the effective dose and circulation time (Li *et al*., 1999, Semple *et al*., 1998).

In an attempt at addressing this matter, two main strategies have emerged. The first and most common method involves surface modification of liposomes with biocompatible polymers, such as poly(ethylene glycol) (PEG), which sterically inhibit contact between serum proteins and the liposomal bilayer (Papahadjopoulos *et al*., 1991, Torchilin *et al*., 1994). The second strategy involves increasing the mechanical strength of the bilayer so as to render it more resistant to the destabilising action of serum proteins. This may be achieved through the incorporation of rigid, membrane-stabilising lipids such as cholesterol (Chol) in liposome formulations (Sułkowski *et al*., 2005).

As such, the following observations were made:

- Deregulated expression of the *c-myc* proto-oncogene initiates transformation of normal cells, promotes tumourigenesis and is a common feature of a wide variety of cancers.
- Inhibition of *c-myc* expression may induce loss of the neoplastic phenotype, and this fact may be exploited in the design and development of more effective cancer treatment strategies.
- Silencing of *c-myc* expression in cancer cells can be achieved by the endogenous mechanism of RNAi via the introduction of correctly designed siRNA molecules.
- The success of any anti-*c-myc* siRNA strategy hinges on faithful delivery of siRNA molecules.
- Cationic liposomes have shown promise as siRNA carriers. However, unfavourable liposome-serum interactions and early elimination represent major limiting factors.
- It was concluded that further design and optimisation of liposome formulations is necessary before their full potential as siRNA carriers can be profitably harnessed.

Initially, much research was centred on enhancing liposome performance by improving the cationic lipid component. Consequently, numerous cationic lipids were synthesised with features which include novel ionisable headgroups that impart the positive charge and improve interactions with siRNA (Desigaux *et al*., 2007, Mével *et al*., 2010), cleavable linkages that minimise toxicity (Zheng *et al*., 2014), and pH-sensitive moieties to promote siRNA release within the cell (Sato *et al*., 2012). It was later shown that variations in the nature and quantity of the helper lipid and addition of surface appendages, when combined with a given cationic lipid gives liposomes with markedly different stabilities, siRNA carrying and protecting capability, cellular uptake characteristics and transfection efficacy (Khatri *et al*., 2014, Wang *et al*., 2013a). Consequently, the potential for formulation enhancement with a given, promising cationic lipid is extensive. The monocationic cholesterol derivative *N*,*N*-dimethylaminopropylamidosuccinyl-cholesterylformylhydrazide (MS09) is one such lipid. Having only been investigated in co-formulation with the conventional helper lipid dioleoylphosphatidylethanolamine (DOPE), MS09 showed potential in siRNA delivery that merits further development (Daniels *et al*., 2013). Hence, this study has focused on the effect of substituting Chol, as the helper lipid in pegylated and non-pegylated MS09 liposomes, in an attempt to achieve lipoplexes capable of safely and

successfully delivering siRNA molecules directed against a clinically relevant gene, *c-myc*, into cancer cells.

1.2 Aim and objectives

The aim of this study was to formulate cationic delivery systems, based on the cationic lipid, MS09; and to evaluate their potential as siRNA carriers *in vitro*, towards the development of a simple, yet effective anti-*c-myc* liposomal onconanotherapeutic agent. In order to achieve this aim, the objectives of the study were as follows:

- To formulate liposomes containing MS09 and bilayer-stabilising agents, namely, the helper lipid, Chol, and a pegylated lipid.
- To determine the optimum ratio of MS09 to Chol for liposome formation.
- To assess siRNA-binding, lipoplex formation and siRNA-protecting capabilities of liposomes.
- To characterise liposomes and siRNA lipoplexes according to size, morphology and zeta potential.
- To investigate cell tolerance and the siRNA-delivery capabilities of liposomes, in transformed and non-transformed human cell lines.
- To compare the characteristics of new liposome formulations with that of liposomes containing the conventional helper lipid, DOPE, and a commercially available liposomal transfection reagent.
- To apply the best-performing lipoplex to the delivery of anti-*c-myc* siRNA in cell lines representative of cancers that are known to overexpress *c-myc*.
- To quantify the effect of transfection with the selected lipoplex on oncogenic *c-myc* expression at the mRNA and protein levels.
- To evaluate the impact of transfection with the selected lipoplex on cancer cell migration and proliferation.

1.3 Significance of the study

Cancer is a leading cause of death world-wide. According to the American Cancer Society, deaths due to cancer outnumber those due to acquired immune deficiency syndrome (AIDS), malaria and tuberculosis combined (American Cancer Society, 2015). At present, cancer treatment mainly involves surgical removal of tumours, the administration of anti-cancer drugs and/or radiation depending on the type and stage of the disease. Despite advances in understanding tumourigenesis and disease progression, current cancer treatments are limited by harsh and possibly persistent side-effects, the possibility of recurrences, and are heavily dependent on early detection and diagnosis for success (DeSantis *et al*., 2014). With the global cancer burden projected to increase to 21.7 million new cases and 13 million deaths by the year 2030, it is clear that more effective treatment strategies are required (American Cancer Society, 2015).

Research into the genetics of cancer cells has identified the altered activity of the *c-myc* proto-oncogene as an important element in the initiation and maintenance of the cancerous state. Silencing of oncogenic *c-myc* by endogenous cellular machinery using appropriately designed siRNA molecules could reverse transformation, and presents a potential therapeutic alternative. The current study is important to the field of cancer gene therapy for the following reasons. Given that aberrant *c-myc* expression is a feature of a wide variety of malignancies, advances in the design of appropriate *c-myc*-silencing systems may eventually prove useful in treating a broad range of cancers (Vita and Henriksson, 2006). It is worth mentioning at this point that further development of the only lipid nanoparticle-based siRNA therapy against *c-myc* that has been reported to date (Tolcher *et al*., 2015) was terminated in 2016 following early-phase clinical trials. Therefore, safe and clinically feasible lipid-based anti-*c-myc* systems remain to be developed. The design, optimisation and evaluation of new liposomal formulations for siRNA delivery may potentiate this goal.

1.4 Novelty of the study

This study reports on new cationic liposome formulations containing the known cytofectin, MS09, and helper lipid, Chol, with or without PEG-modification for the purposes of siRNA delivery. While MS09 has been investigated in a serum-deficient *in vitro* siRNA application (Daniels *et al*., 2013), the effect of its co-formulation with Chol on siRNA delivery, and its

further application in *c-myc* gene silencing under normal cell culture conditions has not previously been explored.

1.5 Outline of dissertation

This dissertation is presented in the form of five chapters.

Chapter 1 provides the context within which the current study is relevant. The aims and objectives of the study together with its novelty and significance in the field of cancer gene therapy are outlined.

Chapter 2 is a literature review that is focused on the *c-myc* proto-oncogene, the role of the c-Myc oncoprotein in human cancer and its potential as a therapeutic target in the treatment of cancer. Due emphasis is placed on nucleic acid-mediated inhibition of *c-myc*.

Chapter 3 gives detailed information of all experimental work performed, fully outlining all materials and protocols undertaken.

Chapter 4 presents all results obtained with statistical analyses. These are interpreted and discussed in detail.

Chapter 5 concludes the study and gives recommendations for further improvement of the liposomal-siRNA systems reported.

CHAPTER 2 – LITERATURE REVIEW

Oncogenic c-Myc: structure, function and potential for nucleic acid-mediated inhibition in cancer treatment

2.1 Introduction

The *c-myc* proto-oncogene is the most famous member of the *myc* gene family which includes *L-myc* (Nau *et al*., 1985), *N-myc* (Schwab *et al*., 1983), *B-myc* (Ingvarsson *et al*., 1988) and *s-myc* (Sugiyama *et al*., 1989). *c-myc* was first identified in 1982, as a cellular homologue of *v-myc*, the oncogene responsible for the transforming activity of avian retroviruses (Vennstrom *et al*., 1982). The *c-myc* gene encodes a nuclear phosphoprotein (Beimling *et al*., 1985, Ramsay *et al*., 1984), c-Myc, that is a key regulator of cellular activity, largely through its capacity as a transcription factor (Dang, 1999, Dang *et al*., 2006).

Shortly after its discovery, the possibility of oncogenic activation of *c-myc* due to chromosomal translocation was raised (Battey *et al*., 1983), and abnormal *c-myc* expression was correlated with the initiation of cancer (Adams *et al*., 1985). *c-myc* has since been recognised as one of the most frequently deregulated genes in human cancers. Consequently, much attention has been given to the idea that the development of an appropriate strategy for inhibiting oncogenic activity of the c-Myc protein may translate into effective treatment for cancer (McKeown and Bradner, 2014). In this regard, synthetic nucleic acids, having long been recognised as tools for modulating gene expression (Juliano, 2016), were considered.

This review discusses the structural and functional aspects of the *c-myc* gene, its protein product, its importance in cancer and, as such, sets the scene to focus on strategies for nucleic acid-mediated *c-myc* inhibition.

2.2 Structure of the *c-myc* gene

The human *c-myc* gene is located on chromosome 8q24 (Neel *et al*., 1982). It is organised in the form of three exons and two introns (Watt *et al*., 1983) as shown in Figure 2.1. Transcription can be initiated from any of four promoter sequences (Nanbru *et al*., 2001). However, P2, from which, at minimum 75 % of *c-myc* mRNA originates, is the major promoter (Bentley and Groudine, 1986). The *c-myc* locus encodes alternate translation start codons, which give rise to

c-Myc protein isoforms (Blackwood *et al*., 1994). The nuclease hypersensitivity element (NHE) III1 is a key regulator of *c-myc* expression. It serves as a binding site for transcription initiation factors (Postel *et al*., 1989), and harbours a guanine-rich motif that modulates transcription via equilibrium between quadruplex and duplex DNA conformation (Seenisamy *et al*., 2004).

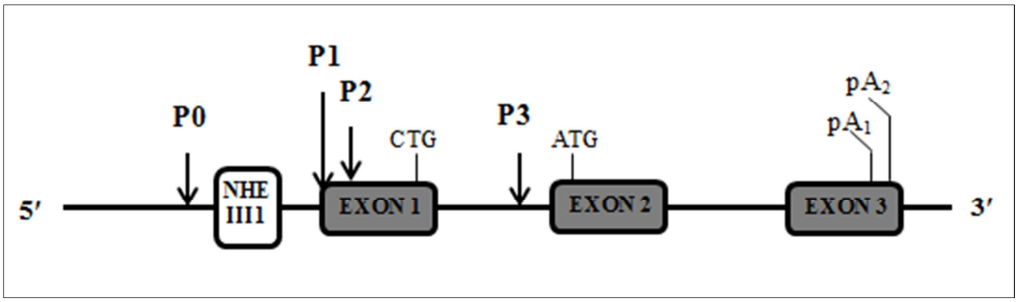

Figure 2.1: A representation of the human *c-myc* gene. The arrows indicate promoters. NHE III1 refers to the nuclease hypersensitivity element III1. CTG and ATG are the alternative start codons for the p67 and p64 protein isoforms, respectively. pA_1 and pA_2 represent polyadenylation signals. Redrawn and adapted from Chen *et al*. (2014) and Nanbru *et al*. (2001).

2.3 Structure of the c-Myc protein

The *c-myc* gene specifies any of three protein isoforms, depending on the promoter sequence and translation start site involved. The major c-Myc protein, designated as p64, is of 64 kDa and occurs when translation of *c-myc* mRNA from any of the four promoters begins at the AUG codon of exon 2. As shown in Figure 2.2, the 439 amino acid polypeptide chain of p64 is broadly divided into the amino-terminal domain (NTD), central domain and carboxy-terminal domain (CTD).

The CTD permits binding between the c-Myc transcription factor and regulatory regions of its target genes. This region harbours the basic helix-loop-helix (HLH) leucine zipper (LZ) motif that is characteristic of the Myc protein family. Importantly, the HLHLZ motif permits dimerization with its obligate partner protein, the Myc-associated factor X (Max) (Blackwood and Eisenman, 1991). The basic amino acid residues of the CTD specify binding of the c-Myc/Max dimer to CACGTG enhancer box (E-box) consensus sequences (Papoulas *et al*., 1992), in the proximal promoter region of its target genes (Kato *et al*., 1992, Zeller *et al*., 2006).

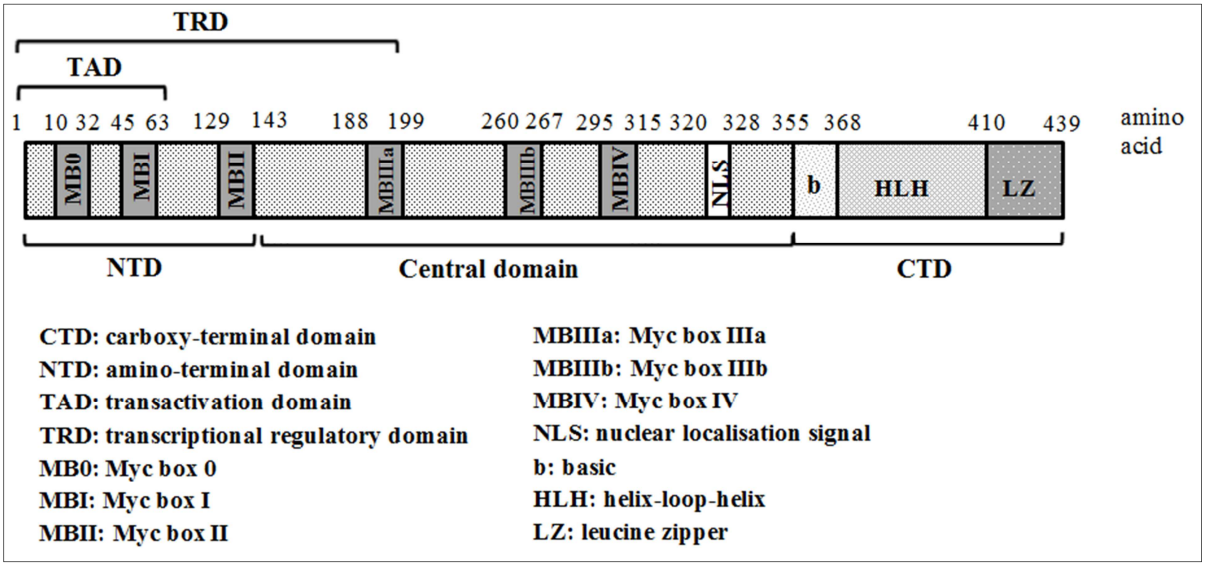

Figure 2.2: Structural organisation of human c-Myc protein, p64. Redrawn and adapted from Pelengaris *et al*. (2002) and Zhang *et al*. (2017b).

Several conserved peptide sequences, known as Myc boxes, play a major role in modulating the level and activity of the c-Myc protein, primarily by serving as docking sites for various protein factors. Myc box I (MBI) and Myc box II (MBII), within the NTD, have been the most widely studied. MBI harbours sites for phosphorylation (Henriksson *et al*., 1993) and *O*-glycosylation (Chou *et al*., 1995) that regulate the protein's lifespan. MBI also associates with proteins such as p107 (Gu *et al*., 1994) and TATA-binding protein (TBP) (McEwan *et al*., 1996), which either promote or repress its activity on target genes. Recently, the existence of a second transactivation domain (TAD), Myc box 0 (MB0), believed to induce the expression of a different set of target genes from MBI, was reported (Zhang *et al*., 2017b). MBII is associated with assembly of the transcription machinery (further details are provided in section 2.4), and has been linked with cellular transformation (Penn *et al*., 1990).

Three other conserved motifs, Myc box IIIa (MBIIIa), Myc box IIIb (MBIIIb) and Myc box IV (MBIV), have been identified within the central region. MBIIIa is required for transcriptional repression, negatively regulates apoptosis and contributes towards cellular transformation *in vitro* and *in vivo* (Herbst *et al*., 2005). MBIIIb serves as a binding site for the WD40-repeat protein, WDR5, and this facilitates the interaction with target chromosomal regions (Thomas *et al*., 2015). The same group later demonstrated that MBIV is necessary for the association of c-Myc with the transcriptional co-regulator, host cell factor-1 (HCF-1) (Thomas *et al*., 2016).

The NTD is the main point of variation among the three isoforms. A 67 kDa polypeptide resulting from translation of *c-myc* mRNA at the CUG start site of exon 1, has an extended N-terminus. This isoform is designated as p67 (Blackwood *et al*., 1994, Hann *et al*., 1988). The third isoform, c-Myc S, is a smaller protein of 45 kDa that is translated from an AUG start codon downstream of the p64 translation initiation site (Spotts *et al*., 1997). Although c-Myc S lacks a functional TAD, it is capable of mediating many biological functions that the other isomers carry out (Xiao *et al*., 1998). *In vivo* studies later performed by Benassayag and coworkers (2005), showed that all three isoforms simultaneously exist within normal cells in ratios that depend on the cell status. In 2010, it was reported that a post-translational cleavage of the full length c-Myc polypeptide results in Myc-nick, which lacks a CTD. The absence of a nuclear localisation signal (NLS) restricts Myc-nick to the cytoplasm where it appears to influence cytoskeletal changes involved in cell differentiation (Conacci-Sorrell *et al*., 2010).

2.4 c-Myc as a transcription factor

It is estimated that c-Myc participates in the regulation of 10-15 % of all genes (Zeller *et al*., 2006), and these encompass genes transcribed by any of the three RNA polymerases (Oskarsson and Trumpp, 2005). Chromatin immunoprecipitation coupled with pair-end ditag sequencing analysis in human B cells showed that over 4000 genomic loci could serve as c-Myc binding sites (Zeller *et al*., 2006). Consequently, many and varied target genes and gene networks of c-Myc have been identified and, in this way, its influence within the cell has become more fully understood.

One of the earliest elucidated roles of c-Myc was its involvement in the cell cycle. Serial analysis of gene expression in primary human umbilical vein endothelial cells identified genes encoding the cell cycle regulators, cyclin-dependent kinase 4, cyclin E binding protein 1, and cyclin B as direct targets (Menssen and Hermeking, 2002). The same study showed that c-Myc may preserve the integrity of the genome during replication through its induction of DNA repair genes. c-Myc regulates energy generation and metabolism, and was found to directly activate genes involved in mitochondrial replication and biogenesis (Kim *et al*., 2008). c-Myc also co-ordinates various biosynthetic pathways. Its role in protein synthesis has been highlighted by studies which show that c-Myc directly activates the transcription of genes encoding ribosomal RNA (rRNA) (Grandori *et al*., 2005) and ribosomal proteins (Guo *et al*., 2000), and controls the maturation of

rRNA (Schlosser *et al*., 2003). In addition, c-Myc is implicated in the transcription of genes involved in the synthesis of lipids (Edmunds *et al*., 2014, Morrish *et al*., 2010) and nucleotides (Liu *et al*., 2008b). c-Myc influences cell adhesion and structure through its activity on the expression of genes which encode proteins of the extracellular matrix and cytoskeleton (Coller *et al*., 2000). More recently, Wang *et al*. (2013b) showed that c-Myc regulates microRNA (miRNA) expression through its interaction with the promoter of the gene that encodes Drosha, which is the enzyme responsible for processing primary-miRNA precursors. The above are intended as examples of key biological functions mediated by c-Myc and, by no means, cover the complexities of the c-Myc target gene network (Dang *et al*., 2006). In fact, in one study, 49 direct targets were identified to be genes which encoded other transcription factors (Zeller *et al*., 2006). As such c-Myc is believed to impact, either directly or indirectly, almost all cellular processes and is referred to as a '*global regulator of transcription*' (Dang *et al*., 2006).

Given that its role as a transcription factor has been widely publicised, a few accepted mechanisms of c-Myc-mediated transcription are briefly discussed. The interaction of c-Myc with Max is essential for its activity (Amati *et al*., 1993). X-ray structures revealed that c-Myc forms a heterodimer with Max via the LZ protein motif, and this positions the basic peptide helices of c-Myc for insertion into the major groove of the DNA target E-box (Nair and Burley, 2003). Once the c-Myc/Max dimer has bound to the E-box, transcription of the target gene is either activated or repressed, depending on the interaction of c-Myc with other protein factors.

An accepted mechanism of c-Myc-mediated transactivation (Figure 2.3) proposes that MBII recruits the transformation/transcription domain-associated protein (TRRAP) which in turn associates with histone acetyltransferases such as, general control of amino acid synthesis protein-5 (GCN5) and TIP60 (McMahon *et al*., 1998; McMahon *et al*., 2000). The acetylation of histones renders the DNA at the target location accessible for binding of the chromatin remodelling complex (Li *et al*., 2007) and encourages transcription by RNA polymerases (Arabi *et al*., 2005, Kenneth *et al*., 2007).

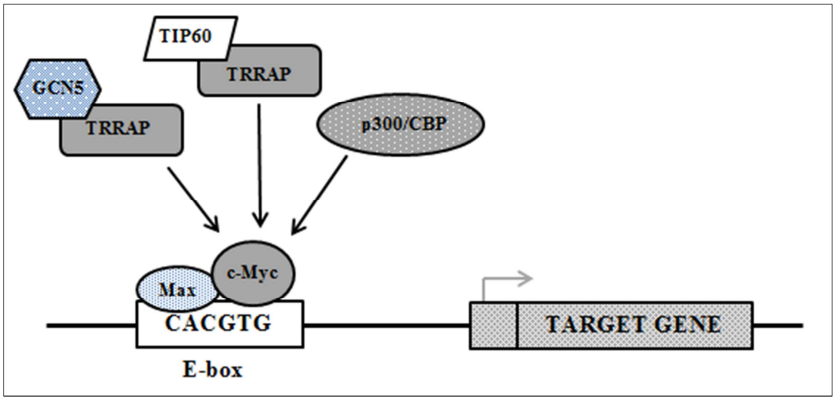

Figure 2.3: c-Myc mediated-transcriptional activation. c-Myc, when associated with Max, recruits histone acetyltransferases GCN5 or TIP60 via TRRAP; or the p300/CBP complex to activate transcription of target genes. The grey arrow indicates transcription initiation and progression. Redrawn and adapted from Cole and Cowling (2008) and Dang (2012).

It was initially accepted that c-Myc exerted its role in transcription via the collaboration of protein complexes with its NTD. However, Vervoorts and coworkers (2003) demonstrated that the cAMP response element binding protein (CBP), which has histone acetyltransferase activity, binds to the CTD of c-Myc. CBP, in association with p300, serves as a positive cofactor for c-Myc function and is believed to interact with the RNA polymerase II (RNA pol II) complex (Cowling and Cole, 2007).

Genes repressed by c-Myc are generally those that restrict cell growth and proliferation. These include genes which encode inhibitors of the cell cycle (Claassen and Hann, 2000), tumour-suppressive miRNAs (Zhang *et al*., 2012) and cell-adhesion molecules (Gebhardt *et al*., 2006). The most common mechanism of transrepression involves the association of c-Myc with the Myc-interacting zinc finger protein-1 (Miz-1) transcription factor (Figure 2.4).

Miz-1 binds to the initiator element (Inr) of promoter sequences, where it activates transcription of genes and is associated with strong growth inhibitory effects in the cell (Peukert *et al*., 1997, Si *et al*., 2010). The c-Myc CTD binds to Miz-1 (Gartel and Shchors, 2003) and this competitively inhibits the binding of p300 (Staller *et al*., 2001). Instead Dnmt3a is recruited, and this methylates the promoter sequences (Brenner *et al*., 2005). In this way, the regulatory region of the gene cannot access an important transcriptional co-factor and receives a modification that brings about gene repression.

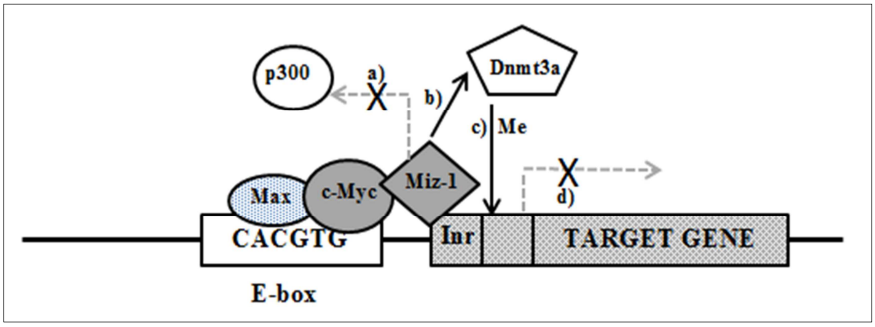

Figure 2.4: c-Myc-mediated transcriptional repression. c-Myc, when associated with Max, binds to Miz-1, **a)** preventing its association with p300, and **b)** recruits Dnmt3 that **c)** methylates the promoter region and, as such, prevents **d)** Miz-1 from promoting transcription of the target gene. Inr denotes an initiator element. Redrawn and adapted from Tansey (2014).

Other mechanisms of c-Myc-mediated gene repression were put forward following studies on growth arrest genes (Gartel and Shchors, 2003). It was shown that c-Myc, in the absence of Max, inhibits the transcriptional activity of another zinc finger transcription factor namely, Sp1, by either binding to Sp1 or the Smad-Sp1 complex (Feng *et al*., 2002, Gartel *et al*., 2001).

Although most c-Myc activity in normal cellular processes and cancer has been attributed to its role in transcription, it is worth mentioning that evidence exists for transcription-independent functions of c-Myc (Cole and Cowling, 2008). In this regard, Cowling and Cole (2007) reported that c-Myc can regulate translation by inducing mRNA cap methylation. In addition, c-Myc directly controls DNA replication by recruiting components of the pre-replicative complex during DNA replication (Dominguez-Sola *et al*., 2007).

2.5 c-Myc in normal cells

c-myc is among the first genes to be expressed when cells are exposed to mitogens and is therefore known as an '*immediate early response gene*' (Henriksson and Lüscher, 1996, Lemaitre *et al*., 1996). c-Myc levels in normal cells vary in response to internal signals for cell proliferation and the external environment (Gardner *et al*., 2002). In quiescent cells, *c-myc* is expressed at low levels such that its protein product is hardly detectable. However, with mitogenic stimuli *c-myc* mRNA and protein levels increase rapidly. The *c-myc* expression continues through the cell cycle and drops to basal levels as cells return to their resting state (Waters *et al*., 1991).

Shichiri *et al*. (1993) showed that cell proliferation is sensitive to small changes in *c-myc* expression, and that regulated expression of *c-myc* is essential for maintaining normal cellular status. Therefore c-Myc levels and activity in the cell are, under normal conditions, stringently regulated. Control points include the transcriptional regulation of the *c-myc* gene itself (Eick and Bornkamm, 1986, Bentley and Groudine, 1986), the activity of translation initiation factor eIF4E which ensures that only faithful *c-myc* mRNA transcripts are exported to the cytoplasm (Culjkovic *et al*., 2006); the short half-life of *c-myc* mRNA (Dani *et al*., 1984), post-translational modifications such as phosphorylation, acetylation and ubiquitinylation (Vervoorts *et al*., 2006); and proteins which either directly interact with c-Myc (Dai *et al*., 2007) or influence its dimerization with Max (Grandori *et al*., 2000).

2.6 Activation of *c-myc* in human cancer

Genetic alterations of the *c-myc* gene and molecules or pathways responsible for its regulation can cause deviations from the rigorously controlled expression of *c-myc*, such that the protein product is expressed at abnormally high levels, is constitutively expressed at varying levels and/or no longer responds to external stimuli. This phenomenon is known as oncogenic activation (Pelengaris *et al*., 2002). The major mechanisms of *c-myc* activation are discussed below.

The earliest genetic alteration of *c-myc* identified was translocation, which places the gene under the control of very active gene regulatory elements. A defining feature of Burkitt's Lymphoma is the juxtaposition of *c-myc* to the constitutively expressed immunoglobulin (Ig) heavy or light chain genes of chromosomes 2, 14 or 22 in B cells (Dalla-Favera *et al*., 1982). In other B cell-associated cancers, translocated *c-myc* may occur in the proximity of genes that do not encode immunoglobulins. These include the *XBP1*, *KRAS*, *FAM46C* and *CCND1* genes that contribute towards maturation of B cells and disease development (Walker *et al*., 2014). Translocation can also place *c-myc* under the control of super-enhancer elements (Walker *et al*., 2014), which interact with *c-myc* via a common, conserved enhancer-docking site located upstream of the *c-myc* promoter (Schuijers *et al*., 2018). Moreover, instability of the *c-myc* oncogene has been associated with the H-DNA-forming tendency of sequences prevalent at common translocation breakpoints (del Mundo *et al*., 2017).

Rearrangements which occur as a result of recombination of genetic material within chromosome 8, are also responsible for oncogenic activation of *c-myc* in cancers of the blood, albeit to a lesser extent (Ott *et al*., 2013). Point mutations in the region of MBI are common to lymphomas. In particular, mutation of the Thr58 phosphorylation site prevents ubiquitin/proteasome-directed degradation of c-Myc, extends its lifespan and, therefore, encourages tumourigenesis (Bahram *et al*., 2000).

Elevated *c-myc* expression can occur as a result of gene amplification. This phenomenon is a hall-mark of many solid tumours. Several surveys have attempted to quantify *c-myc* copies in different malignancies and present an overview of its frequency. For example, Treszl and coworkers (2004) detected extra copies of the *c-myc* gene in 61 % of nodular melanoma samples tested. Naidu and colleagues (2002) observed *c-myc* amplification in 25 % of 440 primary breast carcinomas. Low to moderate *c-myc* amplification was detected in 32 % of tumours taken from 149 colon cancer patients (Augenlicht *et al*., 1997). Abnormal copy numbers of the *c-myc* gene were also reported in cancers of the brain (Herms *et al*., 2000), head and neck (Baltaci *et al*., 2016), liver (Chan *et al*., 2004), lung (Seo *et al*., 2014), stomach (Hara *et al*., 1998), prostate (Jenkins *et al*., 1997), bladder (Sardi *et al*., 1998) and ovaries (Baker *et al*., 1990). Although *c-myc* amplification has been observed in several primary carcinomas (Abba *et al*., 2004, Hara *et al*., 1998), this event is more frequent in late-stage or metastatic cancers (Bitzer *et al*., 2002, Bubendorf *et al*., 1999, Treszl *et al*., 2004, Wang *et al*., 2002).

Defects in molecules and pathways responsible for *c-myc* regulation can up-regulate *c-myc* expression, in the absence of genetic alterations of the *c-myc* gene itself (Smith *et al*., 1993). A notable example is the APC/β-catenin pathway that negatively regulates *c-myc* expression under normal conditions (He *et al*., 1998). Inactivation of this pathway is most prominent in colorectal carcinoma in which 83 % of tumours harbour mutations in the adenomatous polyposis coli (APC) tumour suppressor gene (Rowan *et al*., 2000). Mutations of β-catenin, which is a transcriptional co-repressor, have been reported in cases of medulloblastoma (Zurawel *et al*., 1998), endometrioid ovarian carcinoma (Palacios and Gamallo, 1998) and hepatoblastoma (Udatsu *et al*., 2001). The aberrant expression of several other *c-myc* regulators, which include haematological and neurological expressed 1 (HN1) (Zhang *et al*., 2017a); the RNA helicase DDX6 (Taniguchi *et al*., 2018); the RNA-binding protein, negative elongation factor E

(NELFE) (Dang *et al*., 2017); the bromodomain and extra-terminal (BET) domain protein, BRD4 (Ba *et al*., 2018); transcription factors such as OVOL1 and OVOL2 (Ito *et al*., 2017); and tumour-suppressor miRNAs such as miRNA 320a (Xie *et al*., 2017); represent other avenues by which *c-myc* overexpression occurs in various forms and sub-forms of human cancer.

Overexpression of the mRNA-stabilising, coding region determinant-binding protein (CRD-BP) also accounts for constitutive expression of *c-myc* in several types of cancer (Doyle *et al*., 2000, Ioannidis *et al*., 2004, Ross *et al*., 2001). *In vitro* experiments have shown that the CRD-BP binds to the coding region stability determinant of *c-myc* mRNA and extends its half-life by protecting it against degradation by endonucleases (Bernstein *et al*., 1992). Stabilisation of *c-myc* mRNA in breast cancer has been linked with abnormally high levels of the signaling protein p62. When overexpressed, p62 inhibits the expression of let-7a and let-7b miRNAs that are ordinarily necessary for *c-myc* mRNA degradation (Xu *et al*., 2017). More recently Abdullah *et al*. (2018) reported that atypical expression of the tyrosine-protein kinase, Src, which acts on the RNA-binding protein, IMP1, stabilised the *c-myc* transcript and, as such, stimulated cell cycle entry in oestrogen receptor-positive breast cancer cells.

In addition to the effect of enhanced *c-myc* mRNA stability, oncogenic activation can occur with abnormal longevity of the c-Myc protein. Gu *et al*. (2017) reported a positive correlation between overexpression of the Ca^{2+}/calmodulin-dependent protein kinase II γ (CAMKIIγ), which stabilises c-Myc by direct phosphorylation at MBI, and T cell lymphomagenesis. In prostate cancer, downregulation of the E3 ubiquitin ligase adaptor speckle-type POZ protein (SPOP) is a common aberration and this prevents c-Myc being marked for degradation (Geng *et al*., 2017). c-Myc stability caused by elevated expression of the ubiquitin-specific protease 22 (USP22) (Kim *et al*., 2017a); proteasome activator subunit 3 (PSME3) (Guo *et al*., 2017); zinc finger protein 746 (ZNF746) (Jung *et al*., 2018); and the calcium-dependent phospholipid-binding protein, Annexin A2 (Ma *et al*., 2017); has been associated with the progression of breast, pancreatic, colon and oesophageal cancers, respectively. Abnormal c-Myc stability may also be conferred through the action of non-protein factors. Yang *et al*. (2017) reported that overexpression of a non-coding circular RNA, circ-Amotl1, which occurs both in patient

tumour samples and cancer cell lines, appeared to encourage c-Myc stability by increasing its retention in the nucleus.

A further mechanism of *c-myc* activation in some cancers involves insertion of viral sequences near the *c-myc* locus. Ferber and colleagues (2003) showed that the integration of the human papilloma virus 18 (HPV 18) sequence in cervical tumours is a non-random event, and this typically occurs at common fragile sites in the genome that are susceptible to other genetic changes. The *c-myc* locus is one such site, at which 30 % of HPV 18 insertions were detected. In a study on invasive genital carcinoma cell lines, elevated *c-myc* mRNA and protein levels were observed only in instances in which insertion of viral DNA occurred in the vicinity of the *c-myc* gene (Peter *et al*., 2006).

2.7 Oncogenic effects of c-Myc

Given that *c-myc* is intrinsic to normal cell maintenance, abnormalities in its expression have far-reaching consequences. Following activation of the *c-myc* gene, the most noticeable effect is on cell proliferation. The aberrantly expressed c-Myc protein (henceforth referred to as oncogenic c-Myc) forces cells to enter the cell cycle and hastens its passage through the G1, G2 and S-phases. Rapid cell division requires a simultaneous increase in the rate of DNA replication, and this often results in replication errors and DNA damage. It was proposed that *c-myc* overexpression caused the accumulation of abnormal DNA replication intermediates, a phenomenon known as replication stress (Robinson *et al*., 2009). Other studies have shown that *c-myc* overexpression causes damage to DNA by mechanisms that are either dependent (Vafa *et al*., 2002) or independent of the generation of reactive oxygen species (Ray *et al*., 2006).

Ordinarily, hyper-proliferation and DNA damage activate protective mechanisms such as apoptotic pathways (Eischen *et al*., 1999, Zindy *et al*., 1998) and DNA damage response signaling (Adachi *et al*., 2001, Sankar *et al*., 2009). Therefore, it was initially believed that defects in these pathways, and the effects of other oncogenes, assisted in c-Myc-mediated tumourigenesis. However, it is possible for oncogenic c-Myc to negate the effects of these pathways by itself, given that, under normal conditions, it regulates pathways that restrain replication stress (Campaner and Amati, 2012) and can attenuate the activity of the tumour suppressor, p53 (Vafa *et al*., 2002). c-Myc leads cells towards immortalisation by preventing the

incremental shortening of telomeres that normally occurs each time a cell divides. In this regard, c-Myc directly controls the expression of human telomerase reverse transcriptase (hTERT), which is the rate limiting component of the telomerase complex (Khattar and Tergaonkar, 2017).

In c-Myc driven cancers, oncogenic c-Myc brings about what authors describe as '*metabolic reprogramming*,' a phenomenon in which normal cellular processes are enhanced to support the growth and energy demands of rapidly dividing cells and survival in the tumour microenvironment (Li and Simon, 2013). For example, cancer cells are known to consume glucose at higher rates than normal cells, and are often characterised by greater reliance on glycolysis as opposed to mitochondrial oxidative phosphorylation as a means of energy generation (Vander Heiden *et al*., 2009). Hu and colleagues (2011) showed, using a switchable model of *c-myc*-driven liver cancer, that the expression of several genes involved in glycolysis are upregulated in tumours, but these are repressed when *c-myc* expression is switched off. Moreover, cells transformed by *c-myc* were shown to undergo extensive apoptosis with glucose deprivation and, as such, are said to display glucose addiction (Shim *et al*., 1998). Cancer cells may also utilise glutamine as an alternative energy source. The induction of *c-myc* in a B-cell model of Burkitt's lymphoma caused increase in mitochondrial glutaminase levels because c-Myc repressed the transcription of regulatory miRNAs (Gao *et al*., 2009). As with glucose, oncogenic c-Myc can establish a dependency on glutamine in cancer cells (Wise *et al*., 2008). While these represent isolated illustrations of oncogenic c-Myc-induced metabolic changes, a multiomics-based study by Satoh *et al*. (2017) highlighted its role in global metabolic reprogramming in cancer cells. This group showed that c-Myc expression in colorectal carcinoma induced at least 215 metabolic reactions by altering the expression of 121 metabolic genes and 39 transporter genes.

Along with changes in nutrient consumption and energy generation, oncogenic c-Myc accelerates biosynthesis. This is evidenced by studies which show that forced expression of *c-myc* caused cells to double their size, protein (Iritani and Eisenman, 1999) and RNA content (Nie *et al*., 2012). In fact, increased ribosomal content appears to be an important step towards cancer in pre-neoplastic cells that overexpress *c-myc* (Barna *et al*., 2008). Furthermore, oncogenic c-Myc can create a dependency in cancer cells on accelerated synthesis of biomolecules, by inducing abnormal transcription of the relevant genes. Such dependencies have

been observed with respect to protein (Aleco *et al*., 2016, Pourdehnad *et al*., 2013) and lipid (Hall *et al*., 2016) synthesis. This heightened metabolism has been correlated with c-Myc-driven suppression of circadian rhythm in cancer cells (Altman *et al*., 2015, Dang, 2016). Oncogenic c-Myc, in association with Miz-1, was shown to bind to non-target E-box motifs of core clock genes and, as such, inhibit their expression (Shostak *et al*., 2016).

Oncogenic c-Myc protects cancer cells and creates a suitable environment for them to thrive. Casey *et al*. (2016) provided evidence that c-Myc promotes survival of neoplastic cells by suppressing the regular anti-tumour immune response. c-Myc overexpression was shown to upregulate the expression of two immune checkpoint proteins on the cell surface i.e. the programmed death-ligand 1 (PD-L1) and the cluster of differentiation 47 (CD47), which prevent cancer cell recognition and elimination, respectively. The oncoprotein plays a key role in maintaining cells within a tumour mass by triggering what is referred to as an '*angiogenic switch'*. This involves upregulating the expression of the vascular endothelial growth factor (VEGF), while reducing the expression of thrombospondin-1, to induce pre-existing blood vessels to develop into a complex vascular network within the tumour (Baudino *et al*., 2002, Dews *et al*., 2006). Other sources show that c-Myc is able to trigger angiogenesis and stromal remodelling by activating an inflammatory response (Shchors *et al*., 2006, Soucek *et al*., 2007). These findings are supported by recent work which directly implicates c-Myc-mediated upregulation of inflammatory pathways in tumour growth (Merve *et al*., 2017) and metastasis (Sun *et al*., 2018).

Metastasis is a well-documented consequence of *c-myc* overexpression. c-Myc induces epithelial-to-mesenchymal transition (EMT), which is a process by which cells acquire invasiveness and motility, through co-operation with other proteins such as the transforming growth factor-β (TGFβ) (Smith *et al*., 2009) and sterol regulatory element-binding protein 1 (SREBP1) (Zhai *et al*., 2018). c-Myc-driven EMT in myelomas was shown to induce vasculogenic mimicry, a process by which new blood vessels are formed *de novo* (Lin *et al*., 2017). c-Myc also promotes tumour cell invasiveness by EMT-independent processes that rely on cell adhesion and/or cytoskeletal reorganisation. For example, c-Myc activates the transcription of the galactoside-binding protein, galectin-1, that encourages the spread of oesophageal cancer to the lymph nodes (Yan *et al*., 2009), and co-operates with the S-phase

kinase-associated protein 2 (Skp2) to promote transcription of the RhoA GTPase that encourages cancer cell motility in metastatic breast cancer (Chan *et al*., 2010).

The general consensus is that these effects can collectively account for the initiation, progression and maintenance of cancer. However, all possible oncogenic effects of c-Myc may not necessarily manifest in all *c-myc*-driven cancers. This notion is supported by research which suggest that c-Myc activity can be cell-specific (Kyo *et al*., 2000). Hence, it appears that c-Myc may transform different cell types in different ways (Dang, 2013).

Two different models of c-Myc-driven tumourigenesis have emerged over the past five years. According to the general amplifier model, oncogenic c-Myc amplifies the expression of all genes that are being expressed in a cell. In this way, all cellular processes are accelerated resulting in extreme disorder within the cell (Lin *et al*., 2012, Nie *et al*., 2012). The idea that oncogenic c-Myc promiscuously activates transcription is supported by earlier research by Fernandez *et al*. (2003). This group demonstrated that overexpression of c-Myc increased the affinity with which it bound to E-box elements of genes that represent, under normal conditions, low affinity targets. More recently, Sabò *et al*. (2014) reported that while c-Myc does have the ability to interact with all active promoters, it does not necessarily do so, and changes cell status by either activating or repressing the transcription of discrete sets of genes. The notion that oncogenic c-Myc acts in a gene-specific manner was further supported by Lorenzin and colleagues (Lorenzin *et al*., 2016, Walz *et al*., 2014) and provides the basis for an alternative model of c-Myc driven tumourigenesis.

2.8 *c-myc* as a target in cancer therapy

Several properties of *c-myc*, as an oncogene, render it a suitable target for cancer treatment. Firstly, the ideal treatment for any disease should target the cause, rather than the symptoms. Its protein product is strongly implicated in the initiation and maintenance of the majority of human cancers and, in its capacity as a transcription factor, functions downstream of other oncogenes (Hermeking, 2003). Hence, preventing its oncogenic activity is, in theory, addressing the root of the problem. Secondly, an oncogene is potentially more suitable a target in cancer therapy than a tumour suppressor gene because it is easier to inhibit accelerated functions in cancer cells than to restore functions that they have lost (Hermeking, 2003). Thirdly, the fact that cancer cells often

display a dependency on the continuous expression of *c-myc* for their maintenance may be exploited in the development of anti-cancer strategies. In this regard, experiments performed with conditional transgenic mouse models showed that *c-myc* inactivation brought about tumour regression and can, in some instances, reverse cancer (Arvanitis and Felsher, 2006). Importantly, Soucek *et al*. (2008) responded to concerns surrounding the impact of systemic *c-myc* inhibition in normal cells with a study which showed that side effects on normal regenerating cells were transient and well tolerated over time. Finally, given that *c-myc* is one of the most frequently altered genes in human cancer, a strategy directed against *c-myc* may potentiate the treatment of a broad range of cancers (Vita and Henriksson, 2006).

2.9 Nucleic acids targeting oncogenic *c-myc*

Direct inhibition of oncogenic c-Myc was initially considered to be difficult to accomplish. Firstly, its primary cellular activity i.e. transcription in the nucleus, is not easily accessible to therapeutic agents. Secondly, the protein lacks enzyme activity and suitable ligand-binding domains that could be targeted by traditional small molecule drugs (McKeown and Bradner, 2014). Although advances in understanding the intricacies of c-Myc regulation and interaction with protein factors have presented new areas of attack for novel small molecule inhibitors (Berthon *et al*., 2016, Chen *et al*., 2014, Neidle, 2016), the option of directly inhibiting expression of the activated *c-myc* gene with synthetic nucleic acids continues to receive attention. In fact, the very idea of nucleic acids as therapeutic agents emerged largely in response to conditions such as cancer that were difficult to treat with conventional treatment (Juliano, 2016).

Nucleic acids designed for the purpose of gene inhibition are typically small DNA or RNA molecules. Their use is primarily based on the concept that homology between the nucleic acid molecule and a region of either *c-myc* DNA or mRNA causes binding, and blocks the processes of transcription or translation, respectively. The discussion to follow has attempted to review the various categories of synthetic nucleic acids that can effect *c-myc* inhibition, and trace their development in the search for more effective cancer treatment modalities.

2.9.1. Antisense oligonucleotides

Antisense oligonucleotides (ASOs) represent a major class of nucleic acids that has been applied to the inhibition of *c-myc*. These short, single-stranded nucleotides are designed with complementarity to a region of the mRNA. The ASO binds to the mRNA and either acts as a substrate for RNase H, which catalyses the cleavage of mRNA; or physically blocks translation. ASOs may be either DNA or RNA in nature. However, ASOs employed for the purpose of *c-myc* inhibition are predominantly DNA oligomers. Moreover, the use of unmodified, phosphodiester nucleotides is discouraged primarily due to poor biological stability. Hence, in most studies modified ASOs were synthesised (Figure 2.5) with the aim of improving stability whilst maintaining specificity for the target sequence (Dias and Stein, 2002).

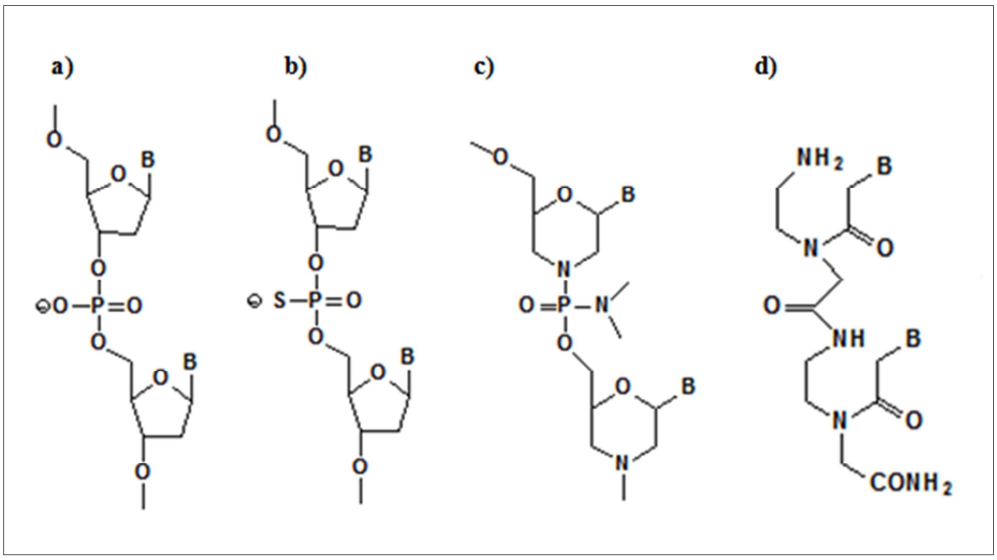

Figure 2.5: Representation of **a)** conventional phosphodiester nucleotides and chemically modified nucleotides **b)** phosphorothioate-linked nucleotides, **c)** phosphorodiamidate morpholino nucleotides and **d)** peptide nucleic acids. B represents a nitrogenous base. Redrawn and adapted from Dias and Stein (2002).

2.9.1.1 Phosphorothioate antisense oligonucleotides

One of the earliest modifications explored, involved attaching individual nucleosides via a phosphorothioate (PS) linkage (Figure 2.5b). This gave an oligomer with approximately ten times greater nuclease resistance than conventional phosphodiester nucleotides (Campbell *et al.*, 1990). Wickstrom *et al.* (1988) synthesised a 15-nucleotide phosphorothioate antisense oligonucleotide (PS-ASO) directed against a hairpin-loop which contained the initiation codon of *c-myc* mRNA. When introduced into human leukemia cells in culture, the PS-ASO reduced

c-Myc levels and inhibited growth in a sequence-specific, dose-dependent manner. This early work suggested the possibility of using *c-myc*-specific PS-ASOs as anti-cancer agents.

Anti-*c-myc* PS-ASOs have since been associated with delivery agents (Junghans *et al*., 2005, Leonetti *et al*., 2001, Pastorino *et al*., 2001, Pastorino *et al*., 2003, Zhang *et al*., 2018) and applied in conjunction with anti-cancer drugs (Citro *et al*., 1998, Leonetti *et al*., 1999, Pastorino *et al*., 2008, Yuan *et al*., 2014) and physical agents, such as ultrasound (Jing *et al*., 2015) to improve efficacy. Notable success was achieved with INX-3280, a 15-nucleotide PS-ASO against *c-myc* (Webb *et al*., 2001), developed by Inex Pharmaceuticals Corporation, which entered clinical trials for treatment of lymphoma and solid tumours. It did not, however, progress beyond the Phase II trial. A modified form, INXC-6295, was later subjected to preclinical studies in solid tumours, but was also not developed further (Whitfield *et al*., 2017).

The use of oligonucleotides as inhibitors of gene expression has expanded with the design of second generation nucleotide analogues. In particular, the phosphorodiamidate morpholino oligomer (PMO), and peptide nucleic acid (PNA) have been incorporated in the design of anti-*c-myc* sequences.

2.9.1.2 Phosphorodiamidate morpholino oligomers

The PMO contains a six-membered morpholine ring instead of the deoxyribose moiety and individual nucleosides are attached by phosphorodiamidate linkage (Figure 2.5c). Unlike the PS backbone, that has affinity for serum and cellular proteins (Levin, 1999), the phosphorodiamidate group is neutral at physiological pH. This reduces the possibility of non-specific effects that limit the use of PS-ASOs (Amantana and Iversen, 2005). PMOs are nuclease, protease and esterase resistant and have demonstrated reasonable stability in biological fluids (Hudziak *et al*., 1996). PMO-mediated gene silencing is not dependent upon the action of RNase H. Instead PMOs inhibit gene expression by causing mis-splicing of pre-mRNA or inhibition of ribosomal assembly (Amantana and Iversen, 2005). The first report of an anti-*c-myc* PMO was made by Hudziak and coworkers (2000). This group showed that a 20-nucleotide PMO reduced c-Myc levels and induced cell cycle arrest in cancer cells *in vitro*. In animal models, this PMO, designated as AVI-4126, sensitised tumour cells to the activity of anti-cancer drugs (Knapp *et al*., 2003), reduced tumour size (Iversen *et al*., 2003), and inhibited metastasis

(Sekhon *et al*., 2008). AVI-4126 was favourably evaluated in clinical safety studies (Iversen *et al*., 2003) and progressed to phase II clinical trials (Stephens, 2004). However, it is unknown as to why AVI-4126 was not further developed (Moreno and Pêgo, 2014).

2.9.1.3 Peptide nucleic acids

The PNA is another class of steric inhibitors of gene expression. Here, the sugar-phosphate backbone is replaced by repeating units of N-(2-aminomethyl)glycine, and the nitrogenous bases are attached to the polyamide skeleton through methylene carbonyl groups (Figure 2.5d). PNAs are known to form highly stable duplexes or triplexes with RNA and DNA respectively, because they are uncharged and do not electrostatically repel the anionic phosphates in naturally-occurring nucleic acids. Consequently, sequence-specific PNAs may inhibit gene expression at the levels of transcription and translation (Shakeel *et al*., 2006).

PNAs directed against *c-myc* have been investigated mainly with a focus on the treatment of Burkitt's lymphoma. In an attempt to overcome any adverse effects resulting from *c-myc* inhibition in normal cells, Cutrona and coworkers (2003) synthesised a PNA complementary to the *Eμ* intronic enhancer at the Ig locus which drives aberrant *c-myc* expression in Burkitt's lymphoma. The PNA inhibited the expression of *c-myc in vitro* by preventing binding of specific nuclear factors to the *Eμ* DNA sequence; and inhibited tumour growth in mice with Burkitt's lymphoma xenografts (Boffa *et al*., 2006). The same animal model was used to evaluate a PNA specific for the *Emu* Ig enhancer (Boffa *et al*., 2005). In these studies PNAs were designed to interact with target DNA duplexes at the *c-myc* locus, rather than with target regions of *c-myc* mRNA. Hence, this represents an antigene approach as opposed to the antisense strategies that have been discussed up until this point.

PNAs directed against *c-myc* have also been linked to hormones and nuclear localisation peptides in order to enhance their cell-specificity (Boffa *et al*., 2000) and nuclear translocation capabilities (Cutrona *et al*., 2000) respectively. More recently, anti-*c-myc* PNAs were loaded into albumin-encapsulated microbubbles for site-specific delivery with ultrasound exposure (He *et al*., 2016).

2.9.2 Clamp-forming oligonucleotides

The clamp-forming oligonucleotide (CFO) is a useful tool in antisense technology. It consists of two covalently linked ASOs in which one oligomer is designed to hybridise with a target mRNA sequence through conventional Watson-Crick base-pairing, while the other forms Hoogsteen base pairs. In this way the CFO surrounds the target sequence as a 'molecular clamp' (Figure 2.6), and this either prevents complete assembly of the translation machinery or physically obstructs elongation of the polypeptide chain (Stewart *et al*., 2001).

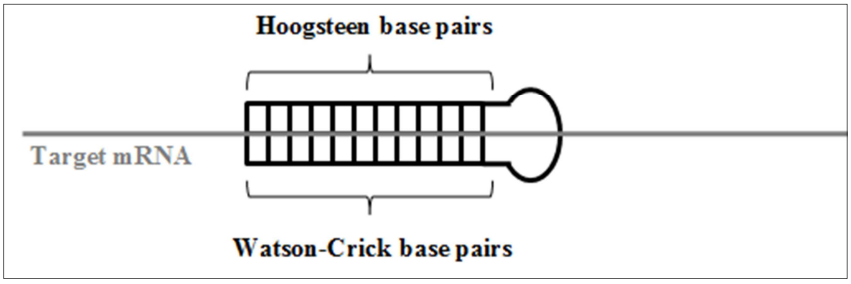

Figure 2.6: Clamp-forming oligonucleotide bound to a complementary sequence on its target mRNA. Redrawn and adapted from Hélène *et al*. (1997).

Stewart and colleagues (2001) designed PS-modified CFOs with complementarity to exons 2 and 3 of murine *c-myc* mRNA. These were modified with psoralen, to permit irreversible binding to the intended mRNA regions through the formation of crosslinks upon activation with ultraviolet light. Gel mobility shift assays and thermal denaturation studies highlighted the sequence-specific association of the ultraviolet-activated CFOs and *c-myc* mRNA. Treatment of B16-F0 murine melanoma cells with activated CFOs reduced *c-myc* expression and inhibited growth far more effectively than standard ASOs. For *in vivo* application, CFOs were modified with the DNA-intercalating agent, acridine, to facilitate strong binding with mRNA at the target regions. CFOs targeting different *c-myc* regions showed variable anti-tumor activity, with the most effective CFO inhibiting tumor growth by 77 % alone, and 82 % in combination with the anti-cancer drug, cisplatin (Stewart *et al*., 2002).

CFOs may also be employed as antigene agents. A recent *in vitro* experiment with human cells showed that CFOs designed with homology to the NHE III1 inhibited *c-myc* expression by stabilising the quadruplex structure of DNA at the target site and, as such, limited the activity of the *c-myc* promoter (Hao *et al*., 2016).

2.9.3 Triplex-forming oligonucleotides

The triplex-forming oligonucleotide (TFO) is a single-stranded oligonucleotide which binds, via Hoogsteen-type hydrogen bonds, to purine-rich sequences in the major groove of double stranded DNA (Jain *et al*., 2008). The use of TFOs as antigene agents exploits the fact that regulatory regions of most human genes, including *c-myc*, contain polypurine/polypyrimidine tracts and, that the formation of triple helices at these sites prevents the binding of protein factors required for transcription (McGuffie *et al*., 2000).

TFOs were designed to bind to several important control elements of the *c-myc* gene, however TFOs against the P2 promoter have proven most effective (Catapano *et al*., 2000). The performance of *c-myc*-specific TFOs has been enhanced through PS modification (Kim *et al*., 1998, McGuffie *et al*., 2000), complexation with diaminopropane to stabilise DNA triplexes (Thomas *et al*., 1995) and conjugation with the DNA-intercalating agents, acridine (Helm *et al*., 1993) and daunomycin (Carbone *et al*., 2004). The acridine-TFO conjugate was evaluated in human ovarian and cervical carcinoma cell lines, and exerted growth inhibitory effects at a lower concentration than the free TFO (Helm *et al*., 1993). Triple helices formed with the daunomycin-conjugated TFO showed greater stability than its unmodified counterpart. Association with a cationic lipid improved its intracellular accumulation and reduced transcription of *c-myc* by approximately 70 % (Carbone *et al*., 2004). In a related study, daunomycin-conjugated anti-*c-myc* TFOs inhibited growth, induced apoptosis and reduced clonogenic ability in prostate cancer cell lines without affecting the growth of normal cells (Napoli *et al*., 2006). Later, the conjugation of an anti-*c-myc* TFO to an ultrasmall gold nanoparticle, which facilitates intranuclear delivery, was shown to improve its efficacy in a breast cancer cell line (Huo *et al*., 2014).

In general, the TFO binds the purine-rich target strand either in parallel or anti-parallel orientation, depending on its nucleotide sequence (Figure 2.7). McGuffie and Catapano (2002) designed a GTC TFO that was able to simultaneously bind the P2 promoter in both orientations. This TFO formed a triplex at the target site with higher affinity than a conventional P2-targeted TFO, and proved effective at concentrations far lower than was reported for other TFOs (McGuffie and Catapano, 2002).

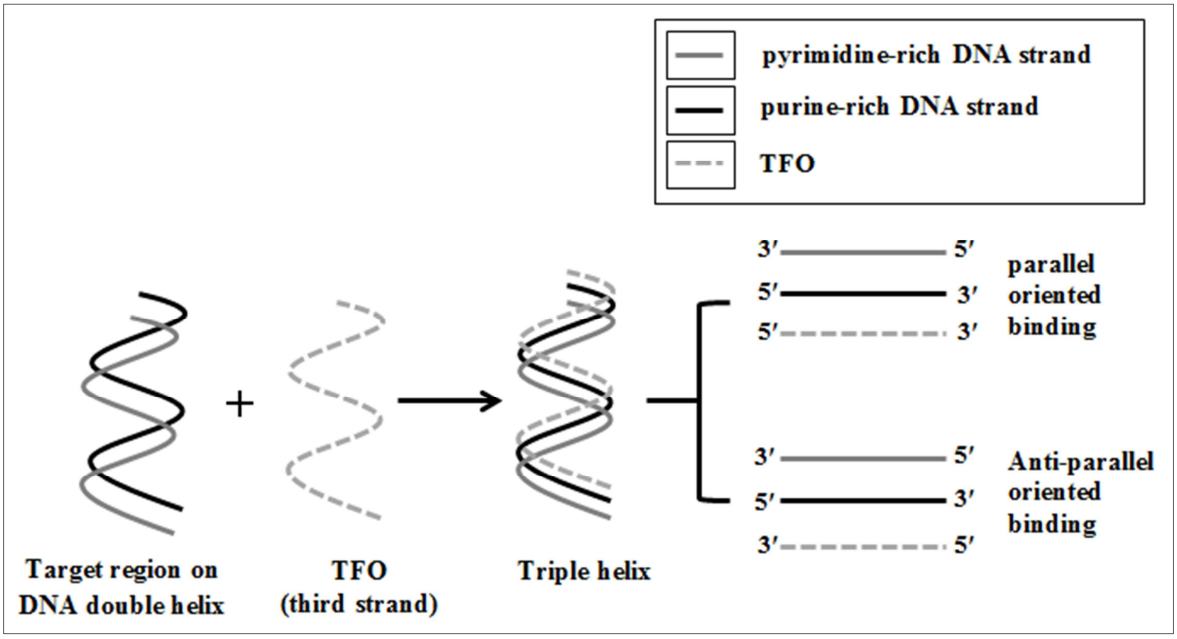

Figure 2.7: Interaction of a triplex-forming oligonucleotide (TFO) with the target region within the major groove of the DNA helix. The TFO may bind either in a parallel or anti-parallel orientation to the purine-rich strand. Redrawn and adapted from Buske *et al.* (2011).

In addition to their well-documented role as steric inhibitors of transcription, TFOs may direct site-specific damage to DNA, inducing replication-independent DNA repair synthesis. This property was exploited in order to augment the activity of an anti-cancer nucleoside analogue, gemcitabine, by increasing its incorporation within DNA at the P2 promoter. Treatment of metastatic breast cancer cells with a combination of a P2-targeted TFO and gemcitabine, reduced cell survival and anchorage-independent growth more effectively than either agent alone (Christensen *et al.*, 2006). This strategy was later shown to inhibit tumour growth in a mouse model of human colon cancer (Boulware *et al.*, 2014).

2.9.4 Decoy oligonucleotides

Decoy oligonucleotides are designed to bear resemblance to transcription factor recognition sequences in order to competitively prevent the transcription factor from binding to regulatory regions of its target genes (Mann and Dzau, 2000). A double-stranded DNA decoy based on the E-box consensus sequence (Figure 2.8) was evaluated in breast carcinoma and neuroblastoma cell lines. The DNA decoy reduced cell proliferation in a dose-dependent manner, when delivered using a cell-penetrating peptide (El-Andaloussi *et al.*, 2005).

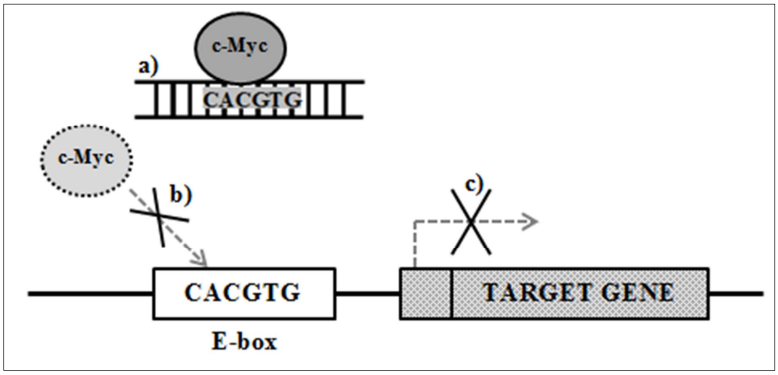

Figure 2.8: Inhibition of gene expression with aid of a decoy oligonucleotide. **a)** The decoy oligomer with transcription factor-binding motif sequesters the transcription factor, **b)** preventing it from binding regulatory regions of the DNA and, as such, **c)** prevents transcription of the target gene. Redrawn and adapted from Fichou and Férec (2006).

Besides competing with regular binding sites of the c-Myc protein, decoy oligonucleotides may be designed to sequester protein factors involved in aberrant transcription of the *c-myc* gene. Such an approach was reported by Seki *et al*. (2006) who designed an 18-mer DNA decoy which harbours a consensus sequence at which the T-cell factor (TCF) binds to the *c-myc* promoter. When introduced into human cell lines via lipid-based delivery the DNA decoy efficiently entered the nucleus, and remained within cells for 72-96 hours. Decoy-mediated inhibition of TCF activity reduced the expression of TCF downstream target genes including *c-myc* and, importantly, growth inhibitory effects were limited to cancer cells.

Simonsson and Henriksson (2002) suggested that a 22-mer guanine-rich DNA oligonucleotide, directed to the NHE III1 reduced *c-myc* expression partly through its decoy-like behavior. The synthetic oligonucleotide, like the sense strand at this site, is able to fold into a quadruplex. When delivered into *c-myc*-overexpressing cells, equilibrium is established between its single-stranded and quadruplex forms. In single-stranded form, the oligonucleotide functions as a TFO i.e. it hybridises with the cytosine-rich strand of the NHE III1 and blocks assembly of the RNA pol II complex. However, when folded as a quadruplex, it prevents promoter activity by serving as an alternative transcription factor-docking site.

More recently, Johari *et al*. (2017) demonstrated the potential for c-Myc decoy oligonucleotides to be used in differentiation therapy, a form of cancer treatment that relies on restoring cancer cells to the normal cell phenotype instead of inducing cancer cell death.

2.9.5 Ribozymes and deoxyribozymes

Catalytic DNA and RNA molecules have also been investigated as gene silencing agents. The hammerhead ribozyme, approximately 30 nucleotides in length, is the smallest naturally occurring self-splicing RNA molecule. The finding that a synthetic hammerhead RNA motif can be engineered to recognise and cleave an RNA sequence other than its own, led to its use in gene silencing experiments (Citti and Rainaldi, 2005). Cheng *et al*. (2000) synthesised a gene encoding a hammerhead ribozyme targeting *c-myc* mRNA, and this was inserted into a plasmid vector. Introduction of the vector by commercial lipid-based transfection into human liver cancer cells reduced *c-myc* expression and this was accompanied by growth inhibition.

Unlike ribozymes, catalytic DNA molecules i.e. deoxyribozymes, do not exist in nature and are identified through *in vitro* selection processes (Silverman, 2005). Deoxyribozymes are considered more favourable gene silencing agents than their RNA counterparts due to the greater biological stability inherent to DNA molecules (Tack *et al*., 2008). Sun *et al*. (1999) reported that an anti-*c-myc* 32-mer single-stranded DNA oligomer successfully cleaved *c-myc* mRNA, reduced c-Myc protein levels and inhibited proliferation of smooth muscle cells.

Thus far, attempts at enhancing the overall efficiency of anti-*c-myc* catalytic nucleic acids have focused on improving intracellular delivery through association with carrier agents (Hudson *et al*., 1996, Tack *et al*., 2008). Furthermore, studies with anti-*c-myc* ribozymes and deoxyribozymes have been confined to *in vitro* experiments.

2.9.6 Small interfering RNA (siRNA)

Small interfering RNA (siRNA) is a short double-stranded RNA (dsRNA) molecule with dinucleotide overhangs at the 3′ end (Figure 2.9). It is one of several classes of small RNA molecules that mediate the naturally occurring gene silencing mechanism known as RNA interference (RNAi). siRNA associates with a network of cytoplasmic proteins to form the RNA-induced silencing complex (RISC), in which it guides the degradation of mRNA bearing a complementary sequence (Pratt and MacRae, 2009).

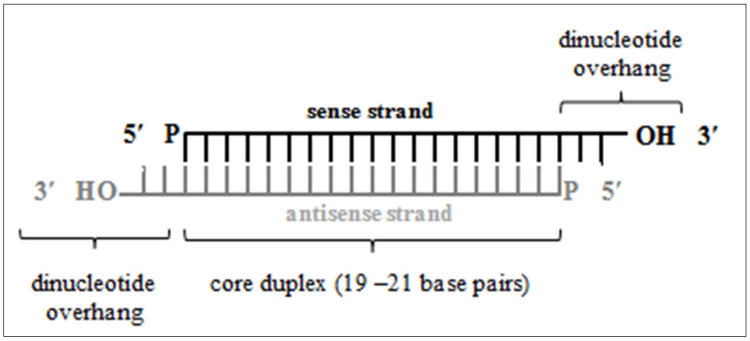

Figure 2.9: A representation of a siRNA molecule showing the core duplex and characteristic overhangs of two nucleotides at the 3′ end. Redrawn and adapted from DeVincenzo (2012).

In theory, effective silencing of any oncogene may be achieved using endogenous cellular machinery, provided that the appropriately designed siRNA molecule is successfully introduced (Aagaard and Rossi, 2007). This, together with evidence that siRNA is manifold more potent a gene silencing agent than antisense oligomers (Bertrand *et al*., 2002), has encouraged extensive research into developing siRNA as a viable treatment for cancer over the past decade (Zuckerman and Davis, 2015). In fact, the development of siRNA-based strategies for the purposes of *c-myc* inhibition has been described as a current '*active field of research*' (Whitfield *et al*., 2017). Therefore much attention has been given to RNAi and potential anti-*c-myc* siRNA approaches in this review.

2.9.6.1 RNA interference (RNAi)

The discovery of RNAi stems from reports, in the early 1990s, of endogenous gene silencing in plants and fungi with the introduction of transgenes and homologous RNA sequences respectively (Napoli *et al*., 1990, Romano and Macino, 1992). However, it was the Nobel Prize-winning work of Fire and Mellow which showed that gene silencing was initiated by dsRNA. Their work demonstrated that silencing of the *unc22* gene in *Caenorhabditis elegans* was many-fold more effective with the introduction of dsRNA than with either the sense or antisense strand alone; gene silencing relied homology between mRNA and the introduced dsRNA; the RNAi effect was hereditary and that the dsRNA worked non-stoichiometrically i.e. only a few molecules of dsRNA were necessary per cell to silence the gene (Fire *et al*., 1998). Further insight into the mechanism of RNAi came with the identification of the cleavage product of long

dsRNA namely, the siRNA molecule, as a key intermediate in the gene silencing process (Elbashir *et al*., 2001).

Long dsRNA can occur within cells as a result of viral invasion and replication, or due to hybridisation of repetitive sequences as in the case of transposons. In the initiation phase of the RNAi pathway, the dsRNA is recognised and cleaved by the RNase III endonuclease DICER in the cytoplasm to yield siRNA molecules (Bernstein *et al*., 2001).

The effector phase, outlined in Figure 2.10, begins when DICER collaborates with other proteins such as transactivating response (TAR) RNA-binding protein (TRBP), to associate the siRNA with the Argonaute 2 (Ago2) protein (Chendrimada *et al*., 2005). These proteins are the main constituents of RISC in humans (MacRae *et al*., 2008). Although the composition of RISC often varies between species, the presence of Argonaute (Ago) proteins is a common feature (Ambrus and Frolov, 2009).

Only one of the strands of the siRNA duplex remains associated with RISC, and serves as a guide strand that eventually specifies the mRNA target. This is the strand that is less thermodynamically stable at its 5′ end (Khvorova *et al*., 2003). Noland and coworkers (2011) proposed that, in humans, the DICER/TRBP dimer repositions the siRNA molecule along the helicase domain of DICER. This region senses thermodynamic stability of both strands of the siRNA duplex, and this possibly orientates the 3′ end of the guide strand towards the Piwi/Argonaute/Zwille (PAZ) domain of Ago2, which binds siRNA through specific recognition of the dinucleotide 3′ overhangs (Lingel *et al*., 2004, Yan *et al*., 2003). The siRNA duplex is unwound, and the second strand of the siRNA molecule, known as the passenger strand, is eliminated by the endonuclease activity of Ago2 during RISC activation (Rand *et al*., 2005). The guide strand directs the active RISC to the target region of mRNA through complementary base pairing interactions. Ago2 catalyses the hydrolysis of phosphodiester bonds of the guide strand-associated region of mRNA between nucleotides 10 and 11, relative to the 5′ end of the guide strand (Elbashir *et al*., 2001). The mRNA fragments are released from the protein complex and are broken down further by cytosolic nucleases, while the active RISC may act upon additional complementary mRNA transcripts (Rana, 2007).

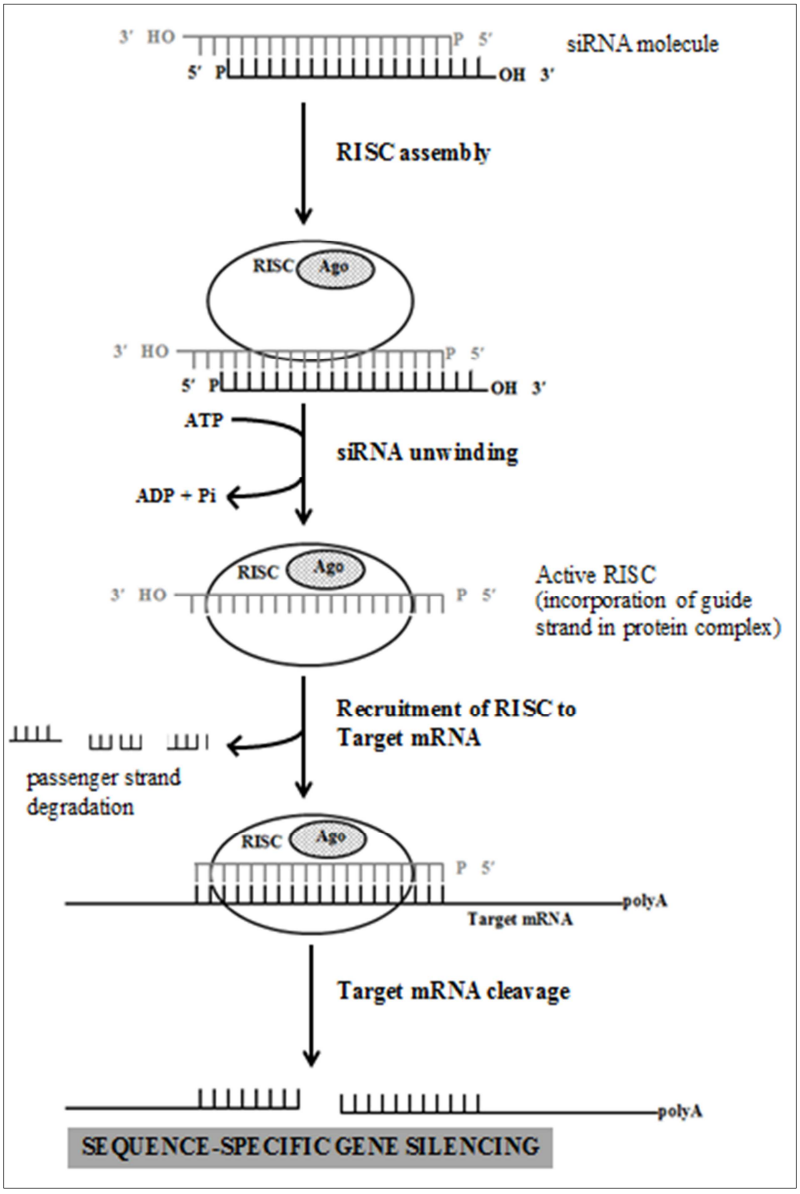

Figure 2.10: Schematic representation of the effector phase of RNAi mediated by siRNA molecules. Redrawn and adapted from Stevenson (2003).

In order for siRNA to be effective in silencing disease-causing genes, intact siRNA must successfully enter the cytoplasm of affected cells. In many instances, the most suitable mode of administering an siRNA treatment would involve injection into the bloodstream (Xu and Wang, 2015). However siRNA is highly susceptible to nuclease digestion (Cao and Ji, 2009). It has been reported that unmodified siRNA in serum has a half-life of 6 minutes (Soutschek *et al.*, 2004). Intravenously introduced siRNA molecules can accumulate in and be eliminated by the kidneys (Van de Water *et al.*, 2006). A further obstacle is that the siRNA molecule will not

simply diffuse across the cell membrane due to inherent physical features such as its size (approximately 14 kDa), hydrophilicity and negative charge (Xu and Wang, 2015).

Modifications of the siRNA molecule which include the introduction of PS linkages, O-methyl or fluoro groups were shown to extend longevity in serum (Braasch *et al*., 2003, Czauderna *et al*., 2003). Conjugation of small biomolecules such as cholesterol, cell-penetrating peptides and RNA aptamers to siRNA, improved pharmacokinetic behavior, intracellular delivery and tumour cell-specificity, respectively (Crombez *et al*., 2009, Soutschek *et al*., 2004, Zhou *et al*., 2008). However chemical alterations to the siRNA molecule can be time-consuming, costly and possibly compromise RNAi activity (Shim *et al*., 1998). For this reason much effort has been focused on the design of delivery agents for unmodified siRNA molecules which will mask its negative charge, protect its integrity, prevent its early removal from the body and facilitate cellular entry. In this regard nanodelivery systems have received much attention, many of which are based on the principle that siRNA can electrostatically associate with positively charged agents (Wang *et al*., 2010). While cationic polymers, co-polymers, dendrimers (Navarro *et al*., 2013) and peptides (Crombez *et al*., 2009) have been assessed, anti-*c-myc* siRNA delivery, like siRNA delivery in general, is predominantly lipid-based (Hope, 2014, Leung *et al*., 2014, Singh *et al*., 2015).

2.9.6.2 Anti-*c-myc* siRNA delivery

Arguably, the most famous lipid-based delivery agent is the liposome, the simplest of which is a self-assembled phospholipid bilayer that encircles an aqueous core in which a variety of molecules may be entrapped (Batzri and Korn, 1973). It is this carrying capability that was exploited for the delivery of several therapeutically important molecules including siRNA. A neutral liposome (Figure 2.11a) composed of dioleoylphosphatidylcholine (DOPC), Chol and distearoylphosphatidylethanolamine-poly(ethylene glycol) (DSPE-PEG) was used to encapsulate and deliver anti-*c-myc* siRNA *in vivo* (Reyes-González *et al*., 2015). Pegylation, the introduction of the PEG polymer, served to create a hydration shell around the liposome that sterically inhibits adverse interparticle associations which reduce nanoparticle longevity in the body (Suk *et al*., 2016). Systemic administration of the DOPC/Chol/DSPE-PEG/siRNA complex reduced the growth of ovarian cancer xenograft tumours, and did not inhibit the growth of cells with low *c-myc* expression (Reyes-González *et al*., 2015). Anti-*c-myc* siRNA delivered via pegylated

DOPC liposomes has also shown promise in the treatment of cisplatin-resistant tumours *in vivo* (Vivas-Mejia *et al*., 2018).

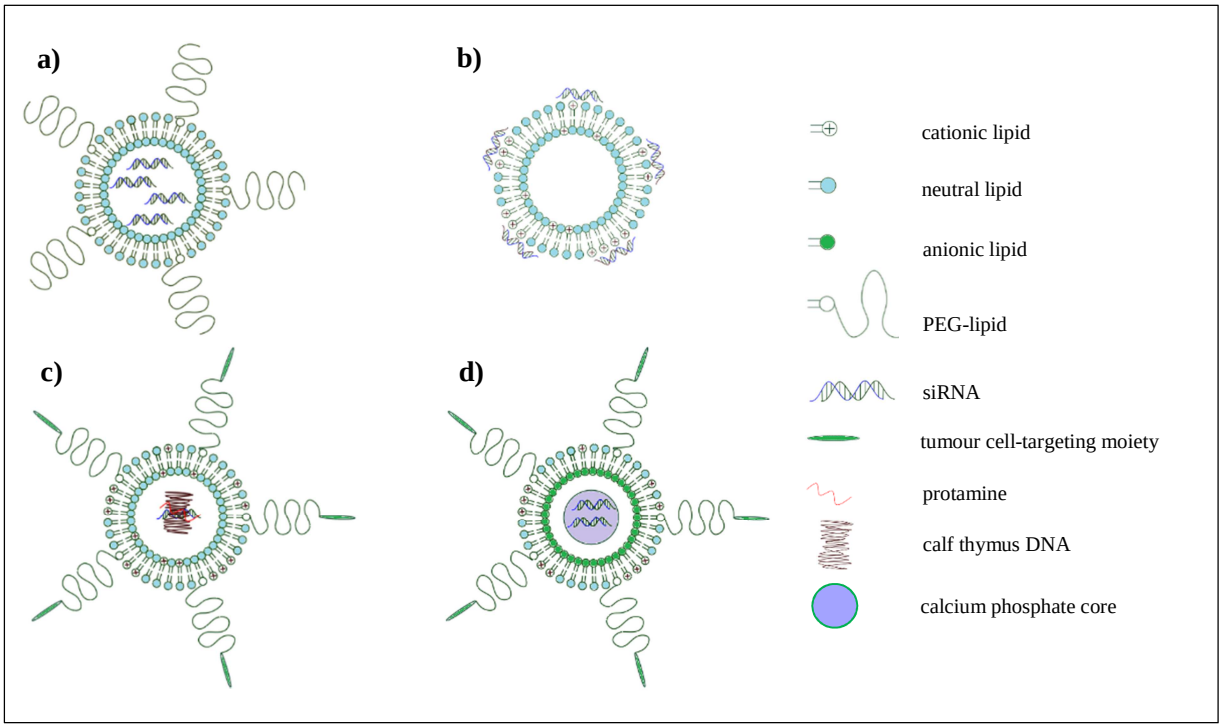

Figure 2.11: Lipid-based delivery agents for anti-*c-myc* siRNA **a)** pegylated, neutral liposome, **b)** cationic liposome, **c)** liposome-polycation-DNA (LPD) nanoparticle and **d)** lipid calcium phosphate (LCP) nanoparticle. Images were created using DesignSpark Mechanical 2.0 software.

Felgner *et al*. (1987) first reported that the hydration of a mixture containing a synthetic cationic lipid and zwitterionic phospholipid gave vesicles that bear a net positive charge, and paved the way for the use of cationic liposomes in nucleic acid delivery. Unlike neutral liposomes in which siRNA must be encapsulated, cationic liposomes electrostatically associate with siRNA to form nanostructures, known as lipoplexes (Khatri *et al*., 2014) (Figure 2.11b). Zhang *et al*. (2009) used the commercially available cationic liposomal reagent, Lipofectamine™ 2000, in association with anti-*c-myc* siRNA, to demonstrate the therapeutic value of siRNA-mediated *c-myc* inhibition in human colon cancer.

Besides being limited to use in cationic liposome formulations, cationic lipids have contributed to the development of more elaborate lipid nanoparticles. For example, Chen *et al*. (2010) used a traditional cationic liposome made up of 1,2-dioleoyl-3-trimethylammonium-propane (DOTAP) and Chol to envelope a core of protamine-bound anti-*c-myc* siRNA and calf thymus DNA. This

is known as a liposome-polycation-DNA (LPD) nanoparticle (Figure 2.11c). Surface modifications included post-inserted PEG chains for steric stabilisation, and a peptide directed to aminopeptidase N, that is overexpressed by cancer cells. Effective siRNA delivery, *c-myc* inhibition and tumour cell apoptosis was noted after these nanoparticles were intravenously administered in a xenograft model. Co-formulation of doxorubicin with siRNA in targeted LPD nanoparticles further improved treatment efficacy (Chen *et al*., 2010). Following the concept of stabilised core/shell lipid nano-assemblies, Zhang *et al*. (2013) used a DOTAP/Chol/PEG formulation as the outer coating of a calcium phosphate core containing anti-*c-myc* siRNA. The resulting lipid calcium phosphate (LCP) nanoparticle was directed to sigma receptor-positive tumour cells by attachment of anisamide to the distal ends of PEG chains (Figure 2.11d). Similar to the findings of Chen *et al*. (2010), co-encapsulation of anti-*c-myc* siRNA and a chemotherapeutic agent, in this case, gemcitabine, gave a more pronounced anti-cancer effect.

Physical agents may prove useful in promoting deposition of systemically introduced liposomal anti-*c-myc* siRNA nanoparticles in tumours. Yang *et al*. (2015) modified a tumour-targeted formulation of 3β[*N*-(*N′*,*N′*-dimethylaminoethane)-carbamoyl] cholesterol (DC-Chol), Chol and DSPE-PEG with a photolabile-caged cell-penetrating peptide to deliver anti-*c-myc* siRNA. The application of near-infrared light at the tumour site activated the cell-penetrating ability of the peptide to allow entry into cancer cells. Liposomes were also used as ultrasound cavitation agents for site-specific release of anti-*c-myc* siRNA conjugated to a cell-penetrating peptide (Xie *et al*., 2016). In both instances, treatment delayed tumour progression in fibrosarcoma xenograft models.

Anti-*c-myc* siRNA has been included in multi-targeted anti-cancer strategies, which involve the combined delivery of siRNAs against several genes implicated in cancer. Song *et al*. (2005) showed that a mixture of siRNAs against *c-myc*, *MDM2* and *VEGF* selectively inhibited tumour growth more effectively than the individual siRNAs. Li *et al*. (2008) co-encapsulated siRNA molecules against the same targets in a pegylated LPD nanocarrier for systemic administration in a murine model of metastatic lung cancer. This treatment simultaneously silenced all three genes in cancerous tissue, reduced metastasis by approximately 80 %, and extended survival time, with minimal toxicity. Similar results were obtained when siRNAs against the aforementioned oncogenes were pooled in pegylated LCP nanoparticles (Yang *et al*., 2011). Later, a mechanistic

study showed that this system impaired the growth of tumours in mice by simultaneously inhibiting cell proliferation and angiogenesis (Yang *et al*., 2012).

Besides delivery via synthetic lipid vesicles, siRNA can also be loaded in exosomes. Exosomes are vesicles that are naturally released by cells for the purposes of intercellular communication, and have come to represent an emerging nanocarrier system for a variety of medically relevant molecules (Ha *et al*., 2016). The potential for exosome-mediated anti-*c-myc* siRNA delivery was demonstrated by Lunavat *et al*. (2016). This group generated exosome-mimetic nanovesicles that successfully entered cells in culture and inhibited *c-myc* expression.

Other organic anti-*c-myc* nanodelivery systems reported are often complex polymer- and peptide-based nanocomposites. For example, Raichur *et al*. (2015) used a layer-by-layer approach to associate anti-*c-myc* siRNA with poly(lactic-co-glycolic acid) hollow nanoparticles. *In vitro* experiments showed that the nanoparticles were taken up by aggressive cancer cells and reduced *c-myc* expression with loss of cell viability. More recently, anti-*c-myc* siRNA has been incorporated in a multifunctional peptide assembly (Bjorge *et al*., 2017) and linked with packaging RNA prior to encapsulation in folate-conjugated, pegylated chitosan nanoparticles (Li *et al*., 2017).

It is also worth mentioning that the use of inorganic nanoparticles in siRNA delivery has been explored in recent years. These are often modified with organic components to improve surface properties and reduce toxicity (Chaudhary *et al*., 2014, Fraga *et al*., 2014, Zhou *et al*., 2009). Attachment of siRNA involves either covalent conjugation, or electrostatic association with positively charged groups introduced on the surface of the nanoparticle (Conde *et al*., 2012, Xia *et al*., 2018). Anti-*c-myc* siRNA carried by PEG- (McCully *et al*., 2015) and poly(ethylene imine)-functionalised (Shaat *et al*., 2016) gold nanoparticles was shown to reduce *c-myc* expression in human cervical and liver cancer cell lines, respectively. In separate *in vivo* experiments, gold nanoparticles modified with polymer shells (Kim *et al*., 2017b), glucose residues (Conde *et al*., 2015) and a RGD tumour-specific peptide (Conde *et al*., 2013) delivered anti-*c-myc* siRNA and suppressed the growth of lung tumours. Polymer-functionalised selenium (Huang *et al*., 2018) and graphene oxide (Imani *et al*., 2018) nanoparticles have also been introduced as potential carriers of anti-*c-myc* siRNA.

2.9.6.3 siRNA-directed transcriptional silencing

Further possibilities for the use of siRNA as tools for gene inhibition emerged from evidence that siRNA molecules homologous to regulatory regions of genes can cause gene silencing at the level of transcription. This phenomenon is known as siRNA-directed transcriptional silencing (RdTS) (Morris *et al*., 2004). The only report to date of RdTS applied to *c-myc* inhibition was presented by Napoli *et al*. (2009). siRNA molecules were designed with complementarity to DNA sequences at the major transcription start site. This achieved *c-myc* silencing in prostate cancer cells when introduced using a commercially available cationic liposome formulation. Importantly, oncogene inhibition was accompanied by anti-cancer effects which included loss of proliferative activity and clonogenic capability. It was shown that the promoter-targeted siRNA molecules formed a complex with non-coding promoter-associated RNA, which was initiated upstream of the transcription start site, and prevented the assembly of the pre-initiation complex in a mechanism that was dependent upon Ago2.

2.9.7 Dicer-substrate siRNA (DsiRNA)

The natural precursor of siRNA i.e. long dsRNA is not a suitable therapeutic agent because it is known to induce an immune response (Clemens, 1997). However, it was reported that short dsRNA molecules, lacking the dinucleotide overhangs that typify siRNA, of between 25 and 30 nucleotides in length, can induce RNAi with greater efficiency than siRNA (Kim *et al*., 2005). The blunt-ended RNA duplex is known as dicer-substrate siRNA (DsiRNA). A possible explanation for this observation was linked with the finding that the dsRNA-processing enzyme, DICER, participates in siRNA loading and RISC assembly. It was put forward that the blunt-ended duplexes were acted upon by the enzyme DICER to yield typical siRNA molecules and that this initial activity, which is unnecessary when pre-formed siRNA is introduced, renders DICER more efficient in its subsequent activities (Rose *et al*., 2005). However, in a more recent study, DsiRNA and conventional siRNA were found to act with comparable efficiency (Carneiro *et al*., 2015).

Like conventional siRNA, DsiRNA requires a vehicle for successful entry. Of significance to this discussion is the fact that pharmaceutical company, Dicerna, reported on a DsiRNA specific for the c-*myc* oncogene, DCR-MYC, delivered using a proprietary EnCore™ lipid nanoparticle. DCR-MYC in this delivery platform is the first, and only anti-*c-myc* RNAi system, to date, to

have reached clinical trials (Tolcher *et al*., 2015). Although the outcome of the initial trial was encouraging, a subsequent trial showed unsatisfactory knockdown efficiency and its development was discontinued (Whitfield *et al*., 2017).

2.9.8 Short hairpin RNA (shRNA)

Knockdown of *c-myc* expression can also be achieved through DNA-directed RNAi, a strategy which generates specific siRNA molecules *in vivo* (Ambesajir *et al*., 2012). This involves the construction of a RNA pol-driven plasmid expression vector into which an antigene sequence of at least 19 nucleotides is inserted, together with appropriate termination signals. When introduced into cells, the antigene sequence is transcribed in the nucleus as a stem-loop structure, which is essentially 2 complementary sequences, 19-22 ribonucleotides in length, linked by a short loop of 4-11 ribonucleotides. This is known as short hairpin RNA (shRNA). The shRNA is exported to the cytoplasm where it is processed by DICER into siRNA molecules and these associate with the RNAi machinery (Taxman *et al*., 2010).

Most experiments with anti-*c-myc* shRNA plasmids have involved their introduction into cells in culture with the aid of commercial cationic lipid transfection reagents. In one such study, plasmid-driven anti-*c-myc* shRNA silenced *c-myc* expression by as much as 80 %, reduced colony forming ability and promoted apoptosis in MCF-7 breast cancer cells (Wang *et al*., 2005). A similar plasmid system impaired proliferation, invasion and motility in the hepatocellular carcinoma cell line, HepG2 (Zhao *et al*., 2013). Hao *et al*. (2008) found that transfection of colon cancer cells with anti-*c-myc* shRNA plasmids not only reduced *c-myc* expression, but also that of the human telomerase reverse transcriptase gene (*hTERT*), which is under the transcriptional regulation of *c-myc*, and also contributes towards carcinogenesis when abnormally expressed.

As with siRNA, the effect of multigene silencing using shRNA expression plasmids was also explored. Song *et al*. (2011) engineered a single plasmid to direct the transcription of shRNAs against *c-myc*, *VEGF*, *hTERT*, and *BIRC5*, which encodes survivin. This produced a more effective anti-cancer effect than shRNA plasmids targeting individual oncogenes. Similarly, Tai *et al*. (2012) observed a synergistic anti-cancer effect, in colon cancer cells, when cells were co-transfected with two shRNA plasmids, each separately targeting *c-myc* and *VEGF*.

Thus far, only one *in vivo* experiment with anti-*c-myc* shRNA has been reported. In this study a poly(ethylene imine)-grafted polyglycidal methacrylate nanoparticle was used as a carrier of the shRNA expression vector. Anti-*c-myc* shRNA delivered in this manner showed anti-cancer activity in murine models of breast and colon cancer (Tangudu *et al*., 2015).

Although anti-*c-myc* shRNA approaches reported to date have primarily relied on RNAi, it is worth mentioning that an shRNA-based system, directed against the P2 promoter, induced transcriptional gene silencing of *c-myc* in hepatocellular carcinoma when delivered via a virosomal carrier (Zakaria *et al*., 2017).

2.10 Final comments

Synthetic nucleic acids designed to inhibit the expression of *c-myc* have, in many instances, induced potent anti-cancer effects *in vitro* and *in vivo*. To date, ASOs, PMOs and DsiRNA were evaluated as alternative cancer treatment in clinical trials, but did not progress further. Whitfield *et al*. (2017) mentioned, in a recent review, that several groups and companies are pursuing the idea of inhibiting *c-myc* at the level of translation as a means of designing a clinically viable anti-*c-myc* agent. Hence RNAi-based strategies are currently significant. Although longer lasting oncogene inhibition can be achieved with DNA-directed RNAi (Takahashi *et al*., 2009), mature siRNA molecules are easily synthesised, and pose fewer delivery concerns as they are of lower molecular weight and do not require genome integration (Wang *et al*., 2010, Xu and Wang, 2015). Hence, siRNA is considered more suitable for therapeutic use (Xu and Wang, 2015). Research to date has emphasised that the development of a siRNA-based approach is largely dependent upon the design of an appropriate nanodelivery system. Of all siRNA carriers explored thus far, the greatest body of knowledge has been generated in the field of lipid-based siRNA delivery, and this has led to the evaluation of several lipid-based RNAi complexes in clinical trials (Barata *et al*., 2016, Zatsepin *et al*., 2016).

Particle stabilisation with Chol and PEG have emerged as important features of lipid-based, anti-*c-myc* siRNA nanoparticles. In addition, most lipid-based nanoparticles reviewed were designed with cancer cell-targeting moieties. While these may render delivery to tumour cells more effective and possibly alleviate short-term effects of *c-myc* inhibition in normal cells, it may not be an entirely necessary feature. This is with reference to findings that presented the feasibility of

systemic *c-myc* inhibition with a non-discriminate *c-myc* inhibitor (Soucek *et al*., 2008) and, that systemic administration of anti-*c-myc* siRNA in non-targeted, pegylated liposomes did not inhibit the growth of cells with low c-Myc levels (Reyes-González *et al*., 2015). Passive targeting, that relies on optimising physical features of the lipid-based nanoparticle to exploit the enhanced permeability and retention effect, can also facilitate effective intratumoural delivery of siRNA (Torchilin, 2011, Maruyama, 2011). In fact, a major issue with the EnCore™ liposomal system, taken up in the clinical trial, was tumour penetration (Zatsepin *et al*., 2016). Furthermore, a passive targeting strategy may pave the way for less elaborate anti-*c-myc* siRNA lipid nanoparticles that can be more easily and economically produced (Deshpande *et al*., 2013). Hence, the current study is aimed at developing traditional cationic lipoplexes as simple but effective lipid-based anti-*c-myc* siRNA delivery agents.

CHAPTER 3 – MATERIALS AND METHODS

3.1 Materials

3.1.1 Liposome preparation and characterisation

DOPE and Chol were obtained from Sigma-Aldrich Chemical Co. (St. Louis, MO, USA). The 1,2-distearoyl-*sn*-glycero-3-phosphoethanolamine-*N*-[methoxy(polyethylene glycol)-2000] (DSPE-PEG_{2000}) was purchased from Avanti Polar Lipids (Albaster, AL, USA). The 2-[-(2-hydroxyethyl)-piperazinyl]-ethanesulphonic acid (HEPES) was from Merck (Darmstadt, Germany). Uranyl acetate solution (2 % $^{w}/_{v}$ in distilled water) and formvar-coated copper grids were supplied by the Microscopy and Microanalysis Unit in the School of Life Sciences (UKZN, Westville).

3.1.2 siRNA duplexes and resuspension

The following was purchased from Thermo Scientific Dharmacon Products (Lafayette, CO, USA): siGENOME non-targeting siRNA #1 (D-001210-01-20), ON-TARGETplus SMARTpool Human MYC (4609) siRNA (L-003282-02-0020), siCONTROL Tox siRNA (D-001500-01), 5× siRNA buffer (B-002000-UB-100, 0.3 M KCl, 30 mM HEPES, 1 mM $MgCl_2$, pH 7.5) and Molecular Grade RNase-free water (B-003000-WB-100). siGENOME non-targeting siRNA #1, with a recognition sequence of 5′-UAG CGA CUA AAC ACA UCA A-3′, has at least four mismatches to all known human, mouse and rat genes. ON-TARGETplus SMARTpool Human MYC (4609) siRNA is a mixture of four anti-*c-myc* siRNA duplexes (Table 3.1). ON-TARGETplus siRNA has a patented dual strand modification designed to reduce off-target effects, and favour RISC-loading of the antisense strand.

Table 3.1: Individual anti-*c-myc* siRNA duplexes in SMARTpool reagent.

Dharmacon code	Target sequence	Molecular weight (g/mol)	Extinction coefficient (L/mol.cm)
J-003282-23	5′-ACG GAA CUC UUG UGC GUA A-3′	13 429.8	371 130
J-003282-24	5′-GAA CAC ACA ACG UCU UGG A-3′	13 429.9	369 973
J-003282-25	5′-AAC GUU AGC UUC ACC AAC A-3′	13 414.9	374 334
J-003282-26	5′-CGA UGU UGU UUC UGU GGA A-3′	13 414.8	374 156

The sequence and physical properties of siCONTROL Tox siRNA are proprietary. The fluorescein isothiocyanate (FITC) labelled dsRNA oligomer (oligo), BLOCK-iT™ Fluorescent Oligo (2013), was obtained from Invitrogen (Carlsbad, CA, USA) as a 20 μM stock suspension in 100 mM KOAc, 30 mM HEPES-KOH, pH 7.4, and 2 mM MgOAc. The RNA duplex has the same length, charge and configuration as standard siRNA, and is designed for the assessment and optimisation of cationic lipid-mediated delivery. The sequence of BLOCK-iT™ Fluorescent Oligo is proprietary, and is not homologous to any known gene.

3.1.3 Liposome-siRNA interactions

Ultrapure™ agarose powder was obtained from Invitrogen (Carlsbad, CA, USA). The ethidium bromide (EtBr) solution (10 mg/ml) and tris(hydroxymethyl)-aminomethane hydrochloride (Tris-HCl) were purchased from Merck (Darmstadt, Germany). SYBR Green II RNA gel stain (10 000× concentrate in dimethylsulphoxide (DMSO)) was from Cambrex BioScience Rockland Inc. (Rockland, ME, USA). Ethylenediaminetetra acetic acid (EDTA) (disodium salt, dihydrate) was from Calbiochem (Darmstadt, Germany). Electrophoresis purity grade sodium dodecylsulphate (SDS) was purchased from Bio-Rad Laboratories (Richmond, CA). Xylene cyanol was supplied by SaarChem (Muldersdrift, SA). Sucrose and bromophenol blue were obtained from Sigma-Aldrich Chemical Co. (St. Louis, MO, USA). Foetal bovine serum (FBS) was sourced from HyClone UK Ltd. (Cramlington, Northumberland). All other chemicals and reagents were of analytical grade and ultrapure water (Direct-Q® 3 ultrapure water purification system, Millipore S.A.S., Molsheim, France) was used throughout.

3.1.4 Cell culture and *in vitro* assays

Human embryonic kidney 293 (HEK293) cells were supplied by the University of Witwatersrand, Medical School, South Africa. Michigan Cancer Foundation 7 (MCF-7) cells (ATCC® HTB-22™) and Human colorectal adenocarcinoma, HT-29, cells (ATCC® HTB-38™) were from the American Type Culture Collection (Manassas, VA, USA). Human colorectal adenocarcinoma, Caco-2, cells were purchased from Highveld Biologicals (PTY) Ltd. (Lyndhurst, South Africa). The following were obtained from Lonza BioWhittaker (Verviers, Belgium): sterile-filtered Eagle's Minimum Essential Medium (EMEM) with L-glutamine, trypsin-EDTA solution (200 mg/L EDTA, 170.000 U trypsin/L) and penicillin/streptomycin mixture (10 000 U/ml penicillin, 10 000 μg/ml streptomycin). Phosphate buffered saline (PBS)

tablets were purchased from Calbiochem (Darmstadt, Germany). Sterile DMSO was supplied by Highveld Biologicals (PTY) Ltd (Lyndhurst, South Africa). The alamarBlue® (AB) cell viability reagent was sourced from Invitrogen (Carlsbad, CA, USA). The 3-(4,5-dimethylthiazol-2-yl)-2,5-diphenyltetrazolium bromide (MTT) and Certistain® acridine orange (AO) zinc chloride double salt were purchased from Merck (Darmstadt, Germany). The 5× cell culture lysis reagent (25 mM Tris-phosphate, pH 7.8; 2 mM dithiothreitol; 2 mM 1,2-diaminocyclohexane-*N*-*N*-*N'*-*N'*-tetra-acetic acid; 10 % ($^{v}/_{v}$) glycerol; 1 % ($^{v}/_{v}$) Triton X-100) was supplied by Promega Corporation (Madison, WI, USA). The following was purchased from Sigma-Aldrich Chemical Co. (St. Louis, MO, USA): bicinchoninic acid (BCA) solution, copper (II) sulphate solution and the protein standard, bovine serum albumin (BSA) (1 mg BSA/ml in 0.15 M NaCl, 0.05 % NaN_3). Lipofectamine™ 3000 (LF3K) reagent was purchased from Invitrogen Life Technologies (Carlsbad, CA, USA). All sterile plasticware for tissue culture was obtained from Corning Inc. (Corning, NY, USA).

3.1.5 Gene expression assays

3.1.5.1 Reverse transcription quantitative real-time PCR (RT-qPCR)

The TRIzol® reagent (15596-026) was obtained from Life Technologies (Carlsbad, CA, USA). All reagents and consumables for RT-qPCR were purchased from Bio-Rad Laboratories (PTY) Ltd (Parkwood, Gauteng, South Africa). The iScript™ genomic DNA (gDNA) Clear complementary DNA (cDNA) Synthesis Kit (1725035) consisted of the following: a 5× reverse transcription (RT) supermix which contains Moloney murine leukemia virus reverse transcriptase, deoxyribonucleoside triphosphates (dNTPs), oligo deoxythymidine (dT), random primers and RNase inhibitor; a 5× no-RT control supermix which contains all aforementioned components except reverse transcriptase; deoxyribonuclease (DNase) I solution; DNase buffer solution; and nuclease-free water. The SsoAdvanced™ Universal SYBR® Green Supermix (1725272) was supplied as a 2× concentrated reagent containing antibody-mediated hot-start Sso7d fusion polymerase, dNTPs, $MgCl_2$, SYBR Green I dye, enhancers, stabilisers and passive reference dyes, including ROX and fluorescein. The following primers were supplied as 20× stock solutions: PrimePCR™ SYBR® Green Assay: MYC, Human (Unique Assay ID: qHsaCID0012921); PrimePCR™ SYBR® Green Assay: ACTB, Human (Unique Assay ID: qHsaCED0036269). The following single-stranded synthetic DNA templates were supplied as

20× stock solutions (20 × 10^6 copies/µl): PrimePCR™ Template for SYBR® Green Assay: MYC, Human; PrimePCR™ Template for SYBR® Green Assay: ACTB, Human. Hard-Shell® 96-well, low profile, semi-skirted polymerase chain reaction (PCR) plates with a clear shell and white wells (HSL9605), 0.2 ml PCR tube strips with domed caps (TBC1202) and Microseal® 'B' adhesive seals (MSB1001) were also purchased.

3.1.5.2 Enzyme-linked immunosorbent assay (ELISA)

Radioimmunoprecipitation assay (RIPA) buffer (50 mM Tris-HCl, pH 8.0, with 150 mM NaCl, 1.0 % Igepal CA-630 (NP-40), 0.5 % sodium deoxycholate, and 0.1 % SDS) and 3,3′,5,5′-Tetramethylbenzidine (TMB) liquid substrate were from Sigma-Aldrich (St. Louis, MO. USA). Na_2CO_3 and $NaHCO_3$ were from Merck (Darmstadt, Germany). The following was purchased from Bio-Rad Laboratories (PTY) Ltd (Parkwood, Gauteng, South Africa): 10× Tris-buffered saline (TBS); 10 % Tween 20, nonionic detergent; and blotting-grade blocker (non-fat dry milk). The following was from Life Technologies (Carlsbad, CA, USA): c-Myc epitope tag antibody 9E11 (AHO0052), a mouse monoclonal antibody raised against a synthetic peptide corresponding to amino acid residues 408-439 of the C-terminus of c-Myc; and goat anti-mouse IgG2A secondary antibody, horseradish peroxidase (HRP) conjugate (M32207). The β-actin antibody (8H10D10), a mouse monoclonal antibody raised against a synthetic peptide corresponding to the amino terminal residue of human β-actin, was purchased from Whitehead Scientific (PTY) Ltd. (Cape Town, South Africa).

3.2 Methods

3.2.1 Synthesis of MS09

MS09 was prepared from cholesterylformylhydrazide hemisuccinate (MS08) via an active ester intermediate (Figure 3.1), according to the published method (Singh and Ariatti, 2006).

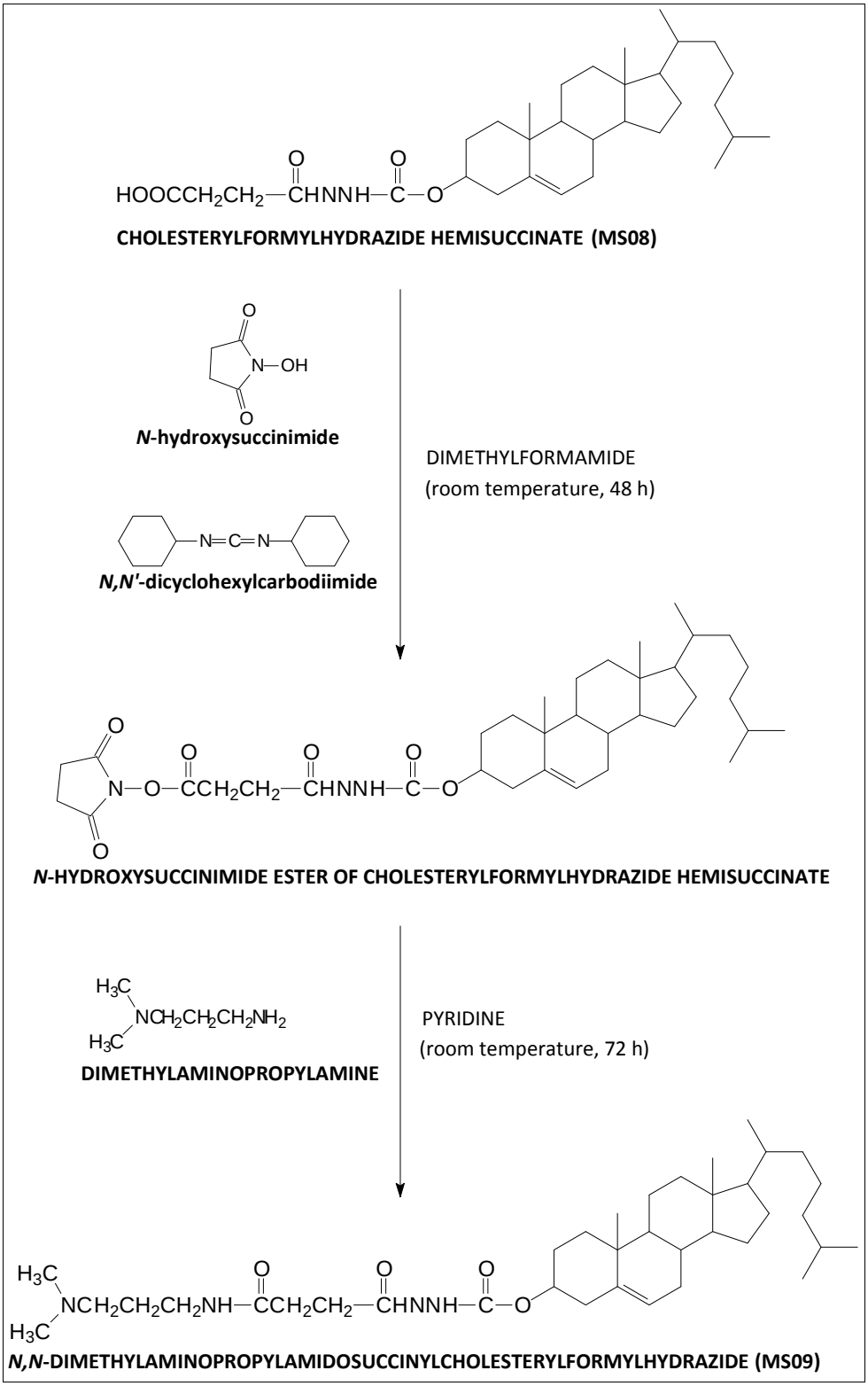

Figure 3.1: Scheme outlining the synthesis of MS09 from MS08 (redrawn and adapted from Singh and Ariatti (2006) using ChemWindow® 6.0, Bio-Rad Laboratories, Sadtler Division, Philadelphia, PA).

3.2.2 Liposome preparation

Liposomes were prepared by a method adapted from Gao and Huang (1991). Stock solutions (10 μg/μl in chloroform) of each lipid component were prepared. These were combined as shown in Table 3.2, and concentrated to a thin film *in vacuo* (Büchi Rotavapor-R rotary evaporator), with additional drying in a Büchi-TO pistol drier (200 mTorr, 25 ˚C, 2 h) to eliminate residual chloroform. The film was rehydrated (4 ˚C, 48 h) in sterile HEPES buffered saline (HBS, 20 mM HEPES, 150 mM NaCl, pH 7.5; 0.5 ml). The suspension was vortexed (2 min) and, thereafter, sonicated (25 ˚C, 10 min) in an Elma, Transsonic (T460/H) bath-type sonicator (Singen, Germany) operating at 35 kHz. Liposome preparations were stored at 4 ˚C, and were sonicated (25 ˚C, 5 min) prior to use.

Table 3.2: Composition of pegylated and non-pegylated cationic liposomes

Liposome	Lipid components (µmol/ 0.5 ml liposome suspension)				Cytofectin concentration			Total lipid concentration		
	MS09	DOPE	Chol	DSPE-PEG_{2000}	µmol/ml	µg/µl	mM	µmol/ml	µg/µl	mM
MS09/DOPE	2	2	-	-	4	2.52	4.00	8.00	5.50	8.00
MS09/Chol (1:1)[a]	2	-	2	-	4	2.52	4.00	8.00	4.06	8.00
MS09/Chol (1:2)[a]	1.33	-	2.67	-	2.66	1.68	2.66	8.00	3.74	8.00
MS09/Chol (1:3)[a]	1	-	3	-	2	1.26	2.00	8.00	3.58	8.00
MS09/DOPE/PEG	1.96	1.96	-	0.08	3.92	2.46	3.92	8.00	5.82	8.00
MS09/Chol/PEG (1:1)[a]	1.96	-	1.96	0.08	3.92	2.46	3.92	8.00	4.42	8.00
MS09/Chol/PEG (1:2)[a]	1.3	-	2.6	0.08	2.6	1.64	2.6	8.00	4.12	8.00
MS09/Chol/PEG (1:3)[a]	0.98	-	2.94	0.08	1.96	1.24	1.96	8.00	3.98	8.00

Note: [a]The ratio in brackets represents the ratio of MS09 to Chol on a molar basis

3.2.3 Characterisation of liposomes

3.2.3.1 Cryogenic transmission electron microscopy (cryo-TEM) of liposomes

Liposome suspensions were diluted (1:15) in HBS, and aliquots (1 µl) were placed on formvar-coated copper grids. Samples were stained with uranyl acetate (1 µl) and allowed to stand at room temperature for 2 min. Excess liquid was removed using filter paper. Samples were flash-frozen by plunging into liquid propane (-170 ˚C), cooled by liquid nitrogen, using a spring-loaded Leica EM CPC cryopreparation system (Leica Microsystems, Vienna, Austria). Grids were immediately transferred to a Gatan cryo-transfer holder (Gatan Inc., Pleasanton, CA, US). Samples were viewed with a JEOL JEM.1010 transmission electron microscope (JEOL Ltd., Tokyo, Japan) at an accelerating voltage of 100 kV, without warming above -150 ˚C. Images were captured using an Olympus MegaView III digital camera in conjunction with SIS iTEM Universal Imaging Platform software (Shinjuku, Japan).

3.2.3.2 Zeta Potential Nanoparticle Tracking Analysis (Z-NTA)

Particle size, zeta (ζ) potential and concentration of liposomes were simultaneously determined using the NanoSight NS500 system fitted with a ZetaSight™ (Malvern Instruments, Worcestershire, UK) module. Liposome suspensions were diluted in a filter-sterilised buffer containing 0.2 mM HEPES, 1.5 mM NaCl, pH 7.5 in accordance with instrument sensitivity limits. Dilutions were as follows: MS09/DOPE, MS09/Chol (1:1), MS09/DOPE/PEG and MS09/Chol/PEG (1:1), 1:7000; MS09/Chol (1:2) and MS09/Chol (1:3), 1:200; MS09/Chol/PEG (1:2) and MS09/Chol/PEG (1:3), 1:300. Samples (1 ml) were introduced into the viewing chamber of the instrument using the on-board sample pump. Particles were visualised with a focused laser beam (405 nm, 60 mW) and the on-board sCMOS camera. Two videos of particle motion were recorded, with the NTA 3.0 build 69 software (Malvern Instruments, Worcestershire, UK), at each of 5 pre-set measurement positions within the chamber upon the application of 10 V, under both positive and negative polarity. Capture duration was set at 60 s for position 1, and at 30 s for positions 2-5. Temperature was maintained at 25 ˚C during measurements. In all instances, sample viscosity of 0.9 cP and a dielectric constant of 80.0 was assumed. Post-capture, the software corrected for electro-osmotic and thermal effects, and calculated zeta potential from individual particle velocities by applying the Henry equation with Smoluchowski approximation. Hydrodynamic diameters were simultaneously calculated from particle tracks using Stokes-Einstein equation. Particle

concentrations were estimated based on the number of particles in the field of view in relation to the scattering volume. The system was flushed with ultrapure water before loading each sample. The quality of the ultrapure water was routinely monitored to confirm the absence of contaminants. Three independent measurements were performed per sample so as to ensure that properties of the sample were not perturbed by electric field cycles of the previous run, and data was presented as the average of the three experiments. Modal size and zeta potential values are given in Chapter 4, section 4.3. Concentrations were reported as follows:

$$\text{Concentration (particles/ml)} = \text{concentration}_{\text{NTA 3.0 build 69}} \times \text{dilution factor}$$

Concentrations were used to estimate the average number of lipid molecules per liposomal vesicle as follows:

$$\text{Average number of lipid molecules/vesicle} = \frac{\text{number of lipid molecules}^{a}\text{/ml}}{\text{average number of vesicles/ml}}$$

[a]Calculated from the total lipid concentration of liposome suspensions (Table 3.2) and Avogrado's constant.

Calculations assumed the absence of particulate contaminants, and estimates are given in Appendix B, Table B1. A sample calculation is given in Appendix C. Note that estimates were made only in the case of stable formulations.

A summary of all other Z-NTA generated data (Tables B2 and B3) together with selected flow profiles, and plots of zeta potential and size *vs*. concentration is presented in Appendix B.

3.2.4 Resuspension of siRNA

The siRNA was resuspended as per manufacturer's instruction. Briefly, siRNA was deposited as a pellet by centrifuging (90 × *g*, 4 ˚C, 60 s) in an Eppendorf 5424 R instrument (Merck, Darmstadt, Germany). The pellet was resuspended by adding 1× siRNA buffer (60 mM KCl, 6 mM HEPES, 0.2 mM $MgCl_2$, pH 7.5; 1 ml) followed by agitation (room temperature, 30 min) on a platform shaker (Stuart Scientific STR6, Surrey, UK) operating at 50 revolutions per minute (rpm), to obtain a final siRNA concentration of 20 μM (0.268 μg/μl, 20 pmol/μl). siRNA stock suspensions were dispensed into RNase-free tubes in aliquots (50 μl) and stored at -80 ˚C (NuAire -86 ˚C Ultralow Freezer, Lasec Laboratory and Scientific Equipment Co.).

3.2.5 Liposome-siRNA binding studies

After characterising all eight liposome suspensions, the following four formulations were investigated further: MS09/DOPE, MS09/Chol (1:1), MS09/DOPE/PEG, and MS09/Chol/PEG (1:1).

3.2.5.1 Gel retardation assays

3.2.5.1.1 Lipoplex assembly

Lipoplexes were assembled at MS09:siRNA ($^{w}/_{w}$) ratios ranging from 4:1 to 28:1 (for the MS09/DOPE formulation) and 8:1 to 32:1 (for all other formulations) in increments of 4. The corresponding N/P ($^{+}/_{-}$) charge ratios were calculated based on the assumption that MS09, with molecular weight of 629 g/mol, carries one positive charge per molecule at physiological pH; while an RNA nucleotide has an average molecular weight of 340 g/mol and carries one negative charge (a sample calculation is given in Appendix C). Varying amounts of liposome were added to a fixed quantity of siGENOME non-targeting siRNA (0.3 μg, 22.5 pmol) to correspond with the aforementioned ratios. Volumes were adjusted to 10 μl with HBS. After brief vortexing (30 s), mixtures were allowed to stand at room temperature for 30 min to permit the formation and maturation of electrostatic complexes. The set-up for the preparation of individual liposome-siRNA complexes is given in Appendix D, Tables D1-D4.

3.2.5.1.2 Preparation of 2 % agarose gels

Agarose powder (0.4 g) was dissolved in water (18 ml) with heating to boiling point. This was cooled to 75 ˚C, and 10× electrophoresis buffer (0.36 M Tris-HCl, 0.3 M NaH_2PO_4, 0.1 M EDTA, pH 7.5; 2 ml) was added. The mixture was poured into a gel casting tray fitted with an eight-well comb (Bio-Rad, Richmond, CA) and allowed to set (room temperature, 40 min).

3.2.5.1.3 Agarose gel electrophoresis

Lipoplexes (10 μl in HBS) were mixed with gel loading buffer (40 % sucrose, 0.25 % xylene cyanol, 0.25 % bromophenol blue; 2.5 μl) and samples (10 μl) were loaded onto 2 % agarose gels. Electrophoresis was carried out for 30 min in a Mini-Sub® Cell GT electrophoresis cell (Bio-Rad, Richmond, CA) containing Tris-phosphate-EDTA (TPE) running buffer (36 mM Tris-HCl, 30 mM NaH_2PO_4, 10 mM EDTA, pH 7.5), using a PowerPac™ Basic power supply unit (Bio-Rad, Richmond, CA) operating at 50 V. Gels were stained with EtBr solution (0.1 μg/ml in

water) for 30 min with gentle agitation (10 rpm, room temperature) on a platform shaker (Stuart Scientific STR6, Surrey, UK). Gels were viewed under ultraviolet transillumination (300 nm) in a Vacutec Syngene G:Box (Syngene, Cambridge, UK) gel documentation system. Images were captured with GeneSnap software, version 7.05.02 (Syngene, Cambridge, UK) following exposure time of 1 s. Densitometric analysis was performed with GeneTools software, version 4.00.00 (Syngene, Cambridge, UK). Bands of siRNA that migrated within the gel represent unbound siRNA. The fluorescence intensities of these bands were expressed as a percentage of the intensity of naked siRNA (0.3 μg, 22.5 pmol) that was loaded in lane 1 of each gel. Hence, the amount of liposome-associated siRNA at each MS09:siRNA ($^{w}/_{w}$) ratio was determined as follows:

$$\%\ \text{bound siRNA} = 100 - \%\ \text{free siRNA}$$

3.2.5.2 Dye displacement assays

3.2.5.2.1 EtBr displacement assay

EtBr (0.4 μg) was added to HBS (200 μl) in 96-well flat-bottom black polystyrene plates. Baseline fluorescence (0 %) was established upon measuring the fluorescence intensity of this solution in a GloMax® Multi+ Detection System (Promega Biosystems, Sunnyvale, CA, USA) using Instinct software, at excitation and emission wavelengths of 525 nm and 600 nm, respectively. siGENOME non-targeting siRNA (1.0 μg, 75 pmol) was introduced, and fluorescence intensity at this point was taken to represent 100 % relative fluorescence. Undiluted liposome suspension was added, stepwise, in 1 μl aliquots, solutions thoroughly mixed after each addition, and allowed to equilibrate in the dark, at room temperature for 4 min before readings were taken. The total volume of liposome suspension introduced was limited to 11 μl, which was approximately 5 % of the initial EtBr-siRNA-HBS mixture by volume, so as to minimise dilution effects. The percentage relative fluorescence upon each addition of liposome was plotted as a function of micrograms of cytofectin.

3.2.5.2.2 SYBR Green displacement assay

The experiment outlined in 3.2.5.2.1 was repeated using SYBR Green II as the RNA-intercalating dye (Dorasamy *et al.*, 2009). The SYBR Green II stock solution was diluted (1:10 000) in HBS, and 202 μl was used to establish baseline fluorescence. Fluorescence intensities upon introduction of siGENOME non-targeting siRNA and liposome were measured

at excitation and emission wavelengths of 497 nm and 520 nm, respectively, and results were reported as described in section 3.2.5.2.1 above.

3.2.5.2.3 Effect of increasing NaCl concentration on liposome-siRNA interactions

The SYBR Green displacement assay was adapted to investigate the strength of liposome-siRNA interactions as follows: Lipoplex suspensions (20 µl in HBS) were assembled with siGENOME non-targeting siRNA (1.0 µg, 75 pmol) and liposome at MS09:siRNA ($^{w}/_{w}$) ratios at which individual formulations attained points of inflection by dye displacement. The fluorescence of SYBR Green II (1:10 000 in HBS; 200 µl) was recorded before and after the addition of lipoplexes (20 µl). Changes in fluorescence were monitored upon addition of 5 M NaCl, stepwise, in aliquots (1 µl). In this way a final NaCl concentration range of 150-400 mM, in increments of 20 mM, was explored. NaCl concentration was not raised beyond 400 mM so as to avoid significant dilution effects with further addition of the NaCl solution. Baseline fluorescence was accounted for, and results were reported as the percentage increase in fluorescence relative to the initial SYBR Green II-lipoplex mixture.

3.2.6 Characterisation of lipoplexes

3.2.6.1 Cryo-TEM

Lipoplexes (10 µl in HBS) were prepared from liposome stock suspensions (1 µl), and siCONTROL Tox siRNA at MS09:siRNA ($^{w}/_{w}$) ratios ranging from 12:1 to 32:1. After incubation (room temperature, 30 min) reaction mixtures were diluted to 20 µl in HBS. Aliquots (1 µl) were cryopreserved and viewed as described for liposomes in 3.2.3.1.

3.2.6.2 Z-NTA

Lipoplexes (10 µl in HBS) were prepared from liposome stock suspensions (1 µl), and siCONTROL Tox siRNA at MS09:siRNA ($^{w}/_{w}$) ratios ranging from 12:1 to 32:1. After incubation (room temperature, 30 min) reaction mixtures were diluted (1:700) in sterile buffer containing 0.2 mM HEPES, 1.5 mM NaCl, pH 7.5, to give particle numbers appropriate to the sensitivity limits of the NS500 system. Videos of particle motion were captured, and data analysis was carried out as described for liposome suspensions in 3.2.3.2.

Particle concentrations were used to estimate the average number of vesicles and siRNA molecules that constitute a single liposome-siRNA nanocomplex, of a given lipoplex suspension, as follows:

1. Average number of vesicles/nanocomplex

$$= \frac{\text{average number of vesicles in 1 µl liposome stock suspension}}{\text{average number of particles/10 µl Lipoplex suspension}^{a}}$$

2. Average number of siRNA molecules/nanocomplex

$$= \frac{\text{number of siRNA molecules}^{b}\text{/10 µl lipoplex suspension}}{\text{average number of particles/10 µl Lipoplex suspension}^{a}}$$

[a]The dilution factor was taken into account.
[b]Calculated from average molar mass of siRNA and Avogrado's constant.

Average estimates of the number of siRNA molecules per nanocomplex were only made in the case of lipoplexes assembled above points which gave maximum dye displacement. At these MS09:siRNA ($^{w}/_{w}$) ratios, it was accepted that lipoplexes were fully formed (Hattori *et al.*, 2013) and all siRNA molecules were taken to be liposome-associated. The absence of contaminants was assumed in all instances. Sample calculations are given in Appendix C, and estimated values are shown in Appendix B, Table B4.

3.2.7 Assessment of batch-to-batch variation

Three independent preparations of each of the MS09/DOPE, MS09/Chol (1:1), MS09/DOPE/PEG and MS09/Chol/PEG (1:1) formulations were made as described in 3.2.2. These were subjected to Z-NTA characterisation and the SYBR Green dye displacement assay as detailed in 3.2.3.2 and 3.2.5.2.2, respectively.

3.2.8 Liposome storage stability studies

Freshly prepared liposome suspensions, MS09/DOPE, MS09/Chol (1:1), MS09/DOPE/PEG and MS09/Chol/PEG (1:1), were characterised by Z-NTA and the SYBR Green dye displacement assay as per protocols given in 3.2.3.2 and 3.2.5.2.2, respectively. The suspensions were stored at 4 ˚C, and the aforementioned experiments were repeated after 5 and 10 months.

3.2.9 Nuclease protection assays

Lipoplexes (10 µl in HBS), each containing siGENOME non-targeting siRNA (0.3 µg, 22.5 pmol), were assembled at MS09:siRNA ($^{w}/_{w}$) ratios of 12:1-32:1. (The corresponding N/P ($^{+}/_{-}$) ratios were between 6.5 and 17.3). These were incubated (37 ˚C, 4 h) with FBS at a final concentration of 10 % ($^{v}/_{v}$). As a control, naked siRNA (0.3 µg, 22.5 pmol) was treated in the same way. Nuclease activity was terminated by the addition of EDTA at a final concentration of 10 mM. Complexes were destabilised by heating (55 ˚C, 25 min) with SDS at a final concentration of 0.5 % ($^{w}/_{v}$). Reaction mixtures were cooled to room temperature and gel loading buffer (3.5 µl) was added. A detailed account of sample preparation and treatment is presented in Appendix D, Tables D5-D8. Samples (10 µl) were subjected to electrophoresis on 2 % agarose gels, followed by densitometry, as described in section 3.2.5.1.3. The siRNA bands that migrated within the gel represent intact siRNA. The fluorescence intensities of these bands were expressed as a percentage of that of untreated siRNA (0.3 µg, 22.5 pmol).

3.2.10 Cell culture and maintenance

3.2.10.1 Reconstitution

Cells in cryogenic ampoules were removed from the biofreezer and placed in a water bath (37 ˚C, 5 min) to thaw. All work pertaining to cell culture was conducted in a class II biological safety cabinet. Cells were transferred into sterile centrifuge tubes and centrifuged (1000 × *g*, 25 ˚C, 3 min) in an Eppendorf 5702 R instrument. The supernatant was discarded and the pellet resuspended in 1 ml growth medium (EMEM supplemented with 10 % ($^{v}/_{v}$) FBS, 100 U/ml penicillin, and 100 µg/ml streptomycin), which was used for cell propagation and *in vitro* experiments throughout the study, unless otherwise specified. Cells were introduced into 25 cm^2 cell culture flasks containing growth medium (4 ml) and maintained at 37 ˚C in a humidified atmosphere with 5 % CO_2 (Steri-Cult CO_2 incubator with class 100 HEPA filtration, Thermo Electron Corporation).

3.2.10.2 Change of medium

Medium was replaced within 24 h of reconstitution, to eliminate residual DMSO and non-adherent cells. Spent medium was discarded and cells were rinsed with PBS (10 mM phosphate buffer, pH 7.4, 140 mM NaCl, 3 mM KCl; 2 ml). Fresh medium (5 ml) was introduced and cells

were returned to the incubator (37 ˚C). Cell growth was monitored on a daily basis using a Nikon TMS inverted microscope (Nikon Instruments, Tokyo, Japan). Any changes in the colour of the growth medium were also noted. Medium was changed every 24-48 h in accordance with these observations. Images of the cells were captured at 200× magnification using an inverted fluorescence microscope (CKX41, Olympus, Japan) operating in bright field mode, in conjunction with Analysis Five Software (Olympus Soft Imaging Solutions, Olympus, Japan).

3.2.10.3 Trypsinisation

Once cells had reached semi-confluency, spent medium was decanted and cells were rinsed with PBS (2 ml). Trypsin-EDTA solution (1 ml) was introduced, and cells were maintained at 37 ˚C for 1-5 min, depending on the cell type. Changes in cell morphology were monitored under the inverted microscope. When cells had rounded-off, medium (2.5 ml) was added to halt further enzyme activity. Cells were dislodged from the surface of the culture vessel with gentle tapping. The contents of the flask were drawn-up and expelled using a sterile pipette, so as to ensure an even distribution of cells in the medium, before being either seeded into multi-well plates for *in vitro* assays, divided among two or more flasks for further propagation, or cryopreserved.

3.2.10.4 Cryopreservation

Cells were trypsinised as described in 3.2.10.3 and recovered as a pellet after centrifugation (1000 × *g*, 25 ˚C, 2 min) in an Eppendorf 5702 R instrument. The pellet was resuspended in medium (1 ml) containing 10 % ($^{v}/_{v}$) DMSO and transferred into cryovials. These were cooled at a rate of -1 ˚C/min in a Nalgene™ Cryo 1 ˚C freezing container (Thermo Fisher Scientific, Waltham, Massachusetts, US) filled with 100 % isopropyl alcohol until a temperature of – 80 °C was attained. Cells were stored in a NuAire -86 ˚C Ultralow Freezer (Lasec Laboratory and Scientific Equipment Co.) for short term storage.

3.2.11 Transfection

3.2.11.1 Transfection with MS09 liposomes

For experiments in 48-well plates, cells were seeded at densities of approximately 4×10^4 cells/well. These were maintained at 37 ˚C for 24 h in order to reach semi-confluency. The initial transfection experiments were conducted within a broad final siRNA concentration

range (57–14 nM). siRNA (0.2 μg per 48-well format) was used as an arbitrary starting point. This amount was sequentially halved.

Lipoplexes were assembled 30 min prior to their introduction to the cells. Transfecting complexes contained 0.2 μg (15 pmol), 0.1 μg (7.5 pmol) or 0.05 μg (3.7 pmol) siRNA and appropriate amounts of liposome to give lipoplexes at MS09:siRNA ($^{w}/_{w}$) ratios of 12:1–32:1. Volumes were adjusted to 10 μl with HBS. In theory, lipoplex suspensions were formulated at siRNA concentrations of 1.5 μM, 0.75 μM and 0.37 μM so as to give final concentrations of 57 nM, 29 nM and 14 nM, respectively, assuming no loss due to pipetting errors (refer to Appendix C for calculations). The corresponding theoretical cytofectin and total lipid concentrations to which cells were exposed are presented in Table 3.3 (a sample calculation is given in Appendix C).

Cells were prepared by draining the wells and adding fresh medium (0.25 ml/well). Lipoplexes (10 μl) were added and cells were incubated at 37 ˚C until assay-specific end-points. Quantities were adjusted, as shown in Table 3.4, for experiments in a 96-well format.

Table 3.3: Final cytofectin and lipid concentrations introduced to cells in transfection experiments

Liposome formulation	Lipid:siRNA ($^{w}/_{w}$)	MS09:siRNA ($^{w}/_{w}$)	N/P ($^{+}/_{-}$)	57 nM siRNA		29 nM siRNA		14 nM siRNA	
				[MS09] (μM)	[Total lipid] (μM)	[MS09] (μM)	[Total lipid] (μM)	[MS09] (μM)	[Total lipid] (μM)
MS09/DOPE	26.2:1	12:1	6.5:1	14.7	29.3	7.4	14.7	3.7	7.3
	34.9:1	16:1	8.7:1	19.6	39.1	9.8	19.6	4.9	9.8
	43.7:1	20:1	10.8:1	24.5	48.8	12.3	24.4	6.2	12.2
	52.4:1	24:1	13.0:1	29.4	58.6	14.7	29.3	7.4	14.7
	61.1:1	28:1	15.1:1	34.2	68.4	17.1	34.2	8.6	17.1
	69.8:1	32:1	17.3:1	39.1	78.1	19.6	39.1	9.8	19.5
MS09/Chol (1:1)	19.3:1	12:1	6.5:1	14.7	29.3	7.4	14.7	3.7	7.3
	25.8:1	16:1	8.7:1	19.6	39.1	9.8	19.6	4.9	9.8
	32.2:1	20:1	10.8:1	24.5	48.8	12.3	24.4	6.2	12.2
	38.7:1	24:1	13.0:1	29.4	58.6	14.7	29.3	7.4	14.7
	45.1:1	28:1	15.1:1	34.2	68.4	17.1	34.2	8.6	17.1
	51.6:1	32:1	17.3:1	39.1	78.1	19.6	39.1	9.8	19.5
MS09/DOPE/PEG	28.4:1	12:1	6.5:1	14.7	30.0	7.4	15.0	3.7	7.5
	37.9:1	16:1	8.7:1	19.6	40.0	9.8	20.0	4.9	10.0
	47.3:1	20:1	10.8:1	24.5	50.0	12.3	25.0	6.2	12.5
	56.8:1	24:1	13.0:1	29.4	60.0	14.7	30.0	7.4	15.0
	66.2:1	28:1	15.1:1	34.2	70.0	17.1	35.0	8.6	17.5
	75.7:1	32:1	17.3:1	39.1	80.0	19.6	40.0	9.8	20.0
MS09/Chol/PEG (1:1)	21.6:1	12:1	6.5:1	14.7	30.0	7.4	15.0	3.7	7.5
	28.8:1	16:1	8.7:1	19.6	40.0	9.8	20.0	4.9	10.0
	35.9:1	20:1	10.8:1	24.5	50.0	12.3	25.0	6.2	12.5
	43.1:1	24:1	13.0:1	29.4	60.0	14.7	30.0	7.4	15.0
	50.3:1	28:1	15.1:1	34.2	70.0	17.1	35.0	8.6	17.5
	57.5:1	32:1	17.3:1	39.1	80.0	19.6	40.0	9.8	20.0

Table 3.4: siRNA quantities and volumes for transfection experiments in 48- and 96-well formats with MS09 liposomes

Well format	Average cell-seeding density (× 10^4 cells/well)	Final siRNA concentration (nM)	siRNA*		Transfecting complex* (µl)	Growth medium* (µl)
			(µg)	(pmol)		
96-well	1.8	58	0.08	6.0	5	100
		29	0.04	3.0	5	100
		14	0.02	1.5	5	100
48-well	4.0	58	0.2	15.0	10	250
		29	0.1	7.5	10	250
		14	0.05	3.7	10	250

*Quantities pertain to a single well

3.2.11.2 Transfection with LF3K

Cells were transfected with the LF3K reagent according to the manufacturer's protocol, dated 10 February 2016 (Publication No. MAN0009872). For a single-well transfection in a 48-well plate, The LF3K reagent (0.75 µl) was added to antibiotic and serum-free EMEM (12.5 µl) and vortexed briefly (3 s). The siRNA (0.1 µg, 7.5 pmol) was diluted in antibiotic and serum-free EMEM (12.5 µl), added to an equal volume of the LF3K-medium mixture and incubated (room temperature, 10 min). The transfecting complex (25 µl) was introduced to semi-confluent cells in fresh complete medium (0.25 ml) to give a final siRNA concentration of 25 nM. Cells were incubated at 37 ˚C until assay-specific end-points. Quantities were appropriately scaled-up or down to accommodate larger or smaller well formats as necessary (Table 3.5). LF3K was used as a positive control in all experiments conducted under standard cell culture conditions.

Table 3.5: Quantities and volumes for LF3K transfections in different well formats

Well format	Average cell-seeding density (× 10^4 cells/well)	siRNA*		LF3K* (µl)	Transfecting complex* (µl)	Growth medium* (µl)
		(µg)	(pmol)			
96-well	1.8	0.04	3.0	0.3	10	100
48-well	4.0	0.1	7.5	0.75	25	250
24-well	8.0	0.2	15.0	1.5	50	500
12-well	15.0	0.4	30.0	3.0	100	1000
6-well	29.0	1.0	75.0	7.5	250	2000

*Quantities pertain to a single well

3.2.12 Cytotoxicity testing

Semi-confluent cells in 48-well plates were treated with lipoplexes assembled from siGENOME non-targeting siRNA at final concentrations of 57 nM, 29 nM and 14 nM as described in 3.2.11. Treatment groups which received naked siRNA at the same final concentrations were also included. Untreated cells were included as positive (100 % cell viability) controls. At 48 h post-transfection, growth medium was aspirated and cell viability was assessed by the MTT (3.2.12.1) and AB (3.2.12.2) assays.

3.2.12.1 MTT assay

Cells were incubated (37 ˚C, 4 h) with 200 µl each of medium and MTT solution (5 mg/ml in PBS) per well. Wells were drained, and formazan crystals were dissolved in DMSO (200 µl/well) to give purple-coloured solutions. Absorbance was read at 540 nm in a Mindray microplate reader, MR-96A (Vacutec, Hamburg, Germany), against pure DMSO as a blank. The percentage cell viability was calculated as follows:

$$\frac{[A_{540\,nm}\ (\text{treated cells}) - A_{540\,nm}\ (\text{blank})]}{[A_{540\,nm}\ (\text{untreated cells}) - A_{540\,nm}\ (\text{blank})]} \times 100$$

3.2.12.2 AB assay

Cells were incubated (37 ˚C, 4 h) with medium (200 µl/well) and AB reagent (20 µl/well). A cell-free control containing the aforementioned quantities of medium and AB reagent was treated in the same way. Medium was transferred into 96-well flat-bottom black plates and fluorescence intensities were read using the GloMax® Multi+ Detection System (Promega Biosystems, Sunnyvale, CA, USA) at excitation and emission wavelengths of 570 nm and 585 nm, respectively. The percentage cell viability was calculated as follows:

$$\frac{[\text{RFU (treated cells)} - \text{RFU (cell-free control)}]}{[\text{RFU(untreated cells)} - \text{RFU (cell-free control)}]} \times 100 \quad \text{….. where RFU is relative fluorescence units}$$

3.2.13 Cellular uptake experiments

3.2.13.1 Quantitative assays

Semi-confluent cells in 96-well plates were treated with lipoplexes assembled from BLOCK-iT™ Fluorescent Oligo, to give final siRNA marker concentrations of 57 nM, 29 nM and 14 nM, as described in section 3.2.11. After 24 h, medium was removed and cells were washed twice with

PBS (60 µl/well). Cells were lysed with 1× lysis buffer (5 mM Tris-phosphate, pH 7.8; 0.4 mM dithiothreitol; 0.4 mM 1,2-diaminocyclohexane-*N*-*N*-*N'*-*N'*-tetra-acetic acid; 2 % $^{v}/_{v}$ glycerol; 0.2 % $^{v}/_{v}$ Triton X-100; 60 µl/well) and gentle agitation (10 rpm, 10 min) on a platform shaker (Stuart Scientific STR6, Surrey, UK). Wells were gently scraped with a micropipette tip to dislodge any remaining cells, and lysates were transferred into 96-well flat-bottom black plates. Fluorescence intensities were quantified with the GloMax® Multi+ Detection System (Promega Biosystems, Sunnyvale, CA, USA) at excitation and emission wavelengths of 494 nm and 519 nm, respectively. The soluble protein concentration of lysates was determined by the BCA assay, with BSA as the protein standard (refer to 3.2.13.2). Fluorescence readings were normalised against protein content, and results were expressed as RFU per mg protein.

3.2.13.2 BCA assay

Standard BSA solutions (ranging from 0 to 30 µg/50 µl in increments of 5 µg/50 µl) were prepared in a final volume of 50 µl with ultrapure water. These were mixed with the BCA working reagent (BCA solution:copper (II) sulfate solution, 50:1 $^{v}/_{v}$; 1 ml) and maintained at 37 ˚C for 30 min. Solutions were cooled to room temperature, and absorbance was measured at 540 nm (Mindray microplate reader, MR-96A, Vacutec, Hamburg, Germany). This data was used to construct a protein standard curve. Lysates were centrifuged (12 000 × *g*, 4 ˚C, 30 s) in an Eppendorf 5424 R instrument to pellet cellular debris. The supernatants (50 µl) were mixed with the BCA working reagent (1 ml) and incubated (37 ˚C, 30 min). The soluble protein concentration of cell lysates was obtained via extrapolation from the standard curve.

3.2.14 Final siRNA and lipid dose for application of anti-*c-myc* lipoplexes

After analysing data from cellular uptake experiments, the following parameters were chosen for gene expression assays:

- Experiments were to be limited to the two *c-myc*-overexpressing cell lines i.e. MCF-7 and HT-29.
- An MS09/Chol (1:1) lipoplex suspension assembled at the MS09:siRNA ($^{w}/_{w}$) ratio of 16:1, was to be evaluated as a new anti-*c-myc* delivery system. An MS09/DOPE lipoplex suspension, at the same MS09:siRNA ($^{w}/_{w}$) ratio, was to be included for comparative purposes.

The strategy adopted was to apply the anti-*c-myc* agents at the minimum final siRNA concentration at which maximum cellular uptake was achieved. In order to select the most appropriate final siRNA and lipid concentrations, cellular uptake experiments were performed with the above-mentioned lipoplexes, within a narrower final siRNA marker concentration range, i.e. 18 nM to 4 nM in decrements of 2 nM, according to the method given in 3.2.13. An AB assay (as outlined in 3.2.12.2) was performed to confirm the absence of cytotoxic effects at the new siRNA and lipid concentrations. siRNA quantities and volumes applicable to experiments in 48- and 96-well format are shown in Table 3.6. The associated final cytofectin and lipid concentrations are given in Table 3.7. Data is presented as a comparison with all other final siRNA concentrations explored.

Table 3.6: siRNA quantities and volumes for transfection with MS09/Chol (1:1) and MS09/DOPE lipoplexes (MS09:siRNA $^{w}/_{w}$ = 16:1) at varying final siRNA concentrations

Well format	**Average cell-seeding density (× 10^4 cells/well)**	**Final siRNA concentration (nM)**	**siRNA***		**Transfecting complex* (µl)**	**Growth medium* (µl)**
			(µg)	**(pmol)**		
96-well	1.8	18	0.026	1.9	5	100
		16	0.023	1.7	5	100
		12	0.017	1.3	5	100
		10	0.014	1.1	5	100
		8	0.011	0.7	5	100
		6	0.008	0.6	5	100
		4	0.005	0.4	5	100
48-well	4.0	18	0.065	4.9	10	250
		16	0.058	4.3	10	250
		12	0.043	3.2	10	250
		10	0.035	2.6	10	250
		8	0.028	1.7	10	250
		6	0.020	1.5	10	250
		4	0.013	1.0	10	250

*Quantities pertain to a single well

Table 3.7: Final cytofectin and lipid concentrations introduced to cells at final siRNA concentrations of 18-4 nM

Liposome formulation			**MS09/Chol (1:1)**	**MS09/DOPE**
MS09:siRNA ($^{w}/_{w}$)			16:1	16:1
Final siRNA concentration (nM)	**18**	**MS09 (µM)**	6.3	6.3
		Total lipid (µM)	12.5	12.5
	16	**MS09 (µM)**	5.6	5.6
		Total lipid (µM)	11.1	11.1
	12	**MS09 (µM)**	4.1	4.1
		Total lipid (µM)	8.2	8.2
	10	**MS09 (µM)**	3.4	3.4
		Total lipid (µM)	6.8	6.8
	8	**MS09 (µM)**	2.7	2.7
		Total lipid (µM)	5.4	5.4
	6	**MS09 (µM)**	2.0	2.0
		Total lipid (µM)	3.9	3.9
	4	**MS09 (µM)**	1.3	1.3
		Total lipid (µM)	2.5	2.5

In all experiments to follow, MS09/Chol (1:1) and MS09/DOPE lipoplexes (MS09:siRNA $^{w}/_{w}$ = 16:1) were introduced to cells at final siRNA concentration of 12 nM. Quantities were adjusted for transfections in different well formats as shown in Table 3.8.

Table 3.8: siRNA quantities and volumes for transfection in different well formats with and MS09/Chol (1:1) and MS09/DOPE lipoplexes (MS09:siRNA $^{w}/_{w}$ = 16:1) at 12 nM final siRNA

Well format	**Average cell-seeding density (× 10^4 cells/well)**	**Final siRNA concentration (nM)**	**siRNA***		**Transfecting complex* (µl)**	**Growth medium* (µl)**
			(µg)	**(pmol)**		
96-well	1.8	12	0.017	1.3	5	100
48-well	4.0	12	0.043	3.3	10	250
24-well	8.0	12	0.085	6.5	20	500
12-well	15.0	12	0.170	13.0	40	1000
6-well	30.0	12	0.340	26.0	80	2000

*Quantities pertain to a single well

3.2.15 Qualitative assessment of cellular uptake under conditions selected for gene expression assays

A qualitative assessment of cellular uptake of MS09/Chol (1:1) and MS09/DOPE lipoplexes in MCF-7 and HT-29 cells was performed. Semi-confluent cells in 12-well plates were treated with lipoplexes assembled with BLOCK-iT™ Fluorescent Oligo at MS09:siRNA ($^{w}/_{w}$) = 16:1, according to the transfection protocol outlined in 3.2.11. Cells received a final siRNA marker concentration of 12 nM (Table 3.8). After 24 h, wells were drained and cells were rinsed with PBS (400 µl). Intracellular fluorescence was observed with an inverted microscope fitted with a CC12 camera, at excitation and emission wavelengths of 494 nm and 519 nm respectively. Images were acquired at 200× magnification using Analysis Five Software (Olympus Soft Imaging Solutions, Olympus, Japan).

3.2.16 Gene expression assays

MCF-7 and HT-29 cells were seeded in 6-well plates and grown to semi-confluency. Cells were transfected according to the protocol given in section 3.2.11 with MS09/Chol (1:1) and MS09/DOPE lipoplexes (MS09:siRNA $^{w}/_{w}$ = 16:1). Lipoplexes were assembled with either siGENOME non-targeting siRNA (henceforth referred to as non-targeting siRNA) or ON-TARGETplus SMARTpool Human MYC siRNA (henceforth referred to as anti-*c-myc* siRNA) to give a final siRNA concentration of 12 nM (Table 3.8). Transfections were carried out in triplicate. Cells were harvested for either total RNA (section 3.2.16.1) or protein (section 3.2.16.3) 48 h after transfection.

3.2.16.1 Total RNA extraction

Total cellular RNA was extracted using TRIzol® Reagent as per manufacturer's instruction. Wells were drained of medium and TRIzol® Reagent (1 ml/well) was added. Cells were drawn up and expelled with a pipette, approximately 10 times, to facilitate lysis. The homogenate was kept at room temperature for 5 min, and then transferred into a 2 ml RNase-free polypropylene microcentrifuge tube, to which chloroform (0.2 ml) was added. The mixture was vigorously shaken for 15 s, and rested (room temperature, 3 min). Phase separation was achieved with centrifugation (12 000 × *g*, 4 ˚C, 15 min), in an Eppendorf 5424 R temperature-controlled centrifuge (Merck, Darmstadt, Germany). The upper aqueous phase was transferred into another microcentrifuge tube and treated (room temperature, 10 min) with 100 % isopropanol (0.5 ml).

RNA was deposited as a gel-like pellet after centrifugation (12 000 × *g*, 4 ˚C, 10 min). The pellet was washed by low-speed vortexing (room temperature, 30 s) in 75 % ($^{v}/_{v}$) ethanol (1 ml) followed by centrifugation (7 500 × *g*, 4 ˚C, 5 min). The ethanol was removed, and the pellet was left to air-dry (room temperature, 10 min) in a laminar-flow cabinet. The pellet was resuspended in RNase-free water (30 µl) by passing the suspension approximately 5 times through a micropipette tip, followed by heating (55 ˚C, 15 min). The NanoDrop 2000c spectrophotometer (Thermo Scientific, Wilmington, DE, USA) was used to measure total RNA concentration, and assess RNA purity. RNA was obtained in good yield (0.58-0.74 µg/µl) and high purity (A_{260}/A_{280} was between 2.03 and 2.11; A_{260}/A_{230} was between 2.0 and 2.30). The integrity of RNA isolates was assessed by agarose gel electrophoresis as described in section 3.2.5.1.3. 28S rRNA, 18S rRNA and 5S rRNA/tRNA bands were clearly evident in all instances. Samples were normalised to 0.057 µg/µl total RNA with RNase-free water and stored, in aliquots (30 µl), in RNase-free tubes, at -80 ˚C, for no more than a month.

3.2.16.2 RT-qPCR

3.2.16.2.1 cDNA synthesis

cDNA synthesis was carried out using the gDNA Clear cDNA Synthesis Kit as per manufacturer's instruction. For a single reaction, the RNA sample (0.8 µg, 14 µl) was mixed with a master mix (2 µl) which contained DNase I (0.5 µl) and DNase buffer (1.5 µl) solutions. Reaction mixtures (16 µl) were prepared, on ice, in PCR tube strips and reactions were carried out in a C1000 Touch™ Thermal Cycler (Bio-Rad Laboratories (PTY) Ltd., Richmond, USA). The DNase reaction was performed as follows: DNA digestion (25 ˚C, 5 min), DNase inactivation (75 ˚C, 5 min), and samples were maintained at 4 ˚C for 10 min. The RT supermix (4 µl) was added and cDNA synthesis was carried out as follows: priming (25 ˚C, 5 min), reverse transcription (46 ˚C, 20 min), RT inactivation (95 ˚C, 1 min) and samples were held at 4 ˚C for 10 min. Two cDNA synthesis reactions per RNA isolate were performed in parallel i.e. one reaction containing the RT supermix and a no-RT control in which the no-RT supermix was added instead. cDNA samples were diluted to a final concentration of 25 ng/µl in nuclease-free water and stored at 4 ˚C, for no more than a week.

3.2.16.2.2 RT-qPCR reactions

The product of each cDNA synthesis reaction was subjected to RT-qPCR. A single reaction mixture (20 µl) contained the following: SsoAdvanced™ Universal SYBR® Green Supermix (10 µl); primers (1 µl) specific for either the target gene, *c-myc* (PrimePCR™ SYBR® Green Assay: MYC, Human) or reference gene, *β-actin* (PrimePCR™ SYBR® Green Assay: ACTB, Human); cDNA sample (25 ng, 1 µl) and nuclease-free water (8 µl). Reaction mixtures in which DNA templates (either PrimePCR™ Template for SYBR® Green Assay: MYC, Human; or PrimePCR™ Template for SYBR® Green Assay: ACTB, Human; 1 µl) were substituted for cDNA served as positive controls. Reaction mixtures in which nuclease-free water (1 µl) was substituted for either primers or cDNA were included as negative controls. All reactions were performed in triplicate. Reaction mixtures were prepared, on ice, in Hard-Shell® 96-well plates and sealed with Microseal® 'B' adhesive seals. Plates were briefly centrifuged and loaded in a C1000 Touch™ Thermal Cycler (CFX 96 Touch™ Real-Time PCR Detection System, Bio-Rad Laboratories (PTY) Ltd.). Reaction conditions were as follows: activation (95 ˚C, 2 min, 1 cycle), denaturation (95 ˚C, 5 s, 40 cycles), annealing/extension (60 ˚C, 30 s, 40 cycles), melt curve (65 ˚C – 95 ˚C in 0.5 ˚C increments, 5 s/step). Data was analysed with CFX Manager™ Software version 3.0 (Bio-Rad Laboratories). *c-myc* expression was normalised to *β-actin* using the $\Delta\Delta C_q$ comparative quantification algorithm.

$$\Delta\Delta C_q = \Delta C_{q(test)} - \Delta C_{q(calibrator)}$$
$$\Delta C_{q(test)} = C_{q(target,\ test)} - C_{q(ref,\ test)}$$
$$\Delta C_{q(calibrator)} = C_{q(target,\ calibrator)} - C_{q(ref,\ calibrator)}$$

where C_q denotes quantification cycle, *target* denotes *c-myc*, *test* denotes treated cells, *ref* denotes the reference gene, *β-actin* and, untreated cells served as the *calibrator*.

3.2.16.3 Total protein extraction

Wells were drained of medium and cells were washed twice with ice-cold PBS (1 ml/well). Cold (4 ˚C) RIPA buffer (100 µl/well) was added and cells were placed on ice for 5 min on a platform shaker (Stuart Scientific STR6, Surrey, UK) operating at 10 rpm. Wells were scraped with a micropipette tip and lysates were transferred to a 0.5 ml sterile microcentrifuge tube. Lysates were clarified by centrifugation (14 000 × *g*, 4 ˚C, 15 min) in an Eppendorf 5424 R instrument (Merck, Darmstadt, Germany). Supernatants were collected and a small volume (10 µl) of each sample was reserved for total protein determination by the BCA assay as described in 3.2.13.2.

Protein concentrations were 2.0-2.6 µg/µl. Lysates were stored at -20 ˚C, for no longer than a month.

3.2.16.4 ELISA

Protein extracts were immobilised onto the wells of a 96-well flat-bottom multi-well plate with 50 mM carbonate-bicarbonate coating buffer, pH 9.6, at 4 ˚C, overnight. Three replicates per isolate were performed. Each well received 10 µg protein in 100 µl coating buffer. The coating buffer was removed and wells were rinsed twice with TBS (20 mM Tris-HCl, pH 7.5, 150 mM NaCl) containing 0.1 % Tween 20 (TBST, 100 µl/well). Wells were treated (room temperature, 1 h) with 5 % non-fat dry milk in TBST (100 µl) with gentle agitation (10 rpm) on a platform shaker (Stuart Scientific STR6, Surrey, UK) to saturate unoccupied attachment sites. The blocking agent was removed and wells were rinsed twice with TBST (100 µl/well). Either c-Myc (1:2000, in TBST) or β-actin (1:10 000, in TBST) primary antibodies were applied (100 µl/well) at room temperature for 1 h. Primary antibodies were removed and wells were washed 4 times with TBST (100 µl/well) for 5 min each, with agitation (10 rpm). The secondary antibody (1:2000, in TBST) was applied (room temperature, 1 h). Wells were drained and washed 4 times with TBST as previously described. TMB (100 µl/well) was applied (room temperature, 30 min). The reaction was terminated by the addition of 2 M H_2SO_4 (100 µl/well) and absorbance was measured at 450 nm (Mindray microplate reader, MR-96A, Vacutec, Hamburg, Germany) against a mixture of TMB (100 µl) and 2 M H_2SO_4 (100 µl), as a blank. Wells containing BSA (10 µg) were treated in the same way, and served as negative controls. Antibody-free and substrate-free controls were also included. Control samples gave negligible corrected absorbance (i.e. less than 1 % of the corrected absorbance of untreated cells treated with primary antibody, secondary antibody and substrate). c-Myc expression was normalised to β-actin and presented relative to untreated cells.

3.2.17 Effects of lipoplex-mediated *c-myc* inhibition

The effects of *c-myc* inhibition on cancer cell migration, proliferation and survival was studied under conditions which mirrored those of the gene expression assays (3.2.16).

3.2.17.1 Wound healing assay

The wound healing assay was adapted from the method reported by Qin and Cheng (2010). Semi-confluent cells in 12-well plates were treated with lipoplexes as per transfection protocol in

3.2.11 and quantities shown in Table 3.8. At 24 h post-transfection a sterile 200 µl micropipette tip was carefully drawn across the diameter of each well so as to create a single, linear wound (t = 0 h). Growth medium was aspirated and cells were rinsed with PBS (0.5 ml/well) to remove any dislodged cells. Fresh medium (1 ml/well) was added. The wounds created were observed with an inverted fluorescence microscope (CKX41, Olympus, Japan), operating in bright field mode, at 100× magnification. Images were captured using Analysis Five Software (Olympus Soft Imaging Solutions, Olympus, Japan). Positions were discretely marked on the edges of wells to permit re-examination of the same field of view at a later stage. Cells were returned to the incubator, and wound closure was monitored 24 h later (t = 24 h). The software facilitated measurements of wound area against calibrated images and results were reported as follows:

$$\text{Normalised wound area (\%)} = \frac{\text{wound area}_{\text{t = 24 h}}\ (\mu m^2)}{\text{wound area}_{\text{t = 0 h}}\ (\mu m^2)} \times 100$$

3.2.17.2 Growth inhibition assays

Lipoplexes were introduced to semi-confluent cells in 48-well plates as per transfection protocol in 3.2.11 and quantities shown in Table 3.8. At 48 h post-transfection, growth inhibition was evaluated by the AB assay as described in section 3.2.12.2.

3.2.17.3 Apoptosis assay

Lipoplexes were introduced to semi-confluent cells in 24-well plates as per transfection protocol in 3.2.11 and quantities shown in Table 3.8. At 48 h post-transfection wells were drained and cells were rinsed with PBS (200 µl/well). Live, apoptotic and necrotic cells were distinguished by the AO/EtBr dual staining method adapted from Maiyo *et al*. (2016). Briefly, cells were stained with AO/EtBr solution (100 µg/ml AO and 100 µg/ml EtBr in PBS; 10 µl/well) with agitation (30 rpm, 25 ˚C, 5 min) on a platform shaker (Stuart Scientific STR6, Surrey, UK). Excess stain was removed by rinsing with PBS (100 µl/well). Cellular changes associated with apoptosis were observed with an inverted fluorescence microscope (CKX41, Olympus, Japan) at excitation and emission wavelengths of 540 nm and 580 nm, respectively. A minimum of 200 cells per well was counted at random fields of view. Images were acquired at 200× magnification using Analysis Five Software (Olympus Soft Imaging Solutions, Olympus, Japan). Results were presented as follows:

$$\text{Live/total apoptotic/early apoptotic/late apoptotic/necrotic cells (\%)} = \frac{[\text{number of live/total apoptotic/early apoptotic/late apoptotic/necrotic cells counted}]}{[\text{total cells counted}]} \times 100$$

3.2.18 Serum tolerance of MS09/Chol (1:1) and MS09/DOPE lipoplexes at MS09:siRNA ($^{w}/_{w}$) = 16:1

Semi-confluent MCF-7 and HT-29 cells in 96-well plates were treated with lipoplexes (5 µl in HBS) assembled with BLOCK-iT™ Fluorescent Oligo, to give a final siRNA marker concentration of 12 nM (Table 3.8) in growth medium (100 µl) containing 10, 30 or 50 % ($^{v}/_{v}$) FBS. After 4 h at 37 ˚C, wells were drained and routine cell culture medium was added. At 24 h post-transfection, intracellular fluorescence was measured and normalised against soluble protein content of cell extracts, as described in section 3.2.13. An AB assay was carried out, as outlined in section 3.2.12.2, so as to confirm cell viability under the new transfection conditions.

3.2.19 Statistical analysis

Statistical analyses were performed using one-way analysis of variance (ANOVA), followed by Tukey's Multiple Comparison Test to compare between groups (GraphPad Prism version 5.04, GraphPad Software Inc., USA). *P* values less than 0.05 were considered significant.

CHAPTER 4 - RESULTS AND DISCUSSION

4.1 Liposome preparation and characterisation

An effective anti-*c-myc* siRNA delivery system, with an uncomplicated design and simple preparation method, may pave the way for the development of an economically feasible and clinically viable onconanotherapeutic agent. This study has focused on a lipid-based delivery agent that is arguably the simplest and easiest to prepare i.e. the traditional cationic liposome prepared by lipid film hydration.

MS09 (Figure 4.1a), a cationic lipid that previously gave good *in vitro* gene silencing capability when formulated into liposomes (Daniels *et al*., 2013), was the chosen cytofectin. Several features of this lipid render it suitable for the development of cationic liposomal siRNA carriers. Firstly, the molecule is built upon the rigid cholesterol ring system that permits its stable incorporation within a lipid bilayer. Secondly, the tertiary amino headgroup, that is protonated at physiological pH, permits electrostatic binding of nucleic acids. Moreover, a spacer of 12 atoms promotes interaction with nucleic acids by reducing steric hindrance between the headgroup region and cholesterol anchor (Singh and Ariatti, 2006). Finally, the carbamoyl bond, which tethers the spacer and headgroup elements to the fused ring system is biodegradable following release of the nucleic acid and augurs well for the biocompatibility (Gao and Huang, 1991) of MS09 liposomal systems.

To date, MS09 has only been evaluated in co-formulation with the zwitterionic phospholipid, DOPE (Figure 4.1b) (Daniels *et al*., 2013, Singh and Ariatti, 2006). The cone-shaped ethanolamine headgroup favours bilayer transition from the ordered lamellar to inverted hexagonal phase, and this is advantageous during cellular uptake, release and endosomal escape of nucleic acids. As such, DOPE is a commonly used helper lipid in cationic liposome formulations (Mochizuki *et al*., 2013). However, DOPE-containing liposomes may not be suitable for intravenous administration. Li and coworkers (1999) demonstrated early on that DOPE-containing cationic liposomes rapidly disintegrate upon exposure to serum. This can be attributed to the fact that DOPE, which has ionisable groups can interact with serum proteins, and this inhibits its activity (Yang *et al*., 2013). Nonetheless an equimolar mixture of MS09 and DOPE, that previously proved effective in *in vitro* siRNA delivery (Daniels *et al*., 2013) was prepared for comparative purposes.

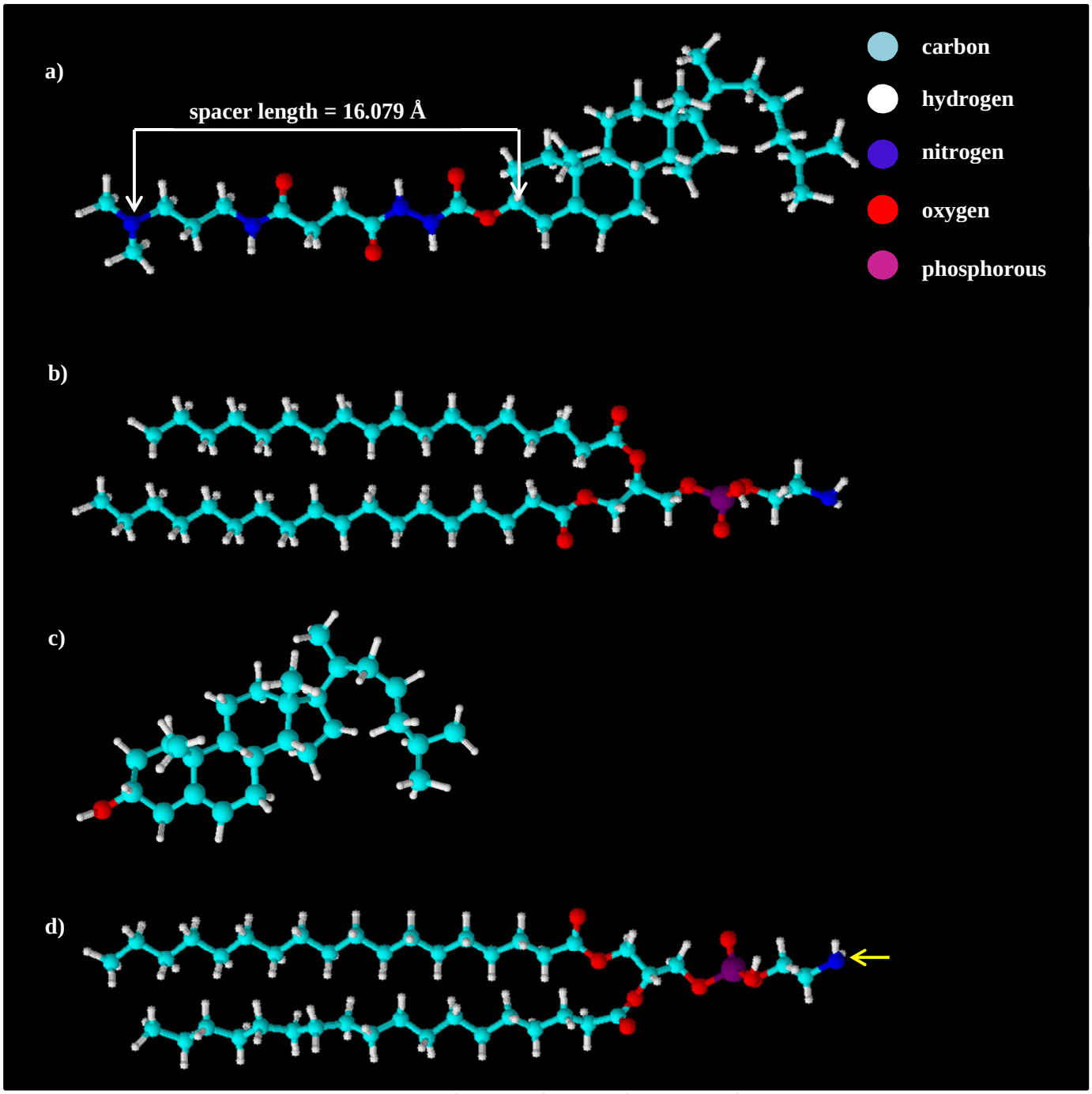

Figure 4.1: Ball and stick models of lipids **a)** MS09, **b)** DOPE, **c)** Chol and **d)** DSPE used in liposome formulations. In a) the spacer length reported was measured as the internuclear distance between the atoms indicated. In d) the yellow arrow shows the point of attachment of the PEG_{2000} chain to the DSPE molecule. Models were generated using ACD/3D Viewer (Advanced Chemistry Development, Inc. (ACD/Labs) Toronto, Ontario, Canada).

Early studies showed that the incorporation of Chol (Figure 4.1c) with phospholipids at 30 mol % or more resulted in the formation of a phase-separated region in the lipid bilayer (Huang *et al*., 1974). This property of Chol liposomes, in the absence of other helper lipids, becomes more pronounced with increasing Chol content, and prevents adverse liposome-protein interactions, aggregation, improves mechanical strength and stability (Epand *et al*., 2003, Huang *et al*., 1974) and can extend circulation time *in vivo* (Semple *et al*., 1996).

The effect of increasing Chol content in MS09 liposomes was studied. Liposomes were formulated with MS09 and Chol at molar ratios of 1:1, 1:2 and 1:3. Higher ratios were not explored, as it was reasoned that incorporating Chol at higher concentrations would reduce the number of cytofectin molecules present in the bilayer by more than 60 %. This is a dramatic reduction in the number of cationic centres available for siRNA binding. A further consideration was that groups which have focused on studying the effect of high Chol content in cationic liposome formulations, before the current study was initiated, had done so within the context of plasmid DNA (pDNA) delivery only (Yang *et al*., 2013, Zhang and Anchordoquy, 2004). Given that siRNA is markedly smaller than pDNA, it cannot condense further (Spagnou *et al*., 2004) and a larger quantity of liposome is required to bind a fixed quantity of siRNA when compared with pDNA (Zhang *et al*., 2010); Chol content did not exceed 75 mol % in this study. Chol concentration below 50 mol % was not investigated in light of the established correlation between high Chol content and improved stability of liposomes formulated with a monocationic cholesteryl cytofectin, DC-Chol (Yang *et al*., 2013).

Transmission electron micrographs show that MS09/DOPE and MS09/Chol (1:1) formulations formed unilamellar vesicles. Vesicles of the MS09/DOPE suspension were predominantly round (Figure 4.2a), similar to those reported by Daniels *et al*. (2013). However, substitution of DOPE with Chol at the same molar ratio gave some irregularly shaped vesicles (Figure 4.2b). Formulations with greater Chol content appeared poorly hydrated and visibly settled out of suspension even with extended sonication time. Consequently, images of these formulations show an aggregated mass of lipid (Figure 4.2c,d).

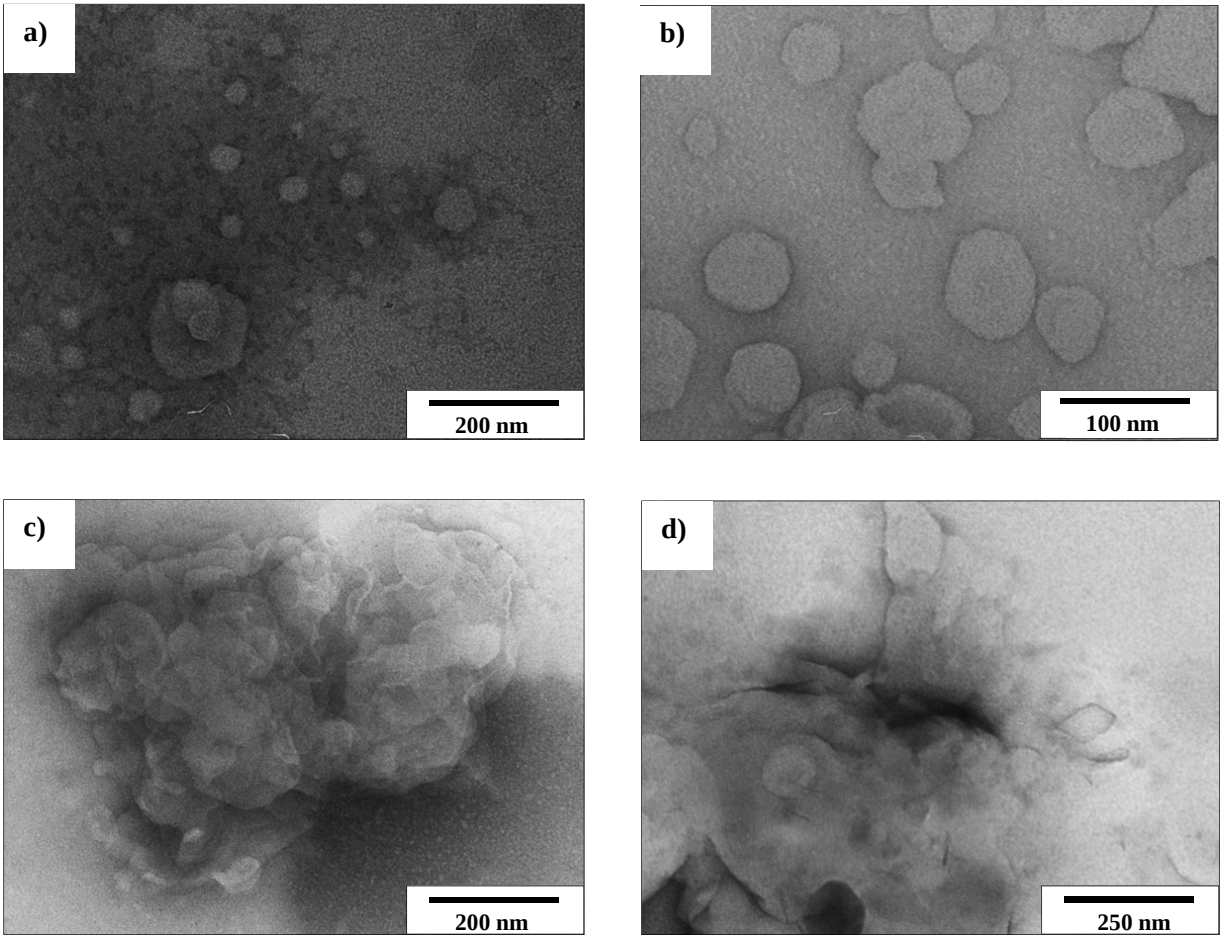

Figure 4.2: Transmission electron micrographs of non-pegylated cationic liposomes: **a)** MS09/DOPE, **b)** MS09/Chol (1:1), **c)** MS09/Chol (1:2), **d)** MS09/Chol (1:3). Liposome suspensions were stained with uranyl acetate and cryopreserved prior to viewing.

Steric stabilisation of liposomes through pegylation was attempted. The simplest method of PEG-modification, pre-pegylation, in which PEG chains are attached to the liposomal bilayer prior to the introduction of siRNA molecules, was opted for. This is in keeping with one of the main themes of the study i.e. to maintain simplicity of carrier design and preparation. Several issues were taken into consideration with regard to polymer size, the nature of the PEG-lipid conjugate and the amount of PEG-lipid incorporated in liposome formulations. Firstly, pegylated lipid derivatives have micelle forming tendencies and this imposes a limit on the concentration at which these lipids can be stably incorporated in liposomal bilayers. As the length of a PEG chain attached to a hydrocarbon skeleton increases, so too does the ratio of the polar region of the lipid relative to its apolar component; and this disturbs the organisation of the bilayer (Photos *et al.*, 2003). Therefore PEG of molecular weight 2000, as opposed to longer polymer chains was

chosen in the form of a commonly used DSPE (Figure 4.1d) lipid conjugate known to stabilise the lamellar phase of the bilayer (Che *et al*., 2015). The commercially available PEG-lipid, DSPE-PEG_{2000}, employed in this study has served as a component of the first Food and Drug Administration-approved anti-cancer liposomal drug, and is therefore favourable in terms of safety and biocompatibility (Allen and Cullis, 2013). A further concern with regard to pre-pegylation is that the presence of polymer chains on the surface may shield cationic groups and hinder the binding of siRNA (Daniels *et al*., 2013, Zhang *et al*., 2010). Finally, too high a PEG density can interfere with the lipoplex-cell association necessary for cellular uptake (Deshpande *et al*., 2004).

Buyens *et al*. (2012) commented that if siRNA molecules are to be complexed with liposomes through simple mixing, liposomes should have low PEG densities. In the interest of achieving a balance between liposome stability and siRNA-binding through pre-pegylation, DSPE-PEG_{2000} was incorporated at what has come to be accepted as a commonly employed concentration for both *in vitro* and *in vivo* use i.e. 2 mol % (Betker *et al*., 2013a). At this concentration, PEG assumes what is referred to as the "mushroom" conformational regime, in which the polymer forms isolated grafts on the bilayer surface. Unlike the "brush" configuration, achieved with greater than 5 mol % PEG-lipids, in which polymer chains interact to form a dense hydrated network around the liposome; pegylation at 2 mol % permits partial exposure of the bilayer (de Gennes, 1980).

Pegylated MS09/DOPE and MS09/Chol (1:1) formulations formed stable suspensions upon lipid film hydration. While tubular vesicles were evident in the MS09/DOPE/PEG suspension (Figure 4.3a), the MS09/Chol/PEG (1:1) formulation gave vesicles (Figure 4.3b) which largely resembled its non-pegylated counterpart. It is likely that the membrane rigidity conferred by Chol, resulted in vesicles that were more resistant to distortion upon the incorporation of a relatively small amount of DSPE-$PEG_{2000.}$

Pegylated suspensions of MS09/Chol (1:2) and MS09/Chol (1:3) formulations were more readily hydrated than their non-pegylated counterparts. Electron micrographs show some unilamellar vesicles in both instances (Figure 4.3c,d). However, particles did settle out of suspension after two days at 4 ˚C. Hence 2 mol % pegylation failed to abolish the inherent instability of these formulations. It appears that unlike the cytofectins DOTMA and DC-Chol, which reportedly

formed stable suspensions with up to 80 mol % Chol (Yang *et al*., 2013, Zhang and Anchordoquy, 2004), MS09 is incompatible with more than 50 mol % Chol.

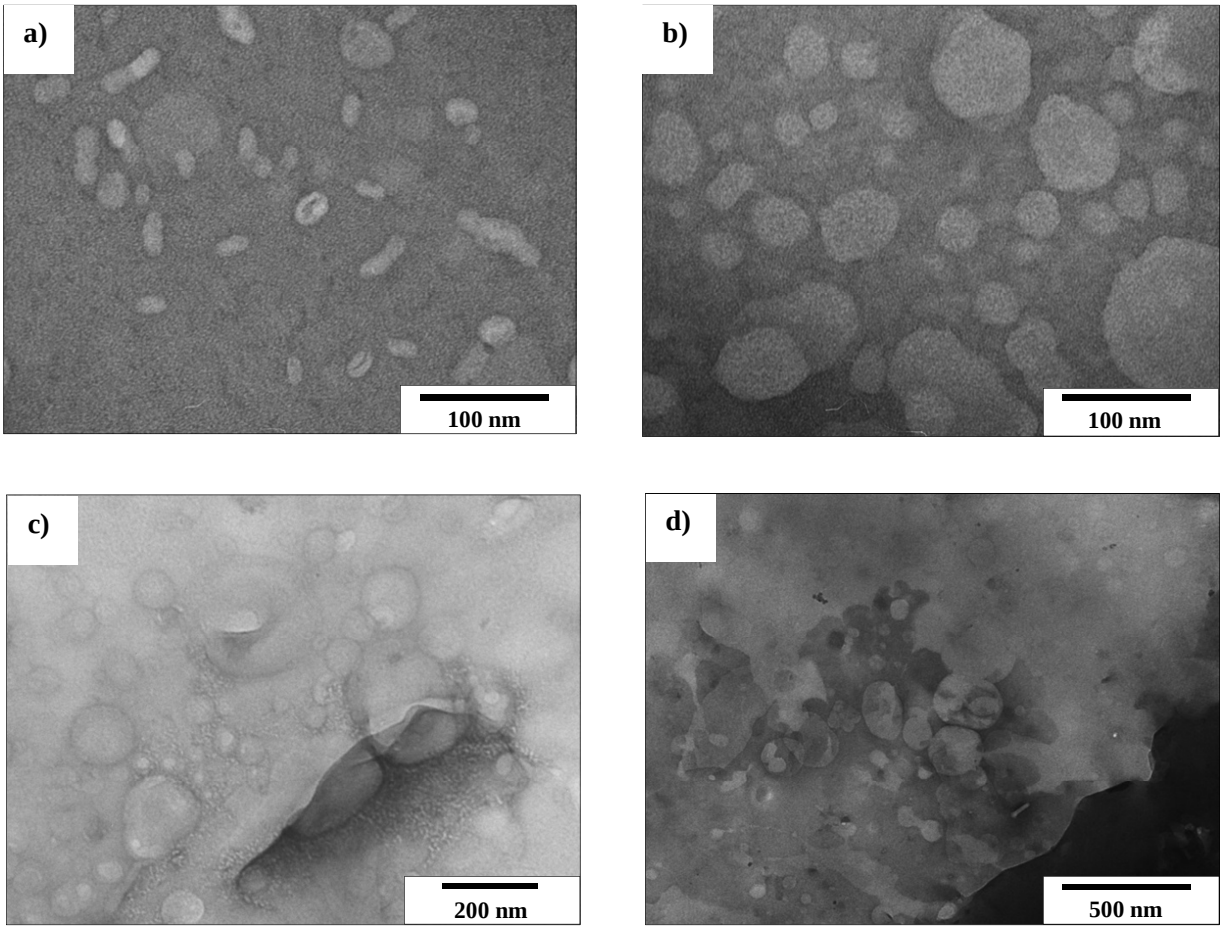

Figure 4.3: Transmission electron micrographs of pegylated cationic liposomes: **a)** MS09/DOPE/PEG, **b)** MS09/Chol/PEG (1:1), **c)** MS09/Chol/PEG (1:2), **d)** MS09/Chol/PEG (1:3). Samples were stained with uranyl acetate and cryopreserved prior to viewing.

It appears that stable incorporation of high Chol concentrations is dependent on the interaction of Chol with other lipids in the formulation. This notion is supported by an early study with pegylated distearoylphosphatidylcholine/Chol liposomes in which high Chol content gave fragile, unstable nanoparticles (Maruyama *et al*., 1992). The incorporation of higher DSPE-PEG_{2000} concentrations was not attempted in accordance with the poor siRNA-binding, cellular uptake and gene silencing that others have observed with pre-pegylated cationic liposomes (Daniels *et al*., 2013, Santel *et al*., 2006).

Liposome preparations were characterised according to size and zeta potential by Z-NTA (Figure 4.4a,b). NTA is a recent addition to nanoparticle characterisation. The NTA system calculates hydrodynamic diameter by tracking the movement of individual particles in a suspension. This provides a more accurate representation of particle size than was possible with the intensity-weighted measurements obtained by traditional light scattering techniques (Wilson and Green, 2017). Combination of NTA instrumentation with a zeta module i.e. an electrophoresis system to apply current to the sample, allows zeta potential to be simultaneously measured (Griffiths *et al*., 2011).

The visible instability of the MS09/Chol (1:2) and MS09/Chol (1:3) formulations was corroborated by the Z-NTA data. The general acceptance is that nanoparticles with zeta potentials between +30 and -30 mV are predisposed towards aggregation over time. In both instances, particles greater than 300 nm in size were detected with zeta potentials close to zero, and this is a clear indication of aggregation tendencies (Griffiths *et al*., 2011). While PEG-modification is known to increase the hydrodynamic diameter of nanoparticles and reduce zeta potential due to charge shielding (Tomasetti *et al*., 2016), visible settling of the pegylated MS09/Chol (1:2) and MS09/Chol (1:3) formulations cannot be ignored.

Further proof of vesicle aggregation was obtained from NTA-derived concentration estimates. The particle concentration of suspensions with more than 50 mol % Chol was roughly an order of magnitude less than that of liposomes formulated from MS09 and Chol in equimolar quantities (Figure 4.4c). In contrast, the concentration of MS09/DOPE, MS09/DOPE/PEG, MS09/Chol (1:1) and MS09/Chol/PEG (1:1) suspensions, all of which are statistically similar in size and zeta potential, did not differ significantly ($P > 0.05$, for all comparisons).

Given that the final lipid concentration of all formulations was kept constant, i.e. 8 mM, and, that many more lipid molecules would be involved in the formation of large structures as opposed to smaller ones, it follows that the particle concentration of pegylated and non-pegylated MS09/Chol (1:2) and MS09/Chol (1:3) formulations is much lower than those that were able to accommodate the stable formation of smaller vesicles.

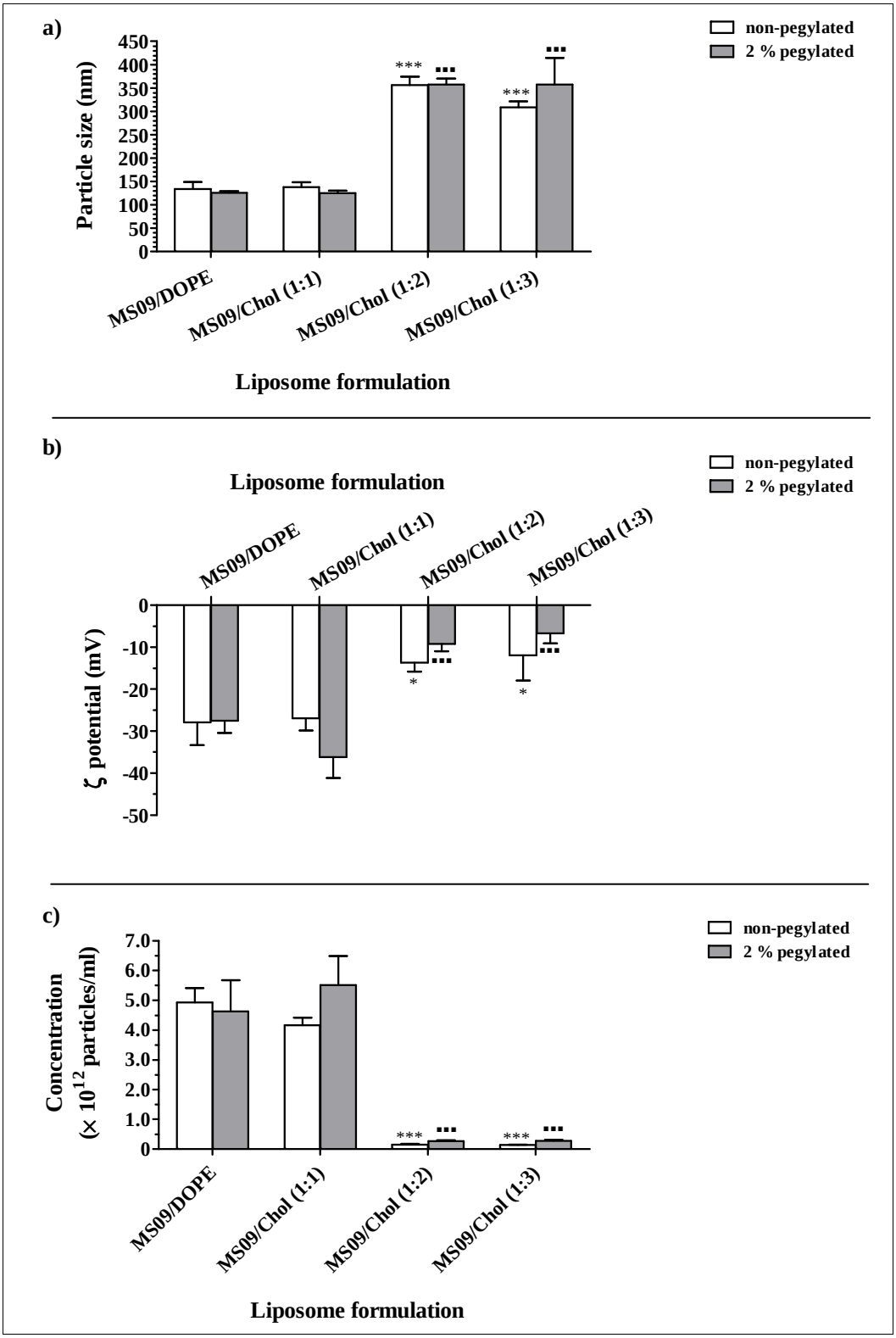

Figure 4.4: Liposome **a)** size, **b)** ζ potential and **c)** vesicle concentration, according to Z-NTA. Each column represents the mean ± SD (*n = 3*). **P* < 0.05, ****P* < 0.001 *vs.* MS09/Chol (1:1); ▪▪▪*P* < 0.001 *vs.* MS09/Chol/PEG (1:1).

With regards to the stable preparations i.e. MS09/DOPE, MS09/DOPE/PEG, MS09/Chol (1:1) and MS09/Chol/PEG (1:1), liposome size was far below 200 nm and sufficient to be classified as small unilamellar vesicles. While there were no significant differences in size or zeta potential across the four preparations, electron micrographs suggest that pegylated vesicles may, in fact, be smaller. Here again, the contribution of the hydrophilic PEG-chains, which can extend away from the bilayer into the external aqueous environment, to the hydrodynamic radius of a vesicle (Tomasetti *et al*., 2016) provides a likely explanation for the similar sizes of pegylated and non-pegylated vesicles. It appears that substitution of DOPE with Chol at the same molar ratio had no significant effect on size or zeta potential. In this regard, Yang and colleagues (2013) commented that Chol is not likely to influence the electrical surface potential of liposomes because it does not bear an ionisable group.

Of note is the fact that all formulations gave negative zeta potentials, contrary to what is expected of cationic carriers. Zeta potential measurements are based on the interaction of the particle with ions in the medium in which it is dispersed. Therefore, the composition of the dispersant influences the zeta potential of a suspended particle. In this instance liposomes were dispersed in HEPES buffer. Zwitterions such as HEPES can influence the zeta potential of a bilayer depending on the orientation of the molecule's ionisable groups relative to the membrane (Koerner *et al*., 2011) in the electrical double layer, and this could possibly account for the Z-NTA measurements obtained. Therefore, in this instance, negative zeta potential values do not necessarily imply that the liposomes would be unable to associate with siRNA molecules. Hence, siRNA-binding studies with MS09/Chol (1:1), MS09/Chol/PEG (1:1), MS09/DOPE and MS09/DOPE/PEG formulations was carried out.

4.2 siRNA-binding studies

The gel retardation assay is widely documented as the first step in assessing the siRNA-binding capability of cationic lipid-based carriers (Ceballos *et al*., 2010, Dorasamy *et al*., 2012, Han *et al*., 2008, Suh *et al*., 2009). This assay is based on the premise that the migration of siRNA on agarose gel is retarded in an electric field when bound to the carrier due to the formation of large electroneutral complexes that are unable to permeate the gel matrix. Figure 4.5a shows the association of siRNA with the MS09/DOPE liposome formulation.

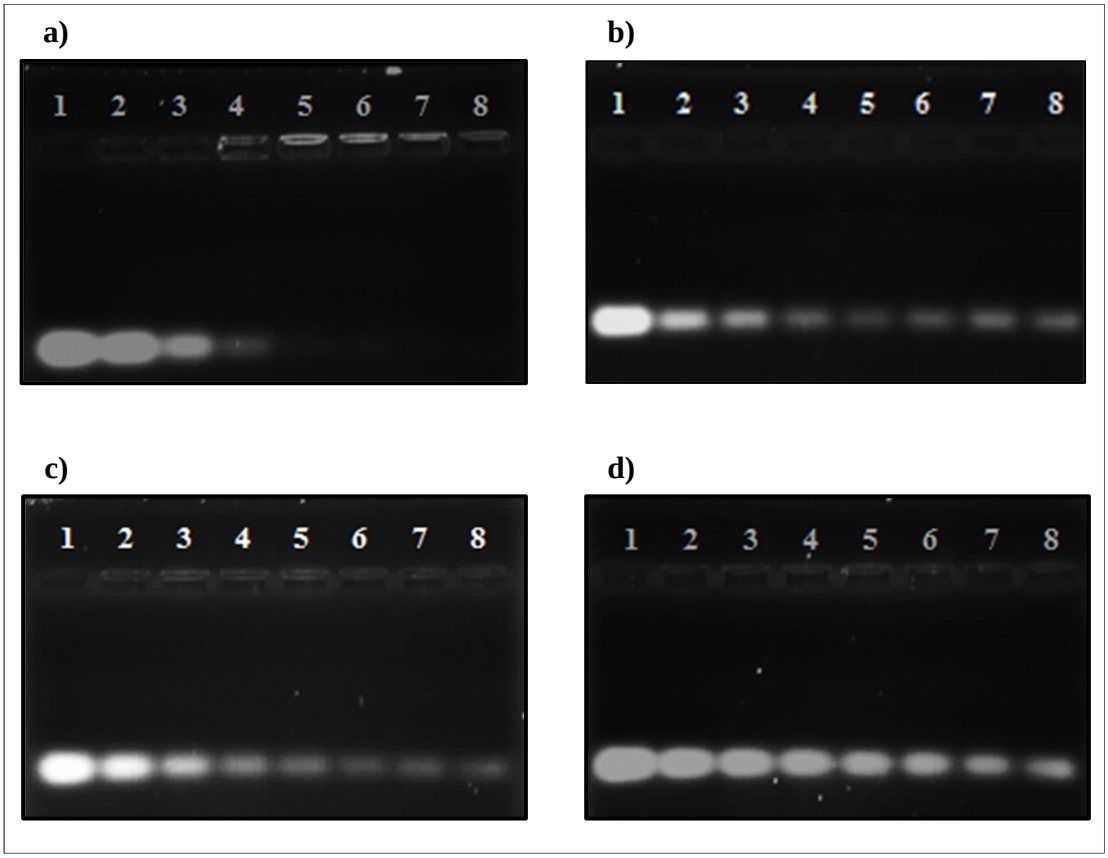

Figure 4.5: Gel retardation study of the binding interactions between siRNA and cationic liposomes. Incubation mixtures (10 µl) contained siRNA (0.3 µg) and varying amounts of liposome to correspond with increasing amounts of cytofectin. **a)** MS09/DOPE, *lanes 1-8* (0, 1.4, 2.8, 4.2, 5.6, 7.0, 8.4, 9.8 µg MS09); **b)** MS09/Chol (1:1), **c)** MS09/DOPE/PEG, **d)** MS09/Chol/PEG (1:1), *lanes 1-8* (0, 2.8, 4.2, 5.6, 7.0, 8.4, 9.8, 11.2 µg MS09).

As the amount of liposome relative to siRNA was increased across lanes 2 to 8, more siRNA became liposome associated. This was observed as a gradual decrease in the intensity of the siRNA band that migrated into the gel, accompanied by siRNA retained in the wells in the form of lipoplexes. Fluorescence in the wells (Figure 4.5a, lanes 4-8) is indicative of intact siRNA that has formed complexes with liposomes. In this study, MS09/DOPE was the only formulation to fully prevent the electrophoretic migration of siRNA.

Figures 4.5b-d show that although the expected gradual decrease in unbound siRNA was observed with increasing liposome content, with respect to the MS09/Chol (1:1), MS09/DOPE/PEG and MS09/Chol/PEG (1:1) formulations, unbound siRNA was evident at all MS09:siRNA ($^{w}/_{w}$) ratios explored. Although retention of siRNA in the wells was not observed

in these instances, it is possible for the lipoplexes to have floated out of the well and into the electrophoresis buffer. Together with densitometric analysis (Figure 4.6), it appears that the binding of siRNA by these liposome formulations increased up until a point, whereupon free siRNA in the gel persisted despite further addition of liposome. This MS09:siRNA ($^{w}/_{w}$) ratio was taken as the end-point binding ratio (point of maximum binding) of these liposomes.

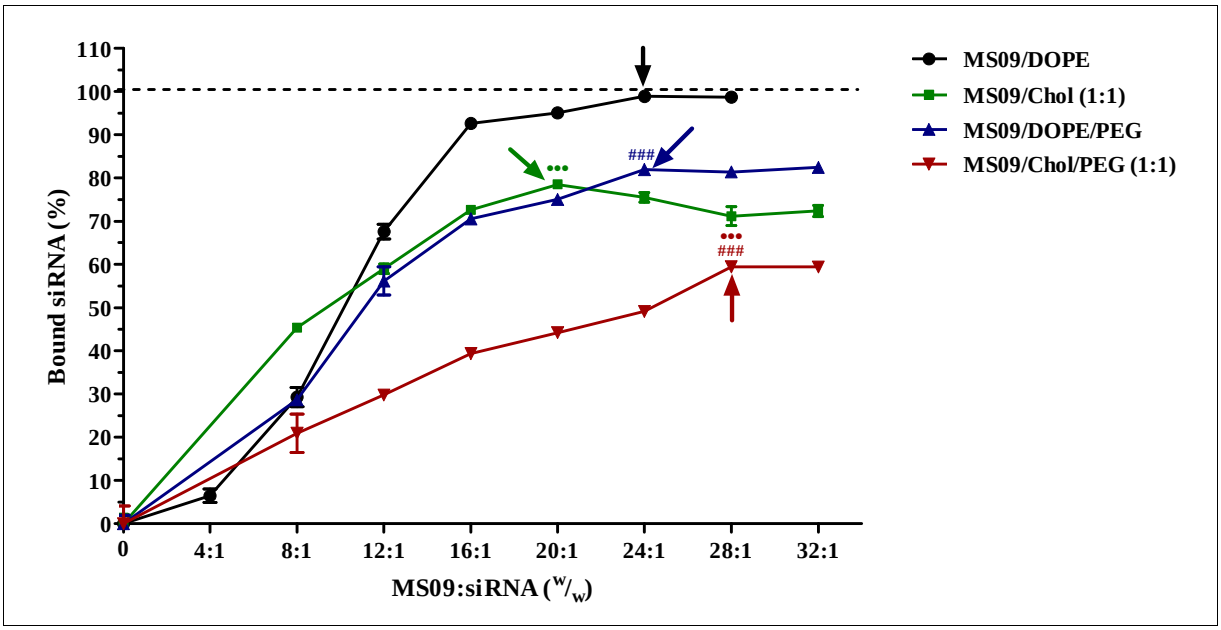

Figure 4.6: siRNA-binding capacity of liposome formulations at varying MS09:siRNA ($^{w}/_{w}$) ratios, as determined by densitometry following gel retardation electrophoresis. Data is presented as the mean ± SD (n = 3). The point at which each formulation best bound siRNA is indicated by an arrow. $^{###}P < 0.001$ *vs.* non-pegylated counterpart, $^{•••}P < 0.001$ *vs.* DOPE-containing counterpart at the respective MS09:siRNA ($^{w}/_{w}$) ratio at which maximum siRNA was bound.

Densitometry showed that, for pegylated preparations, the amount of free siRNA in the gel, beyond the point of maximum binding, was nearly constant. However, in the case of the MS09/Chol (1:1) formulation, an increase in liposome content beyond end-point was accompanied by a decrease in the amount of liposome-bound siRNA. A similar aberration in siRNA binding patterns was observed by Khatri and coworkers (2014) at high lipid:siRNA ratios. This group suggested that, in some instances, incomplete charge titration at very high ratios may attract additional siRNA as a second, more loosely bound layer around the liposome and this is observed as an increase in free siRNA on agarose gel.

The association of siRNA with liposomes was also studied in fluorescence quenching assays. In this set of experiments, one of two nucleic acid intercalating dyes, either EtBr or SYBR Green II, was employed. The assays are based on the concept that the dyes fluoresce strongly when associated with siRNA, but are displaced with the addition of cationic liposomes which bind to the siRNA. Dye displacement is manifested as a drop in fluorescence. Upon successive addition of liposome, fluorescence is gradually quenched. Eventually a point of inflection, which represents complete or maximum siRNA-binding, is reached when fluorescence stabilises irrespective of further addition of liposome. Figure 4.7 shows that all four liposomes in this study were able to displace the siRNA-associated dyes, albeit to different extents, depending on their affinity for siRNA. Had the observed drop in fluorescence occurred as a result of siRNA degradation rather than complex formation, it is likely that fluorescence readings would have eventually approximated the baseline measurements that were taken prior to the introduction of siRNA in incubation mixtures. As suggested by gel retardation experiments, the MS09/DOPE formulation demonstrated the best siRNA-binding capability. Although the points of inflection for dye displacement assays of MS09/Chol (1:1) and MS09/DOPE/PEG were attained at the same and marginally lower MS09:siRNA ($^{w}/_{w}$) ratios respectively, MS09/DOPE achieved the greatest degree of dye displacement.

The maximum dye displacement (Table 4.1) and the MS09:siRNA ($^{w}/_{w}$) ratio at which this value was recorded (Table 4.2) for individual liposome formulations, using both dyes, were in good agreement. However, points of inflection were more clearly defined in assays in which SYBR Green II served as the intercalating dye. This could be explained by the fact that SYBR Green is more sensitive and has greater affinity for RNA (Dorasamy *et al*., 2009).

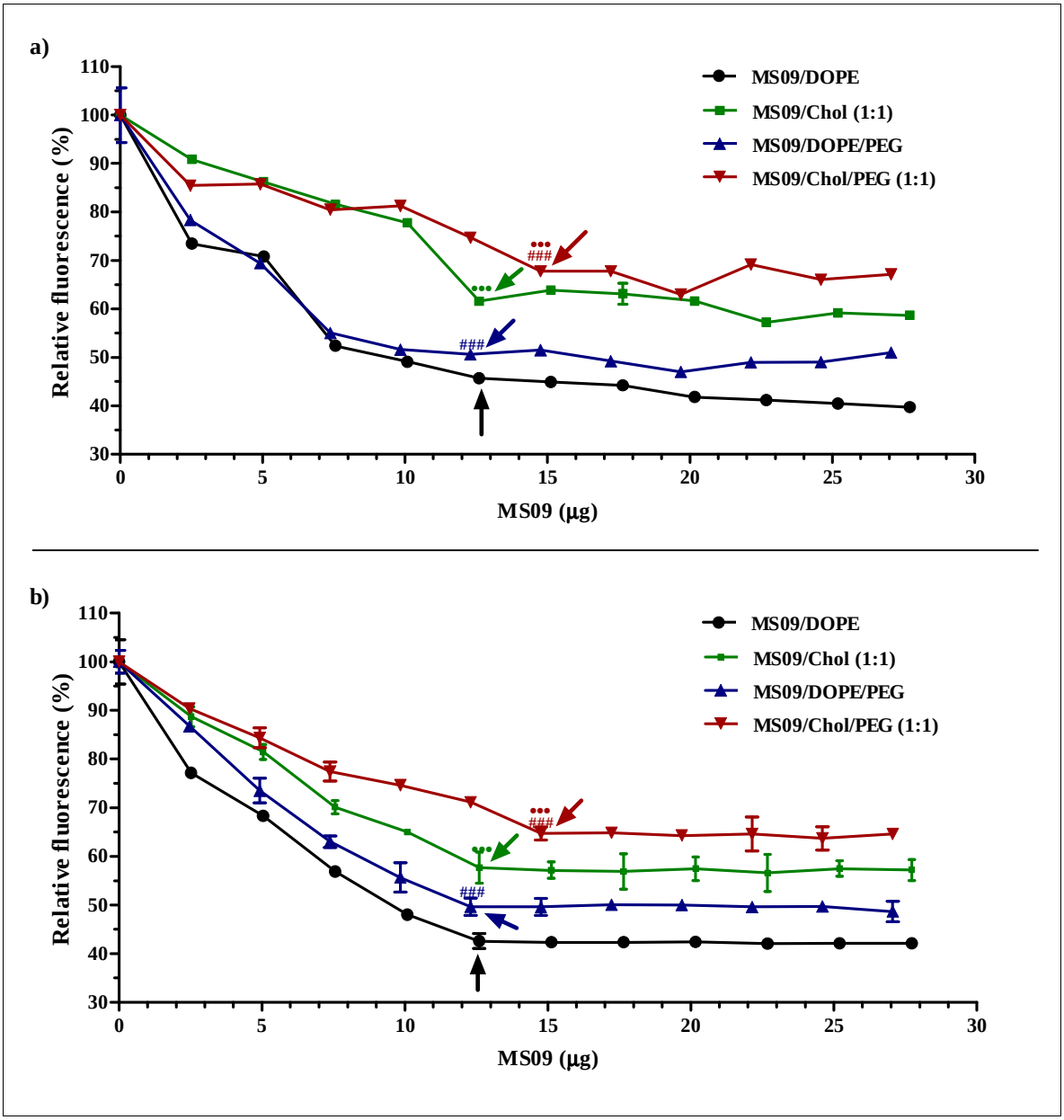

Figure 4.7: Dye displacement assays of liposome formulations. Incubation mixtures contained HBS, siRNA (1 µg) and either **a)** EtBr or **b)** SYBR Green II. Liposomes were introduced stepwise, in aliquots (1 µl). Data is shown as the mean ± SD (*n = 3*). The point of inflection i.e. maximum siRNA-binding, in each case, is shown by an arrow. $^{###}P < 0.001$ *vs.* non-pegylated counterpart, $^{•••}P < 0.001$ *vs.* DOPE-containing counterpart at point of inflection.

Table 4.1: Maximum dye displacement achieved by liposome formulations

Liposome formulation	Maximum dye displacement[a] (%)	
	EtBr[b]	SYBR Green II[b,c]
MS09/DOPE	54.3 ± 0.1	57.4 ± 1.6
MS09/Chol (1:1)	38.9 ± 0.8	42.3 ± 3.2
MS09/DOPE/PEG	49.4 ± 0.1	50.3 ± 1.8
MS09/Chol/PEG (1:1)	32.2 ± 0.1	35.3 ± 1.3

Notes:
[a]Maximum dye displacement (%) = 100 % – relative fluorescence (%) recorded at point of inflection
[b]Each value represents the mean ± SD (n = 3)
[c]In all instances, $P > 0.05$ for maximum dye displacement recorded as per SYBR Green II displacement *vs.* EtBr displacement

Table 4.2: Comparison of gel retardation and dye displacement assays in evaluating liposome siRNA-binding capability

Liposome formulation	Point of maximal siRNA-binding								
	Gel retardation assay[a]			Dye displacement assays					
				EtBr			SYBR Green II		
	Lipid:siRNA ($^{w}/_{w}$)	MS09:siRNA ($^{w}/_{w}$)	N/P ($^{+}/_{-}$)	Lipid:siRNA ($^{w}/_{w}$)	MS09:siRNA ($^{w}/_{w}$)	N/P ($^{+}/_{-}$)	Lipid:siRNA ($^{w}/_{w}$)	MS09:siRNA ($^{w}/_{w}$)	N/P ($^{+}/_{-}$)
MS09/DOPE	52.4:1	24.0:1	13.0:1	27.5:1	12.6:1	6.8:1	27.5:1	12.6:1	6.8:1
MS09/Chol (1:1)	32.2:1	20.0:1	10.8:1	20.3:1	12.6:1	6.8:1	20.3:1	12.6:1	6.8:1
MS09/DOPE/PEG	56.8:1	24.0:1	13.0:1	29.1:1	12.3:1	6.7:1	29.1:1	12.3:1	6.7:1
MS09/Chol/PEG (1:1)	50.3:1	28.0:1	15.2:1	26.5:1	14.8:1	8.0:1	26.5:1	14.8:1	8.0:1

Note:
[a]The point of maximal-binding reported is as per densitometric analysis of agarose gels

Often, dye displacement assays are performed in conjunction with gel retardation assays to provide supporting information (Dorasamy *et al*., 2012, Naicker *et al*., 2014, Singh and Ariatti, 2006). However, in this study, the assays were in poor agreement. Table 4.2 shows that MS09:siRNA ($^{w}/_{w}$) ratios at which maximum siRNA-binding was obtained by gel retardation were roughly twice those obtained by dye displacement. This discrepancy, as well as the apparent incomplete siRNA-binding observed by gel retardation, may be accounted for by the fact that siRNA can be coaxed off a fully-formed nanoparticle under conditions of electrophoresis, due to weak siRNA-carrier interactions (Hattori *et al*., 2013, Hattori *et al*., 2014). Therefore, according to Hattori and colleagues (2013), it can be accepted that siRNA lipoplexes are fully-formed at MS09:siRNA ($^{w}/_{w}$) ratios above that at which maximum dye displacement was recorded. Nonetheless, both assays showed similar trends in the comparative siRNA-binding capabilities of the four formulations i.e.
MS09/DOPE > MS09/DOPE/PEG > MS09/Chol (1:1) > MS09/Chol/PEG (1:1).

The aforementioned comparative siRNA-binding capabilities were further corroborated by considering the effect of increasing ionic strength on liposome-siRNA interactions (Figure 4.8). Given that the interaction between siRNA and cationic liposomes is electrostatic, excess counterions in solution disturbs this association and causes release of siRNA. siRNA release was monitored, through its interaction with the SYBR Green II dye, as an increase in fluorescence; and the ability of lipoplexes to resist destabilisation by NaCl was taken as a measure of the strength of the liposome-siRNA interaction. MS09/DOPE, which demonstrated the best binding affinity, required more NaCl than the other formulations to weaken the liposome-siRNA interaction, and released less siRNA at the highest concentration explored. Release of siRNA by MS09/Chol (1:1) and MS09/DOPE/PEG formulations was initiated at the same point i.e. 320 mM NaCl. However, the extent of lipoplex destabilisation at this point, as evidenced by the difference in relative fluorescence increase, was greater ($P < 0.05$) with MS09/Chol (1:1); and this indicates a comparatively weaker association with siRNA. As expected, the MS09/Chol/PEG (1:1) formulation, which showed the weakest siRNA-binding capability, was least tolerant of increasing ionic strength.

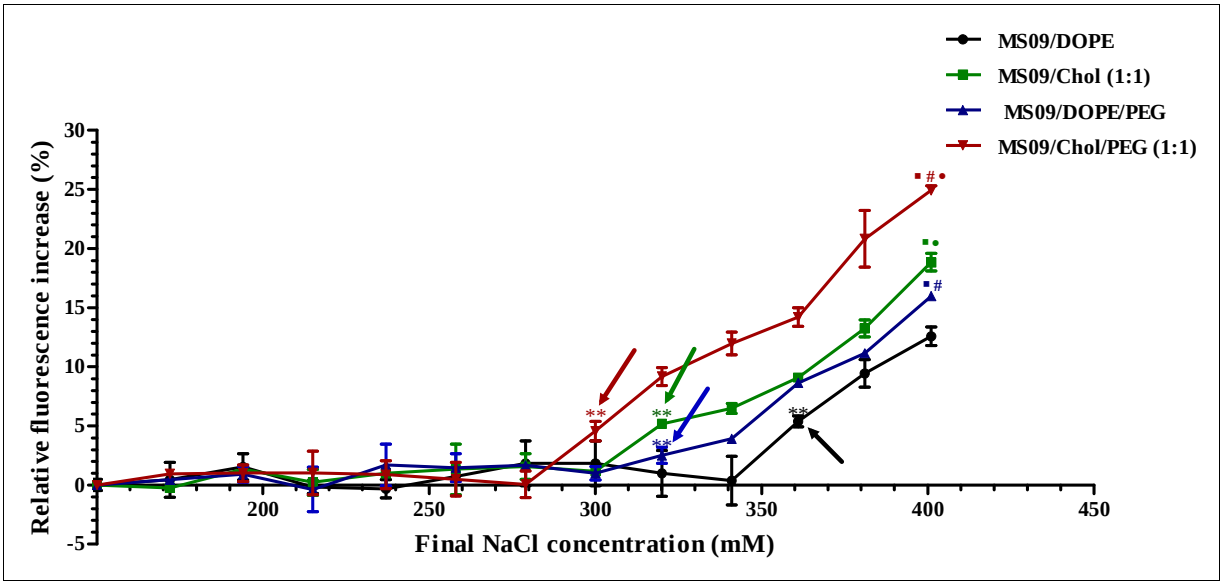

Figure 4.8: The effect of increasing ionic strength on liposome-siRNA interactions. Changes in fluorescence were monitored after stepwise addition of 5 M NaCl to a mixture of SYBR Green II and lipoplexes in HBS. Lipoplexes were assembled at the following MS09:siRNA ($^{w}/_{w}$) ratios: MS09/DOPE, 12.6:1; MS09/Chol (1:1), 12.6:1; MS09/DOPE/PEG, 12.3:1; and MS09/Chol/PEG (1:1), 14.8:1. Each point represents the mean ± SD (n = 3). A significant increase in relative fluorescence compared with the initial SYBR Green II-lipoplex mixture at 150 mM NaCl was taken as the point at which lipoplex destabilisation was initiated, and is indicated by an arrow. $^{**}P < 0.01$ *vs*. relative fluorescence increase at 150 mM NaCl; $^{▪}P < 0.05$ *vs*. MS09/DOPE, $^{\#}P < 0.05$ *vs.* non-pegylated counterpart, $^{•}P < 0.05$ *vs.* DOPE-containing counterpart, at 400 mM NaCl.

Consistent with data obtained in related studies (Daniels *et al*., 2013, Zhang *et al*., 2010), all assays reported thus far show that pegylation of liposomes reduced siRNA-binding affinity. This is because, PEG chains, when tethered to the liposomal bilayer, may conceal cationic groups on the surface (Zhao and Song Zhuang, 2011), and this can impede the association with the siRNA molecules. In fact, Zhang and colleagues (2010) showed that the incorporation of as little as 1 mol % PEG with a DC-Chol/DOPE formulation, gave liposomes which did not completely retard the migration of siRNA on agarose gel.

Interestingly, replacing DOPE with Chol at the same molar ratio in MS09 formulations had a more profound effect on siRNA-binding than the incorporation of 2 mol % PEG. That is, the siRNA interaction with MS09/Chol (1:1) was weaker than that displayed by both MS09/DOPE and MS09/DOPE/PEG liposomes. It is possible that Chol may have induced arrangement of cytofectin molecules during vesicle formation, such that a greater number of cationic centres were positioned inwards rather than on the surface of the bilayer. A further explanation may arise

from the fact that Chol is a more rigid lipid than DOPE and results in liposomal bilayers that are less malleable. Therefore, during the process of lipoplex formation, the Chol-containing liposomes may not change conformation as easily as their DOPE-containing counterparts to completely encompass siRNA molecules. This could result in residual or poorly-associated siRNA that can easily migrate in an agarose gel or associate with an intercalating dye. In relation to this, an early study with DOTAP/Chol liposomes demonstrated that Chol widened the interlamellar spaces of the resultant lipoplexes and, as such, reduced the association with ASOs (Weisman *et al*., 2004).

However, a weak liposome-siRNA interaction does not necessarily imply that the formulation in question will perform poorly overall and does not provide sufficient grounds to prevent its further testing. In some instances, weakly bound siRNA may be more easily released from the lipoplex within the cell, to give better transfection activity - provided that the liposome can adequately protect its cargo, the lipoplex remains stable in circulation and has the appropriate physical characteristics to permit cellular entry, among other factors (Nguyen *et al*., 2008). For this reason, all four formulations were evaluated further. Prior to performing the siRNA-binding studies, the aim was to clearly establish the minimum amount of liposome required for total binding of a fixed amount of siRNA, and to apply this optimum MS09:siRNA ($^{w}/_{w}$) ratio to the subsequent experiments. To compensate for the lack of a clear end-point in the gel retardation assays, and its poor correlation with the fluorescence quenching experiments, it was decided that liposome-siRNA complexes prepared across a range of MS09:siRNA ($^{w}/_{w}$) ratios i.e. 12:1-32:1, encompassing end-points obtained with both gel retardation and dye displacement assays, would be evaluated further.

4.3 Lipoplex characterisation

Electron microscopy gave visual proof of the formation of liposome-siRNA complexes with all four formulations at all MS09:siRNA ($^{w}/_{w}$) ratios explored. Figures 4.9-4.12 show that, overall, lipoplexes assumed structures that were different from the liposomal vesicles shown in Figures 4.2a,b and 4.3a,b, and emphasise the heterogeneity of the liposome-siRNA complexes. This is a consequence of the way in which liposomes and siRNA assemble to form lipoplexes.

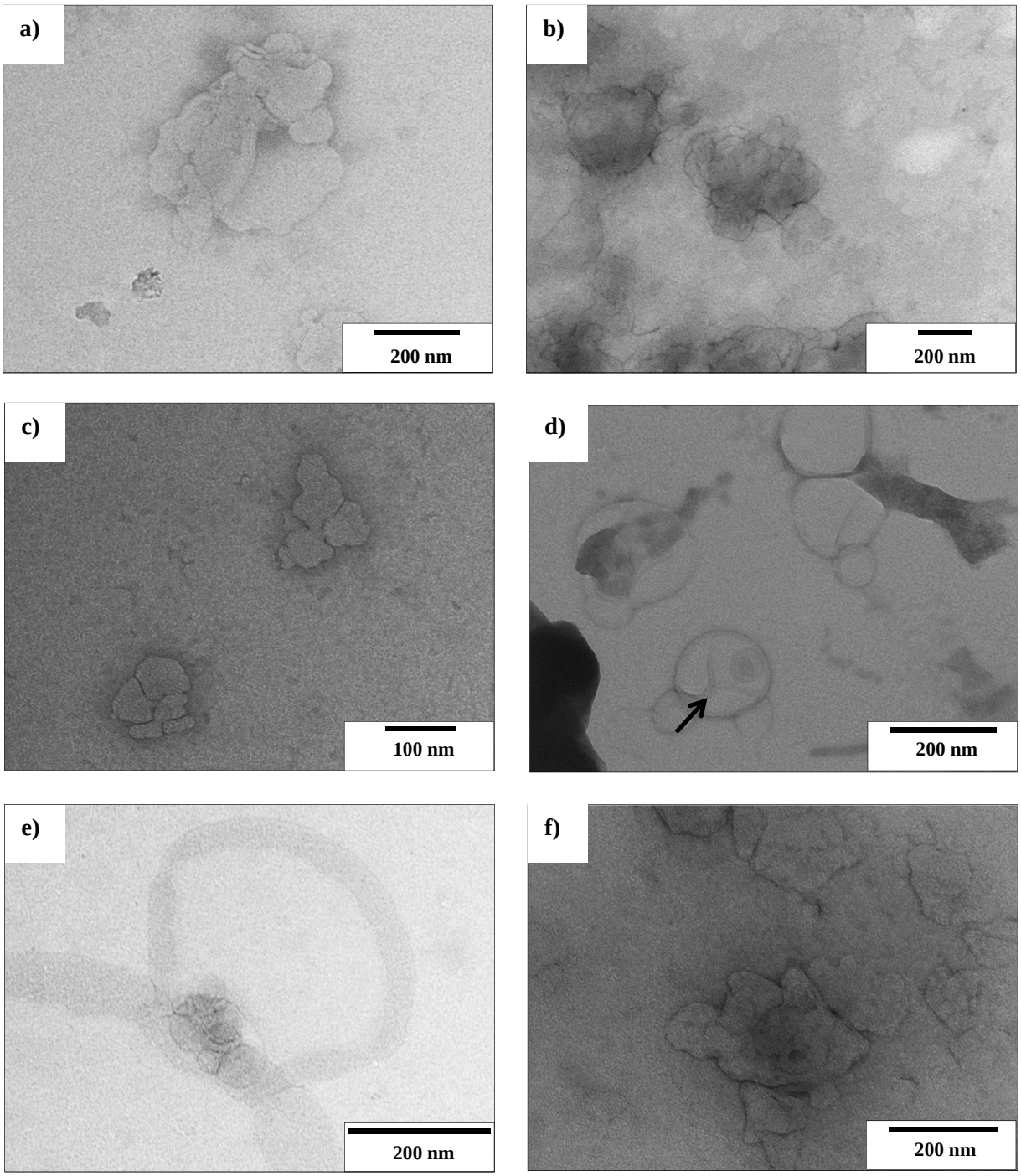

Figure 4.9: Transmission electron micrographs of MS09/DOPE lipoplexes assembled at MS09:siRNA ($^{w}/_{w}$) ratios of **a)** 12:1, **b)** 16:1, **c)** 20:1, **d)** 24:1, **e)** 28:1 and **f)** 32:1. The black arrow shows a bilamellar lipoplex structure.

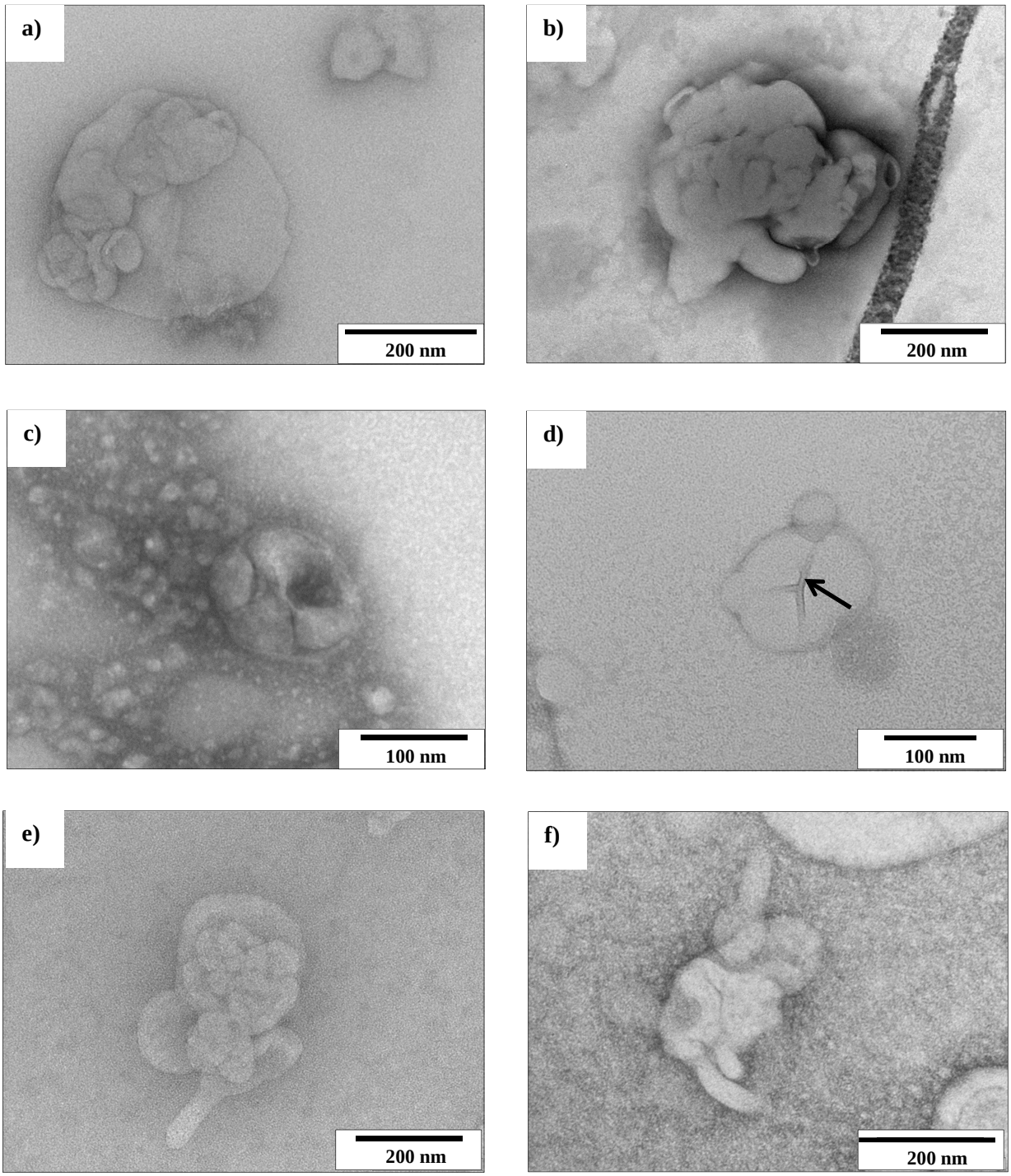

Figure 4.10: Transmission electron micrographs of MS09/Chol (1:1) lipoplexes assembled at MS09:siRNA ($^{w}/_{w}$) ratios of **a)** 12:1, **b)** 16:1, **c)** 20:1, **d)** 24:1, **e)** 28:1 and **f)** 32:1. The black arrow shows a bilamellar lipoplex structure.

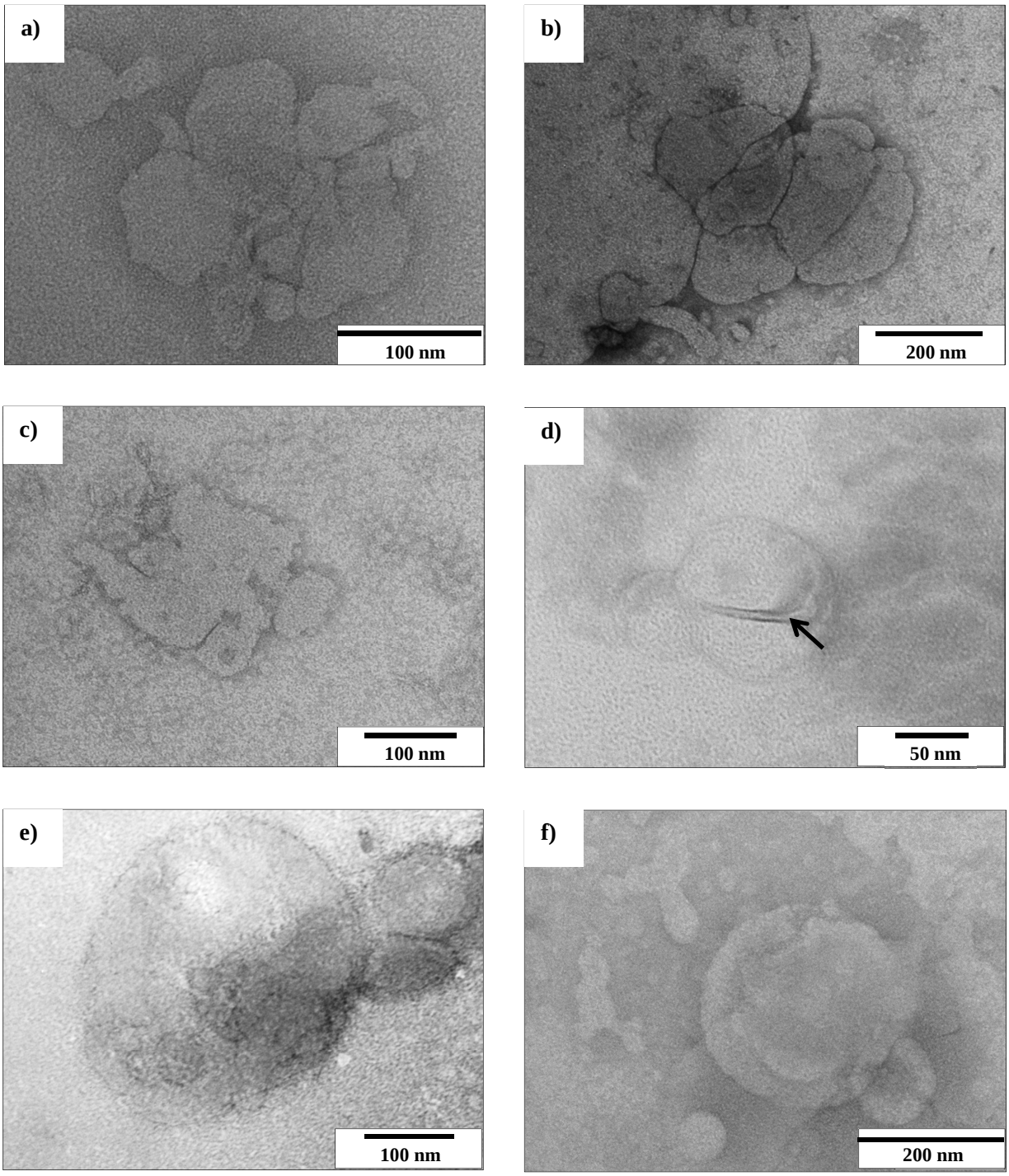

Figure 4.11: Transmission electron micrographs of MS09/DOPE/PEG lipoplexes assembled at MS09:siRNA ($^{w}/_{w}$) ratios of **a)** 12:1, **b)** 16:1, **c)** 20:1, **d)** 24:1, **e)** 28:1 and **f)** 32:1. The black arrow indicates a bilamellar lipoplex structure.

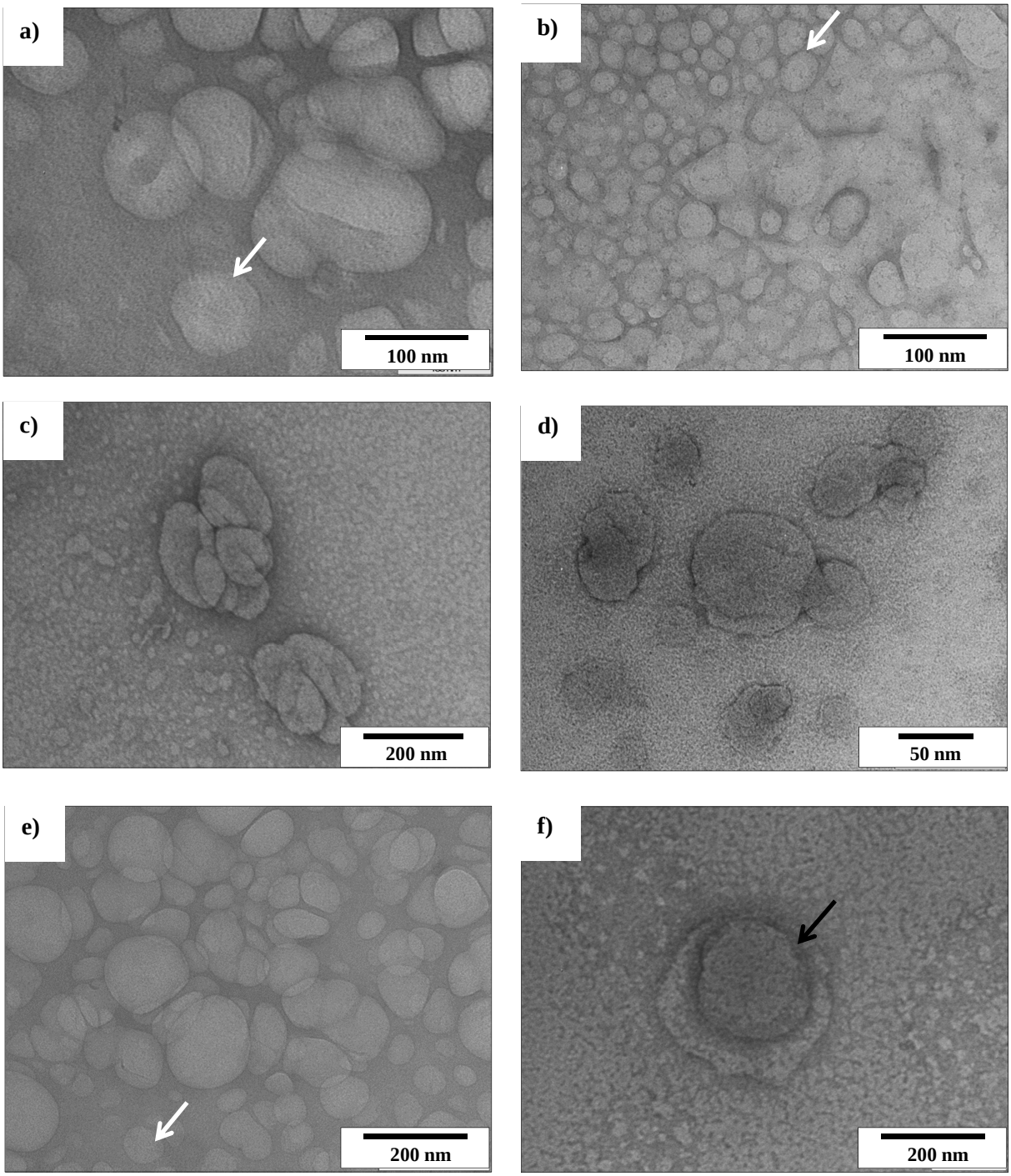

Figure 4.12: Transmission electron micrographs of MS09/Chol/PEG (1:1) lipoplexes assembled at MS09:siRNA ($^{w}/_{w}$) ratios of **a)** 12:1, **b)** 16:1, **c)** 20:1, **d)** 24:1, **e)** 28:1 and **f)** 32:1. The white and black arrows indicate "free" vesicles and bilamellar lipoplex structures, respectively.

Research by Desigaux *et al.* (2007) and Geusens *et al*. (2009) suggested that, during lipoplex formation, the siRNA is sandwiched between successive lipid bilayers to form multilayered structures. Bilamellar structures were observed with all formulations at high MS09:siRNA ($^{w}/_{w}$) ratios (Figures 4.9d, 4.10d, 4.11d, 4.12f). However, the most prominent siRNA lipoplex structures noted in this study were irregular aggregates of smaller vesicles (for example, Figures 4.9a,b,c) that were similar to those reported by others (Daniels *et al*., 2013, Dorasamy *et al*., 2012).

Structures that resembled liposomal vesicles were observed in some MS09/Chol/PEG (1:1) lipoplex suspensions (Figure 4.12a,b,e). While it is possible for free liposomes to exist when the relative proportion of lipid to nucleic acid is high in a lipoplex suspension (Xu *et al*., 1999), this does not account for their presence at the lower MS09:siRNA ($^{w}/_{w}$) ratios of 12:1 and 16:1. A possibility was presented by Khatri and coworkers (2014) who showed that pegylated DOTAP/DOPE/hydrogenated soybean phosphatidylcholine/Chol liposomes permitted only a single monolayer interaction with siRNA and assumed spherical, unilamellar structures. This indication of surface-attachment of siRNA on the liposomal bilayer is additional proof of the weak binding interaction between MS09/Chol/PEG (1:1) liposomes and siRNA.

Collectively, the aforementioned published works show that differences in liposome composition, the behavior of individual lipids and the relative proportions of liposome and siRNA are important factors governing the structures that are formed when liposomes associate with siRNA. Consistent with these studies, the lipoplex morphology observed varied according to the liposome formulation involved and the MS09:siRNA ($^{w}/_{w}$) ratio at which the lipoplexes were assembled.

Besides lipoplex morphology, size and zeta potential represent two important physical parameters by which lipoplexes are characterised. As discussed in a review of lipid-based siRNA delivery by Schroeder and colleagues (2010) , these properties are valuable as determinants of lipoplex performance because they impact on the circulation time of lipoplexes in the body, accumulation at target sites, interaction with cells, the efficacy of cellular uptake and, ultimately, gene silencing activity. The size and zeta potential of lipoplexes as measured by Z-NTA is represented in Figure 4.13a,b.

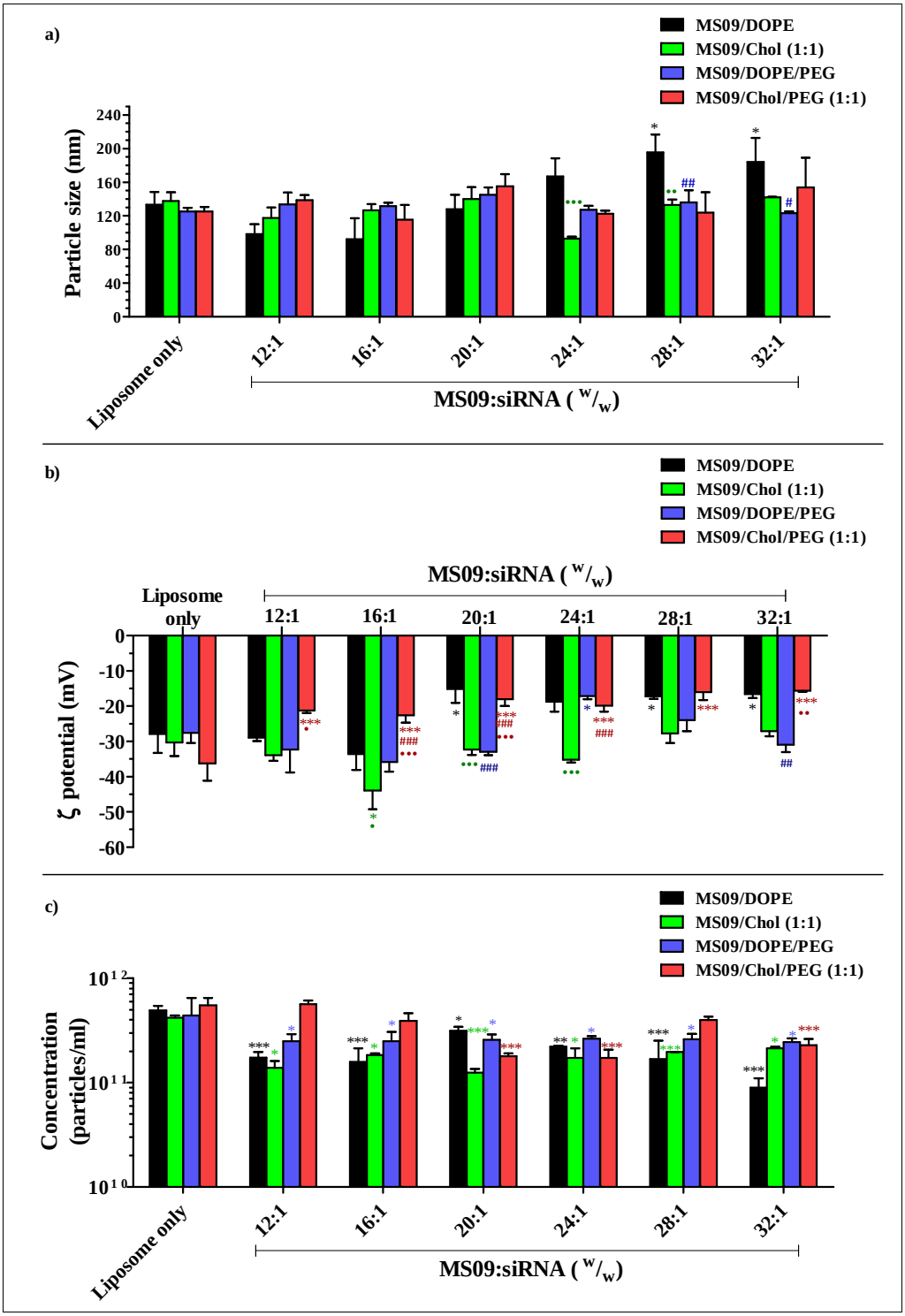

Figure 4.13: Characterisation of lipoplexes by Z-NTA. The **a)** size, **b)** ζ potential and **c)** concentration of lipoplexes assembled at varying MS09:siRNA ($^{w}/_{w}$) ratios was measured. For comparative purposes, liposome concentrations plotted represent vesicle concentrations in incubation mixtures (10 µl) for the preparation of lipoplex suspensions. Each column represents the mean ± SD (n =3). *P < 0.05, **P < 0.01, ***P < 0.001 *vs.* Liposome only; $^{\#}P$ < 0.05, $^{\#\#}P$ < 0.01, $^{\#\#\#}P$ < 0.001 *vs.* non-pegylated counterpart; $^{\bullet}P$ < 0.05, $^{\bullet\bullet}P$ < 0.01, $^{\bullet\bullet\bullet}P$ < 0.001 *vs.* DOPE-containing counterpart.

The association of liposomal vesicles and change in conformation of cationic bilayers upon siRNA binding often produces complexes that are larger in size than the free liposomal vesicles (Desigaux *et al*., 2007, Geusens *et al*., 2009, Weisman *et al*., 2004). While cryo-TEM gave visual proof of changes in vesicle morphology upon lipoplex formation, all lipoplexes were not significantly different in size from the parent liposomal vesicles, with the exception of MS09/DOPE lipoplexes at MS09:siRNA ($^{w}/_{w}$) ratios of 28:1 and 32:1. This could be ascribed to the particle sizing technique employed in this study. In general, earlier studies relied on light scattering techniques which are known to give size measurements that are more representative of larger particles in a sample. This is especially true of samples with high heterogeneity, such as lipoplexes. NTA, however, which provides number-weighted measurements, is free from such bias and better suited for determining lipoplex size (Wilson and Green, 2017).

Although the addition of siRNA to liposomes, in most instances, did not appear to alter particle size, it did have a bearing on nanoparticle concentration (Figure 4.13c). The value of nanoparticle concentration as an additional parameter for the characterisation of lipid-based nanoparticles was recently demonstrated (de Morais Ribeiro *et al*., 2018). In this study, noticeable differences between the concentration of lipoplex and parent liposome suspensions confirmed an interaction between liposomes and siRNA, and provided information that correlates with cryo-TEM characterisation. A significant reduction in particle number upon introduction of siRNA to a fixed volume of liposome suggests the involvement of several vesicles in the formation of a single siRNA lipoplex (Table B4, Appendix B). This supports the observed morphologies of lipoplexes as composites of smaller vesicles and bilamellar structures. The only instances in which lipoplex concentration was statistically similar to that of the parent liposome, were MS09/Chol/PEG (1:1) complexes at MS09:siRNA ($^{w}/_{w}$) ratios of 12:1, 16:1 and 28:1. Interestingly, these were the lipoplex suspensions in which “free” vesicles were evident by cryo-TEM (Figure 4.12a,b,e). Concentration measurements of these suspensions support the previously mentioned possibility of large numbers of single vesicles to which siRNA is likely to be surface-attached.

It is clear that NTA and cryo-TEM provided complementary data towards complete characterisation of lipoplexes. However, representations of particle size were often in poor agreement. Some representative lipoplexes appeared either larger (for example, Figures 4.9a,b;

4.10a,b) or smaller (for example, Figure 4.12d) than the NTA measurements indicate. This is mainly because TEM gives a limited view of the sample. Even multiple images of a sample at different positions on a TEM grid may fail to provide as accurate a representation of particle size as NTA, which resolves and accounts for individual particles. Furthermore, it is possible for samples to either spread out or shrink on the grid during sample preparation (Almgren *et al*., 2000). Although cryo-TEM does provide very useful information regarding the structure of siRNA lipoplexes (Kuntsche *et al*., 2011), particle sizes are likely to be inaccurately represented if a study relies on cryo-TEM alone (Gaumet *et al*., 2008).

All lipoplexes were below 200 nm in size (Figure 4.13a). More specifically, all lipoplexes were smaller than 150 nm with the exception of MS09/DOPE lipoplexes assembled at MS09:siRNA ($^{w}/_{w}$) ratios of 24:1-32:1, and MS09/Chol/PEG (1:1) lipoplexes at the MS09:siRNA ($^{w}/_{w}$) ratio of 20:1. This is of importance for passive targeting of tumour cells via the enhanced permeability and retention (EPR) effect, a strategy that takes advantage of the irregularities of tumour vasculature for the accumulation of therapeutic nanoparticles. This approach is primarily based on designing nanoparticles of suitable size such that they will not pass through the tight junctions of normal blood vessels, but can access tumour cells by passing through their more permeable vasculature, and are retained because of reduced lymphatic drainage (Greish, 2010). In a review of liposome-based systems for systemic delivery, Buyens and coworkers (2012) stated that lipoplexes greater than 150 nm can easily accumulate in tumours. In a more recent publication, 200 nm was reported as the general upper limit for tumour cell entry via EPR (Kobayashi *et al*., 2014). While, this augurs well for the performance of these lipoplexes, their ability to maintain a small size in a biological system is a significant factor governing their overall efficacy.

Like the free liposome suspensions, all lipoplexes displayed negative zeta potential which ranged from –16 mV to -44 mV (Figure 4.13b). Although it is accepted that the net positive charge of lipoplexes allows for binding to anionic membrane-associated proteoglycans to initiate cellular uptake (Mislick and Baldeschwieler, 1996), it is also possible for siRNA lipoplexes with negative zeta potential to enter cells and successfully facilitate gene silencing. Resina and colleagues (2009) showed that cells take up anionic lipoplexes through an energy independent pathway and hypothesised that this occurred via lipid exchange at the plasma membrane. More

recently, however, Kapoor and colleagues showed that siRNA lipoplexes with negative zeta potentials were internalised by breast cancer cells via endocytosis and, that cellular uptake was dependent upon the activity of microtubules and actin (Kapoor and Burgess, 2013, Kapoor and Burgess, 2012). In fact, negatively charged lipid-based siRNA nanocomplexes may be useful as they can avoid aggregation through interaction with erythrocytes and anionic proteins in biological fluids, and have also been associated with lower toxicities than complexes that carry a net positive charge (Hattori *et al*., 2014, Tagalakis *et al*., 2014). Hence, the physical properties displayed by the lipoplexes under investigation thus far warrant further assessment.

4.4 Assessment of batch-to-batch variation

Lipid-film hydration is among the simplest methods by which liposomes can be prepared (Zhang, 2017). To assess whether or not this method can yield liposome suspensions of consistent quality, the effect of batch-to-batch variation on the physical characteristics and siRNA-binding ability of liposomes was studied. Z-NTA data (Figure 4.14) showed that there was no significant difference in the size, zeta potential and vesicle concentration of independently prepared batches of the same liposome formulation. Figure 4.15 shows that maximum dye displacement and the MS09:siRNA ($^{w}/_{w}$) ratio at which this was achieved was consistent across all three batches of a given formulation. The results suggest that the pegylated and non-pegylated MS09/DOPE and MS09/Chol (1:1) formulations can be reproducibly prepared by lipid-film hydration under standard laboratory conditions. Importantly, this confirms that data generated from the preparation of additional liposomes, as was required during the latter stages of this study, was not influenced by physical changes in liposomes and/or siRNA-binding.

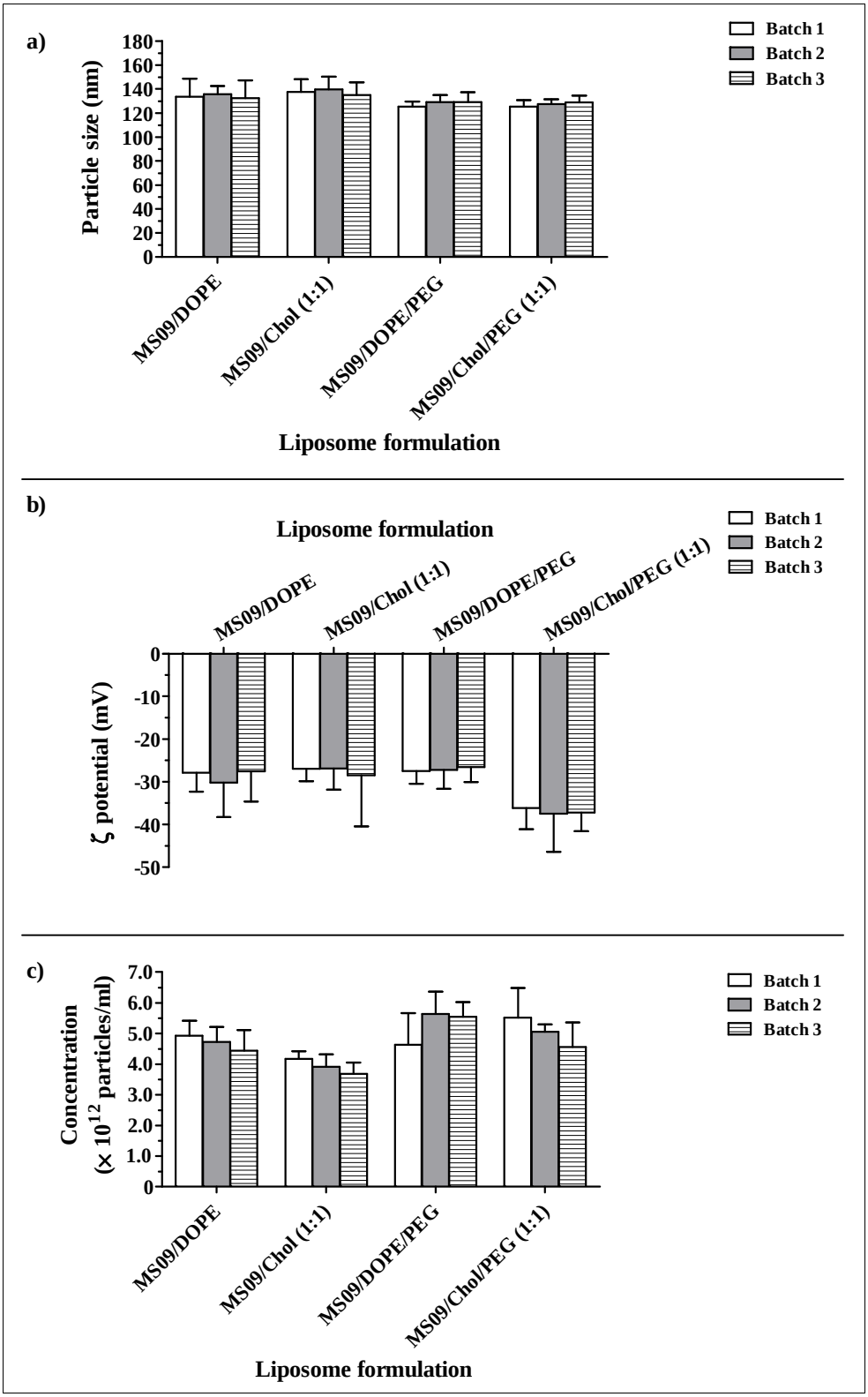

Figure 4.14: Effect of batch-to-batch variation on vesicle **a)** size, **b)** ζ potential and **c)** concentration of liposome suspensions. Each column represents the mean ± SD (n = 3). In all instances, $P > 0.05$ with respect to the following: Batch 2 and 3 *vs.* Batch 1, and Batch 3 *vs.* Batch 2.

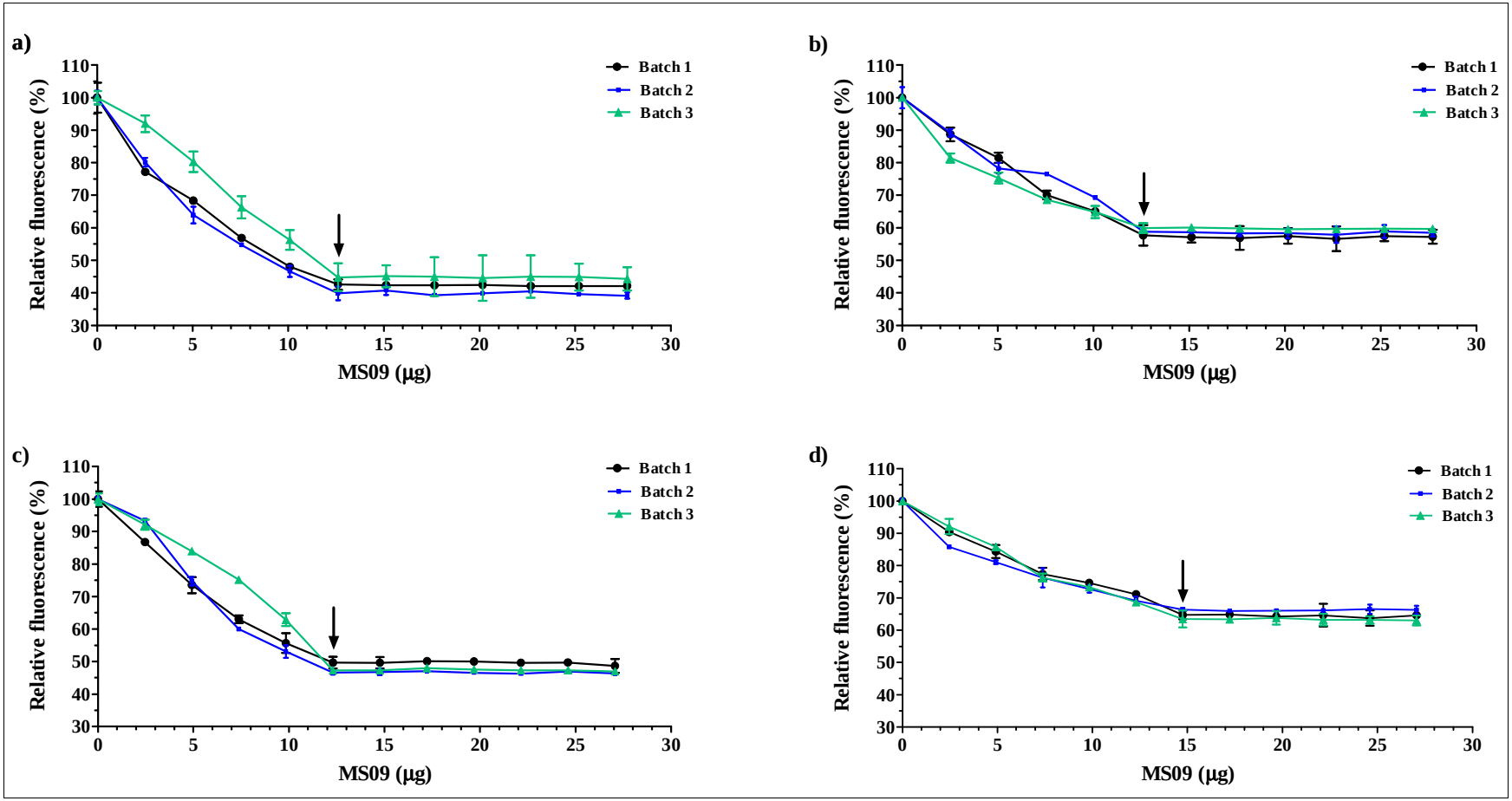

Figure 4.15: Effect of batch-to-batch variation on siRNA-binding capability of liposomes **a)** MS09/DOPE, **b)** MS09/Chol (1:1), **c)** MS09/DOPE/PEG and **d)** MS09/Chol/PEG (1:1). siRNA-binding was assessed by the SYBR Green dye displacement assay. Each point represents the mean ± SD (n = 3). In each case, an arrow indicates the point of inflection. $P > 0.05$ with respect to the following: Batch 2 and 3 *vs.* Batch 1, and Batch 3 *vs.* Batch 2, at point of inflection.

4.5 Liposome storage stability studies

In a recent review of liposomes for drug delivery, Yadav *et al*. (2017) commented that the shelf-life and stability of a liposome suspension has a bearing on its suitability as a pharmaceutical agent. Often, in order to achieve a thermodynamically favourable state, liposomal vesicles aggregate when stored, and this can reduce therapeutic efficacy. For this reason, the effect of the routine storage conditions employed in this study on the physical characteristics and siRNA-binding abilities of liposome suspensions was investigated. No significant changes in vesicle size (Figure 4.16a), zeta potential (Figure 4.16b) or concentration (Figure 4.16c) were noted after a 5 month-long storage at 4 ˚C. Furthermore, the siRNA-binding affinity of each formulation (Figure 4.17) was not appreciably altered. The results confirm that all four liposome suspensions remained stable for at least 5 months when stored in the refrigerator.

However, some changes did occur after a further 5 months at 4 ˚C with the MS09/DOPE formulation. A significant increase in the size of MS09/DOPE vesicles was observed after 10 months, and this was associated with a change in zeta potential (less negative and closer to 0). This evidence of aggregation was further corroborated by a drop in concentration. This is consistent with the inverse relationship between size and nanoparticle concentration validated by de Morais Ribeiro *et al*. (2018) when monitoring the stability of lipid-based nanoparticles.

Although the above-mentioned changes did not affect the overall maximum dye displacement attainable by the MS09/DOPE formulation, a shift in the point of inflection was observed i.e. more liposome was required to achieve the original degree of dye displacement (Figure 4.17a). This is a likely consequence of vesicle aggregation. Due to the fact that multiple small liposomes collectively provide a larger surface area than when fused as a single large liposome, it is possible that vesicle aggregation may have reduced the surface area for siRNA-binding. This could account for the larger quantity of liposome required to bind the same amount of siRNA as the freshly prepared suspension.

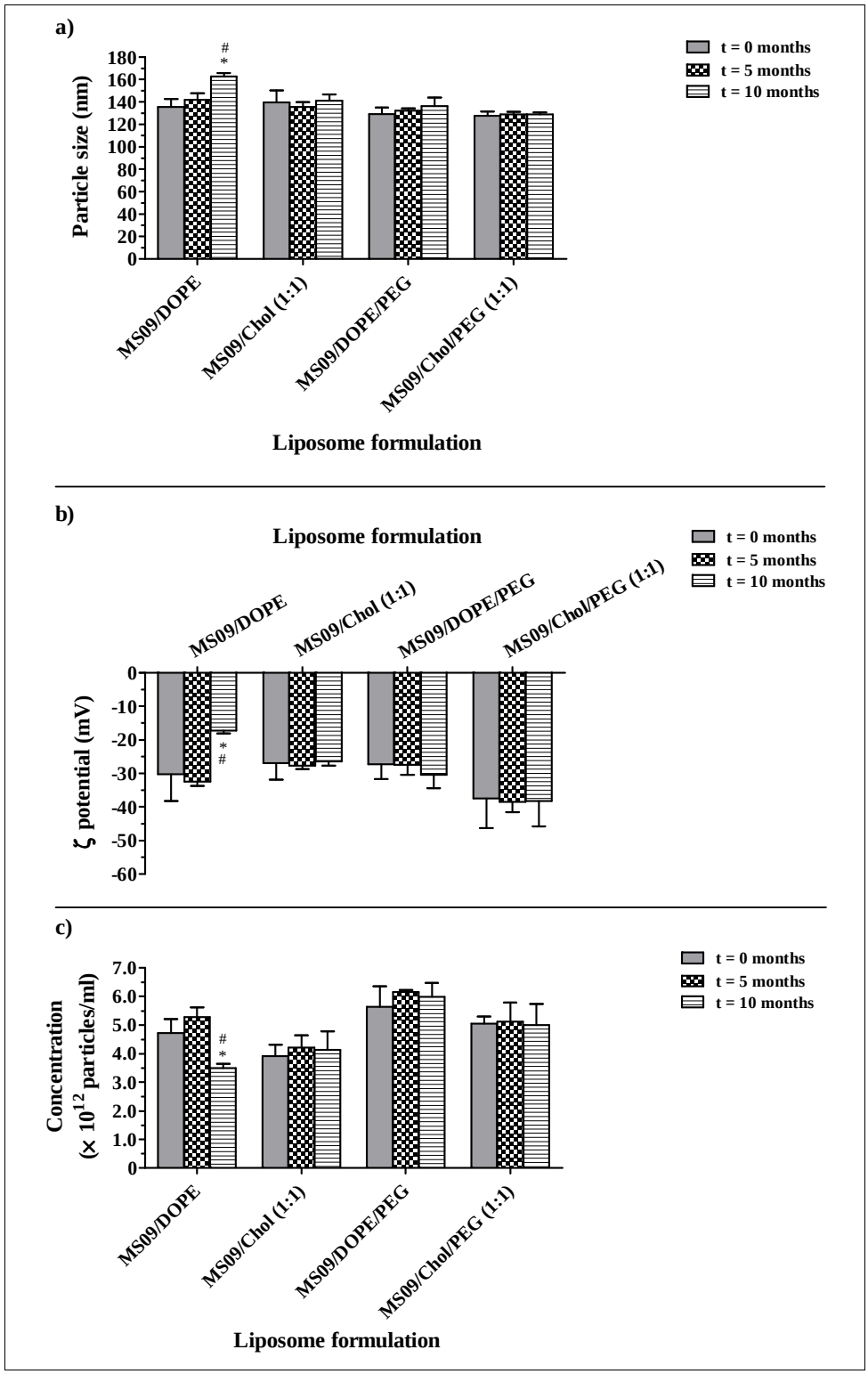

Figure 4.16: Effect of long-term storage at 4 ˚C on vesicle **a)** size, **b)** ζ potential and **c)** concentration of liposome suspensions. Each column represents the mean ± SD (n = 3). $^{*}P < 0.05$ *vs.* t = 0 months; $^{\#}P < 0.05$ *vs.* t = 5 months.

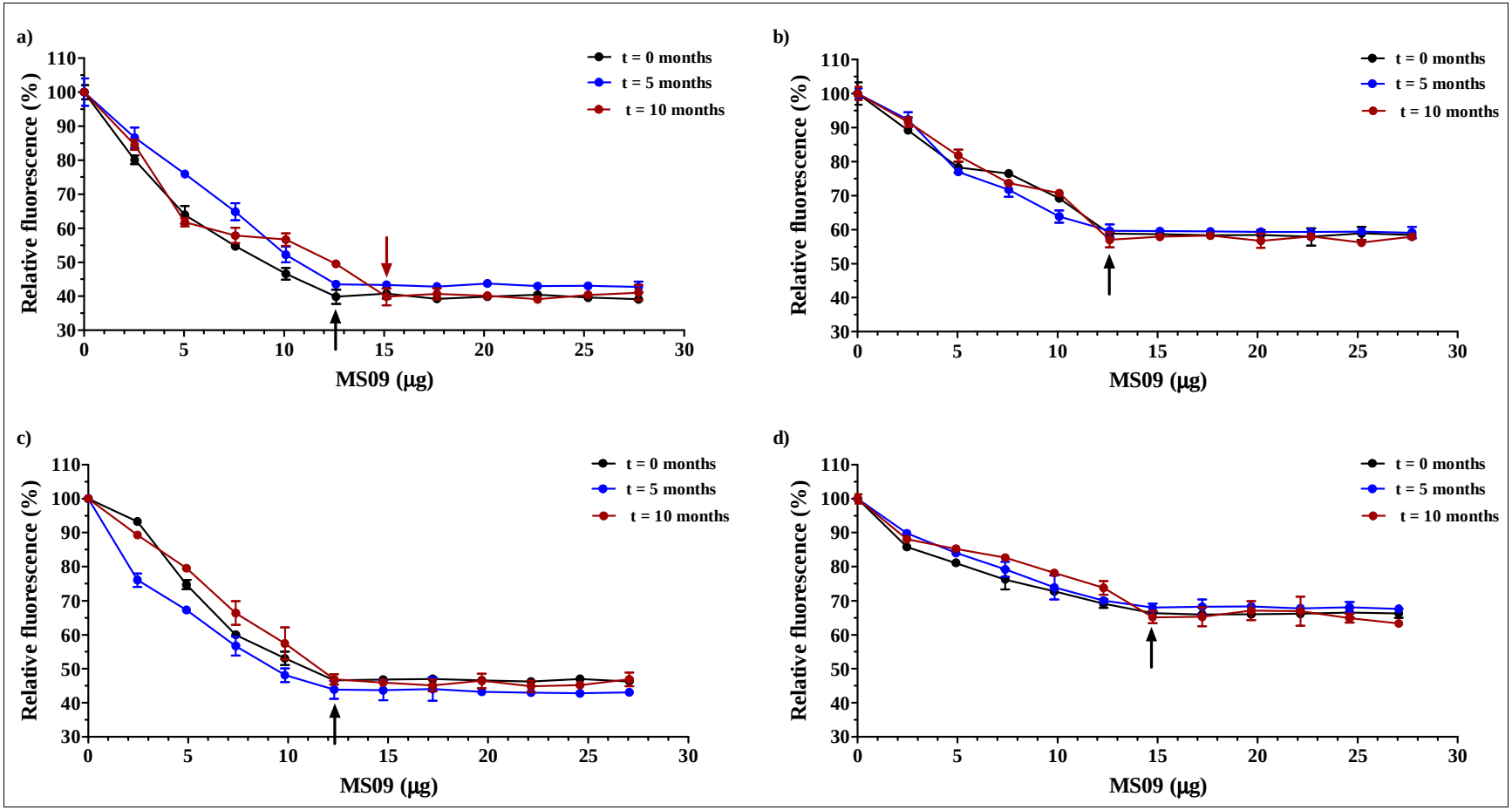

Figure 4.17: Effect of long-term storage at 4 ˚C on siRNA-binding ability of liposomes **a)** MS09/DOPE, **b)** MS09/Chol (1:1), **c)** MS09/DOPE/PEG and **d)** MS09/Chol/PEG (1:1). siRNA-binding was assessed by the SYBR Green dye displacement assay. A black arrow shows the point of inflection for freshly prepared (t = 0 months) liposome suspensions in each instance. Any change in the point of inflection is highlighted by a red arrow. Results are presented as the mean ± SD (*n* = 3). $P > 0.05$ with respect to the following t = 5 and 10 months *vs*. t = 0 months, and t = 5 months *vs*. t = 10 months, at point of inflection.

In contrast, extended storage at 4 ˚C did not significantly affect the physical characteristics or siRNA-binding capabilities of both pegylated formulations and the non-pegylated Chol-containing formulation. It appears that substitution of DOPE with Chol had a similar effect on maintaining stability of MS09 liposomes as 2 % pegylation within the monitored timespan.

On a positive note, NTA confirmed that no degradation, as would have been shown by a decrease in concentration without an accompanied increase in particle size, (de Morais Ribeiro *et al*., 2018) of vesicles in any of the formulations occurred during storage.

4.6 Nuclease protection assays

Attempts at lipid-mediated siRNA delivery are often frustrated by adverse interactions with serum. To this end, the siRNA-protecting capability of each liposome preparation was evaluated after a 4 h long incubation in serum, at the concentration used in routine cell culture, at physiological temperature. siRNA was released with a detergent treatment and its integrity on agarose gels gave an indication of the degree of protection afforded by each liposome formulation. Figure 4.18 shows that, while naked siRNA was entirely degraded under the experimental conditions employed (lane 2 of each gel), intact siRNA bands, less intense than the untreated control, were clearly visible in all instances. This shows that all formulations partially protected siRNA at the respective MS09:siRNA ($^{w}/_{w}$) ratios explored.

siRNA released from non-pegylated liposomes migrated as a single band and to the same extent in the gel as untreated siRNA (Figure 4.18a,b). However, in gels showing the serum nuclease protection capability of pegylated liposomes (Figure 4.18c,d) two distinct siRNA bands, one with slower mobility and markedly less intense than native siRNA, were noted. Zhang *et al*. (2006) observed a similar phenomenon following SDS-mediated release of siRNA from a pegylated liposome formulation. According to this group, the slower moving band should be less negatively charged or have higher molecular weight than native siRNA. Two possibilities were put forward. Firstly, in the event that detergent treatment did not completely destroy the lipid component of lipoplexes, siRNA could bind to a few intact cytofectin molecules. Secondly, since SDS is anionic it may bind to cationic lipids in aqueous solution, and a triple complex made up of siRNA, SDS and remaining cytofectin molecules could account for the appearance of such a band on the gel.

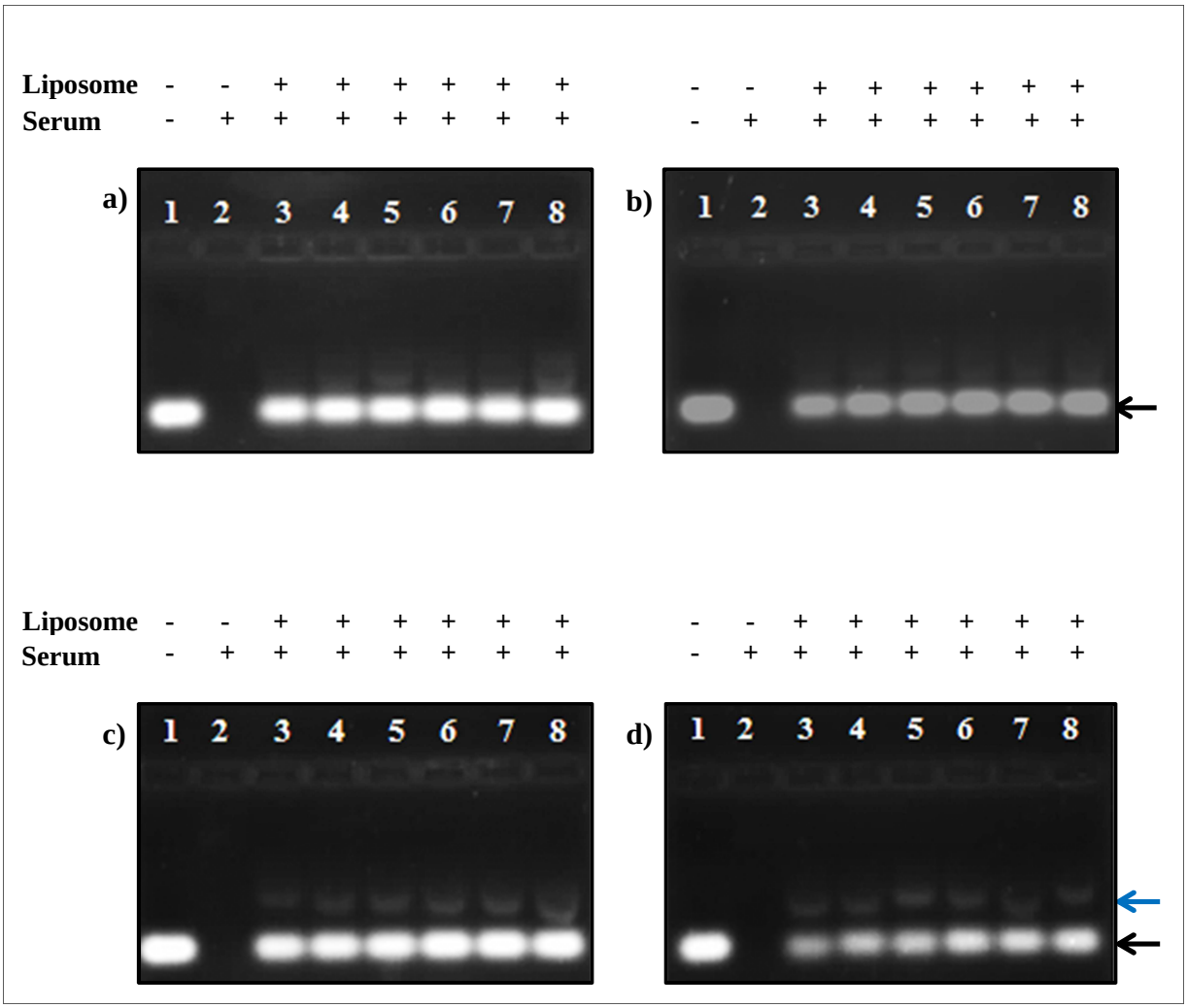

Figure 4.18: Nuclease protection capability of **a)** MS09/DOPE, **b)** MS09/Chol (1:1), **c)** MS09/DOPE/PEG and **d)** MS09/Chol/PEG (1:1) liposomes in FBS at 37 ˚C for 4 h. In each gel, *lane 1* contained undigested siRNA, *lane 2*, serum-digested siRNA and *lanes 3-8*, serum-exposed lipoplexes at varying MS09:siRNA ($^{w}/_{w}$) ratios (12:1, 16:1, 20:1, 24:1, 28:1 and 32:1, respectively). Intact siRNA and a second siRNA band with reduced mobility are shown by black and blue arrows, respectively.

Densitometric analysis of gels (Figure 4.19) gave further insight into the comparative siRNA-protecting capabilities of liposomes.

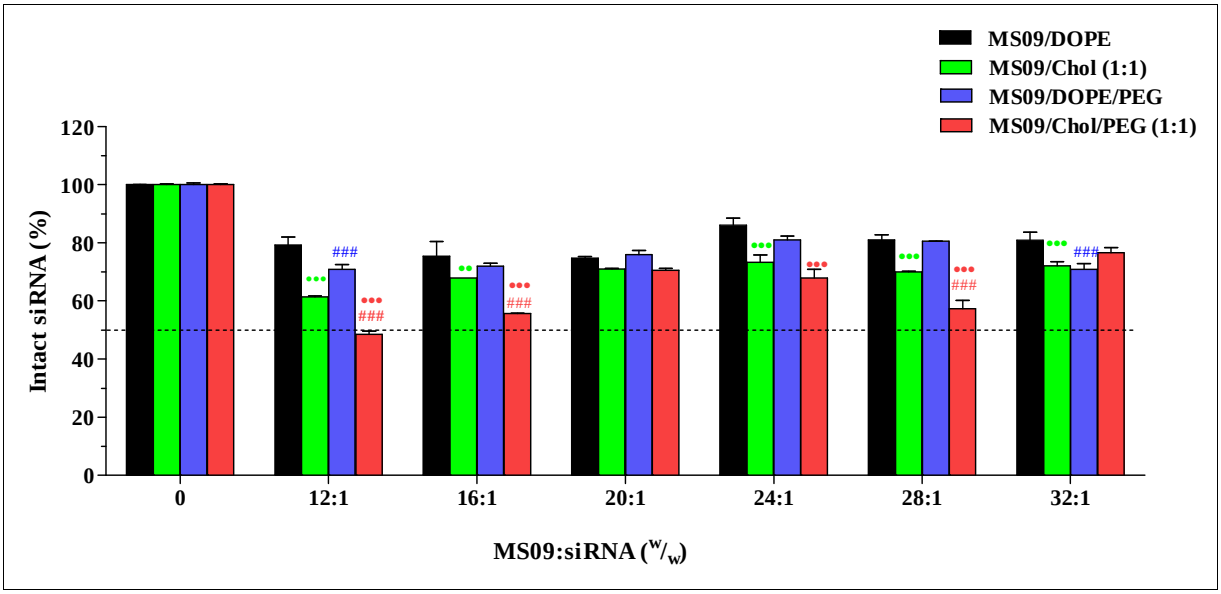

Figure 4.19: siRNA-protecting capacity of liposomes in the presence of 10 % serum, at 37 ˚C for 4 h. Intact siRNA associated with lipoplexes was quantified following nuclease digestion assays, and expressed as a percentage of untreated siRNA. Data is presented as the mean ± SD (n = 3). $^{###}P < 0.001$ *vs*. non-pegylated counterpart, $^{••}P < 0.01$, $^{•••}P < 0.001$ *vs*. DOPE-containing counterpart.

It was observed that individual liposome formulations achieved the best protection of siRNA (Table 4.3) at MS09:siRNA ($^{w}/_{w}$) ratios which gave lipoplexes with bilamellar structure (Figures 4.9d, 4.10d, 4.11d, 4.12f). This is consistent with the fact that siRNA concealed within stable lamellar structures is more likely to avoid interaction with serum than surface-bound siRNA (Khatri *et al*., 2014).

Table 4.3: MS09:siRNA ($^{w}/_{w}$) ratios at which liposomes attained maximum siRNA protection

Liposome formulation	**MS09:siRNA ($^{w}/_{w}$)**	**siRNA protected[a] (%)**
MS09/DOPE	24:1	86 ± 3
MS09/Chol (1:1)	24:1	73 ± 3[c]
MS09/DOPE/PEG	24:1	82 ± 1[b]
MS09/Chol/PEG (1:1)	32:1	77 ± 2[b]

Notes:
[a]Each value represents the mean ± SD (n = 3)
[b]$P > 0.05$ *vs*. non-pegylated counterpart
[c]$P < 0.05$ *vs*. DOPE-containing counterpart

In contrast, the lowest siRNA protection efficiencies were recorded with structures that resembled free vesicles. These were the MS09/Chol/PEG (1:1) lipoplexes at MS09:siRNA ($^{w}/_{w}$)

ratios of 12:1, 16:1 and 28:1, which protected only 49, 56 and 57 % siRNA, respectively. This is consistent with the previously mentioned weak, surface-association of siRNA and liposomal vesicles prevalent at these ratios, given that the exposed siRNA is highly susceptible to nuclease attack (Khatri *et al*., 2014).

At the lowest MS09:siRNA ($^{w}/_{w}$) ratio explored, i.e. 12:1, the extent to which siRNA was protected by a given formulation correlates with the relative siRNA-binding affinities demonstrated in section 4.2. However, this relationship does not hold true at the higher ratios. In fact, maximum protection of siRNA achieved by the MS09/DOPE formulation at the MS09:siRNA ($^{w}/_{w}$) ratio of 24:1 was not significantly different from that achieved by MS09/DOPE/PEG liposomes at the same ratio. Similarly, the highest levels of intact siRNA maintained by MS09/Chol (1:1) and MS09/Chol/PEG (1:1) were comparable albeit at different ratios.

The results show that while pegylation of liposomes gave lower siRNA-binding affinity, it did not impact on the maximum siRNA-protecting capabilities attainable by these formulations, provided that due attention is paid to optimising the lipid:siRNA mixing ratio. Given that PEG chains prevent destabilisation of lipoplexes by acting as a barrier between the lipoplex and serum components, the effect of pre-pegylation at 2 mol % towards conferring stability in serum appears to compensate for the associated reduction in siRNA-binding.

The effect of substituting Chol with DOPE on the serum stability of MS09 formulations was also considered. Maximum intact siRNA of 73 % afforded by MS09/Chol (1:1) liposomes at the MS09:siRNA ($^{w}/_{w}$) ratio of 24:1 was significantly less than that of MS09/DOPE. Figure 4.6 of section 4.2 shows that, at this ratio, 25 % of siRNA was likely to be surface-associated, as it was so loosely bound that it was coaxed off during electrophoresis. Such siRNA is readily detached from the liposomal bilayer upon exposure to serum and is acted upon by nucleases (Buyens *et al*., 2008). However, differences in maximum siRNA protection achieved by MS09/Chol/PEG (1:1) and MS09/DOPE/PEG liposomes were not significant. Given that, according to the gel retardation pattern, only 60 % of siRNA appeared to have been bound by the MS09/Chol/PEG (1:1) formulation, the results imply that the PEG chains can shield even weakly associated siRNA. Hence, pegylation appears useful for maintaining siRNA-protecting

capabilities of liposomes in the presence of a substitution which, in this instance, reduces siRNA-binding and protection of MS09 liposomes when introduced alone.

Of relevance is the fact that maximum siRNA protection for DOPE-containing formulations was recorded at the MS09:siRNA ($^{w}/_{w}$) ratio at which siRNA was best retarded on agarose gel (Figure 4.6). Here lipoplexes capable of optimum siRNA-binding, were also capable of optimum protection within the range of MS09:siRNA ($^{w}/_{w}$) ratios explored. In the case of Chol-containing formulations, lipoplexes assembled at MS09:siRNA ($^{w}/_{w}$) higher than that at which the best retardation of siRNA was achieved, gave the best protection of siRNA. This can be ascribed to the lower affinity of these liposomes for siRNA, even at the point of maximum binding, such that additional liposome is required to produce structures in which more of siRNA molecules are concealed, and is therefore less accessible to serum nucleases.

4.7 Cell lines and maintenance

Four adherent cell lines were used in this study, namely, HEK293, Caco-2, MCF-7 and HT-29. Healthy quiescent cells express low levels of steady state mRNA (Lindsten *et al*., 1988) and the associated protein is barely detectable (Kyo *et al*., 2000). However, regulated transient increases in *c-myc* expression do occur as cells proliferate (Eisenman, 2014). In this study, a non-transformed cell line, HEK293, which was shown to express *c-myc* very weakly by western blot (Liu *et al*., 2008a), was used as a control.

The human breast adenocarcinoma, MCF-7, and colorectal adenocarcinoma, HT-29, cell lines were selected as *in vitro* models of cancers with deregulated *c-myc* expression. The MCF-7 cell line was introduced by Soule and colleagues (1973), and has since become the most widely used breast cancer cell line. This is mainly because it provides a convenient model for the study of the oestrogen receptor (ER), hormone-response and ER-targeted treatment (Lee *et al*., 2015). Of significance to this study, amplification of the *c-myc* oncogene was shown in the MCF-7 cell line (Rummukainen *et al*., 2001). Furthermore, MCF-7 cells harbour palindromic rearrangements which are believed to drive amplification of this oncogene (Guenthoer *et al*., 2012). Finally, *c-myc* overexpression in this cell line was statistically correlated with amplification of the oncogene (Hyman *et al*., 2002).

Early studies showed that HT-29 cells harbour between 4 and 6 copies of the *c-myc* locus, and express oncogenic c-Myc under all culture conditions (Forgue-Lafitte *et al*., 1989). HT-29 cells also bear a mutant, truncated APC tumour suppressor gene (Hsi *et al*., 1999), and this contributes towards sustained *c-myc* expression in most colon carcinomas (He *et al*., 1998). These features, defects in the APC/β-catenin pathway (Sparks *et al*., 1998) and/or *c-myc* gene amplification (Augenlicht *et al*., 1997) are common to colorectal carcinomas, making HT-29 a good representative of this type of cancer.

A second human colorectal adenocarcinoma cell line, Caco-2, has the ability to regulate expression of *c-myc* (Hulla *et al*., 1995). A recent study showed that endogenous *c-myc* expression is lower in this cell line than in HT-29 (Mazzoccoli *et al*., 2016). Caco-2 cells were selected for two main reasons: firstly, for testing the effects of lipoplexes in different cell lines derived from cancer of the same organ, i.e. for comparison with HT-29; and secondly, for testing the effects of lipoplexes in a cancer cell line capable of regulable *c-myc* expression.

All cell lines were successfully propagated after reconstitution by routinely changing growth medium and performing trypsinisation. Sufficient stock of each cell line was maintained with regular cryopreservation. Images of semi-confluent and trypsinised cells are shown in Figures 4.20 and 4.21 respectively.

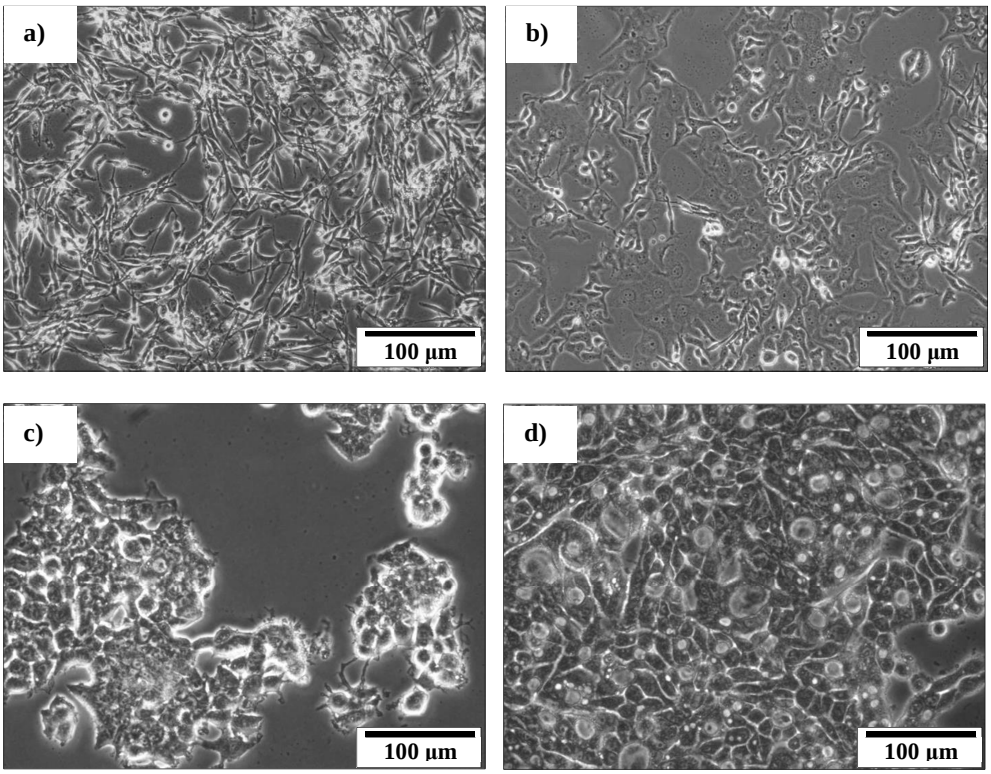

Figure 4.20: Semi-confluent **a)** HEK293, **b)** Caco-2, **c)** MCF-7 and **d)** HT-29 cells. Cells were viewed using an inverted microscope at 200× magnification.

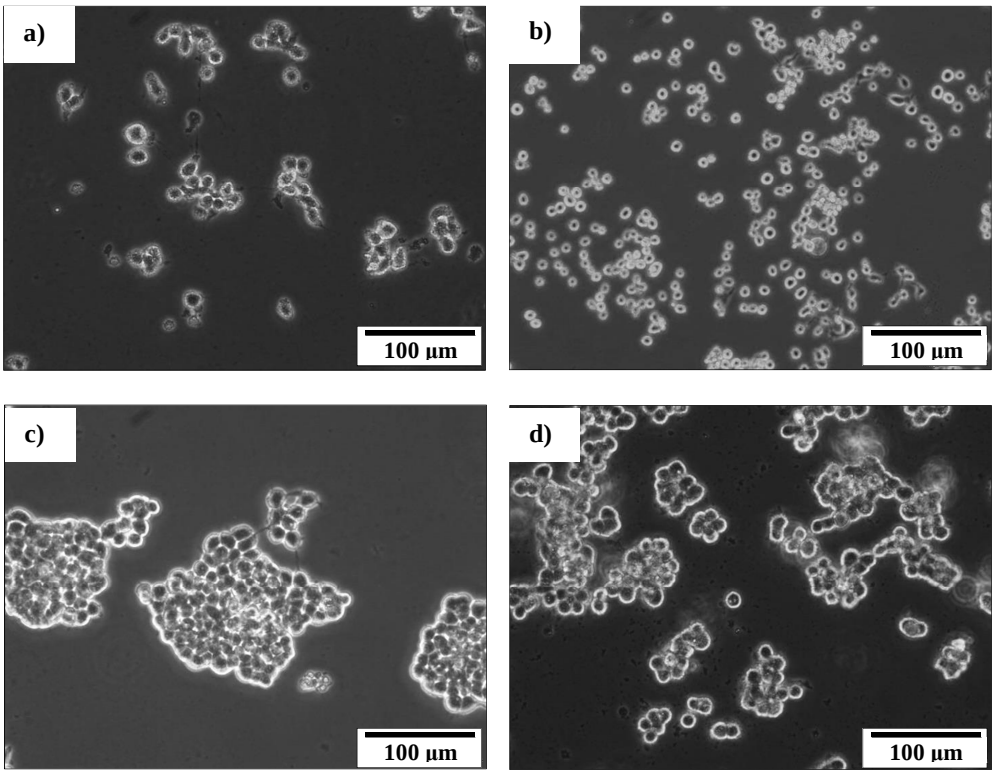

Figure 4.21: Trypsinised **a)** HEK293, **b)** Caco-2, **c)** MCF-7 and **d)** HT-29. Cells were viewed using an inverted microscope at 200× magnification.

4.8 The effect of lipoplexes on cell growth

Any new liposome-siRNA delivery system must be investigated for potential cytotoxic effects. In a review of the toxicity associated with siRNA nanoparticles, Xue *et al*. (2014) commented that even seemingly harmless lipids can cause toxicity when combined with other lipids. Moreover, for the purposes of this study, it was important that any growth inhibitory effects in cancer cells be attributed solely to the RNAi effects of successfully delivered anti-*c-myc* siRNA, and not due to any intrinsic harmful effect of the liposomal carrier complexes.

In this study, cellular tolerance of lipoplexes was evaluated according to two assays, namely the MTT and AB assays. This is in keeping with suggestions that the use of more than one assay is necessary to generate meaningful cytotoxicity profiles (Rampersad, 2012). The MTT assay is based on the principle that enzymes of the mitochondria and other organelles (Stockert *et al*., 2012) of living cells reduce soluble MTT, a tetrazolium salt, to purple formazan crystals (Figure 4.22a).

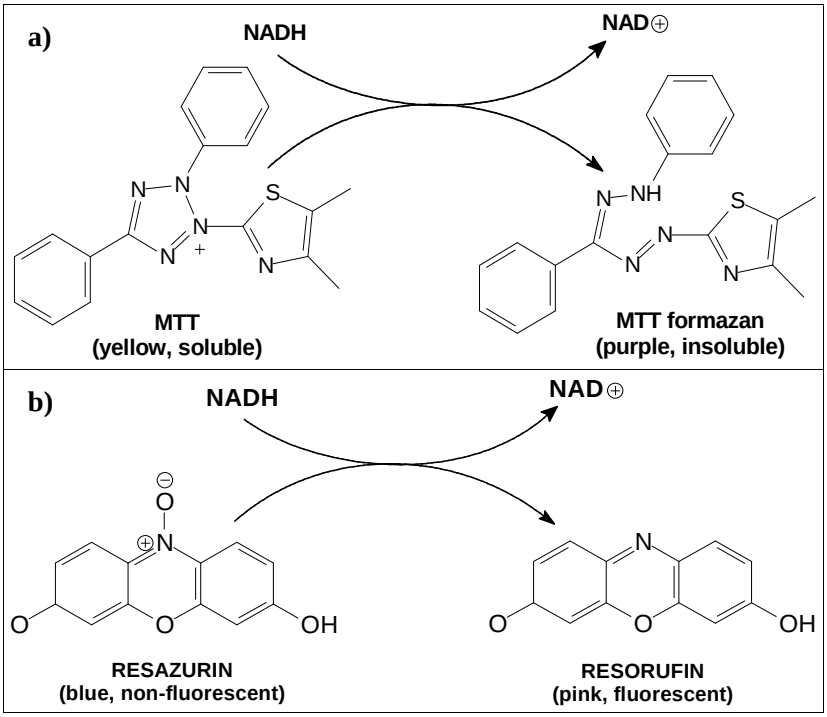

Figure 4.22: Reduction of **a)** MTT and **b)** resazurin to formazan and resorufin products, respectively. Redrawn and adapted from Riss *et al*. (2004) using ChemWindow® 6.0, Bio-Rad Laboratories (Sadtler Division, Philadelphia, PA).

Once solubilised, the intensity of the resultant purple solution correlates with the extent of MTT reduction and, as a consequence, the number of living cells present (Fotakis and Timbrell, 2006). The active agent of AB is resazurin, a blue non-fluorescent dye that is permeable to biological membranes. Resazurin is reduced by cytoplasmic and mitochondrial enzymes to a pink, strongly fluorescent product, resorufin (Figure 4.22b), that is subsequently excreted (O'Brien *et al*., 2000). The amount of resorufin in the growth medium is an indicator of metabolic activity and is proportional to the number of viable cells (Fields and Lancaster, 1993).

Cytotoxicity testing was performed under the same conditions as those employed in cellular uptake and gene silencing experiments, except that lipoplexes were assembled with non-targeting siRNA so as to rule out the possibility of cell death due to silencing of any functional genes. Care was taken to reduce the possibility of the assays being influenced by osmotic effects by assembling siRNA lipoplexes in HBS (Singh *et al*., 2007). This buffer maintains optimum osmolarity (290 mosmol/kg) for cultured human cells because it mirrors that of human plasma (Freshney, 2005). Furthermore, MTT and AB assays were performed in parallel, to minimise technical errors associated with plating of cells and preparation of lipoplex suspensions.

A comparison of Figures 4.23-4.28 shows that, in general, the AB assay confirmed trends in cell survival that were observed by the MTT assay. However, in some instances, cell viability as per the MTT assay appeared higher. This is apparent, for example, by comparing the MTT and AB cell viability data of the MS09/DOPE/PEG formulation at MS09:siRNA ($^{w}/_{w}$) ratios of 12:1-24:1, with 57 nM siRNA in the HEK293 cell line (Figures 4.23a, 4.24a). There is evidence to suggest that larger cells with more mitochondria reduce MTT at a higher rate (Jabbar *et al*., 1989), and that defective mitochondria may retain the ability to reduce MTT (Sieuwerts *et al*., 1995). In addition, it is possible for cells that have detached from the culture vessel to continue reducing MTT, leading to overestimated cell viabilities by this assay (Hamid *et al*., 2004). In fact, several sources mention that the AB assay is more sensitive (Davoren *et al*., 2007, O'Brien *et al*., 2000, Patel *et al*., 2013). Henceforth, the cell viability percentages mentioned refer to data obtained via the AB assay.

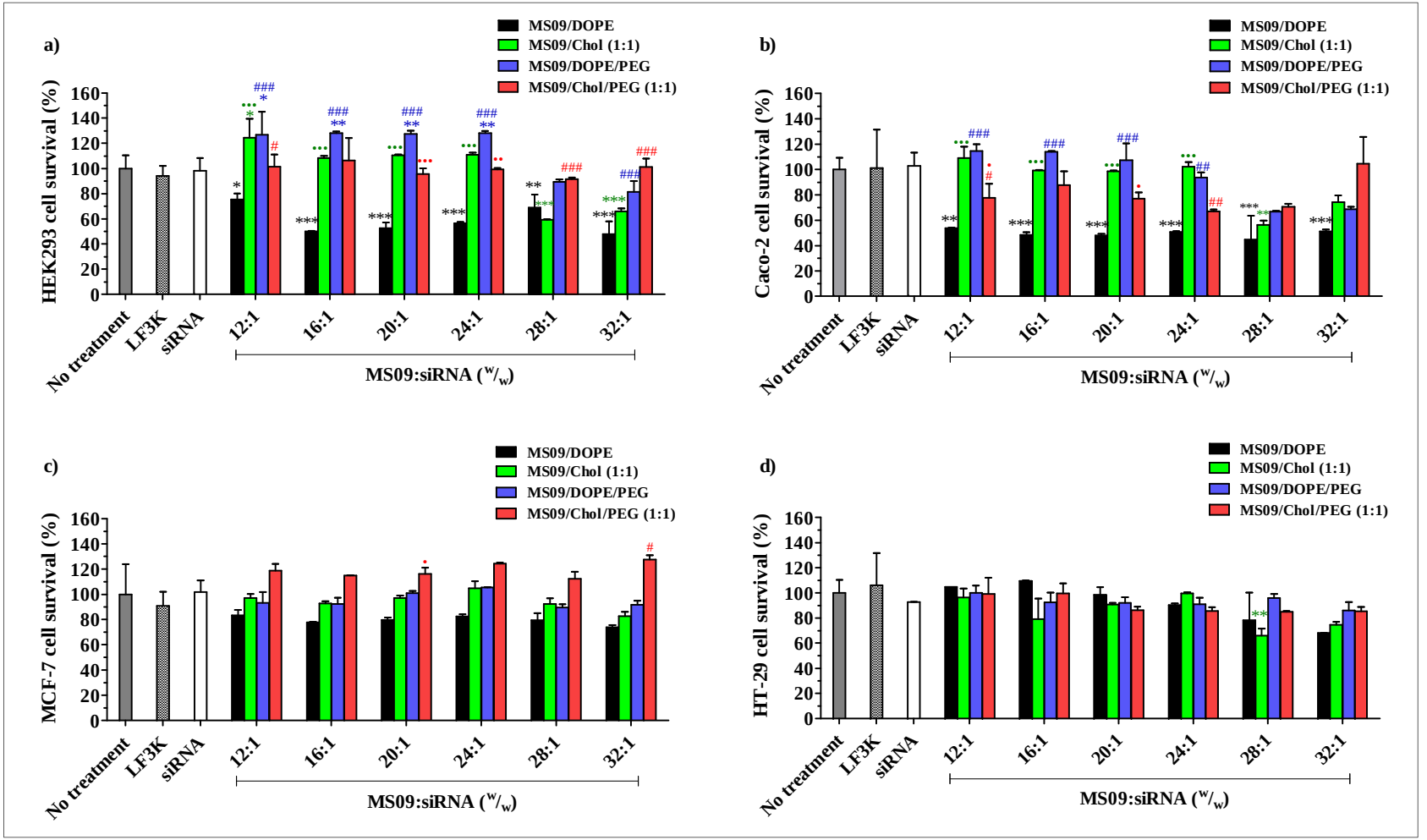

Figure 4.23: MTT viability assays with lipoplexes at final siRNA concentration of 57 nM. The growth response of **a)** HEK293, **b)** Caco-2, **c)** MCF-7 and **d)** HT-29 cells to lipoplexes, assembled with non-targeting siRNA at varying MS09:siRNA ($^{w}/_{w}$) ratios, was assessed 48 h after transfection. LF3K denotes Lipofectamine™ 3000, and transfections were as per manufacturer's instruction. Each column represents the mean ± SD (n = 3). $^{*}P < 0.05$, $^{**}P < 0.01$, $^{***}P < 0.001$ *vs.* untreated cells; $^{\#}P < 0.05$, $^{\#\#}P < 0.01$, $^{\#\#\#}P < 0.001$ *vs.* the non-pegylated counterpart; $^{\bullet}P < 0.05$, $^{\bullet\bullet}P < 0.01$, $^{\bullet\bullet\bullet}P < 0.001$ *vs*. the DOPE-containing counterpart.

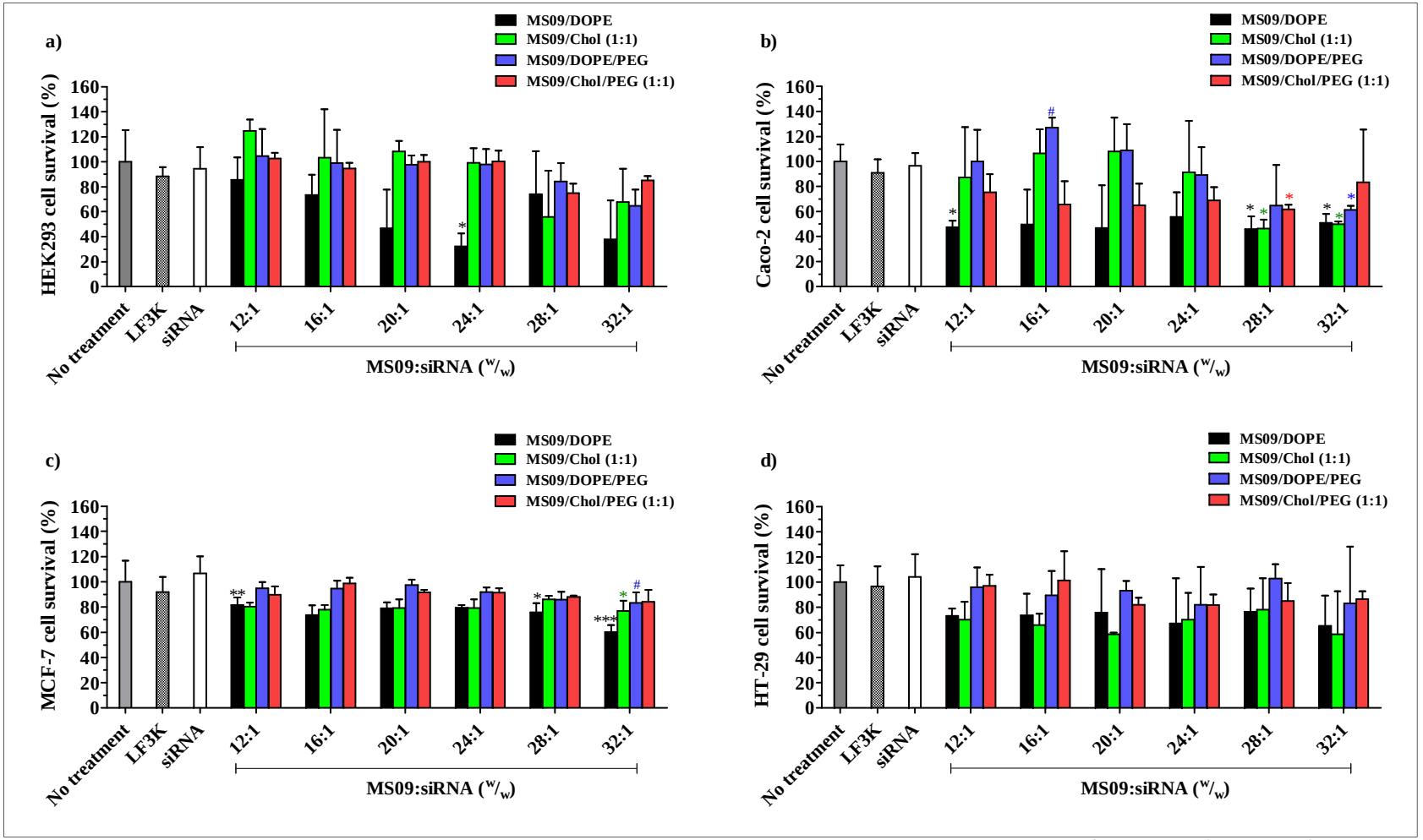

Figure 4.24: AB viability assays with lipoplexes at final siRNA concentration of 57 nM. The growth response of **a)** HEK293, **b)** Caco-2, **c)** MCF-7 and **d)** HT-29 cells to lipoplexes, assembled with non-targeting siRNA at varying MS09:siRNA ($^{w}/_{w}$) ratios, was assessed 48 h after transfection. LF3K denotes Lipofectamine™ 3000, and transfections were as per manufacturer's instruction. Each column represents the mean ± SD (n = 3). $^{*}P < 0.05$, $^{**}P < 0.01$, $^{***}P < 0.001$ *vs.* untreated cells; $^{\#}P < 0.05$ *vs.* the non-pegylated counterpart.

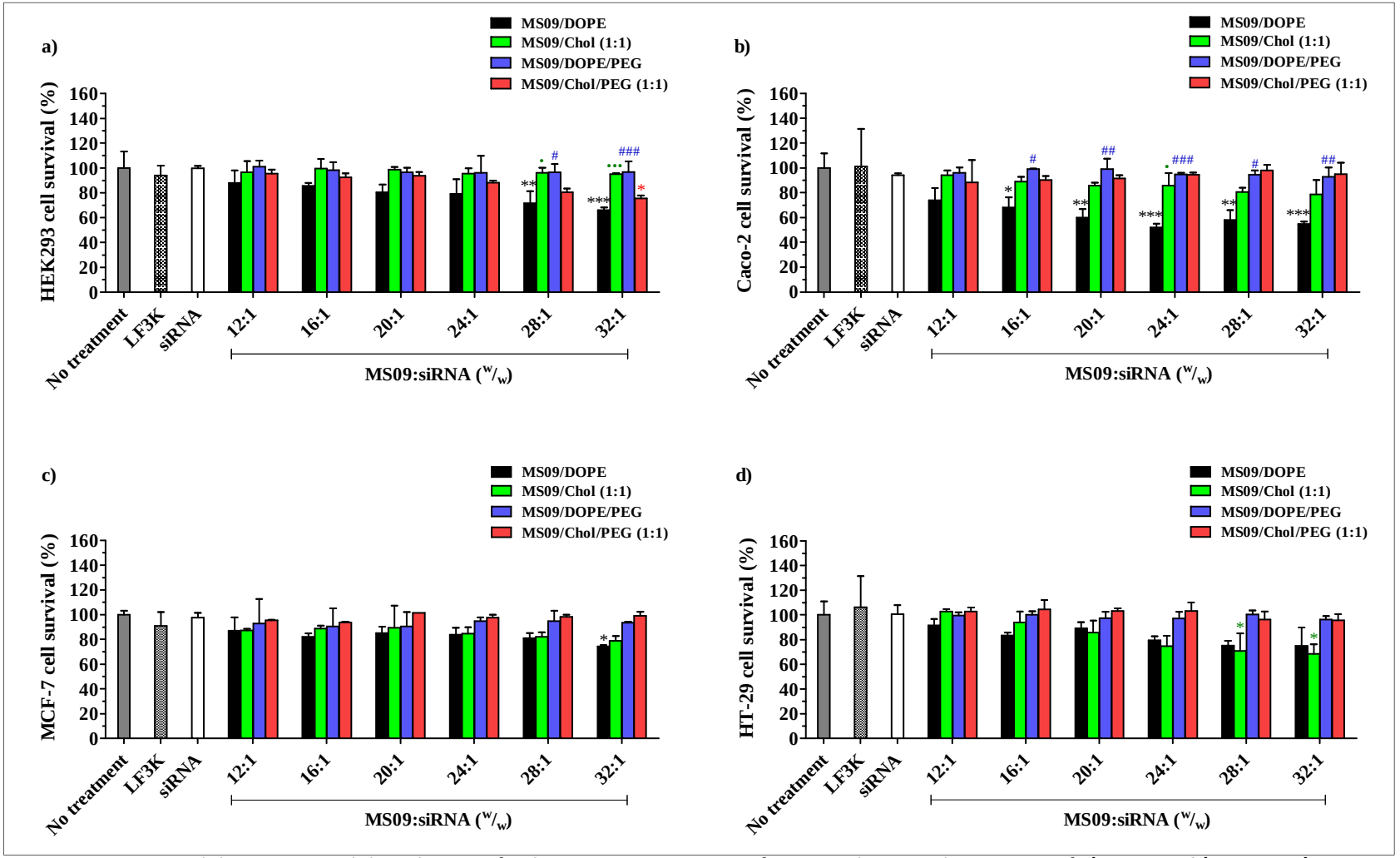

Figure 4.25: MTT viability assays with lipoplexes at final siRNA concentration of 29 nM. The growth response of **a)** HEK293, **b)** Caco-2, **c)** MCF-7 and **d)** HT-29 cells to lipoplexes, assembled from liposomes and non-targeting siRNA at varying MS09:siRNA ($^{w}/_{w}$) ratios, was assessed 48 h after transfection. LF3K denotes Lipofectamine™ 3000, and transfections were as per manufacturer's instruction. Each column represents the mean ± SD (n = 3). $^{*}P < 0.05$, $^{**}P < 0.01$, $^{***}P < 0.001$ *vs.* untreated cells; $^{\#}P < 0.05$, $^{\#\#}P < 0.01$, $^{\#\#\#}P < 0.001$ *vs.* the non-pegylated counterpart; $^{\bullet}P < 0.05$, $^{\bullet\bullet\bullet}P < 0.001$ *vs*. the DOPE-containing counterpart.

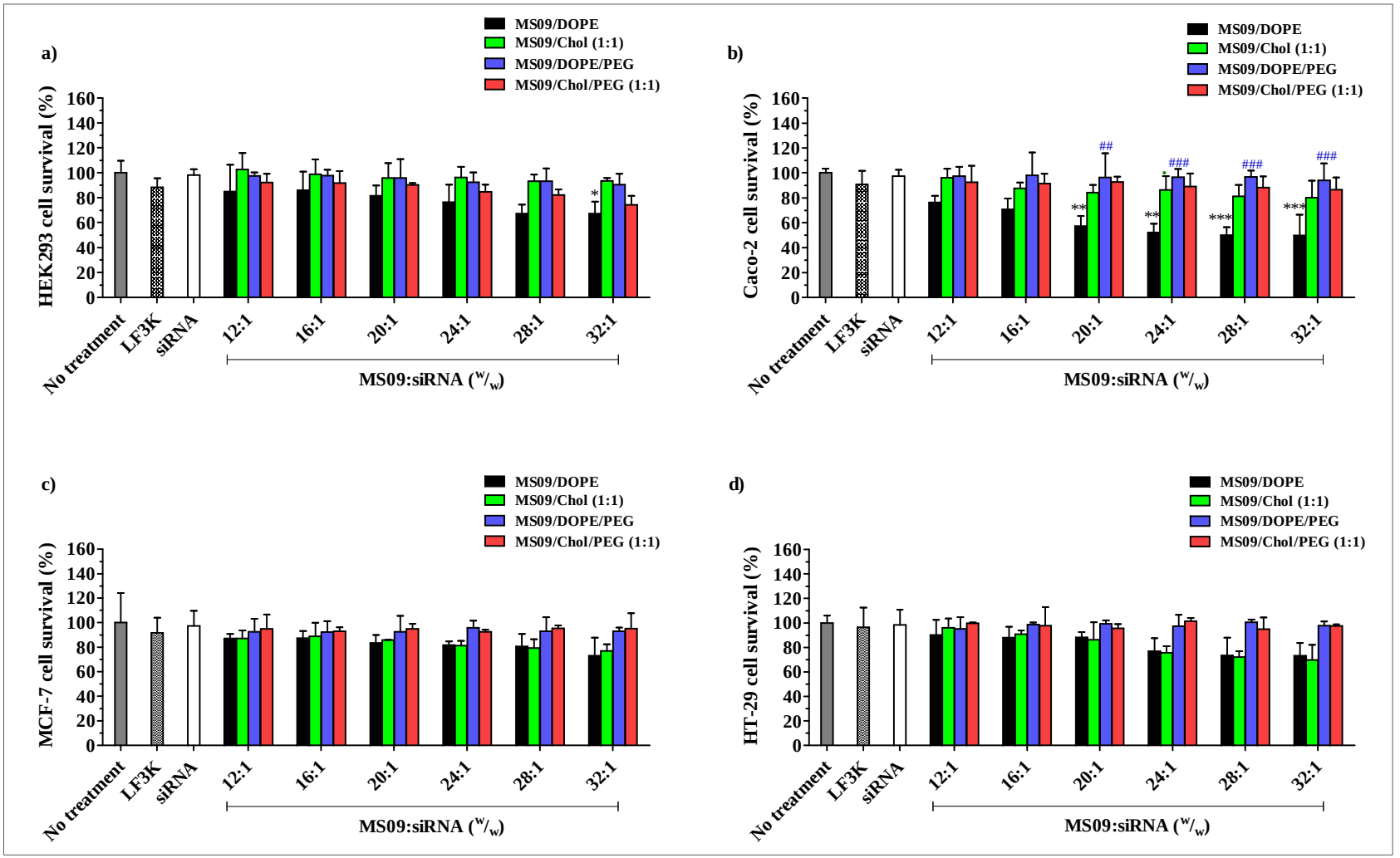

Figure 4.26: AB viability assays with lipoplexes at final siRNA concentration of 29 nM. The growth response of **a)** HEK293, **b)** Caco-2, **c)** MCF-7 and **d)** HT-29 cells to lipoplexes, assembled from liposomes and non-targeting siRNA at varying MS09:siRNA ($^{w}/_{w}$) ratios, was assessed 48 h after transfection. LF3K denotes Lipofectamine™ 3000, and transfections were as per manufacturer's instruction. Each column represents the mean ± SD (n = 3). $^{*}P < 0.05$, $^{**}P < 0.01$, $^{***}P < 0.001$ *vs.* untreated cells; $^{\#\#}P < 0.01$, $^{\#\#\#}P < 0.001$ *vs.* the non-pegylated counterpart; $^{\bullet}P < 0.05$ *vs*. the DOPE-containing counterpart.

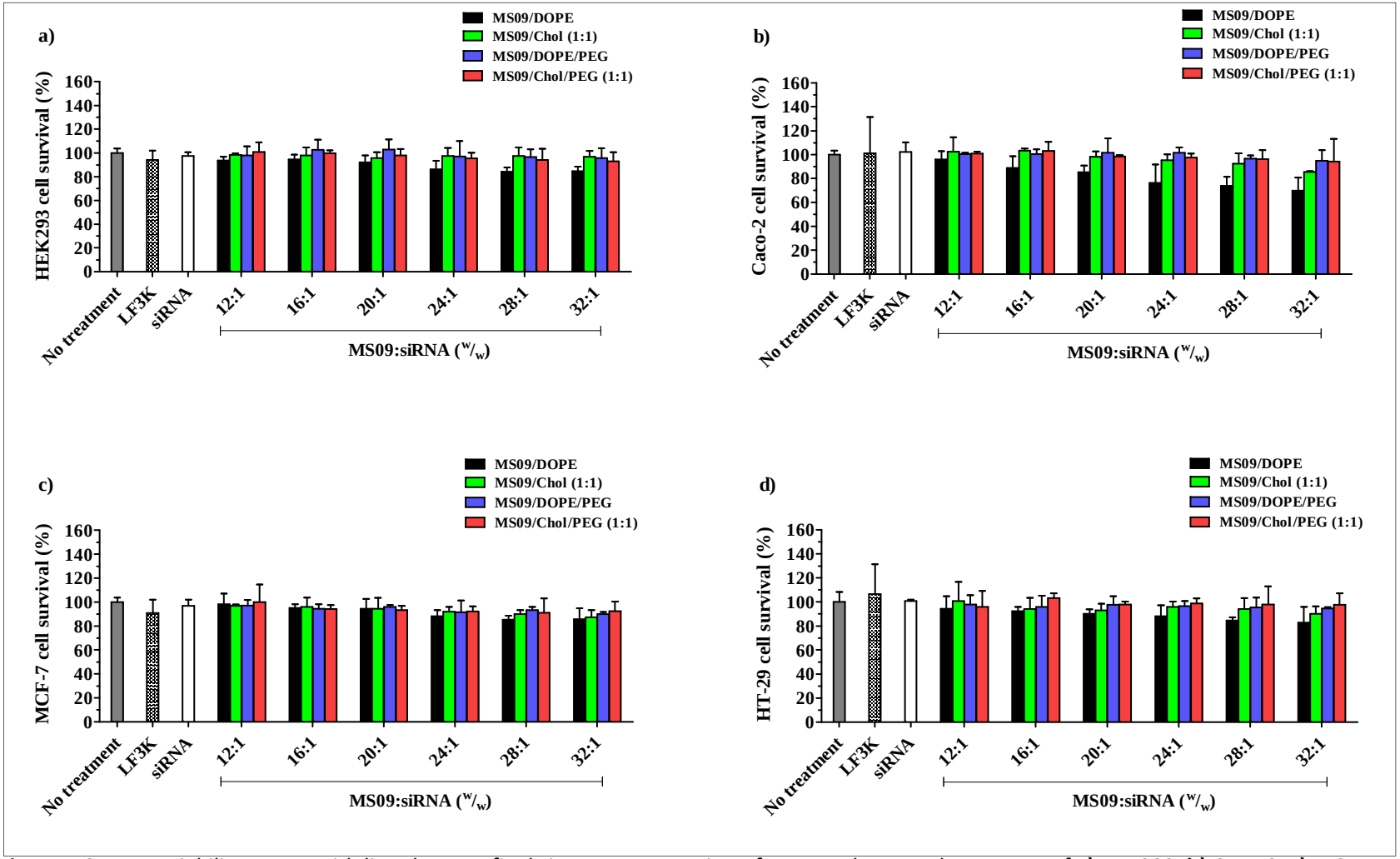

Figure 4.27: MTT viability assays with lipoplexes at final siRNA concentration of 14 nM. The growth response of **a)** HEK293, **b)** Caco-2, **c)** MCF-7 and **d)** HT-29 cells to lipoplexes, assembled from liposomes and non-targeting siRNA at varying MS09:siRNA ($^{w}/_{w}$) ratios, was assessed 48 h after transfection. LF3K denotes Lipofectamine™ 3000, and transfections were as per manufacturer's instruction. Each column represents the mean ± SD (n = 3). $P > 0.05$ *vs.* untreated cells, non-pegylated and DOPE-containing counterparts.

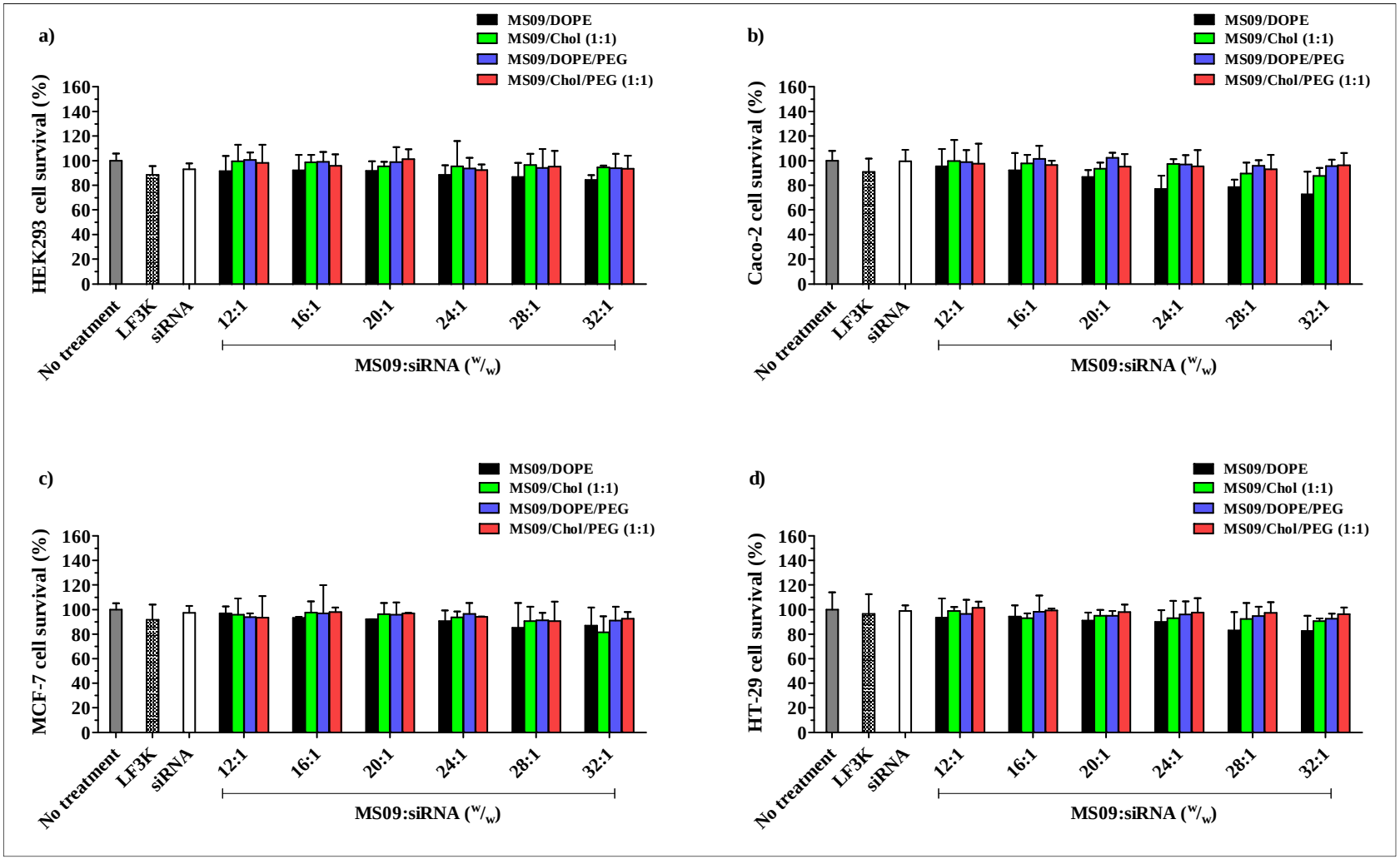

Figure 4.28: AB viability assays with lipoplexes at final siRNA concentration of 14 nM. The growth response of **a)** HEK293, **b)** Caco-2, **c)** MCF-7 and **d)** HT-29 cells to lipoplexes, assembled from liposomes and non-targeting siRNA at varying MS09:siRNA ($^{w}/_{w}$) ratios, was assessed 48 h after transfection. LF3K denotes Lipofectamine™ 3000, and transfections were as per manufacturer's instruction. Each column represents the mean ± SD (n = 3). $P > 0.05$ *vs.* untreated cells, non-pegylated and DOPE-containing counterparts.

As expected, no significant reduction in viability was detected upon treatment of all cell lines with naked siRNA at the same concentrations as contained in lipoplexes. Cells retained viability of at least 88 % with exposure to LF3K-siRNA complexes. However, the cellular growth response to MS09 lipoplexes varied with liposome composition, the MS09:siRNA ($^{w}/_{w}$) ratio, final siRNA and lipid concentration and, were often cell-specific.

Maximum growth inhibition of 67 % was recorded with the MS09/DOPE formulation at an MS09:siRNA ($^{w}/_{w}$) ratio of 24:1, at 57 nM siRNA in HEK293 cells (Figure 4.24a). Significant cell death with this formulation was also noted in Caco-2 (Figure 4.24b) and MCF-7 cells (Figure 4.24c). Poor cell survival at high MS09:siRNA ($^{w}/_{w}$) ratios can be attributed to the sensitivity of these cell types to the high cytofectin concentrations applied. Cationic lipids induce cytotoxicity mainly by association with the plasma membrane and consequent inhibition of protein kinase C (Farhood *et al*., 1992, Zelphati and Szoka, 1996). This causes the formation of transmembrane pores and possibly disturbs signal transduction (Das *et al*., 2016). Other adverse effects of cationic lipids include vacuolisation of cytoplasm, slow cell division, cell shrinkage, lysis and necrosis (Lappalainen *et al*., 1994, Mishra *et al*., 2004). Interestingly, significant cell death was also observed at the lowest MS09:siRNA ($^{w}/_{w}$) ratio explored, i.e. 12:1, in Caco-2 and MCF-7 cells. It is possible that these lipoplexes were well suited for cellular uptake in the aforementioned cell lines and, when used in such quantities so as to deliver 57 nM siRNA, accumulated within the cells at high concentrations that impeded cell growth. Hence the effective lipid dose with these lipoplexes could have been higher than with other lipoplexes assembled from the same formulation.

Besides the effect of lipid concentration, the effective siRNA dose, i.e. the actual number of siRNA molecules that successfully enter the cell in an intact form, can also impact adversely on cell survival. There is evidence to suggest that excess intracellular siRNA can saturate the RNAi machinery and cause toxicity by competitively inhibiting miRNA-mediated silencing pathways (Grimm, 2011). RISC concentration in the cell is estimated at 3-5 nM, which corresponds to approximately 10^{3}-10^{4} protein complexes per cell. Therefore, RISC saturation can, in theory, occur with as few as 10^{3}-10^{4} intact and successfully delivered siRNA molecules (Alagia and Eritja, 2016). However, the unfavourable effects of RISC saturation can be avoided by applying siRNA at the lowest effective dose possible (Grimm, 2011, Jackson and Linsley, 2010). Halving

the siRNA and associated lipid concentrations abolished any growth inhibitory effects with MS09/DOPE lipoplexes in MCF-7 cells (Figure 4.26c) and improved cell survival in the HEK293 (Figure 4.26a) and Caco-2 cell lines (Figure 4.26b). A further 50 % reduction in siRNA and lipid dose was necessary to avoid cytotoxic effects in the latter cell lines (Figures 4.28a,b).

In general, cell survival after exposure to the MS09/Chol (1:1) formulation was better than its DOPE-containing counterpart. Significant loss of cell viability was noted only in three instances i.e. in Caco-2 cells at MS09:siRNA ($^{w}/_{w}$) ratios of 28:1 and 32:1 (Figure 4.24b) and MCF-7 cells at a ratio of 32:1 (Figure 4.24c), at 57 nM siRNA. The observation that this formulation was better tolerated than MS09/DOPE could be ascribed to Chol being an endogenous lipid. Another possibility is presented by the fact that DOPE is pH-sensitive while Chol is not. Interestingly, this property of DOPE, which is often marked as important for transfection, has also been associated with toxicity, because it causes destabilisation of lysosomes and release of debris within the cell. Consequently, replacing DOPE with a pH-insensitive lipid, which is unable to interfere with the lysosomal membrane, was shown to reduce the toxicity of cationic liposomes (Filion and Phillips, 1997).

Pegylated formulations did not significantly inhibit cell growth with the exception of MS09/DOPE/PEG and MS09/Chol/PEG (1:1) lipoplexes at MS09:siRNA ($^{w}/_{w}$) ratios of 32:1 and 28:1, respectively, in Caco-2 cells (Figure 4.24b) and only at the highest siRNA and lipid concentrations at which these complexes were applied. The favourable overall cell survival permitted by pegylated lipoplexes could be a consequence of poor cellular entry due to PEG-inhibited lipoplex-cell interactions.

Differences in the growth response of Caco-2 and HT-29 highlight the issue of cell-specific cytotoxicity. Both cell lines are derived from tumours of the intestinal epithelium. However, Caco-2 cells differentiate to absorptive cells which resemble enterocytes (Rousset, 1986), while HT-29 cells are primarily undifferentiated in culture with some mucous-secreting and columnar absorptive sub-populations (Huet *et al*., 1995). Despite their similar origins, HT-29 cells were more resilient to lipoplex treatment than Caco-2 cells. According to the AB assay, no significant drop in viability of HT-29 cells was noted with any formulation at all MS09:siRNA ($^{w}/_{w}$) ratios, final siRNA and lipid concentrations explored.

4.9 Cellular uptake studies

The cellular uptake of lipoplexes is often correlated with transfection activity (Wang *et al.*, 2013a). In order to assess the ability of lipoplexes to enter cells and deliver siRNA, lipoplexes were assembled with BLOCK-iT™ Fluorescent Oligo, a fluorescein-labelled siRNA marker (Han *et al.*, 2008) that embodies the structural features of a typical siRNA molecule. The oligo permits RISC-independent assessment of siRNA delivery. Once successfully internalised the oligo localises mainly to the nucleus (Fisher *et al.*, 1993) and can be detected through fluorescence measurements. As shown in Figures 4.29-4.31, normalised intracellular fluorescence that was significantly greater than that of control 2, in which cells were treated with the naked oligo alone, was taken to represent successful siRNA delivery.

The best intracellular accumulation of the siRNA marker was observed with non-pegylated liposomes in MCF-7 and HT-29 cells at all siRNA concentrations explored. In fact, some non-pegylated lipoplexes achieved significantly better siRNA delivery than the standard *in vitro* transfection reagent, LF3K. As expected, differences in siRNA delivery were noted with varying MS09:siRNA ($^{w}/_{w}$) ratio, because this parameter influences the physical characteristics of lipoplexes (Khatri *et al.*, 2014, Wang *et al.*, 2013a). These physical features, in turn, have a major bearing on the cellular uptake of lipoplexes (Ma *et al.*, 2007, Rejman *et al.*, 2004a).

Maximum siRNA delivery achieved with MS09/DOPE and MS09/Chol (1:1) liposomes was comparable ($P > 0.05$) at all final siRNA concentrations explored in the MCF-7 and HT-29 cell lines, respectively. However, the mechanisms by which cells internalised lipoplexes assembled from these formulations are likely to have been very different. Alshehri *et al.* (2018) identified, through use of a variety of pharmacological inhibitors, several entry routes for non-pegylated siRNA lipoplexes which contained a monocationic cholesteryl derivative and DOPE. These included clathrin-mediated endocytosis, macropinocytosis and cell membrane cholesterol-dependent processes. With regard to lipoplexes formulated with Chol, it has been suggested that the formation of cholesterol nanodomains in the liposomal bilayer can contribute toward cellular uptake (Xu and Anchordoquy, 2008, Xu and Anchordoquy, 2010). Although the exact mechanisms by which they encourage uptake have not yet been elucidated, it has been put forward that cholesterol domains could interact with cell membrane components such as lipids and specific receptors (Betker *et al.*, 2013b).

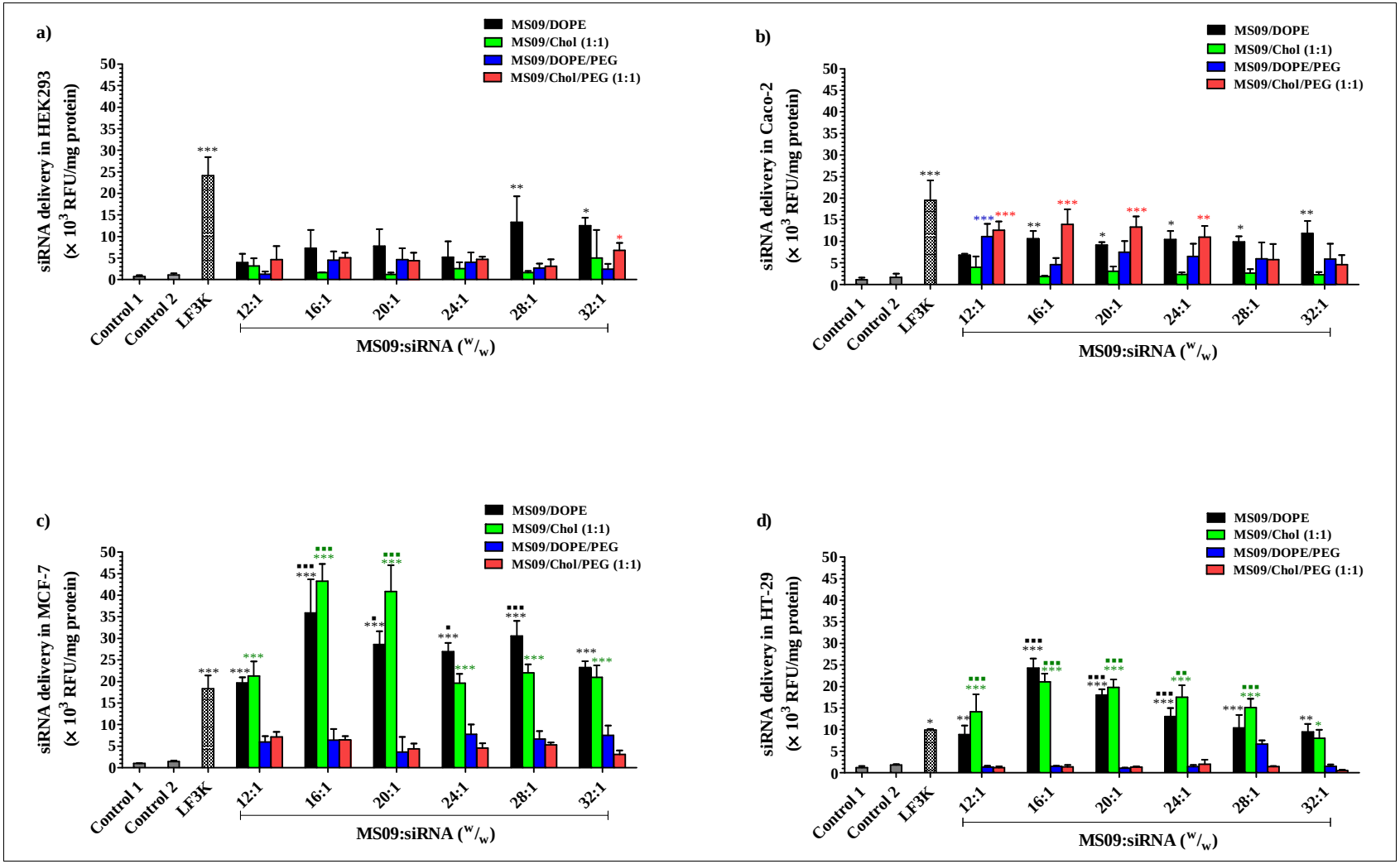

Figure 4.29: siRNA delivery by MS09 lipoplexes at final siRNA concentration of 57 nM in **a)** HEK293, **b)** Caco-2, **c)** MCF-7, and **d)** HT-29 cells. Cells were treated with lipoplexes, which were assembled with BLOCK-iT™ Fluorescent Oligo at varying MS09:siRNA ($^{w}/_{w}$) ratios, for 24 h after which intracellular fluorescence was measured. LF3K denotes Lipofectamine™ 3000, and transfections were as per manufacturer's instruction. Control 1 contained cells only, while control 2 contained cells treated with the naked oligo. Each column represents the mean ± SD (n = 3). $^{*}P < 0.05$, $^{**}P < 0.01$, $^{***}P < 0.001$ *vs.* control 2; $^{▪}P < 0.05$, $^{▪▪}P < 0.01$, $^{▪▪▪}P < 0.001$ *vs.* LF3K.

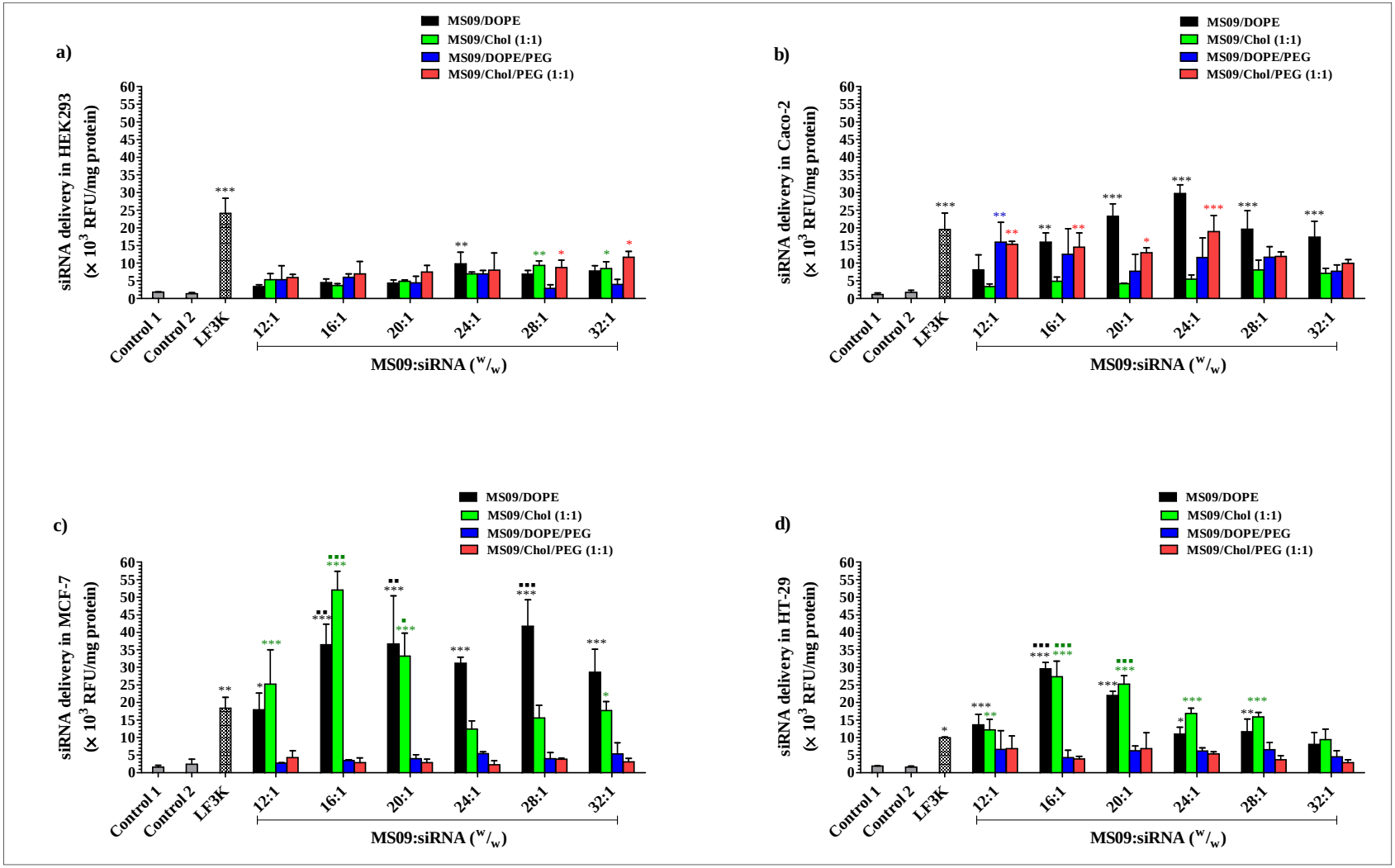

Figure 4.30: siRNA delivery by MS09 lipoplexes at final siRNA concentration of 29 nM in **a)** HEK293, **b)** Caco-2, **c)** MCF-7, and **d)** HT-29 cells. Cells were treated with lipoplexes, which were assembled with BLOCK-iT™ Fluorescent Oligo at varying MS09:siRNA ($^{w}/_{w}$) ratios, for 24 h after which intracellular fluorescence was measured. LF3K denotes Lipofectamine™ 3000, and transfections were as per manufacturer's instruction. Control 1 contained cells only, while control 2 contained cells treated with the naked oligo. Each column represents the mean ± SD (n = 3). $^{*}P < 0.05$, $^{**}P < 0.01$, $^{***}P < 0.001$ *vs.* control 2; $^{▪}P < 0.05$, $^{▪▪}P < 0.01$, $^{▪▪▪}P < 0.001$ *vs.* LF3K.

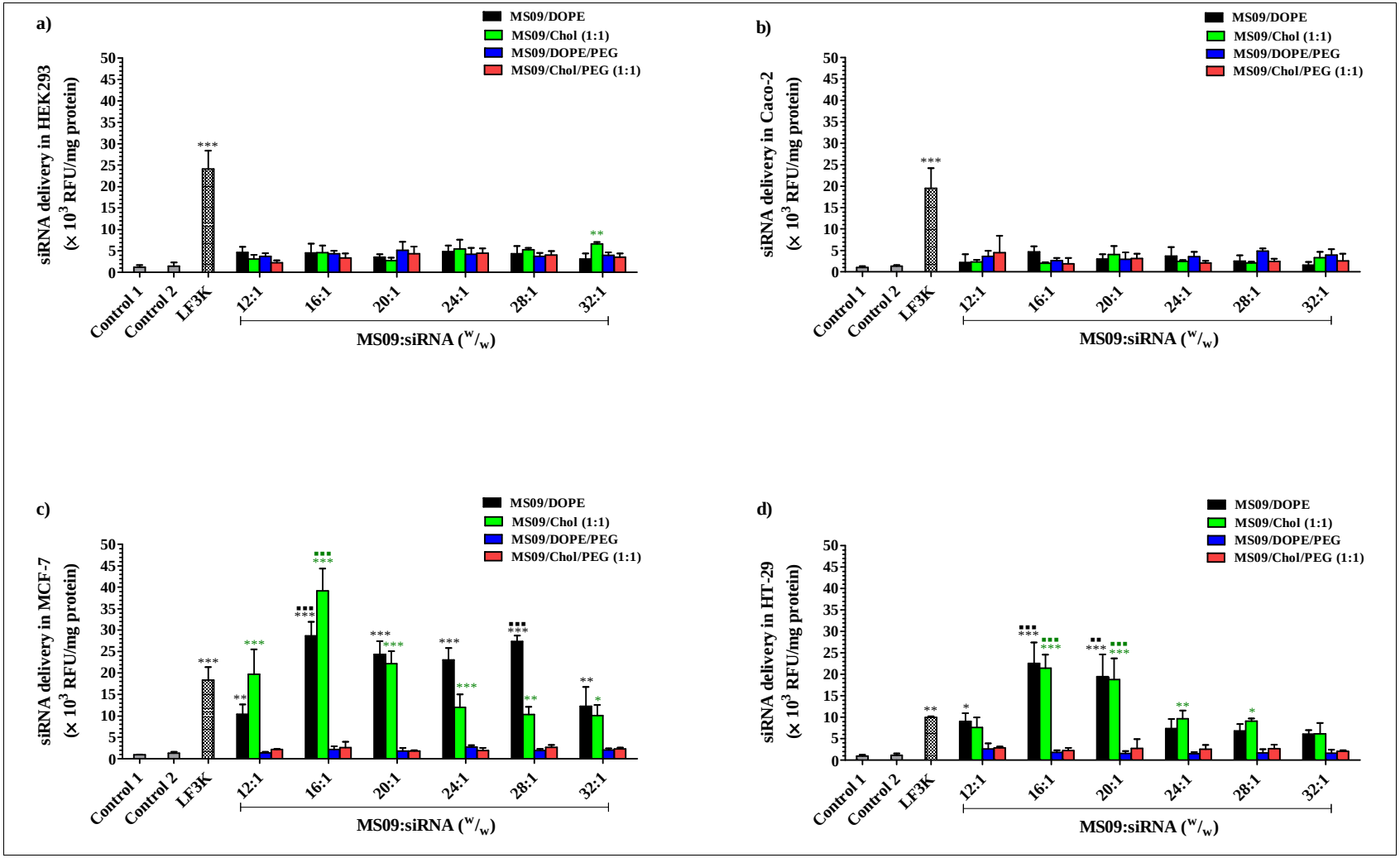

Figure 4.31: siRNA delivery by MS09 lipoplexes at final siRNA concentration of 14 nM in **a)** HEK293, **b)** Caco-2, **c)** MCF-7, and **d)** HT-29 cells. Cells were treated with lipoplexes, which were assembled with BLOCK-iT™ Fluorescent Oligo at varying MS09:siRNA ($^{w}/_{w}$) ratios, for 24 h after which intracellular fluorescence was measured. LF3K denotes Lipofectamine™ 3000, and transfections were as per manufacturer's instruction. Control 1 contained cells only, while control 2 contained cells treated with the naked oligo. Each column represents the mean ± SD (n = 3). $^{*}P < 0.05$, $^{**}P < 0.01$, $^{***}P < 0.001$ *vs.* control 2; $^{▪▪}P < 0.01$, $^{▪▪▪}P < 0.001$ *vs.* LF3K.

Others have shown that Chol-containing lipoplexes may be internalised by fusion with the cell membrane (Pozzi *et al*., 2012). This is supported by more recent work which identified direct membrane fusion as the dominant mechanism for siRNA delivery by Chol-containing, non-pegylated cationic liposomes, in HeLa cells (Lazebnik *et al*., 2016). In this way, Chol lipoplexes can deliver siRNA directly into the cytoplasm and altogether avoid the endolysosomal network. This is a major advantage, given that pathways which involve trafficking via intracellular vesicles are often associated with significant loss of internalised siRNA. It has been estimated that less than 2 % of siRNA escapes from endosomes into the cytoplasm (Gilleron *et al*., 2013). This occurs shortly after cellular uptake, and prior to endosomal maturation and endolysosomal fusion which direct the entrapped siRNA for degradation (Wittrup *et al*., 2015).

Taken together with an earlier study by Lu *et al*. (2009) who demonstrated that the delivery of functional siRNA molecules, i.e. the siRNA molecules that successfully interact with RISC in the cell by cationic liposomes, occurs via a mechanism that involves fusion of liposomal and cell membranes; these findings bode well for the potential efficacy of MS09/Chol (1:1) lipoplexes in gene silencing applications.

By comparison, delivery of the siRNA marker with MS09/DOPE and MS09/Chol (1:1) liposomes in HEK293 and Caco-2 cells was less effective. In the case of MS09/DOPE lipoplexes at 57 and 29 nM final siRNA this can, in most instances, be attributed to poor cell survival at the applied concentrations, as was demonstrated in growth inhibition experiments. In other instances, it is likely that the lipoplex characteristics were not conducive to cellular uptake in these cell lines. Although cell viability was preserved in the presence of MS09/DOPE lipoplexes at 14 nM siRNA, no significant siRNA delivery was noted at any of the MS09:siRNA ($^{w}/_{w}$) ratios explored. It is possible that, at this low concentration, lipoplexes interacted either minimally or not at all with these cells. Nonetheless, the MS09/DOPE formulation performed better than its Chol-containing counterpart in HEK293 and Caco-2 cell lines, even though MS09/Chol (1:1) was, in general, non-toxic. The data suggest that different cell types may harbour preferences for the uptake of lipoplexes depending on both lipid composition and the MS09:siRNA ($^{w}/_{w}$) ratio at which these are assembled. This could be associated with the concept that different lipoplexes may be internalised by different pathways (Ma *et al*., 2007, Rejman *et al*., 2004a) and, that some

cells are better suited towards different modes of uptake than others (Elouahabi and Ruysschaert, 2005).

Pegylated formulations failed to successfully transfer siRNA into MCF-7 and HT-29 cells at all MS09:siRNA ($^{w}/_{w}$) ratios, final lipid and siRNA concentrations explored. It is likely that, in these cell lines, PEG chains prevented cellular uptake altogether through inhibition of the lipoplex-plasma membrane association (Deshpande *et al*., 2004). This adds credence to the notion that favourable cell survival in the presence of pegylated lipoplexes is due to their lack of interaction with the cells. A further possibility, especially in the case of the MS09/DOPE/PEG formulation, is that the lipoplexes may have been endocytosed, but could not escape endolysosomal degradation due to the effects of PEG and DSPE, both of which prevent destabilisation of internal compartments (Fuxin *et al*., 2002, Song *et al*., 2002, Rejman *et al*., 2004b).

Modest delivery of siRNA by pegylated liposomes was, however, noted in the Caco-2 and HEK293 cell lines. In HEK293 cells, only the MS09/Chol/PEG (1:1) formulation gave appreciable normalised fluorescence levels, and this was achieved at high MS09:siRNA ($^{w}/_{w}$) ratios, i.e. 28:1 and 32:1, with 57 and 29 nM final siRNA explored (Figures 4.29a, 4.30a). In contrast, MS09/Chol/PEG (1:1) lipoplexes assembled at lower ratios were taken up by Caco-2 cells (Figures 4.29b, 4.30b). Caco-2 cells are the only cells in this study in which an MS09/DOPE/PEG lipoplex was able to facilitate siRNA delivery, and its performance was comparable with the Chol-containing counterpart. Here again the idea of cells demonstrating different affinities for different liposome formulations could account for the fact that pegylated lipoplexes were, in general, taken up more effectively in this cell line than the other three cell types. Halving the siRNA dose from 57 to 29 nM did not have a significant effect on siRNA delivery by pegylated lipoplexes in both cell lines. However, intracellular accumulation of the siRNA marker was negligible in both cell lines when the dose was halved once more. Collectively, this implies that there exists a minimum lipoplex concentration necessary for cellular uptake, that a limit exists on the amount of a given lipoplex that can accumulate within cells and that these properties are specific to the lipoplex and the cell line involved.

4.10 Selection of an appropriate anti-*c-myc* liposomal agent

To demonstrate the gene silencing effect of anti-*c-myc* siRNA lipoplexes, the two cancer cell lines with deregulated high *c-myc* expression were chosen i.e. MCF-7 and HT-29. Lipoplexes to be investigated as anti-*c-myc* agents were selected based on the following criteria:

- Lipoplexes should be capable of high siRNA delivery at low siRNA and lipid dose in the test cell lines.
- Lipoplexes should be non-cytotoxic in the test cell lines.
- Lipoplexes should have negligible effect in control cell lines.

From the broad final siRNA concentration range investigated (Figures 4.29-4.31), it is evident that the lipoplexes which achieved the highest siRNA delivery at lowest siRNA and lipid concentration, with negligible effect on normal cell growth were assembled from the MS09/Chol (1:1) formulation and its DOPE-containing counterpart, at the MS09:siRNA ($^{w}/_{w}$) ratio of 16:1. At 14 nM siRNA, these lipoplexes were taken up as readily as they were at higher concentrations by both MCF-7 and HT-29 cells, which imply that both cell types have high affinity for these complexes. Hence, these lipoplexes were investigated further. A summary of the characteristics of MS09/Chol (1:1) and MS09/DOPE lipoplexes at the MS09:siRNA ($^{w}/_{w}$) ratio of 16:1, is presented in Appendix E, Table E1. Of note is the observation that, in the case of both formulations, this ratio is below that at which siRNA was best protected and retarded on agarose gels. Internalised siRNA levels detected at these ratios, in both cell lines, were either comparable with or significantly lower than that which was achieved at the MS09:siRNA ($^{w}/_{w}$) ratio of 16:1. This observation was made at all final siRNA concentrations explored, and ties in with previous comments that a weaker liposome-siRNA association may be useful for siRNA release in the cell (Nguyen *et al*., 2008).

At a final siRNA concentration of 14 nM, non-pegylated MS09 lipoplexes at the MS09:siRNA ($^{w}/_{w}$) ratio of 16:1 were shown to be ineffective at delivering the siRNA marker into HEK293 and Caco-2 cells (Figure 4.31a,b) and did not interfere with cell growth (Figure 4.28a,b). This could suggest preferential accumulation of these lipoplexes in cancer cells characterised by deregulated *c-myc* expression, and this could be exploited for the selective treatment of such cancers. Furthermore, the fact that both lipoplexes, at 14 nM siRNA, had negligible effect in the non-transformed cell line, taking into account both the effect on cell

growth and introduction of siRNA, is an added advantage. Although normal cells are able to tolerate *c-myc* inhibition (Soucek *et al*., 2008), a *c-myc*-directed system that does not enter non-cancerous cells, may potentially alleviate any short-term effects of *c-myc* inhibition in healthy cells. The results suggest that it may be possible to achieve cancer cell selectivity of MS09 lipoplexes in the absence of additional liposome modifications, through optimising the lipid:siRNA mixing ratio for lipoplex assembly, lipid and siRNA dose.

It was noted that, in HT-29 cells, siRNA delivery by each non-pegylated liposome was comparable at MS09:siRNA ($^{w}/_{w}$) ratios of 16:1 and 20:1 ($P > 0.05$). However, the lipoplex suspensions at 16:1 were chosen for further study in light of the fact that, at 20:1, a higher lipid concentration would have to be applied. Although lipoplexes at this concentration were found to be harmless in all cell lines tested in this study, a lower lipid dose would be more economically feasible in a clinical setting. Furthermore, given that testing the effects of lipoplexes on cell lines modelled upon all possible cell types in the human body falls beyond the scope of this study, the lower lipid dose is favourable as it reduces the risk of adverse effects in other types of cells. Similar ideas were put forward by Xue *et al.* (2014) in a review of the toxicity of siRNA-based nanomedicine. Consequently, further attention was given to the final siRNA dose at which the selected lipoplexes would be applied (Figure 4.32).

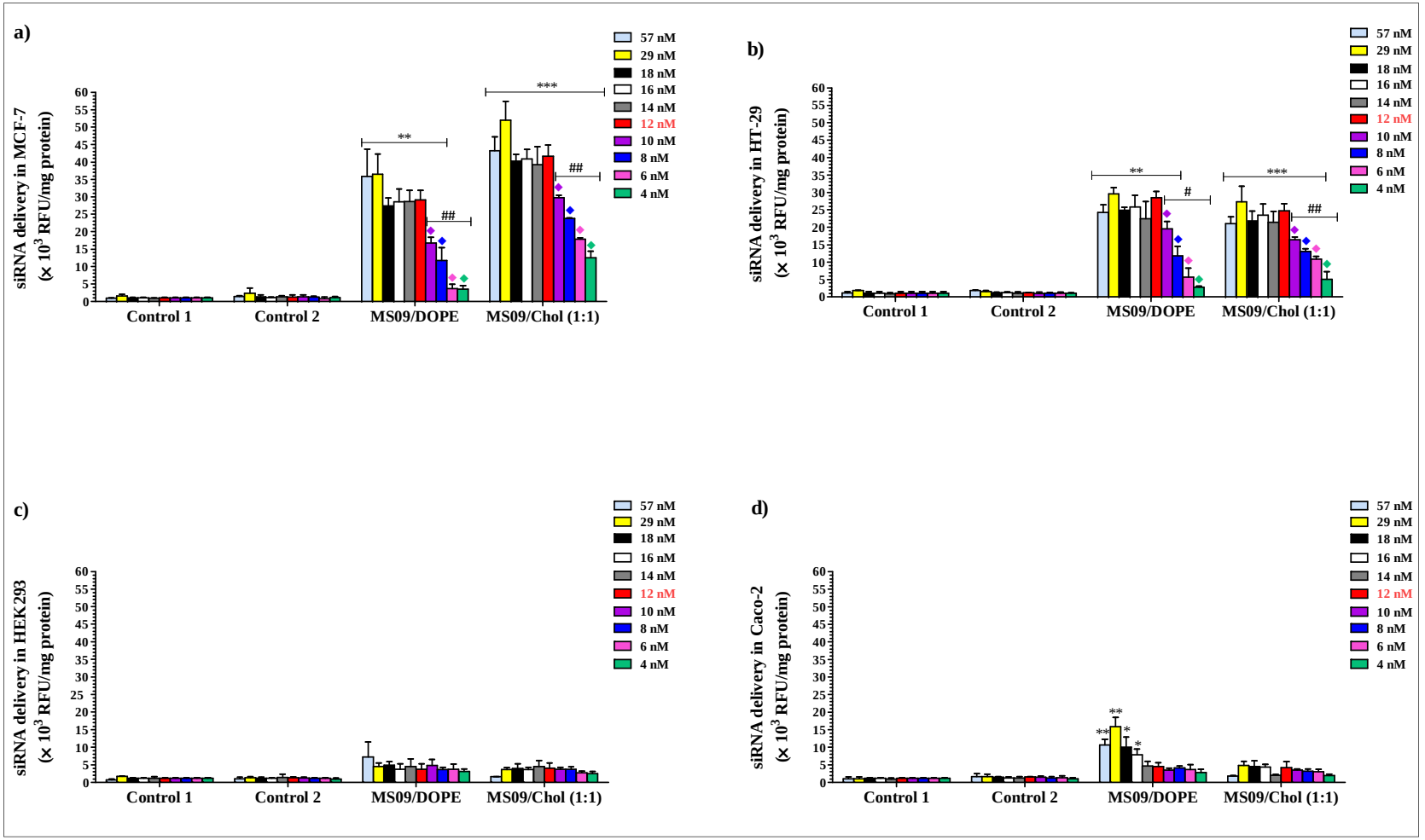

Figure 4.32: Delivery of siRNA by MS09/DOPE and MS09/Chol (1:1) formulations at MS09:siRNA ($^{w}/_{w}$) = 16:1 when introduced at varying final siRNA concentrations. **a)** MCF-7, **b)** HT-29, **c)** HEK293 and **d)** Caco-2 cells were exposed to lipoplexes assembled with BLOCK-iT™ Fluorescent Oligo for 24 h. Controls 1 and 2 represent untreated cells and cells treated with naked BLOCK-iT™ oligo, respectively. Data is presented as the mean ± SD (n = 3). $^{*}P < 0.05$, $^{**}P < 0.01$, $^{***}P < 0.001$ *vs.* control 2; $^{\blacklozenge}P < 0.05$ *vs*. 57 nM, 29 nM and 14 nM siRNA; $^{\#}P < 0.05$, $^{\#\#}P < 0.01$ *vs*. 12 nM siRNA.

In order to ascertain whether or not a final siRNA concentration of 14 nM was, in fact, the minimum applied concentration necessary for maximum lipoplex uptake and siRNA accumulation, cellular uptake experiments with MS09/DOPE and MS09/Chol (1:1) lipoplexes at MS09:siRNA ($^{w}/_{w}$) of 16:1 were carried out within a narrower siRNA concentration range. Figure 4.32a,b shows that there was no significant difference in siRNA delivery via both lipoplexes at final concentrations ranging from 57-12 nM siRNA in MCF-7 and HT-29 cells. Hence, final siRNA concentration of 12 nM was verified to be the lowest required for maximum cellular uptake of both lipoplexes in both cell lines. Further reduction of siRNA concentration significantly decreased siRNA marker delivery in both cell lines. At 6 nM, the siRNA and associated lipid concentration appeared to be too low to facilitate significant uptake with MS09/DOPE lipoplexes in both cell lines. In contrast, internalisation of MS09/Chol (1:1) lipoplexes was detectable at up to 6 nM and 4 nM final siRNA in HT-29 and MCF-7 cells, respectively. Importantly, it was confirmed that the markedly lower normalised intracellular fluorescence measurements obtained, at the newly tested siRNA and lipid concentrations, were not due to cell death (Appendix F, Figure F1a,b) and are, therefore, directly attributable to a dose-dependent decrease in cellular uptake at concentrations below 12 nM.

As proof of principle, the same siRNA concentration range was also tested in the non-target cell lines. Figure 4.32c,d, confirms that no siRNA delivery by MS09/DOPE and MS09/Chol (1:1) lipoplexes occurred in HEK293 and Caco-2 cells at siRNA concentrations below 14 nM. In addition, no significant loss of viability was recorded in these cell lines (Appendix F, Figure F1c,d). Hence, as with lipoplexes introduced at 14 nM final siRNA, it was confirmed that lipoplexes have no significant effect in the HEK293 and Caco-2 cell lines at 12 nM siRNA.

Further proof that the lipoplexes of interest can effectively enter MCF-7 and HT-29 cells, at 12 nM final siRNA, was provided by fluorescence microscopy. The successfully delivered siRNA marker was observed as green fluorescence within the cells (Figures 4.33, 4.34). Fluorescence signals were weak due to the low final concentration of the siRNA marker applied. The possibility of these signals arising from artifacts was ruled out on the grounds that untreated cells were non-fluorescent. Although qualitative assessment by microscopy alone is limited by the field of view, the images presented served as visual evidence of cellular uptake and supported the quantitative data obtained through normalised measurements of intracellular fluorescence.

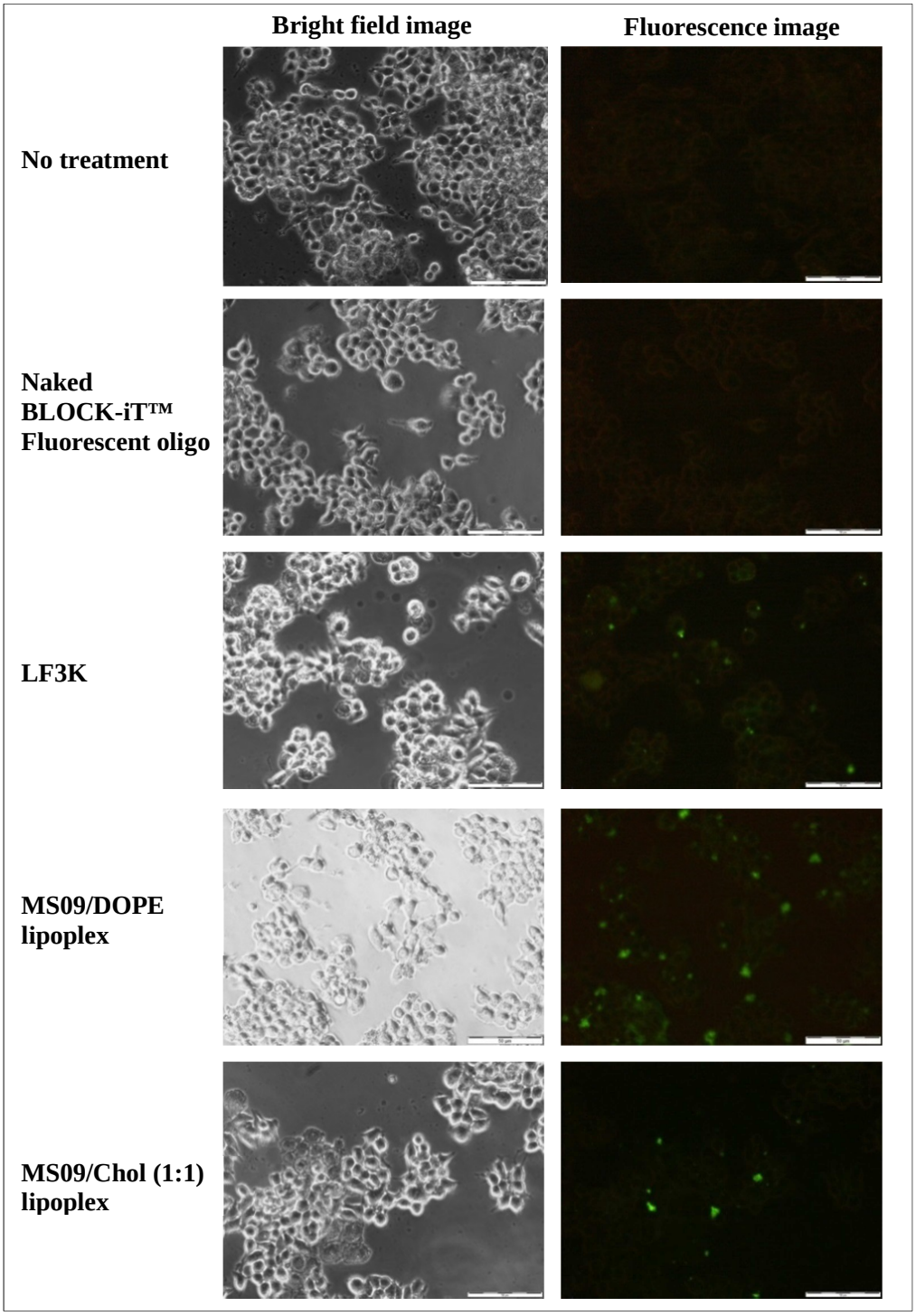

Figure 4.33: Cellular uptake of a fluorescein-labelled siRNA marker in MCF-7 cells, after transfection with MS09/DOPE and MS09/Chol (1:1) lipoplexes. Cells were transfected with lipoplexes assembled with BLOCK-iT™ Fluorescent oligo (MS09:siRNA $^{w}/_{w}$ = 16:1) at final concentration of 12 nM for 24 h. LF3K denotes Lipofectamine™ 3000, and transfection was as per manufacturer's instruction. Intracellular fluorescence was monitored using an inverted fluorescence microscope at 200× magnification. The scale bar represents 50 μm in all images.

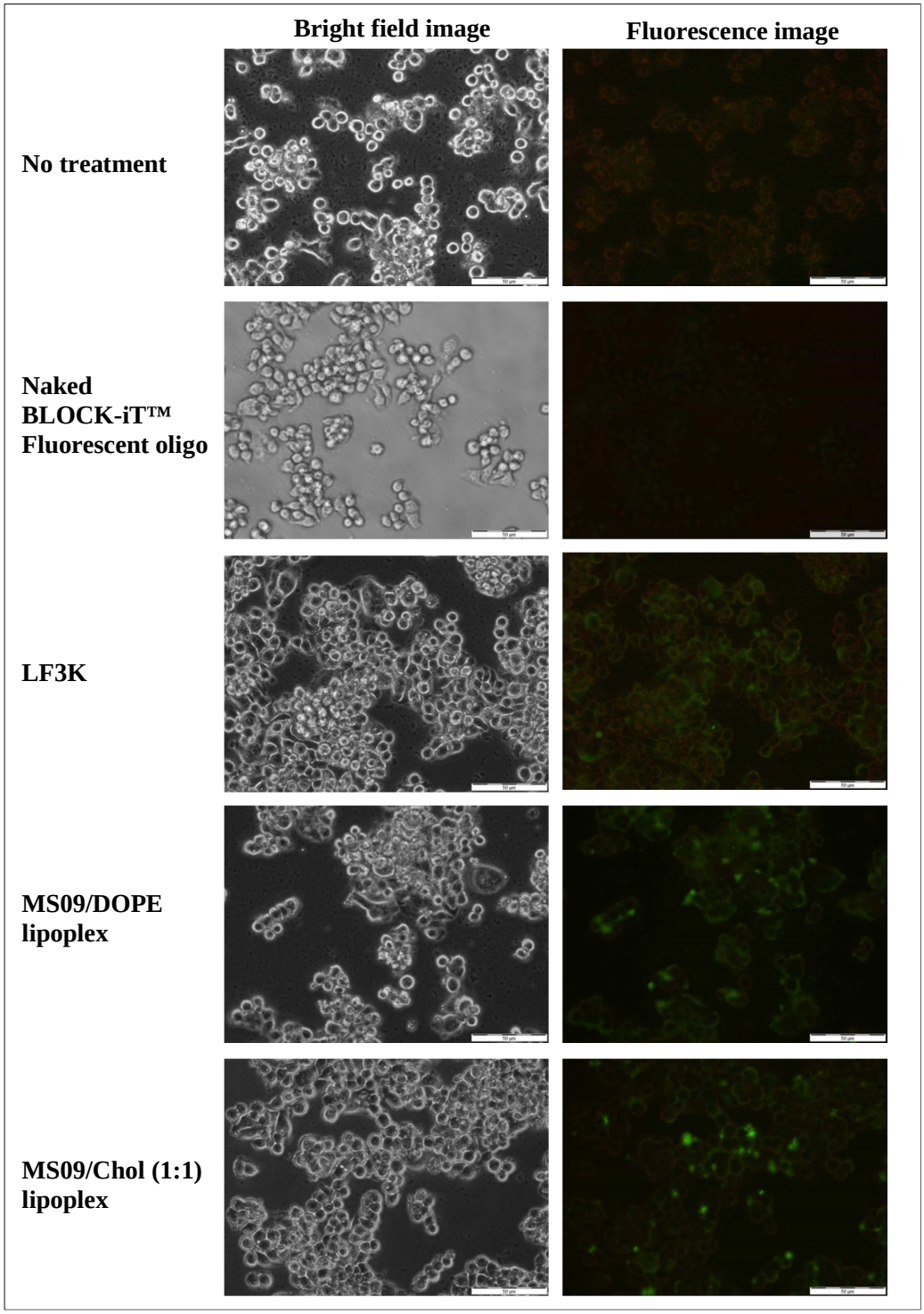

Figure 4.34: Cellular uptake of a fluorescein-labelled siRNA marker in HT-29 cells, after transfection with MS09/DOPE and MS09/Chol (1:1) lipoplexes. Cells were transfected with lipoplexes assembled with BLOCK-iT™ Fluorescent oligo (MS09:siRNA $^{w}/_{w}$ = 16:1) at final concentration of 12 nM for 24 h. LF3K denotes Lipofectamine™ 3000, and transfection was as per manufacturer's instruction. Intracellular fluorescence was monitored using an inverted fluorescence microscope at 200× magnification. The scale bar represents 50 µm in all images.

Consequently the MS09/Chol (1:1) lipoplex assembled at an MS09:siRNA ($^{w}/_{w}$) ratio of 16:1 was investigated as a new anti-*c-myc* agent, at a final siRNA concentration of 12 nM, in comparison with its DOPE-containing counterpart.

4.11 Gene silencing mediated by MS09/Chol (1:1) lipoplexes

Thus far, it has been confirmed that siRNA associated with MS09/Chol (1:1) and MS09/DOPE liposomes at an MS09:siRNA ($^{w}/_{w}$) ratio of 16:1 successfully traverses the plasma membrane and enters MCF-7 and HT-29 cells, at the highest level possible for these formulations in the cell lines tested, when applied at a final concentration of 12 nM. However, the question as to whether the siRNA delivered successfully reaches and engages with the RNAi machinery to inhibit oncogene expression, is critical to this study.

Given that the initial RNAi effect is exerted at the mRNA level, the effect of transfection with anti-*c-myc* lipoplexes on *c-myc* transcripts in cancer cells was studied using RT-qPCR. Figure 4.35 shows a decrease in *c-myc* mRNA only in instances in which a transfecting agent was used to deliver anti-*c-myc* siRNA sequences. Quantification of cellular c-Myc protein by ELISA (Figure 4.36) showed that a drop in *c-myc* mRNA levels was, in all instances, accompanied by a concomitant reduction in protein expression. Complexes assembled with non-targeting siRNA were without effect. This confirms that the observed reduction in *c-myc* mRNA is directly attributable to the RNAi effect of successfully delivered anti-*c-myc* siRNA. Furthermore, the fact that naked anti-*c-myc* siRNA did not influence *c-myc* expression in any way, emphasises that the delivery vehicle is a necessity.

MS09/Chol (1:1) and MS09/DOPE lipoplexes produced significantly more potent gene silencing effects than LF3K in both cell lines. More specifically, in the MCF-7 cell line, MS09 lipoplexes achieved 8- and 3.5-fold greater knockdown of oncogenic *c-myc* than LF3K at the mRNA and protein levels, respectively. In HT-29 cells, the decrease in *c-myc* mRNA and protein was 5- and 2.8-fold more intense with MS09 lipoplexes. This is consistent with the fact that both MS09 lipoplexes were taken up more effectively than LF3K ($P < 0.01$) in MCF-7 and HT-29. The superior performance of MS09 lipoplexes is further highlighted by the fact that these were applied at half the final siRNA concentration as LF3K.

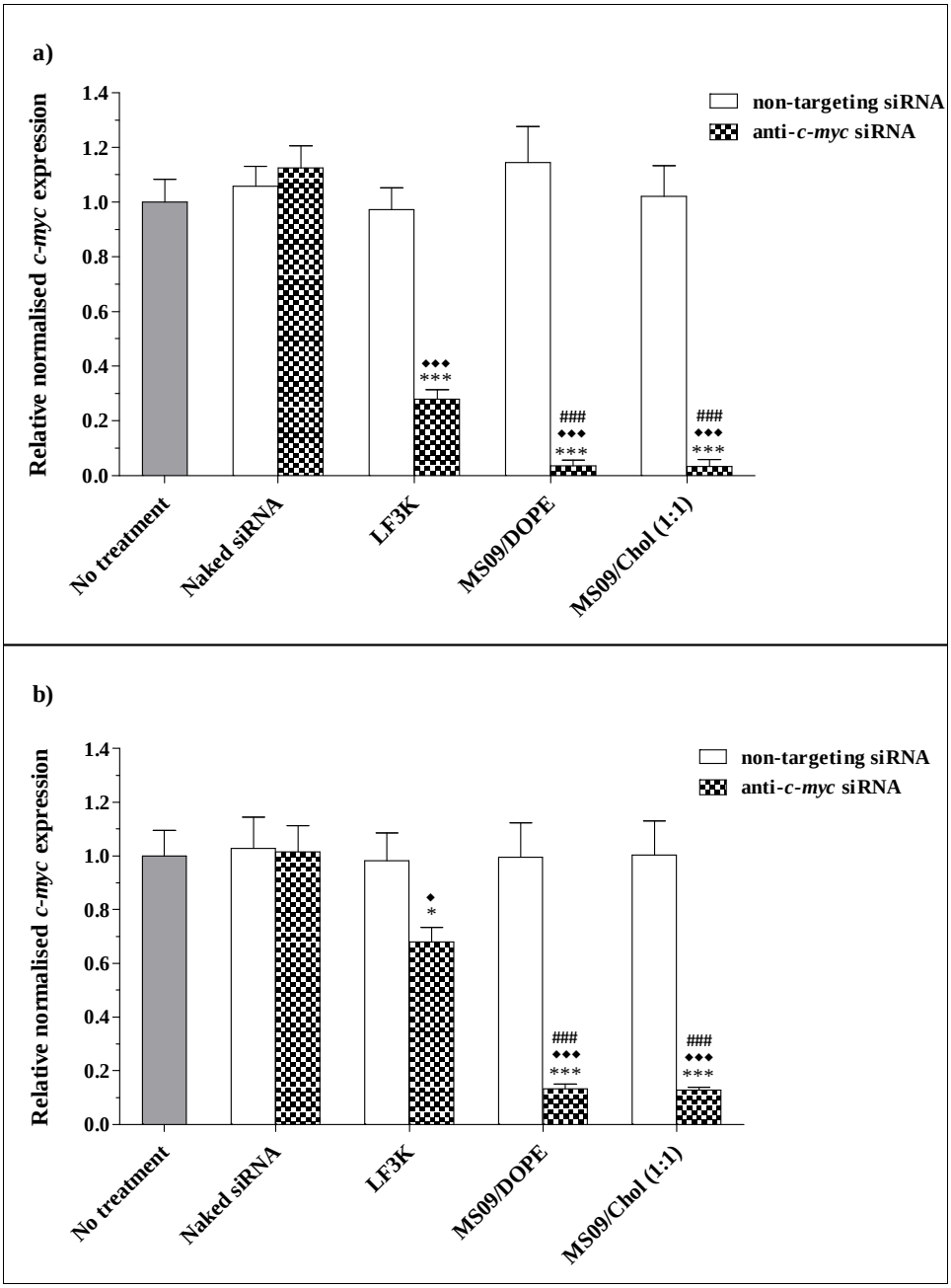

Figure 4.35: The effect of anti-*c-myc* lipoplexes on *c-myc* mRNA expression in **a)** MCF-7 and **b)** HT-29 cells, 48 h after transfection with MS09/DOPE and MS09/Chol (1:1) lipoplexes. Lipoplexes were assembled at MS09:siRNA ($^{w}/_{w}$) ratio of 16:1 and cells received final siRNA concentration of 12 nM. *c-myc* expression was quantified by RT-qPCR and normalised to the *β-actin* reference gene using the $\Delta\Delta C_q$ comparative quantification algorithm. Each column represents the mean ± SD (n = 3). $^{*}P < 0.05$, $^{***}P < 0.001$ *vs*. naked siRNA; $^{\blacklozenge}P < 0.05$, $^{\blacklozenge\blacklozenge\blacklozenge}P < 0.001$ *vs*. non-targeting siRNA; $^{\#\#}P < 0.01$, $^{\#\#\#}P < 0.001$ *vs*. anti-*c-myc* LF3K. $P > 0.05$, with respect to anti-*c-myc* MS09/Chol (1:1) *vs*. anti-*c-myc* MS09/DOPE.

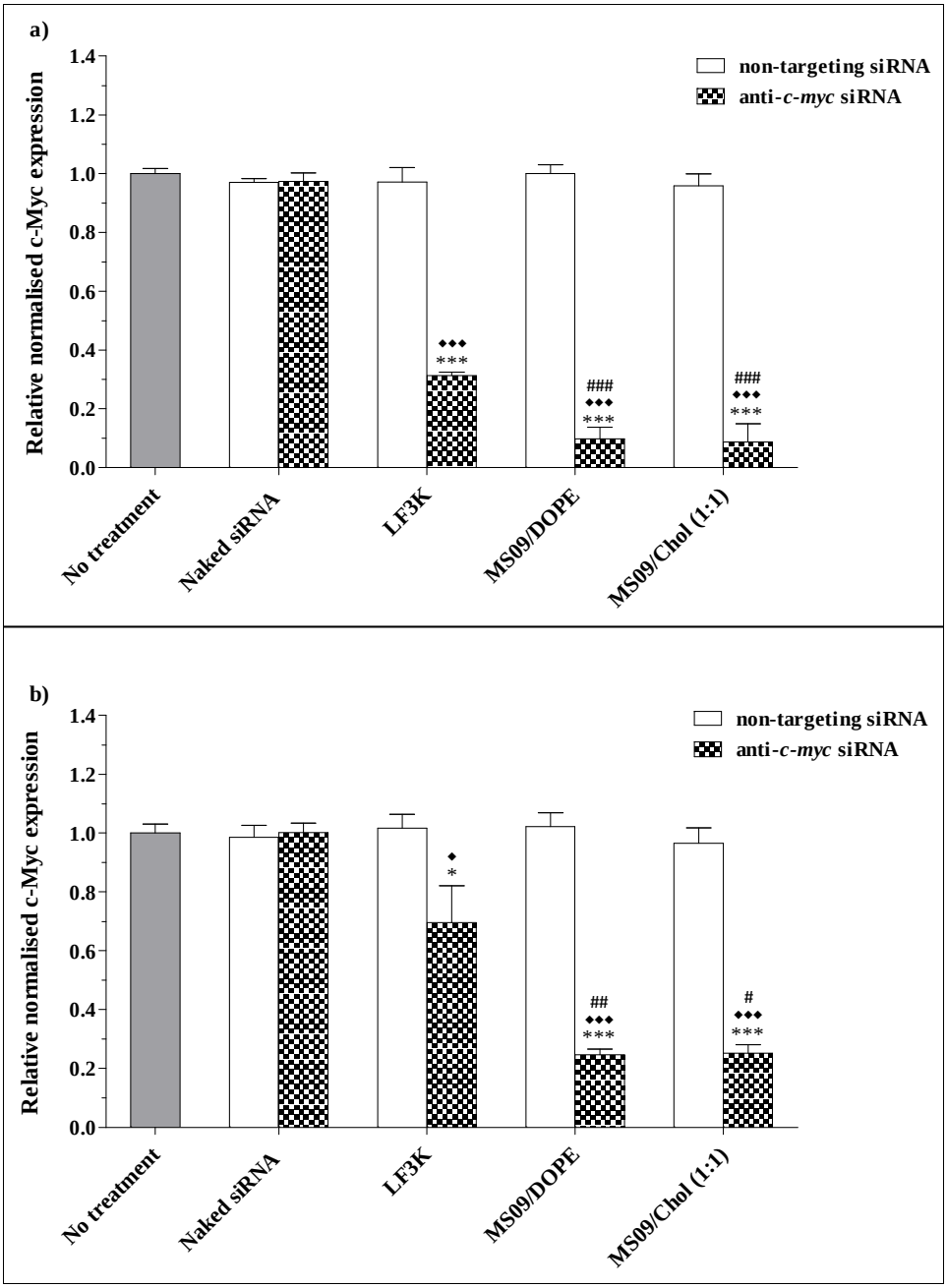

Figure 4.36: The effect of anti-*c-myc* lipoplexes on c-Myc protein expression in **a)** MCF-7 and **b)** HT-29 cells, 48 h after transfection with MS09/DOPE and MS09/Chol (1:1) lipoplexes. Lipoplexes were assembled at MS09:siRNA ($^{w}/_{w}$) ratio of 16:1 and cells received final siRNA concentration of 12 nM. c-Myc expression was quantified by ELISA, and normalised to the internal control, β-actin. Each column represents the mean ± SD (n = 3). $^{*}P < 0.05$, $^{***}P < 0.001$ *vs*. naked siRNA; $^{\blacklozenge}P < 0.05$, $^{\blacklozenge\blacklozenge\blacklozenge}P < 0.001$ *vs*. non-targeting siRNA; $^{\#}P < 0.05$, $^{\#\#}P < 0.01$, $^{\#\#\#}P < 0.001$ *vs*. anti-*c-myc* LF3K. $P > 0.05$, with respect to anti-*c-myc* MS09/Chol (1:1) *vs*. anti-*c-myc* MS09/DOPE.

In HT-29 cells cellular uptake of MS09/Chol (1:1) and MS09/DOPE lipoplexes was comparable ($P > 0.05$). The similar reduction in *c-myc* mRNA and protein observed implies that the MS09 lipoplexes facilitated RISC-engagement of intact anti-*c-myc* siRNA molecules with near-equal efficiency. In contrast, in the MCF-7 cell line, the MS09/Chol (1:1) lipoplex, at 12 nM final siRNA, facilitated more effective siRNA delivery than its DOPE-containing counterpart ($P < 0.05$), but did not give a more pronounced gene silencing effect. Taking into account that, at the point of maximum cellular uptake, a greater number of siRNA molecules enter MCF-7 cells with the MS09/Chol (1:1) lipoplex, saturation of the RNAi machinery is a possibility, especially given the likelihood that this complex releases siRNA directly into the cytoplasm. RISC saturation within a broad siRNA concentration range of 5-100 nM has been reported, and is dependent upon the potency of the siRNA molecules involved (Daniels *et al*., 2013). Given the catalytic nature of siRNA activity, the results suggest that the MS09/Chol (1:1) lipoplex could give useful, or perhaps as effective, gene silencing at final siRNA concentrations below 12 nM in MCF-7 cells. In support of this notion, siRNA delivery by the MS09/Chol (1:1) lipoplex in MCF-7 cells was detectable with as little as 4 nM final siRNA (Figure 4.32a).

It was observed that *c-myc* inhibition at both levels of expression by all transfecting agents was more pronounced in MCF-7 cells than in HT-29 cells ($P < 0.05$). This is underscored by the fact that the HT-29 cell line is considerably more difficult to transfect than other human cell lines (Alameh *et al*., 2010, Cerda *et al*., 2015, Hsi *et al*., 2000). In fact, manufacturers of the LF3K reagent have reported that the HT-29 cell line was among the least efficiently transfected in a wide range of tested mammalian cell lines (http://www.thermofisher.com/us/en/home/brands/product-brand/lipofectamine/lipofectamine-3000.html#sup). This explains the markedly lower cellular uptake (Figure 4.31d) and oncogene knockdown (1.4-fold reduction of *c-myc* at both levels of expression) obtained with LF3K in HT-29 cells. On a more positive note, the fact that MS09 lipoplexes have performed better in a recalcitrant cell line than a standard transfection reagent, could point to their applicability as oncogene silencing agents in other difficult-to-transfect cancer cells, and this adds credence to their potential as broad range anti-*c-myc* agents.

For comparative evaluation as anti-*c-myc* agents, both MS09/Chol (1:1) and MS09/DOPE lipoplexes were tested at the same MS09:siRNA ($^{w}/_{w}$) ratio, final lipid and siRNA concentration.

Although the siRNA-binding and protecting capability, under standard *in vitro* conditions, of MS09/Chol (1:1) was shown to be markedly weaker than its DOPE-containing counterpart at the MS09:siRNA ($^{w}/_{w}$) ratio of 16:1, the MS09/Chol (1:1) lipoplex has proved to be as effective an siRNA carrier and *c-myc*-silencing agent. This could be ascribed to the aforementioned role of cholesterol nanodomains in transfection (Xu and Anchordoquy, 2008, Xu and Anchordoquy, 2010) and the usefulness of Chol-mediated fusion with the cell membrane as a mode of delivering intact siRNA directly to the RNAi apparatus in the cytoplasm (Pozzi *et al*., 2012).

4.12 Anti-cancer effects of anti-*c-myc* lipoplexes

Cancer cell motility is associated with invasiveness and metastatic potential (Paul *et al*., 2017). Oncogenic c-Myc supports cell migration in several ways. For example, oncogenic c-Myc drives the expression of integrins (Boudjadi *et al*., 2016), long non-coding RNA (Hu and Lu, 2015) and microRNA (Li *et al*., 2013) that are known to encourage cell migration. In fact, the truncated form of c-Myc, Myc-nick, was recently shown to accelerate the migration of colon cancer cells by inducing fascin expression and activating the Rho GTPase Cdc42 (Anderson *et al*., 2016).

The impact of transfection with anti-*c-myc* lipoplexes on cell migration was assessed by monitoring the movement of cells into a wound that was created in the cell monolayer (Liang *et al*., 2007). Figures 4.37 and 4.38 show that all complexes containing anti-*c-myc* siRNA were associated with a defect in cell motility. In fact, in cells treated with anti-*c-myc* MS09/Chol (1:1) and MS09/DOPE lipoplexes, the normalised wound area measured after 24 h was wider ($P < 0.01$) (Figure 4.39) and wound margins at 24 h appeared less defined than at 0 h. This could point to loss of cell viability. To confirm this, the AB viability assay was performed.

The AB assay (Figure 4.40) showed that, all transfections with anti-*c-myc* siRNA, with the exception of LF3K in HT-29 cells, were associated with a significant drop in cell viability. This is consistent with a wealth of evidence, as reviewed by Bretones *et al.* (2015) that, downregulating *c-myc* expression inhibits cell cycle progression and mitosis due to its key role in these processes.

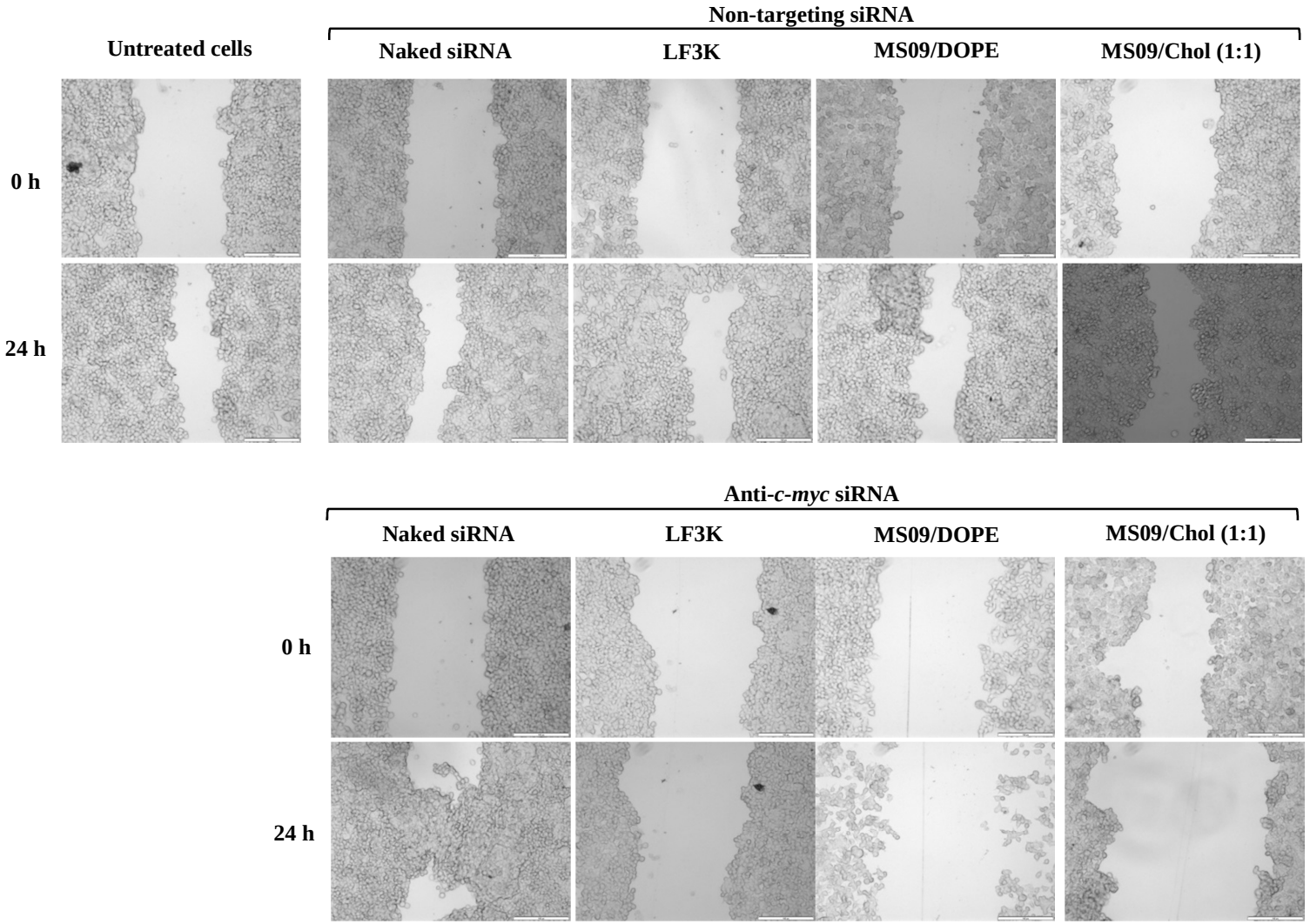

Figure 4.37: Effect of lipoplexes on MCF-7 cell migration. Wounds were created after transfection with MS09/DOPE and MS09/Chol (1:1) lipoplexes (MS09:siRNA $^{w}/_{w}$ = 16:1) at a final siRNA concentration of 12 nM. LF3K denotes Lipofectamine™ 3000 and transfection was as per manufacturer's instruction. Wound closure was monitored after 24 h with an inverted microscope at 100× magnification. Each scale bar represents 100 µm.

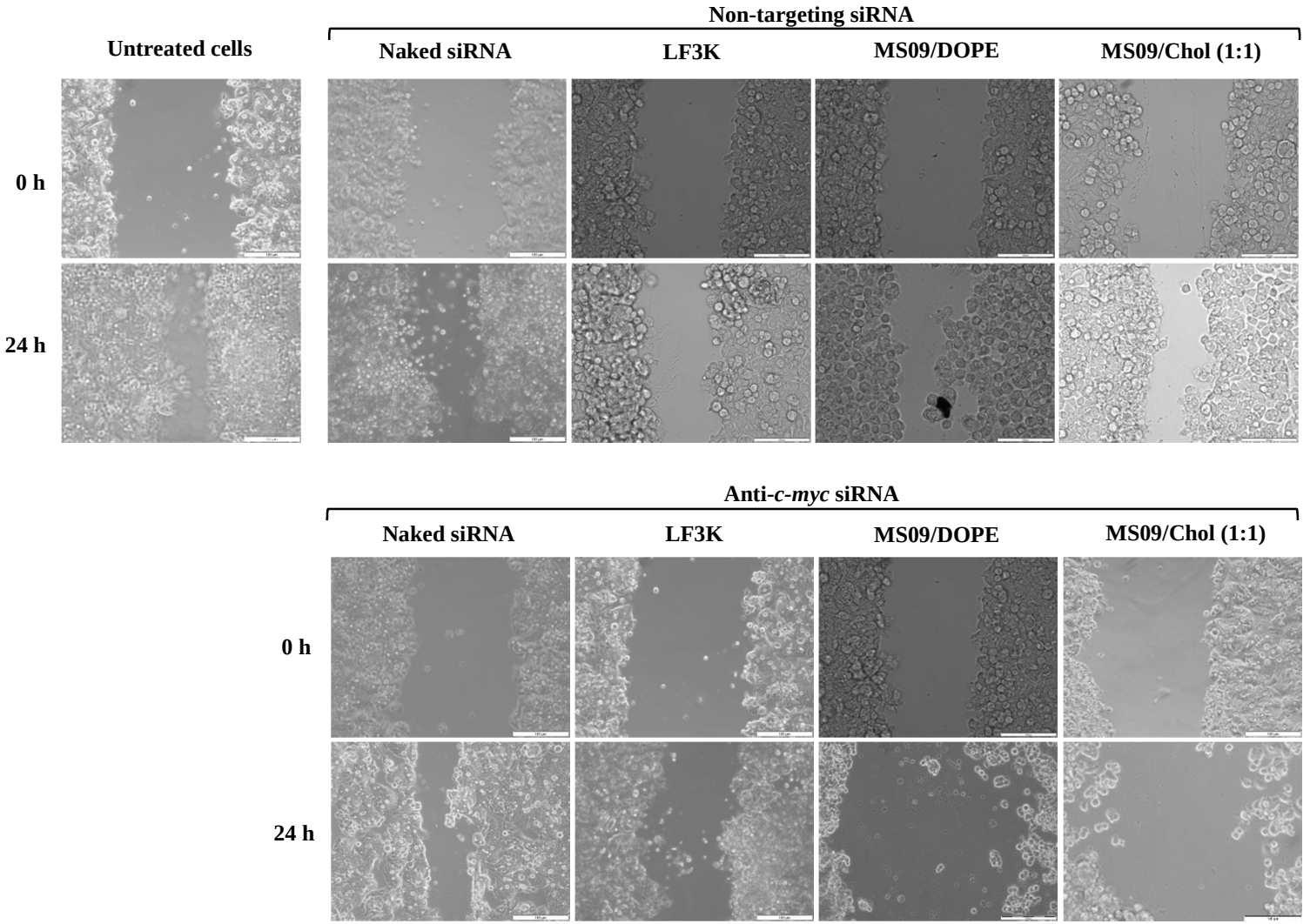

Figure 4.38: Effect of lipoplexes on HT-29 cell migration. Wounds were created after transfection with MS09/DOPE and MS09/Chol (1:1) lipoplexes (MS09:siRNA $^{w}/_{w}$ = 16:1) at a final siRNA concentration of 12 nM. LF3K denotes Lipofectamine™ 3000 and transfection was as per manufacturer's instruction. Wound closure was monitored after 24 h with an inverted microscope at 100× magnification. Each scale bar represents 100 µm.

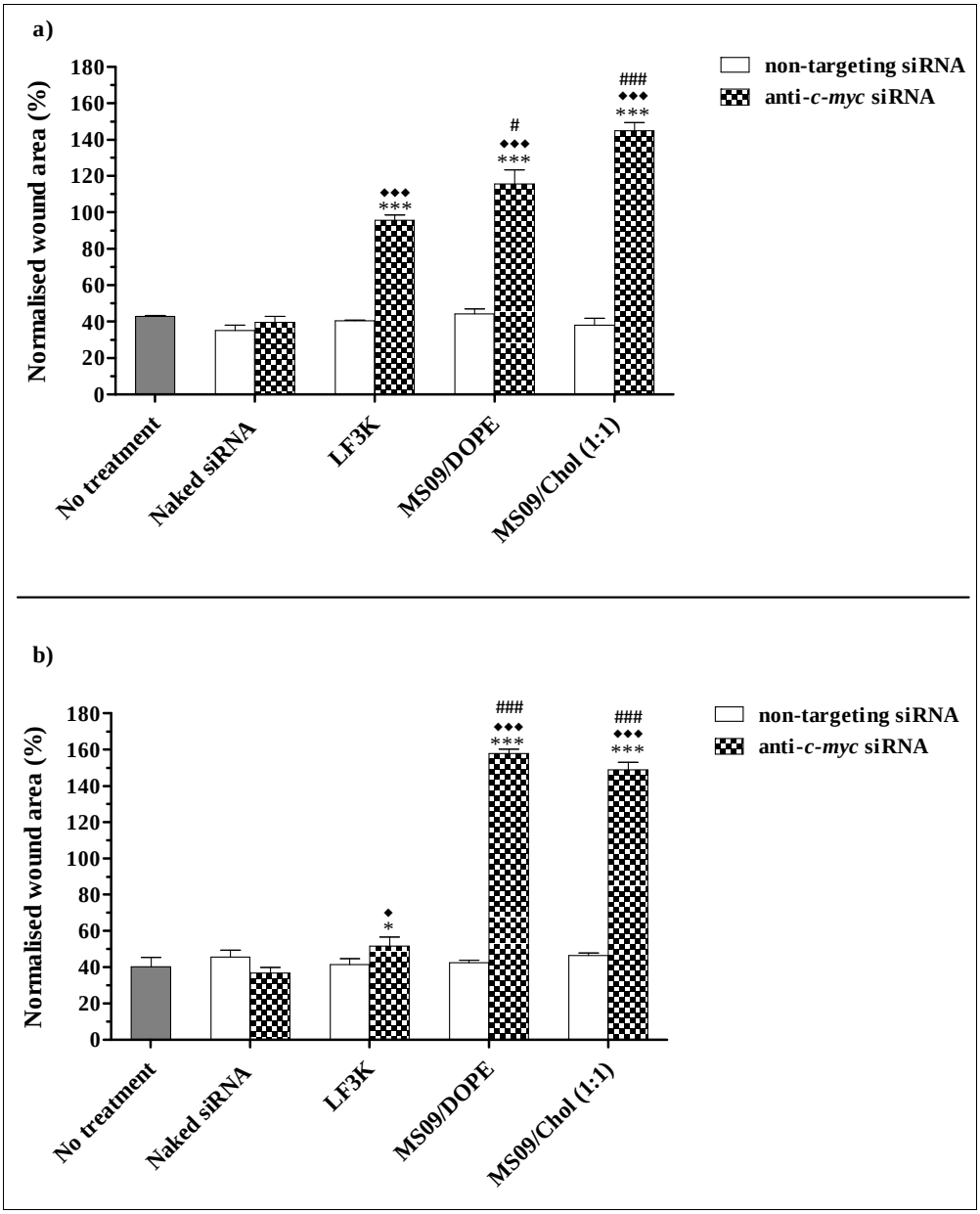

Figure 4.39: Wound healing ability of **a)** MCF-7 and **b)** HT-29 cells after treatment with lipoplexes assembled with either non-targeting or anti-*c-myc* siRNA. Data is presented as the mean ± SD (*n* = 3). $^{*}P < 0.05$, $^{***}P < 0.001$ *vs*. naked siRNA; $^{\blacklozenge}P < 0.05$, $^{\blacklozenge\blacklozenge\blacklozenge}P < 0.001$ *vs*. non-targeting siRNA. $^{\#}P < 0.05$, $^{\#\#\#}P < 0.001$ *vs*. anti-*c-myc* LF3K.

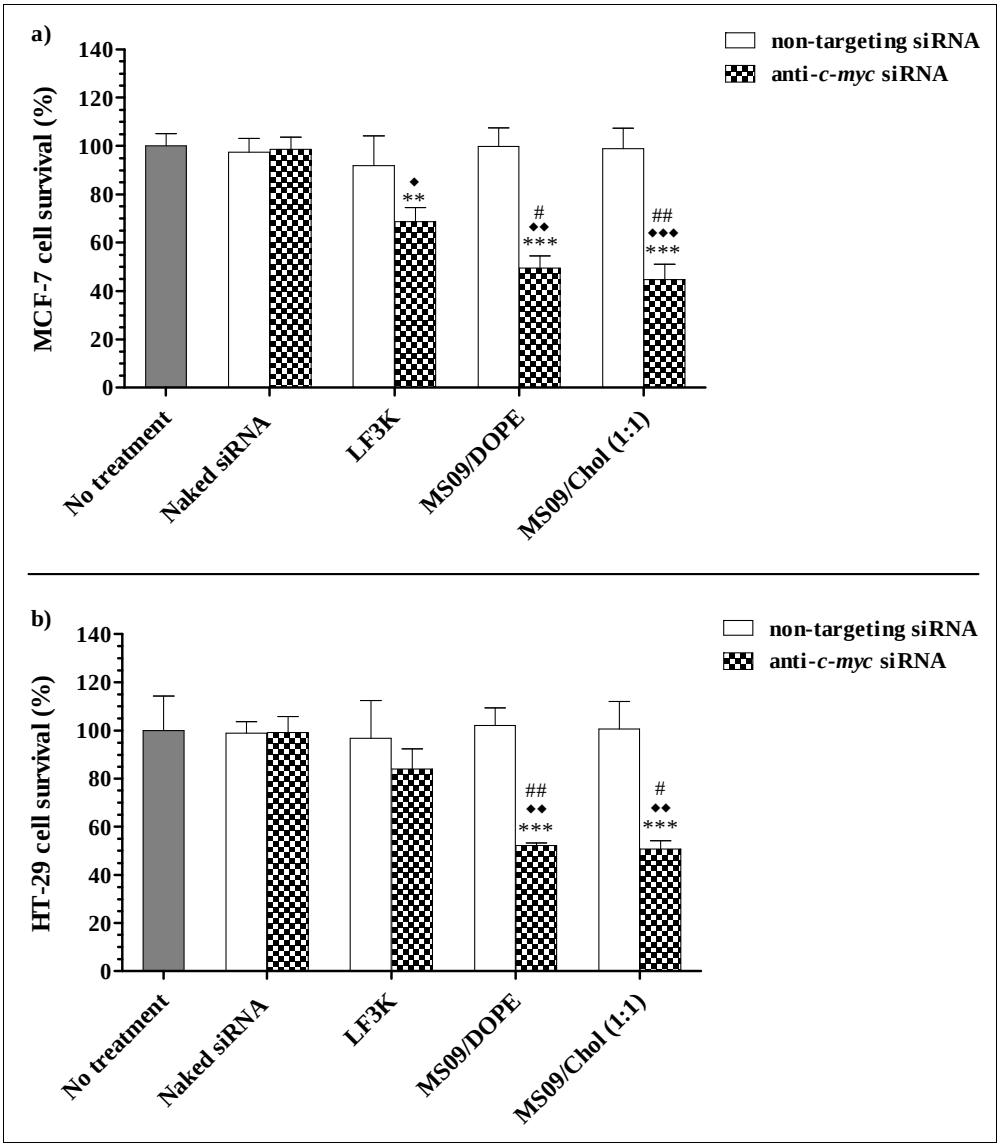

Figure 4.40: Effect of lipoplexes assembled with anti-*c-myc* siRNA on the growth of **a)** MCF-7 and **b)** HT-29 cells. Cells were tested for viability by the AB assay 48 h post-transfection. Data is presented as the mean ± SD (n = 3). $^{**}P < 0.01$, $^{***}P < 0.001$ *vs*. naked siRNA; $^{\blacklozenge}P < 0.05$, $^{\blacklozenge\blacklozenge}P < 0.01$, $^{\blacklozenge\blacklozenge\blacklozenge}P < 0.001$ *vs*. non-targeting siRNA; $^{\#}P < 0.05$, $^{\#\#}P < 0.01$ vs. anti-*c-myc* LF3K. $P > 0.05$ with respect to anti-*c-myc* MS09/Chol (1:1) *vs*. anti-*c-myc* MS09/DOPE.

Cell death can occur by several mechanisms and this is dependent upon the stimulus that cells receive. In treating cancer, a desirable feature is for the treatment to induce death of cancer cells without causing harm to surrounding healthy tissue. For this reason several anti-cancer approaches have attempted to exploit a natural mechanism of cell death such as apoptosis that, under normal conditions, facilitates elimination of damaged and/or harmful cells in a regulated

fashion (Baig *et al*., 2016). To test whether or not the anti-*c-myc* lipoplexes result in cell death via this potentially useful pathway, AO/EtBr dual staining was performed.

The AO/EtBr method is based on the principle that AO enters cells with intact plasma membranes and binds to DNA to emit green fluorescence, while EtBr enters cells with defective membrane integrity and fluoresces red-orange when bound to DNA. Differentiation between normal, early apoptotic, late apoptotic and necrotic cells was made based on observations of nuclear morphology (Figures 4.41, 4.42). Live cells were characterised by a bright green nucleus in the centre of the cell. The nuclei of early apoptotic cells, with undamaged membranes, also stained green, but appeared to be fragmented or condensed. In contrast, the nuclei of late apoptotic cells, with compromised membrane integrity, stained orange with evidence of fragmentation or condensation. Finally, necrotic cells were characterised by an intact bright orange nucleus (Ribble *et al*., 2005).

Figure 4.43 shows that the major mechanism of cell death that was observed by the AB assay after 48 h in cells treated with anti-*c-myc* lipoplexes is, in fact, apoptosis. This observation is supported by several studies which have demonstrated that inhibition of *c-myc* in cancer cells leads to apoptosis (Chen *et al*., 2010, Wang *et al*., 2005, Zhang *et al*., 2009), and this is largely due to the phenomenon of oncogene addiction (Felsher, 2010). Importantly, necrosis, a non-specific form of cell death that is associated with an inflammatory response (Kasibhatla and Tseng, 2003), was negligible in all instances i.e. necrotic cells accounted for less than 3 % of total cells per sample. This implies that MS09/Chol (1:1) and MS09/DOPE-mediated anti-*c-myc* siRNA delivery is capable of destroying cancer cells without damaging healthy tissue.

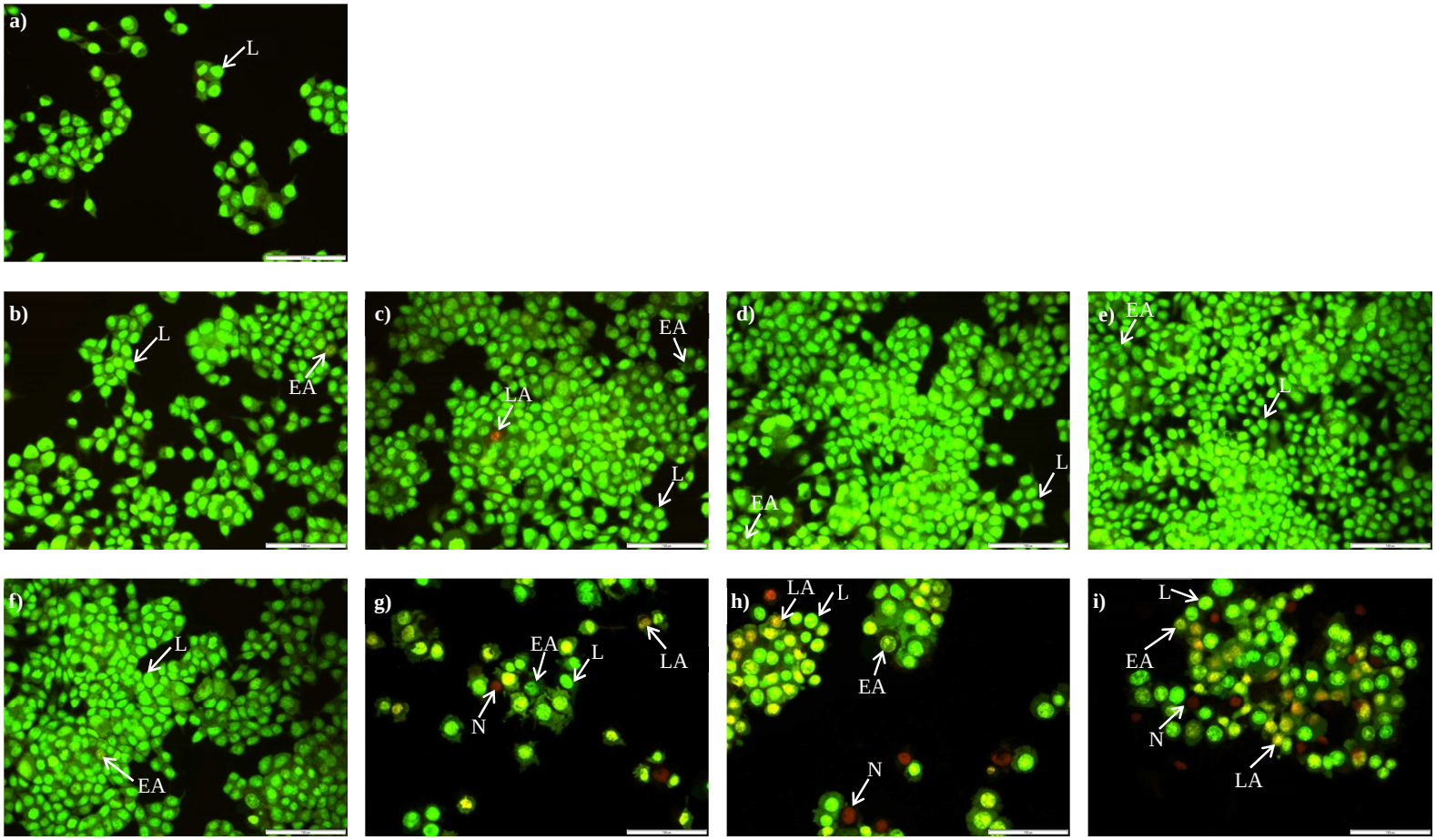

Figure 4.41: Apoptotic potential of anti-*c-myc* and non-targeting lipoplexes in MCF-7 cells. Live and apoptotic cells were visualised by AO/EtBr dual staining, 48 h after transfection with MS09/DOPE and MS09/Chol (1:1) lipoplexes (MS09:siRNA $^{w}/_{w}$ = 16:1) at 12 nM final siRNA concentration. Transfections with Lipofectamine™ 3000 (LF3K) were as per manufacturer's instruction. Cells were observed using an inverted fluorescence microscope at 200× magnification, and one representative field of view per sample is given. Labelled arrows denote the following: L = live, EA = early apoptotic, LA = late apoptotic, N = necrotic. The scale bar represents 100 µm in all images. Treatment groups were as follows:

a) No treatment
b) Naked non-targeting siRNA
c) LF3K with non-targeting siRNA
d) MS09/DOPE lipoplex with non-targeting siRNA
e) MS09/Chol (1:1) lipoplex with non-targeting siRNA
f) Naked anti-*c-myc* siRNA
g) LF3K with anti-*c-myc* siRNA
h) MS09/DOPE lipoplex with anti-*c-myc* siRNA
i) MS09/Chol (1:1) with anti-*c-myc* siRNA

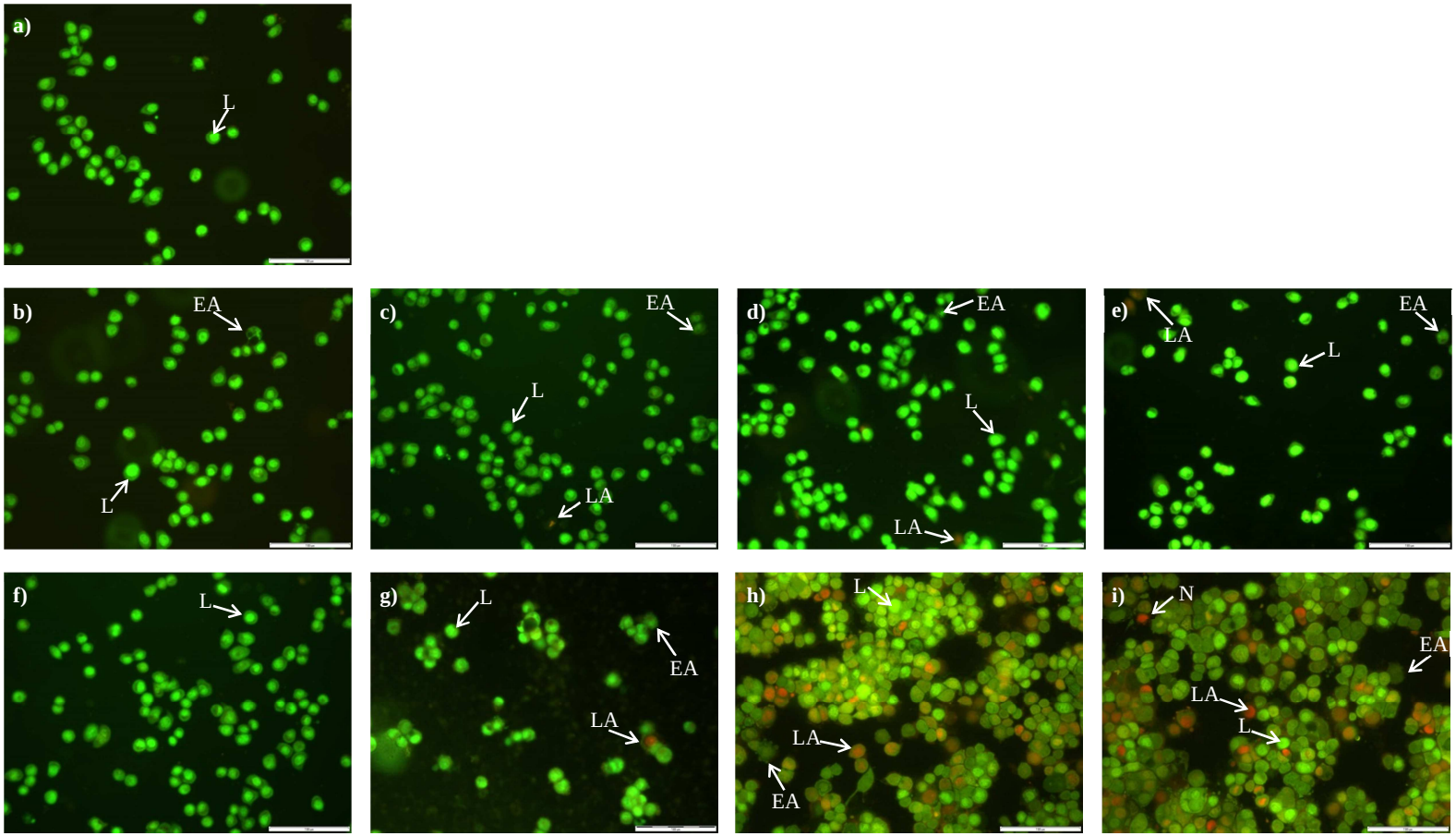

Figure 4.42: Apoptotic potential of anti-*c-myc* and non-targeting lipoplexes in HT-29 cells. Live and apoptotic cells were visualised by AO/EtBr dual staining, 48 h after transfection with MS09/DOPE and MS09/Chol (1:1) lipoplexes (MS09:siRNA $^{w}/_{w}$ = 16:1) at 12 nM final siRNA concentration. Transfections with Lipofectamine™ 3000 (LF3K) were as per manufacturer's instruction. Cells were observed using an inverted fluorescence microscope at 200× magnification, and one representative field of view per sample is given. Labelled arrows denote the following: L = live, EA = early apoptotic, LA = late apoptotic, N = necrotic. The scale bar represents 100 µm in all instances. Treatment groups were as follows:

a) No treatment
b) Naked non-targeting siRNA
c) LF3K with non-targeting siRNA
d) MS09/DOPE lipoplex with non-targeting siRNA
e) MS09/Chol (1:1) lipoplex with non-targeting siRNA
f) Naked anti-*c-myc* siRNA
g) LF3K with anti-*c-myc* siRNA
h) MS09/DOPE lipoplex with anti-*c-myc* siRNA
i) MS09/Chol (1:1) with anti-*c-myc* siRNA

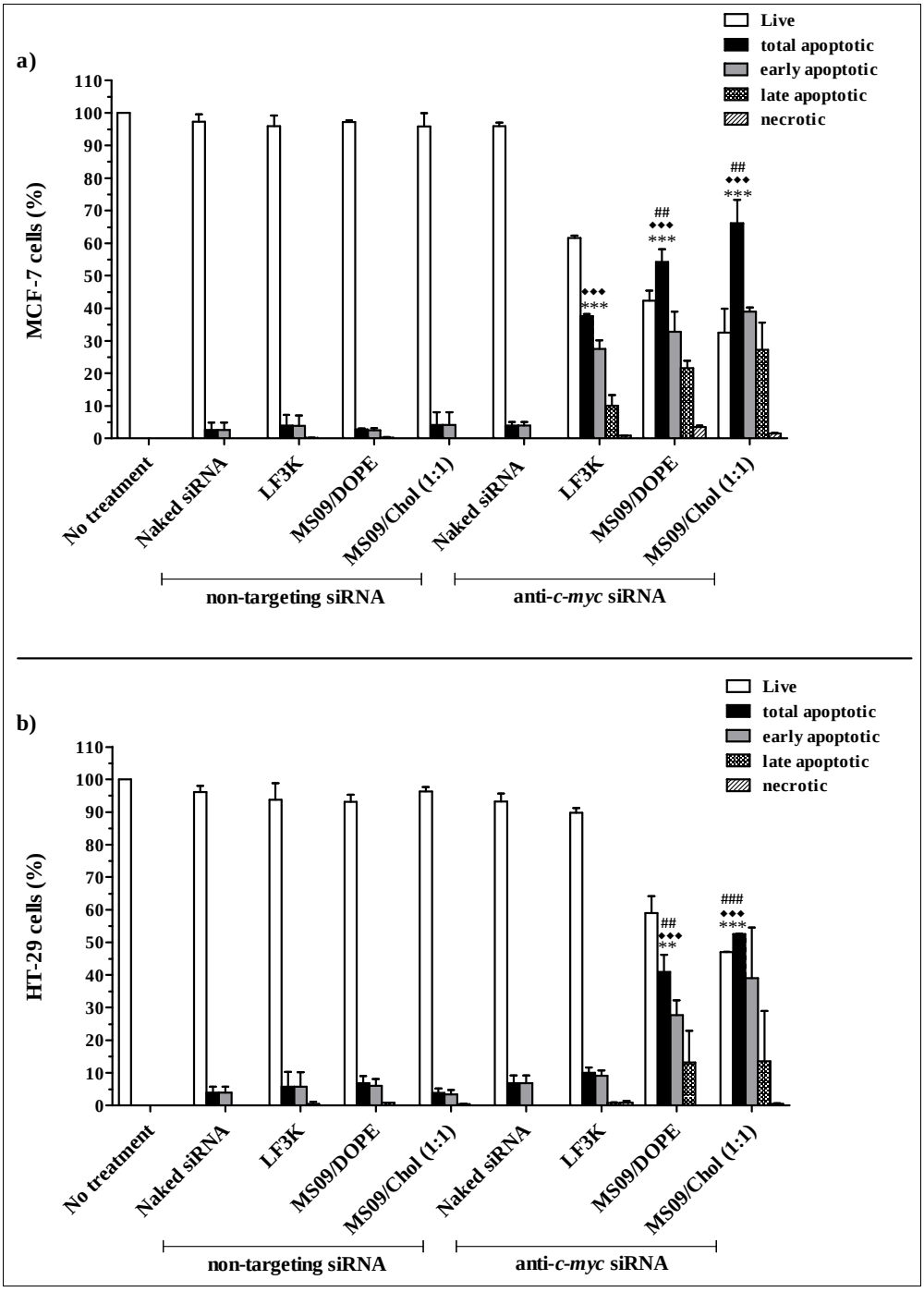

Figure 4.43: Quantification of apoptotic potential of anti-*c-myc* and non-targeted lipoplexes in **a)** MCF-7 and **b)** HT-29 cells. Live, early apoptotic, late apoptotic and necrotic cells were visualised by fluorescence microscopy after AO/EtBr dual staining. At least 200 cells per sample were counted. Data is presented as the mean ± SD (n = 3). $^{**}P < 0.01$, $^{***}P < 0.001$ *vs*. naked siRNA; $^{♦♦♦}P < 0.001$ *vs*. non-targeting siRNA; $^{\#\#}P < 0.01$, $^{\#\#\#}P < 0.001$ *vs*. anti-*c-myc* LF3K. $P > 0.05$ with respect to anti-*c-myc* MS09/Chol (1:1) *vs*. anti-*c-myc* MS09/DOPE.

A significant decrease in *c-myc* expression was correlated with anti-cancer effects, which included inhibition of cancer cell migration, loss of cell viability and elimination of cancer cells through apoptosis, in all instances, with the exception of anti-*c-myc* LF3K in HT-29 cells. Here, modest *c-myc* inhibition slightly impeded cancer cell migration but was too low to induce significant apoptosis and reduce cancer cell numbers within a 48 h period. Of importance, is the observation that lipoplexes assembled with non-targeting siRNA, which had no effect on *c-myc* expression, did not impede the normal migration of cancer cells, and did not significantly influence their growth in any way. The application of anti-*c-myc* siRNA in the absence of a transfecting agent also did not exhibit any anti-cancer activity. Taken together, this confirms that all anti-cancer effects can be ascribed to the RNAi activity of successfully introduced anti-*c-myc* siRNA.

In keeping with the trend observed in the gene silencing experiments, anti-*c-myc* MS09/Chol (1:1) and MS09/DOPE lipoplexes gave better anti-cancer activity than the LF3K reagent, in a given cell line. Furthermore the comparable gene silencing activity mediated by MS09/Chol (1:1) and MS09/DOPE lipoplexes in individual cell lines was coupled with anti-cancer effects of near-equal potency. Although *c-myc* inhibition with MS09 lipoplexes was more pronounced (i.e. 3.8- and 2.8-fold differences at the mRNA and protein levels, respectively) in MCF-7 cells than in HT-29 cells, the associated impact on cell migration, cell growth and extent to which apoptosis was induced, was similar. Here two possible explanations can be put forward. The first is that the level of *c-myc* inhibition required to elicit a given degree of anti-cancer activity differs among cell lines. The second is that, more potent oncogene knockdown does not necessarily correspond with enhanced anti-cancer activity. This notion correlates with previous comments that a lower final siRNA dose may prove as effective in the easier to transfect, MCF-7 cell line.

4.13 Predicting *in vivo* efficacy of the MS09/Chol (1:1) lipoplex

Thus far, it has been demonstrated that both MS09/DOPE and MS09/Chol (1:1) formulations are able to successfully deliver anti-*c-myc* siRNA to the RNAi apparatus, into cancer cells known to overexpress this oncogene. Both formulations were able to achieve knockdown of oncogenic *c-myc* and elicit anti-cancer effects that surpassed the performance of LF3K. Hence, both formulations performed well under standard cell culture conditions, i.e. with 10 % serum. In order to predict *in vivo* efficacy, a serum stability study was performed in higher serum concentrations to resemble physiological conditions more closely (Templeton, 2003, Eliyahu *et al*., 2002).

Figure 4.44 shows the results of cellular uptake experiments performed in medium containing 10, 30 and 50 % serum, with 50 % serum representing physiological concentration (Zhang and Anchordoquy, 2004). If present at higher than normal concentrations, serum could either lead to an abnormal increase in the growth of cultured cells or adversely impact on viability (EL-Ensahsy, 2009). In light of this, 24 h exposure to lipoplexes, as was carried out in all previous cellular uptake experiments, in medium with high serum concentration was deemed impractical. For this reason, cells were exposed to lipoplexes in medium containing the relevant serum concentration for a shorter duration, i.e. 4 h, after which normal growth medium was re-introduced. It was demonstrated that the shorter exposure time did not have a significant effect on cellular uptake of the siRNA marker following transfection in both cell lines ($P > 0.05$, 4 h *vs*. 24 h in 10 % serum). This implies that lipoplexes are either completely taken up, or at least attached to cell membranes within 4 h of application. In addition, this observation validates the exposure time fixed in this set of experiments. Moreover, the new set of transfection conditions employed had no effect on cell growth as confirmed by the AB assay (Appendix F, Figure F2). Hence, any observed reduction in siRNA uptake was as a consequence of the performance of the liposomal carrier at the relevant serum concentration, and not due to any growth inhibitory effects.

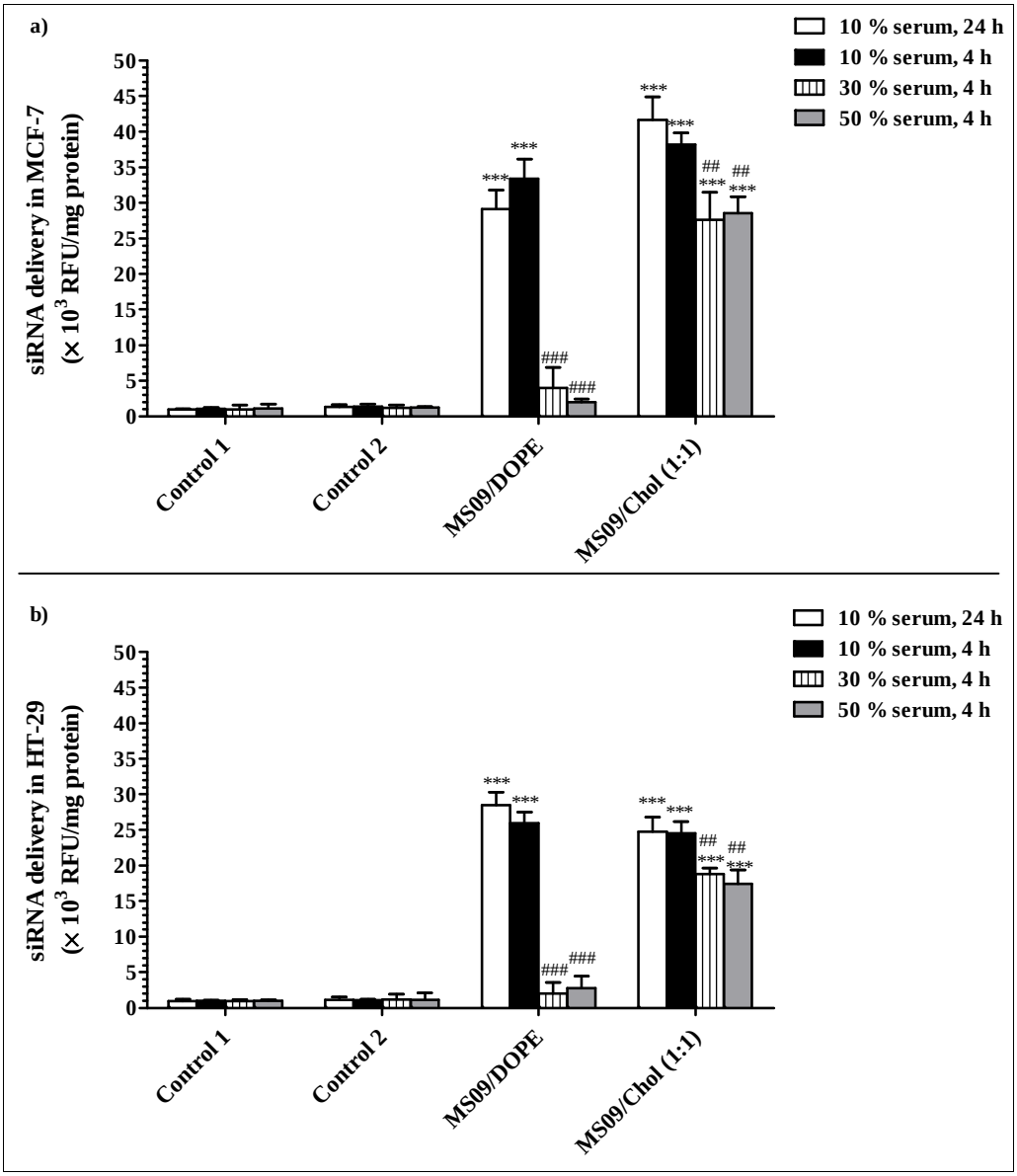

Figure 4.44: The effect of serum concentration on siRNA delivery by MS09/DOPE and MS09/Chol (1:1) lipoplexes in **a)** MCF-7 and **b)** HT-29 cells. Cells were exposed to lipoplexes assembled with BLOCK-iT™ Fluorescent Oligo at MS09:siRNA ($^{w}/_{w}$) ratio of 16:1 for 4 h in medium containing 10, 30 or 50 % serum. Cells received a final oligo concentration of 12 nM. Intracellular fluorescence was measured 24 h post-transfection. Control 1 contained cells only, while control 2 contained cells treated with the naked oligo. Each column represents the mean ± SD (n = 3). $^{***}P < 0.001$ *vs.* control 2; $^{##}P < 0.01$, $^{###}P < 0.001$ *vs.* siRNA delivery in 10 % serum with 4 h exposure to lipoplexes.

Although a significant reduction in siRNA delivery was noted with both formulations in MCF-7 and HT-29 cells when serum concentration was increased from 10 to 30 %, the effect on MS09/DOPE-mediated delivery was more dramatic. In fact, siRNA delivery by MS09/DOPE was negligible in 30 % and 50 % serum in both cell lines. It appears therefore, that the siRNA delivery capability of MS09/DOPE is limited to standard *in vitro* conditions. In contrast, no significant ($P > 0.05$) drop in siRNA delivery by MS09/Chol (1:1) was noted in either cell line when serum concentration was increased from 30 to 50 %.

Despite the weaker siRNA-binding affinity of the MS09/Chol (1:1) formulation, it retains the ability to deliver siRNA at physiological serum concentration due to Chol-conferred stability. Of note, is the fact that normalised intracellular fluorescence after the introduction of MS09/Chol (1:1) lipoplexes in 50 % serum, was significantly ($P < 0.05$) greater, in both cell lines, than levels achieved with the LF3K transfection reagent under standard *in vitro* conditions. This implies that the anti-*c-myc* MS09/Chol (1:1) lipoplex, at MS09:siRNA ($^{w}/_{w}$) ratio of 16:1, would be capable of oncogene silencing and anti-cancer activity at physiological serum concentration, when applied at final lipid and siRNA concentrations of 8.2 μM and 12 nM, respectively.

CHAPTER 5 – SUMMARY AND CONCLUSION

Overexpression of the *c-myc* proto-oncogene features prominently in most human cancers. Early studies established that inhibiting oncogenic *c-myc* expression produced anti-cancer effects. This gave rise to the notion that an appropriate *c-myc* silencing system may provide a broadly applicable and more effective form of cancer treatment, than is currently available. In this regard, several nucleic acid-mediated, antigene and antisense strategies have been explored. Among them *c-myc* silencing approaches based on the use of siRNA molecules, which mediate the natural RNAi mechanism, represent a promising and current area of research (Whitfield *et al*., 2017).

In theory, siRNA molecules with sequences that are complementary to the *c-myc* mRNA transcript will inhibit *c-myc* expression by causing cleavage of *c-myc* mRNA through interaction with the RNAi machinery in the cytoplasm. However, the success of this strategy is largely dependent upon efficient intracellular delivery of siRNA. Consequently the association of anti-*c-myc* siRNA with a variety of carrier agents has been explored, many of which are elaborate multi-component nanosystems. The current study took into account the fact that lipid-based nanoparticles represent the most widely explored class of siRNA carriers to date, and this provided a massive body of knowledge upon which to improve. Moreover, a carrier system with a straightforward design is better suited for routine clinical application, because it is more likely to be easily and economically produced. Hence, this study focused on what is arguably the simplest lipid-based siRNA delivery agent, i.e. the traditional cationic liposome, as the framework for the development of an uncomplicated, but effective anti-*c-myc* onconanotherapeutic agent.

An existing cationic lipid, MS09, which previously demonstrated efficacy within the context of *in vitro* siRNA delivery, served as the foundation for the formulation of novel cationic liposomes. In the interest of developing liposomes capable of maintaining stability and resisting damage within biological fluids, Chol, which provides mechanical strength to lipid bilayers, was included as a helper lipid in novel formulations. As a further stabilising feature, PEG-modification in the form of DSPE-PEG_{2000} was introduced. Liposomes containing equimolar

quantities of MS09 and the conventional helper lipid, DOPE, were included for comparative purposes.

The process of developing an appropriate MS09-based siRNA carrier began with the optimisation of the Chol content of MS09 formulations. Within the range of MS09:Chol molar ratios explored, MS09 was found to be compatible with only 50 mol % Chol, in the presence or absence of DSPE-PEG_{2000} at 2 mol %. Therefore, the study proceeded with four preparations, i.e. the 2 % pegylated and non-pegylated MS09/Chol (1:1) formulations and their DOPE-containing counterparts. Films of these lipid mixtures were successfully hydrated to form small unilamellar liposomes, less than 140 nm in size, with zeta potential between -27 and -36 mV. The lipid film hydration liposome preparation method employed gave liposome suspensions of consistent quality under standard laboratory conditions. Moreover, the substitution of DOPE with Chol and/or incorporation of PEG improved the stability of MS09 liposomes with extended storage time.

The siRNA-binding affinity of liposomes was evaluated based on their ability to retard the migration of siRNA on agarose gels and displace siRNA-intercalated dyes. Although Chol- and PEG-containing liposomes showed weaker siRNA-binding capability than MS09/DOPE, these formulations were carried forward in the study on the grounds that a weaker siRNA-binding interaction may be useful for the release of siRNA at a later stage in the transfection process. Cryo-TEM gave visual proof that all formulations formed complexes with siRNA at MS09:siRNA ($^{w}/_{w}$) ratios of 12:1-32:1. Further evidence of lipoplex formation was obtained by Z-NTA-derived concentration estimates which confirmed the involvement of several liposomal vesicles in a single complex, except in instances in which the liposome-siRNA interaction was markedly tenuous. Lipoplexes were smaller than 200 nm, with zeta potential between -16 and -44 mV. Liposome composition and the MS09:siRNA ($^{w}/_{w}$) ratio at which the complexes were assembled influenced both lipoplex morphology and the degree of protection that siRNA was afforded in the presence of serum. Lipoplexes with bilamellar structures were found to be most effective at protecting siRNA against nuclease attack.

Having confirmed that all formulations formed nanostructures in which siRNA was protected, and which displayed biophysical characteristics conducive to cellular uptake, the interaction of lipoplexes with several human cell lines was investigated. These were the MCF-7 breast cancer

and HT-29 colon cancer cells, both of which overexpress *c-myc*; Caco-2 colon cancer cells that are able to regulate *c-myc* expression; and a non-transformed cell line, HEK293. In order to select the best performing lipoplex, cells received lipoplexes assembled at all characterised MS09:siRNA ($^{w}/_{w}$) ratios (i.e. 12:1-32:1) and these were applied at broad range final siRNA concentrations (i.e. 57-14 nM). Cell viability assays showed that lipoplex-mediated growth inhibition was cell-specific and dependent upon several variables. These included the liposome composition, the MS09:siRNA ($^{w}/_{w}$) ratio at which lipoplexes were formed and the final siRNA and lipid dose. These factors also had a bearing on cellular uptake and siRNA delivery efficiency. Although well tolerated, pegylated lipoplexes gave negligible siRNA delivery in MCF-7 and HT-29 cells. This was largely ascribed to the inhibitory effect of PEG chains on the interaction between the lipoplex and biological membranes. In this regard, the use of cleavable PEG-lipids, designed to shed the polymer upon exposure to specific extra- or intracellular conditions, has been suggested (Fang *et al*., 2017).

By contrast, non-pegylated lipoplexes proved effective even at low final siRNA concentration. The MS09/Chol (1:1) lipoplex at the MS09:siRNA ($^{w}/_{w}$) ratio of 16:1 was most effectively taken up by MCF-7 and HT-29 cells, without compromising cell viability at 14 nM final siRNA. Moreover, at the applied dose, this lipoplex appeared selective for *c-myc*-overexpressing cancer cells, having no significant impact in non-cancerous cells and cancer cells that are able to regulate *c-myc* expression i.e. HEK293 and Caco-2, respectively. Therefore, the MS09/Chol (1:1) lipoplex (MS09:siRNA ($^{w}/_{w}$) ratio = 16:1) was investigated further as a potential *c-myc* silencing agent. A final siRNA concentration of 12 nM was found to be the minimum dose required for maximum cellular uptake of this lipoplex in MCF-7 and HT-29 cells. It was also confirmed that, at this dose, lipoplexes were not internalised by HEK293 and Caco-2 cells and no significant drop in cell numbers was recorded.

Anti-*c-myc* lipoplexes were assembled using a pool of four siRNA duplexes, each with complementarity to a different region of the *c-myc* transcript. At 12 nM final siRNA, the MS09/Chol (1:1) lipoplex dramatically reduced *c-myc* expression at the mRNA and protein levels within a 48 h period in both cell lines. Lipoplex-mediated *c-myc* silencing inhibited the motility of cancer cells and induced cell death. Importantly, cancer cell death was found to occur primarily via the innocuous mechanism of apoptosis which preserves the integrity of normal,

healthy tissue. In all instances, the MS09/Chol (1:1) lipoplex produced more potent *c-myc* silencing and anti-cancer effects than the commercially available transfection reagent, LF3K. Although the DOPE-containing counterpart performed with comparable efficacy under standard cell culture conditions, it will not be effective *in vivo*. This was highlighted by the demonstration that an increase in serum concentration, both approaching and at physiological levels, abolished siRNA delivery by MS09/DOPE. In contrast, the MS09/Chol (1:1) lipoplex retained approximately 70 % siRNA delivery capability in MCF-7 and HT-29 cells when transfections were conducted in 50 % serum. Given the catalytic, non-stoichiometric activity of siRNA, this lipoplex is likely to give clinically useful outcomes *in vivo*. Moreover, the performance of the MS09/Chol (1:1) lipoplex at physiological serum concentration, in the absence of pegylation, ties in with previous work which suggested the use of large quantities of Chol as an alternative to pegylation (Nchinda *et al*., 2002, Templeton *et al*., 1997, Yang *et al*., 2013, Zhang and Anchordoquy, 2004). It is also worth mentioning that further studies with primary cells, which require high serum concentrations to grow, could provide strong supporting data in evaluating lipoplex performance *in vivo*. The current study can be profitably extended by repeating the cellular uptake experiments, as described, in primary cells derived from *c-myc*-driven tumours and, finally, appling the anti-*c-myc* MS09/Chol (1:1) lipoplex to assess oncogene knockdown at physiological serum levels.

The fact that the MS09/Chol (1:1) lipoplex, in the absence of any additional modifications, appears to display specificity for *c-myc*-overexpressing cancer cells, is a point of interest and worthy of further investigation. In order to confirm this phenomenon it is suggested that the cellular uptake of the lipoplex be assessed in several more cell lines, that are representative of other cancers characterised by *c-myc* overexpression. Taking into account that *c-myc* overexpression drives aberrant lipid metabolism (Eberlin *et al*., 2014, Hall *et al*., 2016, Perry *et al*., 2013) and the postulate that cholesterol domains of the lipoplex could facilitate cellular uptake via interaction with plasma membrane components (Betker *et al*., 2013b); it is possible that even subtle differences in composition of the plasma membrane of such cancer cells, as opposed to cells which can regulate *c-myc* levels, may account for the observed affinity for this lipoplex. A comparison of lipid profiles of cells which overexpress *c-myc* and those which do not, combined with an in-depth analysis of the lipoplex uptake mechanism could confirm whether or not this holds true. Such a study could open up further possibilities for targeting the

vast majority of cancers in which *c-myc* is overexpressed while maintaining a simple carrier design.

In summary, several features of the anti-*c-myc* MS09/Chol (1:1) lipoplex point towards its potential as a simple, safe and effective onconanotherapeutic agent. Firstly, the lipoplex is an uncomplicated three-component nanostructure obtained in a convenient two-stage process i.e. reproducible lipid-film hydration of MS09 and Chol to form a stable liposome suspension, followed by electrostatic association with siRNA. Secondly, the lipoplex mediated potent *c-myc* silencing at a relatively low final siRNA and lipid dose, and this destroys cancer cells in a manner that is unlikely to injure healthy cells. Its effectiveness as an anti-cancer agent was highlighted by its ability to facilitate efficient siRNA delivery and oncogene knockdown in recalcitrant cancer cells. Moreover, the physical features of the lipoplex point towards a tendency for selective accumulation at tumour sites. Thirdly, the lipoplex has apparent specificity for *c-myc*-overexpressing cancer cells without adversely affecting non-cancerous cells. Finally, the lipoplex remains capable of siRNA delivery at physiological serum concentrations. These features, taken together, suggest that the anti-*c-myc* MS09/Chol (1:1) lipoplex reported is worthy of further investigation *in vivo*.

REFERENCES

American Cancer Society. 2015. Global Cancer Facts & Figures. 3rd ed. Atlanta: American Cancer Society.

AAGAARD, L. & ROSSI, J. J. 2007. RNAi therapeutics: principles, prospects and challenges. *Advanced Drug Delivery Reviews,* 59**,** 75-86.

ABBA, M. N. C., LAGUENS, R. M., DULOUT, F. N. & GOLIJOW, C. D. 2004. The c-myc activation in cervical carcinomas and HPV 16 infections. *Mutation Research/Genetic Toxicology and Environmental Mutagenesis,* 557**,** 151-158.

ABDULLAH, C., KORKAYA, H., IIZUKA, S. & COURTNEIDGE, S. A. 2018. SRC increases MYC mRNA expression in estrogen receptor-positive breast cancer via mRNA stabilization and inhibition of p53 function. *Molecular and Cellular Biology,* 38**,** e00463-17. DOI:10.1128/MCB.00050-18.

ADACHI, S., OBAYA, A. J., HAN, Z., RAMOS-DESIMONE, N., WYCHE, J. H. & SEDIVY, J. M. 2001. c-Myc is necessary for DNA damage-induced apoptosis in the G2 phase of the cell cycle. *Molecular and Cellular Biology,* 21**,** 4929-4937.

ADAMS, J. M., HARRIS, A. W., PINKERT, C. A., CORCORAN, L. M., ALEXANDER, W. S., CORY, S., PALMITER, R. D. & BRINSTER, R. L. 1985. The c-myc oncogene driven by immunoglobulin enhancers induces lymphoid malignancy in transgenic mice. *Nature,* 318**,** 533-538.

AKHTAR, S. & BENTER, I. 2007. Toxicogenomics of non-viral drug delivery systems for RNAi: potential impact on siRNA-mediated gene silencing activity and specificity. *Advanced Drug Delivery Reviews,* 59**,** 164-182.

ALAGIA, A. & ERITJA, R. 2016. siRNA and RNAi optimization. *Wiley Interdisciplinary Reviews: RNA,* 7**,** 316-329.

ALAMEH, M., JEAN, M., DEJESUS, D., BUSCHMANN, M. D. & MERZOUKI, A. 2010. Chitosanase-based method for RNA isolation from cells transfected with chitosan/siRNA nanocomplexes for real-time RT-PCR in gene silencing. *International Journal of Nanomedicine,* 5**,** 473-481.

ALECO, D., GRITTI, I., NICOLI, P., GIORGIO, M., DONI, M., CONTI, A., BIANCHI, V., CASOLI, L., SABÒ, A. & MIRONOV, A. 2016. The mitochondrial translation machinery as a therapeutic target in Myc-driven lymphomas. *Oncotarget,* 7**,** 72415-72430.

ALLEN, T. M. & CULLIS, P. R. 2013. Liposomal drug delivery systems: from concept to clinical applications. *Advanced Drug Delivery Reviews,* 65**,** 36-48.

ALMGREN, M., EDWARDS, K. & KARLSSON, G. 2000. Cryo transmission electron microscopy of liposomes and related structures. *Colloids and Surfaces A: Physicochemical and Engineering Aspects,* 174**,** 3-21.

ALSHEHRI, A., GRABOWSKA, A. & STOLNIK, S. 2018. Pathways of cellular internalisation of liposomes delivered siRNA and effects on siRNA engagement with target mRNA and silencing in cancer cells. *Scientific Reports,* 8**,** 3748. DOI:10.1038/s41598-018-22166-3.

ALTMAN, B. J., HSIEH, A. L., SENGUPTA, A., KRISHNANAIAH, S. Y., STINE, Z. E., WALTON, Z. E., GOUW, A. M., VENKATARAMAN, A., LI, B. & GORAKSHA-HICKS, P. 2015. MYC disrupts the circadian clock and metabolism in cancer cells. *Cell Metabolism,* 22**,** 1009-1019.

AMANTANA, A. & IVERSEN, P. L. 2005. Pharmacokinetics and biodistribution of phosphorodiamidate morpholino antisense oligomers. *Current Opinion in Pharmacology,* 5**,** 550-555.

AMATI, B., BROOKS, M. W., LEVY, N., LITTLEWOOD, T. D., EVAN, G. I. & LAND, H. 1993. Oncogenic activity of the c-Myc protein requires dimerization with Max. *Cell,* 72**,** 233-245.

AMBESAJIR, A., KAUSHIK, A., KAUSHIK, J. J. & PETROS, S. T. 2012. RNA interference: A futuristic tool and its therapeutic applications. *Saudi Journal of Biological Sciences,* 19**,** 395-403.

AMBRUS, A. M. & FROLOV, M. V. 2009. The Diverse Roles of RNA Helicases in RNAi. *Cell Cycle,* 8**,** 3500-3505.

ANDERSON, S., POUDEL, K. R., ROH-JOHNSON, M., BRABLETZ, T., YU, M., BORENSTEIN-AUERBACH, N., GRADY, W. N., BAI, J., MOENS, C. B. & EISENMAN, R. N. 2016. MYC-nick promotes cell migration by inducing fascin expression and Cdc42 activation. *Proceedings of the National Academy of Sciences,* 113**,** E5481-E5490.

ARABI, A., WU, S., RIDDERSTRALE, K., BIERHOFF, H., SHIUE, C., FATYOL, K., FAHLEN, S., HYDBRING, P., SODERBERG, O., GRUMMT, I., LARSSON, L. G. & WRIGHT, A. P. 2005. c-Myc associates with ribosomal DNA and activates RNA polymerase I transcription. *Nature Cell Biology,* 7**,** 303-310.

ARVANITIS, C. & FELSHER, D. W. 2006. Conditional transgenic models define how MYC initiates and maintains tumorigenesis. *Seminars in Cancer Biology,* 16**,** 313-317.

AUGENLICHT, L. H., WADLER, S., CORNER, G., RICHARDS, C., RYAN, L., MULTANI, A. S., PATHAK, S., BENSON, A., HALLER, D. & HEERDT, B. G. 1997. Low-level c-myc amplification in human colonic carcinoma cell lines and tumors: a frequent, p53-independent mutation associated with improved outcome in a randomized multi-institutional trial. *Cancer Research,* 57**,** 1769-1775.

BA, M., LONG, H., YAN, Z., WANG, S., WU, Y., TU, Y., GONG, Y. & CUI, S. 2018. BRD4 promotes gastric cancer progression through the transcriptional and epigenetic regulation of c-MYC. *Journal of Cellular Biochemistry,* 119**,** 973-982.

BAHRAM, F., VON DER LEHR, N., CETINKAYA, C. & LARSSON, L.-G. 2000. c-Myc hot spot mutations in lymphomas result in inefficient ubiquitination and decreased proteasome-mediated turnover. *Blood,* 95**,** 2104-2110.

BAIG, S., SEEVASANT, I., MOHAMAD, J., MUKHEEM, A., HURI, H. & KAMARUL, T. 2016. Potential of apoptotic pathway-targeted cancer therapeutic research: Where do we stand? *Cell Death & Disease,* 7**,** e2058. DOI:10.1038/cddis.2015.275.

BAKER, V. V., BORST, M. P., DIXON, D., HATCH, K. D., SHINGLETON, H. M. & MILLER, D. 1990. c-myc amplification in ovarian cancer. *Gynecologic Oncology,* 38**,** 340-342.

BALTACI, E., KARAMAN, E., DALAY, N. & BUYRU, N. 2016. Analysıs of gene copy number changes ın head and neck cancer. *Clinical Otolaryngology***,** DOI:10.1111/coa.12686.

BARATA, P., SOOD, A. K. & HONG, D. S. 2016. RNA-targeted therapeutics in cancer clinical trials: Current status and future directions. *Cancer Treatment Reviews,* 50**,** 35-47.

BARNA, M., PUSIC, A., ZOLLO, O., COSTA, M., KONDRASHOV, N., REGO, E., RAO, P. H. & RUGGERO, D. 2008. Suppression of Myc oncogenic activity by ribosomal protein haploinsufficiency. *Nature,* 456**,** 971-975.

BATTEY, J., MOULDING, C., TAUB, R., MURPHY, W., STEWART, T., POTTER, H., LENOIR, G. & LEDER, P. 1983. The human c-myc oncogene: structural consequences of translocation into the IgH locus in Burkitt lymphoma. *Cell,* 34**,** 779-787.

BATZRI, S. & KORN, E. D. 1973. Single bilayer liposomes prepared without sonication. *Biochimica et Biophysica Acta (BBA)-Biomembranes,* 298**,** 1015-1019.

BAUDINO, T. A., MCKAY, C., PENDEVILLE-SAMAIN, H., NILSSON, J. A., MACLEAN, K. H., WHITE, E. L., DAVIS, A. C., IHLE, J. N. & CLEVELAND, J. L. 2002. c-Myc is essential for vasculogenesis and angiogenesis during development and tumor progression. *Genes & Development,* 16**,** 2530-2543.

BEIMLING, P., BENTER, T., SANDER, T. & MOELLING, K. 1985. Isolation and characterization of the human cellular myc gene product. *Biochemistry,* 24**,** 6349-6355.

BENASSAYAG, C., MONTERO, L., COLOMBIÉ, N., GALLANT, P., CRIBBS, D. & MORELLO, D. 2005. Human c-Myc Isoforms Differentially Regulate Cell Growth and Apoptosis in Drosophila melanogaster. *Molecular and Cellular Biology,* 25**,** 9897-9909.

BENTLEY, D. L. & GROUDINE, M. 1986. Novel promoter upstream of the human c-myc gene and regulation of c-myc expression in B-cell lymphomas. *Molecular and Cellular Biology,* 6**,** 3481-3489.

BERNS, K., HIJMANS, E. M. & BERNARDS, R. 1997. Repression of c-Myc responsive genes in cycling cells causes G1 arrest through reduction of cyclin E/CDK2 kinase activity. *Oncogene,* 15**,** 1347-1356.

BERNSTEIN, E., CAUDY, A. A., HAMMOND, S. M. & HANNON, G. J. 2001. Role for a bidentate ribonuclease in the initiation step of RNA interference. *Nature,* 409**,** 363-366.

BERNSTEIN, P. L., HERRICK, D. J., PROKIPCAK, R. D. & ROSS, J. 1992. Control of c-myc mRNA half-life in vitro by a protein capable of binding to a coding region stability determinant. *Genes & Development,* 6**,** 642-654.

BERTHON, C., RAFFOUX, E., THOMAS, X., VEY, N., GOMEZ-ROCA, C., YEE, K., TAUSSIG, D. C., REZAI, K., ROUMIER, C. & HERAIT, P. 2016. Bromodomain inhibitor OTX015 in patients with acute leukaemia: a dose-escalation, phase 1 study. *The Lancet Haematology,* 3**,** e186-e195.

BERTRAND, J.-R., POTTIER, M., VEKRIS, A., OPOLON, P., MAKSIMENKO, A. & MALVY, C. 2002. Comparison of antisense oligonucleotides and siRNAs in cell culture and in vivo. *Biochemical and Biophysical Research Communications,* 296**,** 1000-1004.

BETKER, J. L., GOMEZ, J. & ANCHORDOQUY, T. J. 2013a. The effects of lipoplex formulation variables on the protein corona and comparisons with in vitro transfection efficiency. *Journal of Controlled Release,* 171**,** 261-268.

BETKER, J. L., KULLBERG, M., GOMEZ, J. & ANCHORDOQUY, T. J. 2013b. Cholesterol domains enhance transfection. *Therapeutic delivery,* 4**,** 453-462.

BITZER, M., STAHL, M., ARJUMAND, J., REES, M., KLUMP, B., HEEP, H., GABBERT, H. E. & SARBIA, M. 2002. C-myc gene amplification in different stages of oesophageal squamous cell carcinoma: prognostic value in relation to treatment modality. *Anticancer Research,* 23**,** 1489-1493.

BJORGE, J. D., PANG, A. & FUJITA, D. J. 2017. Delivery of gene targeting siRNAs to breast cancer cells using a multifunctional peptide complex that promotes both targeted delivery and endosomal release. *PloS ONE,* 12**,** e0180578. DOI:10.1371/journal.pone.0180578.

BLACKWOOD, E. M. & EISENMAN, R. N. 1991. Max: a helix-loop-helix zipper protein that forms a sequence-specific DNA-binding complex with Myc. *Science,* 251**,** 1211-1217.

BLACKWOOD, E. M., LUGO, T. G., KRETZNER, L., KING, M. W., STREET, A. J., WITTE, O. N. & EISENMAN, R. N. 1994. Functional analysis of the AUG- and CUG-initiated forms of the c-Myc protein. *Molecular Biology of the Cell,* 5**,** 597-609.

BOFFA, L., CUTRONA, G., CILLI, M., MATIS, S., DAMONTE, G., MARIANI, M., MILLO, E., MORONI, M., RONCELLA, S. & FEDELI, F. 2006. Inhibition of Burkitt's lymphoma cells growth in SCID mice by a PNA specific for a regulatory sequence of the translocated c-myc. *Cancer Gene Therapy,* 14**,** 220-226.

BOFFA, L. C., CUTRONA, G., CILLI, M., MARIANI, M. R., MATIS, S., PASTORINO, M., DAMONTE, G., MILLO, E., RONCELLA, S. & FERRARINI, M. 2005. Therapeutically promising PNA complementary to a regulatory sequence for c-myc: pharmacokinetics in an animal model of human Burkitt's lymphoma. *Oligonucleotides,* 15**,** 85-93.

BOFFA, L. C., MARIANI, M. R., DAMONTE, G., ALLFREY, V. G., BENATTI, U. & MORRIS, P. L. 2000. Dihydrotestosterone as a selective cellular/nuclear localization vector for anti-gene peptide nucleic acid in prostatic carcinoma cells. *Cancer Research,* 60**,** 2258-2262.

BOUDJADI, S., CARRIER, J., GROULX, J. & BEAULIEU, J. 2016. Integrin α1β1 expression is controlled by c-MYC in colorectal cancer cells. *Oncogene,* 35**,** 1671-1678.

BOULWARE, S. B., CHRISTENSEN, L. A., THAMES, H., COGHLAN, L., VASQUEZ, K. M. & FINCH, R. A. 2014. Triplex-forming oligonucleotides targeting c-MYC potentiate the anti-tumor activity of gemcitabine in a mouse model of human cancer. *Molecular Carcinogenesis,* 53**,** 744-752.

BRAASCH, D. A., JENSEN, S., LIU, Y., KAUR, K., ARAR, K., WHITE, M. A. & COREY, D. R. 2003. RNA interference in mammalian cells by chemically-modified RNA. *Biochemistry,* 42**,** 7967-7975.

BRENNER, C., DEPLUS, R., DIDELOT, C., LORIOT, A., VIRE, E., DE SMET, C., GUTIERREZ, A., DANOVI, D., BERNARD, D., BOON, T., PELICCI, P. G., AMATI, B., KOUZARIDES, T., DE LAUNOIT, Y., DI CROCE, L. & FUKS, F. 2005. Myc represses transcription through recruitment of DNA methyltransferase corepressor. *The EMBO Journal,* 24**,** 336-346.

BRETONES, G., DELGADO, M. D. & LEÓN, J. 2015. Myc and cell cycle control. *Biochimica et Biophysica Acta (BBA)-Gene Regulatory Mechanisms,* 1849**,** 506-516.

BUBENDORF, L., KONONEN, J., KOIVISTO, P., SCHRAML, P., MOCH, H., GASSER, T. C., WILLI, N., MIHATSCH, M. J., SAUTER, G. & KALLIONIEMI, O.-P. 1999. Survey of gene amplifications during prostate cancer progression by high-throughput fluorescence in situ hybridization on tissue microarrays. *Cancer Research,* 59**,** 803-806.

BUSKE, F. A., MATTICK, J. S. & BAILEY, T. L. 2011. Potential in vivo roles of nucleic acid triple-helices. *RNA biology,* 8**,** 427-439.

BUYENS, K., DE SMEDT, S. C., BRAECKMANS, K., DEMEESTER, J., PEETERS, L., VAN GRUNSVEN, L. A., DU JEU, X. D. M., SAWANT, R., TORCHILIN, V. & FARKASOVA, K. 2012. Liposome based systems for systemic siRNA delivery: stability in blood sets the requirements for optimal carrier design. *Journal of Controlled Release,* 158**,** 362-370.

BUYENS, K., LUCAS, B., RAEMDONCK, K., BRAECKMANS, K., VERCAMMEN, J., HENDRIX, J., ENGELBORGHS, Y., DE SMEDT, S. C. & SANDERS, N. N. 2008. A fast and sensitive method for measuring the integrity of siRNA-carrier complexes in full human serum. *Journal of Controlled Release,* 126**,** 67-76.

CAMPANER, S. & AMATI, B. 2012. Two sides of the Myc-induced DNA damage response: from tumor suppression to tumor maintenance. *Cell Division,* 7**,** DOI:10.1186/1747-1028-7-6.

CAMPBELL, J. M., BACON, T. A. & WICKSTROM, E. 1990. Oligodeoxynucleoside phosphorothioate stability in subcellular extracts, culture media, sera and cerebrospinal fluid. *Journal of Biochemical and Biophysical Methods,* 20**,** 259-267.

CAO, B. & JI, A. M. 2009. Construction of small interfering RNA targeting mouse vascular endothelial growth factor receptor-2: its serum stability and gene silencing efficiency in vitro. *Nan Fang Yi Ke Da Xue Xue Bao,* 29**,** 864-867.

CARBONE, G. M., MCGUFFIE, E., NAPOLI, S., FLANAGAN, C. E., DEMBECH, C., NEGRI, U., ARCAMONE, F., CAPOBIANCO, M. L. & CATAPANO, C. V. 2004. DNA binding and antigene activity of a daunomycin-conjugated triplex-forming oligonucleotide targeting the P2 promoter of the human c-myc gene. *Nucleic Acids Research,* 32**,** 2396-2410.

CARNEIRO, B., BRAGA, A. C. S., BATISTA, M. N., HARRIS, M. & RAHAL, P. 2015. Evaluation of canonical siRNA and Dicer substrate RNA for inhibition of hepatitis C virus genome replication–a comparative study. *PloS ONE,* 10**,** e0117742. DOI:10.1371/journal.pone.0117742.

CASEY, S. C., TONG, L., LI, Y., DO, R., WALZ, S., FITZGERALD, K. N., GOUW, A., BAYLOT, V., GUTGEMANN, I., EILERS, M. & FELSHER, D. W. 2016. MYC Regulates the Anti-Tumor Immune Response through CD47 and PD-L1. *Science,* 352**,** 227-231.

CATAPANO, C. V., MCGUFFIE, E. M., PACHECO, D. & CARBONE, G. M. 2000. Inhibition of gene expression and cell proliferation by triple helix-forming oligonucleotides directed to the c-myc gene. *Biochemistry,* 39**,** 5126-5138.

CEBALLOS, C., KHIATI, S., PRATA, C. A., ZHANG, X. X., GIORGIO, S., MARSAL, P., GRINSTAFF, M. W., BARTHELEMY, P. & CAMPLO, M. 2010. Cationic nucleoside lipids derived from universal bases: A rational approach for siRNA transfection. *Bioconjugate Chemistry,* 21**,** 1062-1069.

CERDA, M. B., BATALLA, M., ANTON, M., CAFFERATA, E., PODHAJCER, O., PLANK, C., MYKHAYLYK, O. & POLICASTRO, L. 2015. Enhancement of nucleic acid delivery to hard-to-transfect human colorectal cancer cells by magnetofection at laminin coated substrates and promotion of the endosomal/lysosomal escape. *RSC Advances,* 5**,** 58345-58354.

CHAN, C.-H., LEE, S.-W., LI, C.-F., WANG, J., YANG, W.-L., WU, C.-Y., WU, J., NAKAYAMA, K. I., KANG, H.-Y. & HUANG, H.-Y. 2010. Deciphering the transcriptional complex critical for RhoA gene expression and cancer metastasis. *Nature Cell Biology,* 12**,** 457-467.

CHAN, K.-L., GUAN, X.-Y. & NG, I. O.-L. 2004. High-throughput tissue microarray analysis of c- myc activation in chronic liver diseases and hepatocellular carcinoma. *Human Pathology,* 35**,** 1324-1331.

CHAUDHARY, S., UMAR, A. & MEHTA, S. 2014. Surface functionalized selenium nanoparticles for biomedical applications. *Journal of Biomedical Nanotechnology,* 10**,** 3004-3042.

CHE, J., I OKEKE, C., HU, Z.-B. & XU, J. 2015. DSPE-PEG: a distinctive component in drug delivery system. *Current Pharmaceutical Design,* 21**,** 1598-1605.

CHEN, B.-J., WU, Y.-L., TANAKA, Y. & ZHANG, W. 2014. Small molecules targeting c-Myc oncogene: promising anti-cancer therapeutics. *International Journal of Biological Sciences,* 10**,** 1084-1096.

CHEN, Y., WU, J. J. & HUANG, L. 2010. Nanoparticles targeted with NGR motif deliver c-myc siRNA and doxorubicin for anticancer therapy. *Molecular Therapy,* 18**,** 828-834.

CHENDRIMADA, T. P., GREGORY, R. I., KUMARASWAMY, E., NORMAN, J., COOCH, N., NISHIKURA, K. & SHIEKHATTAR, R. 2005. TRBP recruits the Dicer complex to Ago2 for microRNA processing and gene silencing. *Nature,* 436**,** 740-744.

CHENG, J., LUO, J., ZHANG, X., HU, J., HUI, H., WANG, C. & STERN, A. 2000. Inhibition of cell proliferation in HCC-9204 hepatoma cells by a c-myc specific ribozyme. *Cancer Gene Therapy,* 7**,** 407-412.

CHOU, T.-Y., DANG, C. V. & HART, G. W. 1995. Glycosylation of the c-Myc transactivation domain. *Proceedings of the National Academy of Sciences USA,* 92**,** 4417-4421.

CHRISTENSEN, L. A., FINCH, R. A., BOOKER, A. J. & VASQUEZ, K. M. 2006. Targeting oncogenes to improve breast cancer chemotherapy. *Cancer Research,* 66**,** 4089-4094.

CITRO, G., D'AGNANO, I., LEONETTI, C., PERINI, R., BUCCI, B., ZON, G., CALABRETTA, B. & ZUPI, G. 1998. C-myc antisense oligodeoxynucleotides enhance the efficacy of cisplatin in melanoma chemotherapy in vitro and in nude mice. *Cancer Research,* 58**,** 283-289.

CITTI, L. & RAINALDI, G. 2005. Synthetic hammerhead ribozymes as therapeutic tools to control disease genes. *Current Gene Therapy,* 5**,** 11-24.

CLAASSEN, G. F. & HANN, S. R. 2000. A role for transcriptional repression of p21CIP1 by c-Myc in overcoming transforming growth factor β-induced cell-cycle arrest. *Proceedings of the National Academy of Sciences USA,* 97**,** 9498-9503.

CLEMENS, M. J. 1997. PKR—a protein kinase regulated by double-stranded RNA. *The International Journal of Biochemistry & Cell Biology,* 29**,** 945-949.

COLE, M. D. & COWLING, V. H. 2008. Transcription-independent functions of MYC: regulation of translation and DNA replication. *Nature Reviews Molecular Cell Biology,* 9**,** 810-815.

COLLER, H. A., GRANDORI, C., TAMAYO, P., COLBERT, T., LANDER, E. S., EISENMAN, R. N. & GOLUB, T. R. 2000. Expression analysis with oligonucleotide microarrays reveals that MYC regulates genes involved in growth, cell cycle, signaling, and adhesion. *Proceedings of the National Academy of Sciences USA,* 97**,** 3260-3265.

CONACCI-SORRELL, M., NGOUENET, C. & EISENMAN, R. N. 2010. Myc-nick: A cytoplasmic cleavage product of Myc that promotes α-tubulin acetylation and cell differentiation. *Cell,* 142**,** 480-493.

CONDE, J., AMBROSONE, A., SANZ, V., HERNANDEZ, Y., MARCHESANO, V., TIAN, F., CHILD, H., BERRY, C. C., IBARRA, M. R. & BAPTISTA, P. V. 2012. Design of multifunctional gold nanoparticles for in vitro and in vivo gene silencing. *Acs Nano,* 6**,** 8316-8324.

CONDE, J., TIAN, F., HERNANDEZ, Y., BAO, C., BAPTISTA, P. V., CUI, D., STOEGER, T. & JESUS, M. 2015. RNAi-based glyconanoparticles trigger apoptotic pathways for in vitro and in vivo enhanced cancer-cell killing. *Nanoscale,* 7**,** 9083-9091.

CONDE, J., TIAN, F., HERNÁNDEZ, Y., BAO, C., CUI, D., JANSSEN, K.-P., IBARRA, M. R., BAPTISTA, P. V., STOEGER, T. & JESÚS, M. 2013. In vivo tumor targeting via nanoparticle-mediated therapeutic siRNA coupled to inflammatory response in lung cancer mouse models. *Biomaterials,* 34**,** 7744-7753.

COWLING, V. H. & COLE, M. D. 2007. The Myc transactivation domain promotes global phosphorylation of the RNA polymerase II carboxy-terminal domain independently of direct DNA binding. *Molecular and Cellular Biology,* 27**,** 2059-2073.

CROMBEZ, L., ALDRIAN-HERRADA, G., KONATE, K., NGUYEN, Q. N., MCMASTER, G. K., BRASSEUR, R., HEITZ, F. & DIVITA, G. 2009. A new potent secondary amphipathic cell–penetrating peptide for siRNA delivery into mammalian cells. *Molecular Therapy,* 17**,** 95-103.

CULJKOVIC, B., TOPISIROVIC, I., SKRABANEK, L., RUIZ-GUTIERREZ, M. & BORDEN, K. L. 2006. eIF4E is a central node of an RNA regulon that governs cellular proliferation. *The Journal of Cell Biology,* 175**,** 415-426.

CUTRONA, G., CARPANETO, E. M., PONZANELLI, A., ULIVI, M., MILLO, E., SCARFÌ, S., RONCELLA, S., BENATTI, U., BOFFA, L. C. & FERRARINI, M. 2003. Inhibition of the translocated c-myc in Burkitt's lymphoma by a PNA Complementary to the Eμ Enhancer. *Cancer Research,* 63**,** 6144-6148.

CUTRONA, G., CARPANETO, E. M., ULIVI, M., RONCELLA, S., LANDT, O., FERRARINI, M. & BOFFA, L. C. 2000. Effects in live cells of a c-myc anti-gene PNA linked to a nuclear localization signal. *Nature Biotechnology,* 18**,** 300-303.

CZAUDERNA, F., FECHTNER, M., DAMES, S., AYGÜN, H., KLIPPEL, A., PRONK, G. J., GIESE, K. & KAUFMANN, J. 2003. Structural variations and stabilising modifications of synthetic siRNAs in mammalian cells. *Nucleic Acids Research,* 31**,** 2705-2716.

DAI, M. S., ARNOLD, H., SUN, X. X., SEARS, R. & LU, H. 2007. Inhibition of c-Myc activity by ribosomal protein L11. *The EMBO Journal,* 26**,** 3332-3345.

DALLA-FAVERA, R., BREGNI, M., ERIKSON, J., PATTERSON, D., GALLO, R. C. & CROCE, C. M. 1982. Human c-myc onc gene is located on the region of chromosome 8 that is translocated in Burkitt lymphoma cells. *Proceedings of the National Academy of Sciences USA,* 79**,** 7824-7827.

DALLA-FAVERA, R., MARTINOTTI, S., GALLO, R. C., ERIKSON, J. & CROCE, C. M. 1983. Translocation and rearrangements of the c-myc oncogene locus in human undifferentiated B-cell lymphomas. *Science,* 219**,** 963-967.

DANG, C. V. 1999. c-Myc target genes involved in cell growth, apoptosis, and metabolism. *Molecular and Cellular Biology,* 19**,** 1-11.

DANG, C. V. 2012. MYC on the path to cancer. *Cell,* 149**,** 22-35.

DANG, C. V. 2013. MYC, metabolism, cell growth, and tumorigenesis. *Cold Spring Harbor Perspectives in Medicine,* 3**,** a014217. DOI:10.1101/cshperspect.a014217.

DANG, C. V. 2016. A time for MYC: metabolism and therapy. *Cold Spring Harbor Symposia on Quantitative Biology,* 81**,** 79-83.

DANG, C. V., O'DONNELL, K. A., ZELLER, K. I., NGUYEN, T., OSTHUS, R. C. & LI, F. 2006. The c-Myc target gene network. *Seminars in cancer biology,* 16**,** 253-264.

DANG, H., TAKAI, A., FORGUES, M., POMYEN, Y., MOU, H., XUE, W., RAY, D., HA, K. C., MORRIS, Q. D. & HUGHES, T. R. 2017. Oncogenic activation of the RNA binding protein NELFE and MYC signaling in hepatocellular carcinoma. *Cancer Cell,* 32**,** 101-114. e8.

DANI, C., BLANCHARD, J., PIECHACZYK, M., EL SABOUTY, S., MARTY, L. & JEANTEUR, P. 1984. Extreme instability of myc mRNA in normal and transformed human cells. *Proceedings of the National Academy of Sciences USA,* 81**,** 7046-7050.

DANIELS, A., SINGH, M. & ARIATTI, M. 2013. Pegylated and Non-Pegylated siRNA Lipoplexes Formulated with Cholesteryl Cytofectins Promote Efficient Luciferase Knockdown in HeLa tat luc Cells. *Nucleosides, Nucleotides and Nucleic Acids,* 32**,** 206-220.

DAS, J., HAN, J. W., CHOI, Y.-J., SONG, H., CHO, S.-G., PARK, C., SEO, H. G. & KIM, J.-H. 2016. Cationic lipid-nanoceria hybrids, a novel nonviral vector-mediated gene delivery into mammalian

cells: investigation of the cellular uptake mechanism. *Scientific Reports,* 6**,** 29197. DOI:10.1038/srep29197.
DAVOREN, M., HERZOG, E., CASEY, A., COTTINEAU, B., CHAMBERS, G., BYRNE, H. J. & LYNG, F. M. 2007. In vitro toxicity evaluation of single walled carbon nanotubes on human A549 lung cells. *Toxicology In Vitro,* 21**,** 438-448.
DE GENNES, P. 1980. Conformations of polymers attached to an interface. *Macromolecules,* 13**,** 1069-1075.
DE MORAIS RIBEIRO, L. N., COUTO, V. M., FRACETO, L. F. & DE PAULA, E. 2018. Use of nanoparticle concentration as a tool to understand the structural properties of colloids. *Scientific Reports,* 8**,** DOI:10.1038/s41598-017-18573-7.
DEL MUNDO, I. M. A., ZEWAIL-FOOTE, M., KERWIN, S. M. & VASQUEZ, K. M. 2017. Alternative DNA structure formation in the mutagenic human c-MYC promoter. *Nucleic Acids Research,* 45**,** 4929-4943.
DESANTIS, C. E., LIN, C. C., MARIOTTO, A. B., SIEGEL, R. L., STEIN, K. D., KRAMER, J. L., ALTERI, R., ROBBINS, A. S. & JEMAL, A. 2014. Cancer treatment and survivorship statistics, 2014. *CA: A Cancer Journal for Clinicians,* 64**,** 252-271.
DESHPANDE, M. C., DAVIES, M. C., GARNETT, M. C., WILLIAMS, P. M., ARMITAGE, D., BAILEY, L., VAMVAKAKI, M., ARMES, S. P. & STOLNIK, S. 2004. The effect of poly (ethylene glycol) molecular architecture on cellular interaction and uptake of DNA complexes. *Journal of Controlled Release,* 97**,** 143-156.
DESHPANDE, P. P., BISWAS, S. & TORCHILIN, V. P. 2013. Current trends in the use of liposomes for tumor targeting. *Nanomedicine,* 8**,** 1509-1528.
DESIGAUX, L., SAINLOS, M., LAMBERT, O., CHEVRE, R., LETROU-BONNEVAL, E., VIGNERON, J.-P., LEHN, P., LEHN, J.-M. & PITARD, B. 2007. Self-assembled lamellar complexes of siRNA with lipidic aminoglycoside derivatives promote efficient siRNA delivery and interference. *Proceedings of the National Academy of Sciences USA,* 104**,** 16534-16539.
DEVINCENZO, J. P. 2012. The promise, pitfalls and progress of RNA-interference-based antiviral therapy for respiratory viruses. *Antiviral Therapy,* 17**,** 213-225.
DEWS, M., HOMAYOUNI, A., YU, D., MURPHY, D., SEVIGNANI, C., WENTZEL, E., FURTH, E. E., LEE, W. M., ENDERS, G. H. & MENDELL, J. T. 2006. Augmentation of tumor angiogenesis by a Myc-activated microRNA cluster. *Nature Genetics,* 38**,** 1060-1065.
DIAS, N. & STEIN, C. A. 2002. Antisense Oligonucleotides: Basic Concepts and Mechanisms. *Molecular Cancer Therapeutics,* 1**,** 347-355.
DOMINGUEZ-SOLA, D., YING, C. Y., GRANDORI, C., RUGGIERO, L., CHEN, B., LI, M., GALLOWAY, D. A., GU, W., GAUTIER, J. & DALLA-FAVERA, R. 2007. Non-transcriptional control of DNA replication by c-Myc. *Nature,* 448**,** 445-451.
DORASAMY, S., NARAINPERSAD, N., SINGH, M. & ARIATTI, M. 2012. Novel targeted liposomes deliver siRNA to hepatocellular carcinoma cells in vitro. *Chemical Biology & Drug Design,* 80**,** 647-656.
DORASAMY, S., SINGH, M. & ARIATTI, M. 2009. Rapid and sensitive fluorometric analysis of novel galactosylated cationic liposome interaction with siRNA. *African Journal of Pharmacy and Pharmacology,* 3**,** 632-635.
DOYLE, G. A., BOURDEAU-HELLER, J. M., COULTHARD, S., MEISNER, L. F. & ROSS, J. 2000. Amplification in human breast cancer of a gene encoding a c-myc mRNA-binding protein. *Cancer Research,* 60**,** 2756-2759.
EBERLIN, L. S., GABAY, M., FAN, A. C., GOUW, A. M., TIBSHIRANI, R. J., FELSHER, D. W. & ZARE, R. N. 2014. Alteration of the lipid profile in lymphomas induced by MYC overexpression. *Proceedings of the National Academy of Sciences USA,* 111**,** 10450-10455.
EDMUNDS, L. R., SHARMA, L., KANG, A., LU, J., VOCKLEY, J., BASU, S., UPPALA, R., GOETZMAN, E. S., BECK, M. E. & SCOTT, D. 2014. c-Myc programs fatty acid metabolism and dictates acetyl-CoA abundance and fate. *Journal of Biological Chemistry,* 289**,** 25382-25392.

EGUCHI, A., MEADE, B. R., CHANG, Y.-C., FREDRICKSON, C. T., WILLERT, K., PURI, N. & DOWDY, S. F. 2009. Efficient siRNA delivery into primary cells by a peptide transduction domain–dsRNA binding domain fusion protein. *Nature Biotechnology,* 27**,** 567-571.
EICK, D. & BORNKAMM, G. W. 1986. Transcriptional arrest within the first exon is a fast control mechanism in c-myc gene expression. *Nucleic Acids Research,* 14**,** 8331-8346.
EISCHEN, C. M., WEBER, J. D., ROUSSEL, M. F., SHERR, C. J. & CLEVELAND, J. L. 1999. Disruption of the ARF-Mdm2-p53 tumor suppressor pathway in Myc-induced lymphomagenesis. *Genes & Development,* 13**,** 2658-2669.
EISENMAN, R. N. 2014. *The Myc/Max/Mad Transcription Factor Network*, Springer Berlin Heidelberg.
EL-ANDALOUSSI, S., JOHANSSON, H., MAGNUSDOTTIR, A., JÄRVER, P., LUNDBERG, P. & LANGEL, Ü. 2005. TP10, a delivery vector for decoy oligonucleotides targeting the Myc protein. *Journal of Controlled Release,* 110**,** 189-201.
EL-ENSAHSY, H. A. 2009. Serum Concentration Effects on the Kinetics and Metabolism of HeLa-S3 Cell Growth and Cell Adaptability for Successful Proliferation in Serum Free Medium. *World Applied Sciences Journal,* 6**,** 608-615.
ELBASHIR, S. M., LENDECKEL, W. & TUSCHL, T. 2001. RNA interference is mediated by 21-and 22-nucleotide RNAs. *Genes & Development,* 15**,** 188-200.
ELIYAHU, H., SERVEL, N., DOMB, A. & BARENHOLZ, Y. 2002. Lipoplex-induced hemagglutination: potential involvement in intravenous gene delivery. *Gene Therapy,* 9**,** 850-858.
ELOUAHABI, A. & RUYSSCHAERT, J.-M. 2005. Formation and intracellular trafficking of lipoplexes and polyplexes. *Molecular Therapy,* 11**,** 336-347.
EPAND, R. M., HUGHES, D. W., SAYER, B. G., BOROCHOV, N., BACH, D. & WACHTEL, E. 2003. Novel properties of cholesterol–dioleoylphosphatidylcholine mixtures. *Biochimica et Biophysica Acta (BBA) - Biomembranes,* 1616**,** 196-208.
FANG, Y., XUE, J., GAO, S., LU, A., YANG, D., JIANG, H., HE, Y. & SHI, K. 2017. Cleavable PEGylation: a strategy for overcoming the "PEG dilemma" in efficient drug delivery. *Drug Delivery,* 24**,** 22-32.
FARHOOD, H., BOTTEGA, R., EPAND, R. M. & HUANG, L. 1992. Effect of cationic cholesterol derivatives on gene transfer and protein kinase C activity. *Biochimica et Biophysica Acta (BBA)-Biomembranes,* 1111**,** 239-246.
FELGNER, P. L., GADEK, T. R., HOLM, M., ROMAN, R., CHAN, H. W., WENZ, M., NORTHROP, J. P., RINGOLD, G. M. & DANIELSEN, M. 1987. Lipofection: a highly efficient, lipid-mediated DNA-transfection procedure. *Proceedings of the National Academy of Sciences USA,* 84**,** 7413-7417.
FELSHER, D. W. 2010. MYC Inactivation Elicits Oncogene Addiction through Both Tumor Cell–Intrinsic and Host-Dependent Mechanisms. *Genes & Cancer,* 1**,** 597-604.
FENG, X. H., LIANG, Y. Y., LIANG, M., ZHAI, W. & LIN, X. 2002. Direct interaction of c-Myc with Smad2 and Smad3 to inhibit TGF-beta-mediated induction of the CDK inhibitor p15(Ink4B). *Molecular Cell,* 9**,** 133-143.
FERBER, M. J., THORLAND, E. C., BRINK, A. A., RAPP, A. K., PHILLIPS, L. A., MCGOVERN, R., GOSTOUT, B. S., CHEUNG, T. H., CHUNG, T. K. H. & FU, W. Y. 2003. Preferential integration of human papillomavirus type 18 near the c-myc locus in cervical carcinoma. *Oncogene,* 22**,** 7233-7242.
FERNANDEZ, P. C., FRANK, S. R., WANG, L., SCHROEDER, M., LIU, S., GREENE, J., COCITO, A. & AMATI, B. 2003. Genomic targets of the human c-Myc protein. *Genes & Development,* 17**,** 1115-1129.
FICHOU, Y. & FÉREC, C. 2006. The potential of oligonucleotides for therapeutic applications. *Trends in Biotechnology,* 24**,** 563-570.
FIELDS, R. & LANCASTER, M. 1993. Dual-attribute continuous monitoring of cell proliferation/cytotoxicity. *American Biotechnology Laboratory,* 11**,** 48-50.

FILION, M. C. & PHILLIPS, N. C. 1997. Toxicity and immunomodulatory activity of liposomal vectors formulated with cationic lipids toward immune effector cells. *Biochimica et Biophysica Acta (BBA) - Biomembranes,* 1329**,** 345-356.

FIRE, A., XU, S., MONTGOMERY, M. K., KOSTAS, S. A., DRIVER, S. E. & MELLO, C. C. 1998. Potent and specific genetic interference by double-stranded RNA in Caenorhabditis elegans. *Nature,* 391**,** 806-811.

FISHER, T. L., TERHORST, T., CAO, X. & WAGNER, R. W. 1993. Intracellular disposition and metabolism of fluorescently-labled unmodified and modified oligouncleotides microijjected into mammalian cells. *Nucleic Acids Research,* 21**,** 3857-3865.

FORGUE-LAFITTE, M. E., COUDRAY, A. M., BREANT, B. & MESTER, J. 1989. Proliferation of the human colon carcinoma cell line HT29: autocrine growth and deregulated expression of the c-myc oncogene. *Cancer Research,* 49**,** 6566-6571.

FOTAKIS, G. & TIMBRELL, J. A. 2006. In vitro cytotoxicity assays: comparison of LDH, neutral red, MTT and protein assay in hepatoma cell lines following exposure to cadmium chloride. *Toxicology Letters,* 160**,** 171-177.

FRAGA, S., BRANDÃO, A., SOARES, M. E., MORAIS, T., DUARTE, J. A., PEREIRA, L., SOARES, L., NEVES, C., PEREIRA, E. & DE LOURDES BASTOS, M. 2014. Short-and long-term distribution and toxicity of gold nanoparticles in the rat after a single-dose intravenous administration. *Nanomedicine: Nanotechnology, Biology and Medicine,* 10**,** 1757-1766.

FRESHNEY, R. 2005. *Culture of animal cells, a manual of basic technique,* New Jersey, John Wiley & Sons Inc.

FUXIN, S., WASUNGU, L., NOMDEN, A., STUART, M. C., POLUSHKIN, E., ENGBERTS, J. B. & HOEKSTRA, D. 2002. Interference of poly (ethylene glycol)–lipid analogues with cationic-lipid-mediated delivery of oligonucleotides; role of lipid exchangeability and non-lamellar transitions. *Biochemical Journal,* 366**,** 333-341.

GAO, P., TCHERNYSHYOV, I., CHANG, T.-C., LEE, Y.-S., KITA, K., OCHI, T., ZELLER, K. I., DE MARZO, A. M., VAN EYK, J. E. & MENDELL, J. T. 2009. c-Myc suppression of miR-23a/b enhances mitochondrial glutaminase expression and glutamine metabolism. *Nature,* 458**,** 762-765.

GAO, X. & HUANG, L. 1991. A novel cationic liposome reagent for efficient transfection of mammalian cells. *Biochemical and Biophysical Research Communications,* 179**,** 280-285.

GARDNER, L., LEE, L. & DANG, C. 2002. The c-Myc oncogenic transcription factor. *Encyclopedia of cancer* 2nd ed.: Academic Press.

GARTEL, A. L. & SHCHORS, K. 2003. Mechanisms of c-myc-mediated transcriptional repression of growth arrest genes. *Experimental Cell Research,* 283**,** 17-21.

GARTEL, A. L., YE, X., GOUFMAN, E., SHIANOV, P., HAY, N., NAJMABADI, F. & TYNER, A. L. 2001. Myc represses the p21(WAF1/CIP1) promoter and interacts with Sp1/Sp3. *Proceedings of the National Academy of Sciences USA,* 98**,** 4510-4515.

GAUMET, M., VARGAS, A., GURNY, R. & DELIE, F. 2008. Nanoparticles for drug delivery: The need for precision in reporting particle size parameters. *European Journal of Pharmaceutics and Biopharmaceutics,* 69**,** 1-9.

GEBHARDT, A., FRYE, M., HEROLD, S., BENITAH, S. A., BRAUN, K., SAMANS, B., WATT, F. M., ELSÄSSER, H.-P. & EILERS, M. 2006. Myc regulates keratinocyte adhesion and differentiation via complex formation with Miz1. *The Journal of Cell Biology,* 172**,** 139-149.

GENG, C., KAOCHAR, S., LI, M., RAJAPAKSHE, K., FISKUS, W., DONG, J., FOLEY, C., DONG, B., ZHANG, L. & KWON, O.-J. 2017. SPOP regulates prostate epithelial cell proliferation and promotes ubiquitination and turnover of c-MYC oncoprotein. *Oncogene,* 36**,** 4767-4777.

GEUSENS, B., LAMBERT, J., DE SMEDT, S., BUYENS, K., SANDERS, N. & VAN GELE, M. 2009. Ultradeformable cationic liposomes for delivery of small interfering RNA (siRNA) into human primary melanocytes. *Journal of Controlled Release,* 133**,** 214-220.

GIL, J., KERAI, P., LLEONART, M., BERNARD, D., CIGUDOSA, J. C., PETERS, G., CARNERO, A. & BEACH, D. 2005. Immortalization of primary human prostate epithelial cells by c-Myc. *Cancer Research,* 65**,** 2179-2185.

GILLERON, J., QUERBES, W., ZEIGERER, A., BORODOVSKY, A., MARSICO, G., SCHUBERT, U., MANYGOATS, K., SEIFERT, S., ANDREE, C. & STÖTER, M. 2013. Image-based analysis of lipid nanoparticle–mediated siRNA delivery, intracellular trafficking and endosomal escape. *Nature Biotechnology,* 31**,** 638-646.

GRANDORI, C., COWLEY, S. M., JAMES, L. P. & EISENMAN, R. N. 2000. The Myc/Max/Mad network and the transcriptional control of cell behavior. *Annual Review of Cell and Developmental Biology,* 16**,** 653-699.

GRANDORI, C., GOMEZ-ROMAN, N., FELTON-EDKINS, Z. A., NGOUENET, C., GALLOWAY, D. A., EISENMAN, R. N. & WHITE, R. J. 2005. c-Myc binds to human ribosomal DNA and stimulates transcription of rRNA genes by RNA polymerase I. *Nature Cell Biology,* 7**,** 311-318.

GREISH, K. 2010. Enhanced permeability and retention (EPR) effect for anticancer nanomedicine drug targeting. *Cancer Nanotechnology: Methods and Protocols,* 624**,** 25-37.

GRIFFITHS, D., BERNT, W., HOLE, P., SMITH, J., MALLOY, A. & CARR, B. 2011. Zeta Potential Measurement of Nanoparticles by Nanoparticle Tracking Analysis (NTA). *NSTI-Nanotech,* 1.

GRIMM, D. 2011. The dose can make the poison: lessons learned from adverse in vivo toxicities caused by RNAi overexpression. *Silence,* 2**,** DOI:10.1186/1758-907X-2-8.

GU, W., BHATIA, K., MAGRATH, I. T., DANG, C. V. & DALLA-FAVERA, R. 1994. Binding and suppression of the Myc transcriptional activation domain by p107. *Science,* 264**,** 251-254.

GU, Y., ZHANG, J., MA, X., KIM, B.-W., WANG, H., LI, J., PAN, Y., XU, Y., DING, L., YANG, L., GUO, C., WU, X., WU, J., WU, K., GAN, X., LI, G., LI, L., FORMAN, S. J., CHAN, W.-C., XU, R. & HUANG, W. 2017. Stabilization of the c-Myc Protein by CAMKIIγ Promotes T Cell Lymphoma. *Cancer Cell,* 32**,** 115-128.e7.

GUENTHOER, J., DIEDE, S. J., TANAKA, H., CHAI, X., HSU, L., TAPSCOTT, S. J. & PORTER, P. L. 2012. Assessment of palindromes as platforms for DNA amplification in breast cancer. *Genome Research,* 22**,** 232-245.

GUO, J., HAO, J., JIANG, H., JIN, J., WU, H., JIN, Z. & LI, Z. 2017. Proteasome activator subunit 3 promotes pancreatic cancer growth via c-Myc-glycolysis signaling axis. *Cancer letters,* 386**,** 161-167.

GUO, Q. M., MALEK, R. L., KIM, S., CHIAO, C., HE, M., RUFFY, M., SANKA, K., LEE, N. H., DANG, C. V. & LIU, E. T. 2000. Identification of c-myc responsive genes using rat cDNA microarray. *Cancer Research,* 60**,** 5922-5928.

HA, D., YANG, N. & NADITHE, V. 2016. Exosomes as therapeutic drug carriers and delivery vehicles across biological membranes: current perspectives and future challenges. *Acta Pharmaceutica Sinica B,* 6**,** 287-296.

HALL, Z., AMENT, Z., WILSON, C. H., BURKHART, D. L., ASHMORE, T., KOULMAN, A., LITTLEWOOD, T., EVAN, G. I. & GRIFFIN, J. L. 2016. Myc expression drives aberrant lipid metabolism in lung cancer. *Cancer Research,* 76**,** 4608-4618.

HAMID, R., ROTSHTEYN, Y., RABADI, L., PARIKH, R. & BULLOCK, P. 2004. Comparison of alamar blue and MTT assays for high through-put screening. *Toxicology In Vitro,* 18**,** 703-710.

HAN, S.-E., KANG, H., SHIM, G. Y., SUH, M. S., KIM, S. J., KIM, J.-S. & OH, Y.-K. 2008. Novel cationic cholesterol derivative-based liposomes for serum-enhanced delivery of siRNA. *International Journal of Pharmaceutics,* 353**,** 260-269.

HANN, S. R., KING, M. W., BENTLEY, D. L., ANDERSON, C. W. & EISENMAN, R. N. 1988. A non-AUG translational initiation in c-myc exon 1 generates an N-terminally distinct protein whose synthesis is disrupted in Burkitt's lymphomas. *Cell,* 52**,** 185-95.

HAO, H., NANCAI, Y., LEI, F., XIONG, W., WEN, S., GUOFU, H., YANXIA, W., HANJU, H., QIAN, L. & HONG, X. 2008. siRNA directed against c-Myc inhibits proliferation and downregulates

human telomerase reverse transcriptase in human colon cancer Colo 320 cells. *Journal of Experimental & Clinical Cancer Research,* 27**,** DOI:10.1186/1756-9966-27-27.
HAO, T., GAERIG, V. C. & BROOKS, T. A. 2016. Nucleic acid clamp-mediated recognition and stabilization of the physiologically relevant MYC promoter G-quadruplex. *Nucleic Acids Research,* 44**,** 11013-11023.
HARA, T., OOI, A., KOBAYASHI, M., MAI, M., YANAGIHARA, K. & NAKANISHI, I. 1998. Amplification of c-myc, K-sam, and c-met in gastric cancers: detection by fluorescence in situ hybridization. *Laboratory Investigation; A Journal of Technical Methods and Pathology,* 78**,** 1143-1153.
HATTORI, Y., NAKAMURA, A., ARAI, S., NISHIGAKI, M., OHKURA, H., KAWANO, K., MAITANI, Y. & YONEMOCHI, E. 2014. In vivo siRNA delivery system for targeting to the liver by poly-l-glutamic acid-coated lipoplex. *Results in Pharma Sciences,* 4**,** 1-7.
HATTORI, Y., NAKAMURA, T., OHNO, H., FUJII, N. & MAITANI, Y. 2013. siRNA delivery into tumor cells by lipid-based nanoparticles composed of hydroxyethylated cholesteryl triamine. *International Journal of Pharmaceutics,* 443**,** 221-229.
HE, T.-C., SPARKS, A. B., RAGO, C., HERMEKING, H., ZAWEL, L., DA COSTA, L. T., MORIN, P. J., VOGELSTEIN, B. & KINZLER, K. W. 1998. Identification of c-MYC as a target of the APC pathway. *Science,* 281**,** 1509-1512.
HE, X., WU, D., JI, J., LING, W., CHEN, X. & CHEN, Y. 2016. Ultrasound microbubble-carried PNA targeting to c-myc mRNA inhibits the proliferation of rabbit iliac arterious smooth muscle cells and intimal hyperplasia. *Drug Delivery,* 23**,** 2482-2487.
HÉLÈNE, C., GIOVANNANGELI, C., GUIEYSSE-PEUGEOT, A. L. & PRASEUTH, D. Sequence-specific control of gene expression by antigene and clamp oligonucleotides. Ciba Foundation Symposium, 1997. Citeseer, 94-106.
HELM, C. W., SHRESTHA, K., THOMAS, S., SHINGLETON, H. M. & MILLER, D. M. 1993. A Unique c-myc-Targeted Triplex-Forming Oligonucleotide Inhibits the Growth of Ovarian and Cervical Carcinomas in Vitro. *Gynecologic Oncology,* 49**,** 339-343.
HENRIKSSON, M., BAKARDJIEV, A., KLEIN, G. & LÜSCHER, B. 1993. Phosphorylation sites mapping in the N-terminal domain of c-myc modulate its transforming potential. *Oncogene,* 8**,** 3199-3209.
HENRIKSSON, M. & LÜSCHER, B. 1996. Proteins of the Myc network: essential regulators of cell growth and differentiation. *Advances in Cancer Research,* 68**,** 109-182.
HERBST, A., HEMANN, M. T., TWORKOWSKI, K. A., SALGHETTI, S. E., LOWE, S. W. & TANSEY, W. P. 2005. A conserved element in Myc that negatively regulates its proapoptotic activity. *EMBO Reports,* 6**,** 177-183.
HERMEKING, H. 2003. The MYC oncogene as a cancer drug target. *Current Cancer Drug Targets,* 3**,** 163-175.
HERMEKING, H., RAGO, C., SCHUHMACHER, M., LI, Q., BARRETT, J. F., OBAYA, A. J., O'CONNELL, B. C., MATEYAK, M. K., TAM, W. & KOHLHUBER, F. 2000. Identification of CDK4 as a target of c-MYC. *Proceedings of the National Academy of Sciences,* 97**,** 2229-2234.
HERMS, J., NEIDT, I., LÜSCHER, B., SOMMER, A., SCHÜRMANN, P., SCHRÖDER, T., BERGMANN, M., WILKEN, B., PROBST-COUSIN, S. & HERNÁIZ-DRIEVER, P. 2000. C-MYC expression in medulloblastoma and its prognostic value. *International Journal of Cancer,* 89**,** 395-402.
HOLT, J., REDNER, R. & NIENHUIS, A. 1988. An oligomer complementary to c-myc mRNA inhibits proliferation of HL-60 promyelocytic cells and induces differentiation. *Molecular and Cellular Biology,* 8**,** 963-973.
HOPE, M. J. 2014. Enhancing siRNA delivery by employing lipid nanoparticles. *Therapeutic Delivery,* 5**,** 663-673.

HSI, L. C., ANGERMAN-STEWART, J. & ELING, T. E. 1999. Introduction of full-length APC modulates cyclooxygenase-2 expression in HT-29 human colorectal carcinoma cells at the translational level. *Carcinogenesis,* 20**,** 2045-2049.

HSI, L. C., BAEK, S. J. & ELING, T. E. 2000. Lack of cyclooxygenase-2 activity in HT-29 human colorectal carcinoma cells. *Experimental Cell Research,* 256**,** 563-570.

HU, S., BALAKRISHNAN, A., BOK, R. A., ANDERTON, B., LARSON, P. E., NELSON, S. J., KURHANEWICZ, J., VIGNERON, D. B. & GOGA, A. 2011. 13 C-Pyruvate Imaging Reveals Alterations in Glycolysis that Precede c-Myc-Induced Tumor Formation and Regression. *Cell metabolism,* 14**,** 131-142.

HU, T. & LU, Y.-R. 2015. BCYRN1, a c-MYC-activated long non-coding RNA, regulates cell metastasis of non-small-cell lung cancer. *Cancer Cell International,* 15**,** DO1:10.1186/s12935-015-0183-3.

HUANG, C.-H., SIPE, J. P., CHOW, S. & MARTIN, R. B. 1974. Differential interaction of cholesterol with phosphatidylcholine on the inner and outer surfaces of lipid bilayer vesicles. *Proceedings of the National Academy of Sciences USA,* 71**,** 359-362.

HUANG, W., LIANG, Y., SANG, C., MEI, C., LI, X. & CHEN, T. 2018. Therapeutic Nanosystems Co-deliver Anticancer Drugs and Oncogene SiRNA to Achieve Synergetic Precise Cancer Chemo-gene Therapy. *Journal of Materials Chemistry B,* 6**,** 3013-3022.

HUANG, Y., HONG, J., ZHENG, S., DING, Y., GUO, S., ZHANG, H., ZHANG, X., DU, Q. & LIANG, Z. 2011. Elimination Pathways of Systemically Delivered siRNA. *Molecular Therapy,* 19**,** 381-385.

HUDSON, A. J., LEWIS, K. J., RAO, M. V. & AKHTAR, S. 1996. Biodegradable polymer matrices for the sustained exogenous delivery of a biologically active c-myc hammerhead ribozyme. *International Journal of Pharmaceutics,* 136**,** 23-29.

HUDZIAK, R. M., BAROFSKY, E., BAROFSKY, D. F., WELLER, D. L., HUANG, S. B. & WELLER, D. D. 1996. Resistance of morpholino phosphorodiamidate oligomers to enzymatic degradation. *Antisense and Nucleic Acid Drug Development,* 6**,** 267-272.

HUDZIAK, R. M., SUMMERTON, J., WELLER, D. D. & IVERSEN, P. L. 2000. Antiproliferative effects of steric blocking phosphorodiamidate morpholino antisense agents directed against c-myc. *Antisense and Nucleic Acid Drug Development,* 10**,** 163-176.

HUET, G., KIM, I., DE BOLOS, C., LO-GUIDICE, J., MOREAU, O., HEMON, B., RICHET, C., DELANNOY, P., REAL, F. & DEGAND, P. 1995. Characterization of mucins and proteoglycans synthesized by a mucin-secreting HT-29 cell subpopulation. *Journal of Cell Science,* 108**,** 1275-1285.

HULLA, W., KÁLLAY, E., KRUGLUGER, W., PETERLIK, M. & CROSS, H. S. 1995. Growth control of human colon-adenocarcinoma-derived Caco-2 cells by vitamin-D compounds and extracellular calcium in vitro: relation to c-myc-oncogene and vitamin-D-receptor expression. *International Journal of Cancer,* 62**,** 711-716.

HUO, S., JIN, S., MA, X., XUE, X., YANG, K., KUMAR, A., WANG, P. C., ZHANG, J., HU, Z. & LIANG, X.-J. 2014. Ultrasmall gold nanoparticles as carriers for nucleus-based gene therapy due to size-dependent nuclear entry. *ACS Nano,* 8**,** 5852-5862.

HYMAN, E., KAURANIEMI, P., HAUTANIEMI, S., WOLF, M., MOUSSES, S., ROZENBLUM, E., RINGNÉR, M., SAUTER, G., MONNI, O. & ELKAHLOUN, A. 2002. Impact of DNA amplification on gene expression patterns in breast cancer. *Cancer Research,* 62**,** 6240-6245.

IMANI, R., PRAKASH, S., VALI, H. & FAGHIHI, S. 2018. Polyethylene glycol and octaarginine n dual-functionalized nano-graphene oxide: An optimization for efficient nucleic acids delivery. *Biomaterials Science,* 6**,** 1636-1650.

INGVARSSON, S., ASKER, C., AXELSON, H., KLEIN, G. & SÜMEGI, J. 1988. Structure and expression of B-myc, a new member of the myc gene family. *Molecular and Cellular Biology,* 8**,** 3168-3174.

IOANNIDIS, P., KOTTARIDI, C., DIMITRIADIS, E., COURTIS, N., MAHAIRA, L., TALIERI, M., GIANNOPOULOS, A., ILIADIS, K., PAPAIOANNOU, D. & NASIOULAS, G. 2004.

Expression of the RNA-binding protein CRD-BP in brain and non-small cell lung tumors. *Cancer Letters,* 209**,** 245-250.
IRITANI, B. M. & EISENMAN, R. N. 1999. c-Myc enhances protein synthesis and cell size during B lymphocyte development. *Proceedings of the National Academy of Sciences USA,* 96**,** 13180-13185.
ITO, T., TSUJI, G., OHNO, F., NAKAHARA, T., UCHI, H. & FURUE, M. 2017. Potential role of the OVOL1–OVOL2 axis and c-Myc in the progression of cutaneous squamous cell carcinoma. *Modern Pathology,* 30**,** 919-927.
IVERSEN, P. L., ARORA, V., ACKER, A., MASON, D. H. & DEVI, G. R. 2003. Efficacy of antisense morpholino oligomer targeted to c-myc in prostate cancer xenograft murine model and a Phase I safety study in humans. *Clinical Cancer Research,* 9**,** 2510-2519.
JABBAR, S., TWENTYMAN, P. & WATSON, J. 1989. The MTT assay underestimates the growth inhibitory effects of interferons. *British Journal of Cancer,* 60**,** 523-528.
JACKSON, A. L. & LINSLEY, P. S. 2010. Recognizing and avoiding siRNA off-target effects for target identification and therapeutic application. *Nature Reviews Drug Discovery,* 9**,** 57-67.
JAIN, A., WANG, G. & VASQUEZ, K. M. 2008. DNA triple helices: biological consequences and therapeutic potential. *Biochimie,* 90**,** 1117-1130.
JENKINS, R. B., QIAN, J., LIEBER, M. M. & BOSTWICK, D. G. 1997. Detection of c-myc oncogene amplification and chromosomal anomalies in metastatic prostatic carcinoma by fluorescence in situ hybridization. *Cancer Research,* 57**,** 524-531.
JING, H., CHENG, W., ZHANG, J.-W., HAN, X., SHAO, H. & SUN, Y.-X. 2015. Galactosylated poly-L-lysine targeted microbubbles for ultrasound mediated antisense c-myc gene transfection in hepatocellular carcinoma cells. *Archives of Medical Science: AMS,* 11**,** 292-300.
JOHARI, B., EBRAHIMI-RAD, M., MAGHSOOD, F., LOTFINIA, M., SALTANATPOURI, Z., TEIMOORI-TOOLABI, L., SHARIFZADEH, Z., KARIMIPOOR, M. & KADIVAR, M. 2017. Myc Decoy Oligodeoxynucleotide Inhibits Growth and Modulates Differentiation of Mouse Embryonic Stem Cells as a Model of Cancer Stem Cells. *Anticancer agents in Medicinal Chemistry,* 17**,** 1786-1795.
JULIANO, R. L. 2016. The delivery of therapeutic oligonucleotides. *Nucleic acids research,* 44**,** 6518-6548.
JUNG, J. H., JUNG, D.-B., KIM, H., LEE, H., KANG, S.-E., SRIVASTAVA, S. K., YUN, M. & KIM, S.-H. 2018. Zinc finger protein 746 promotes colorectal cancer progression via c-Myc stability mediated by glycogen synthase kinase 3β and F-box and WD repeat domain-containing 7. *Oncogene***,** DOI: 10.1038/s41388-018-0225-0.
JUNGHANS, M., LOITSCH, S. M., STEINIGER, S. C., KREUTER, J. & ZIMMER, A. 2005. Cationic lipid–protamine–DNA (LPD) complexes for delivery of antisense c-myc oligonucleotides. *European Journal of Pharmaceutics and Biopharmaceutics,* 60**,** 287-294.
KAPOOR, M. & BURGESS, D. J. 2012. Physicochemical characterization of anionic lipid-based ternary siRNA complexes. *Biochimica et Biophysica Acta (BBA) - Biomembranes,* 1818**,** 1603-1612.
KAPOOR, M. & BURGESS, D. J. 2013. Cellular uptake mechanisms of novel anionic siRNA lipoplexes. *Pharmaceutical Research,* 30**,** 1161-1175.
KASIBHATLA, S. & TSENG, B. 2003. Why target apoptosis in cancer treatment? *Molecular Cancer Therapeutics,* 2**,** 573-580.
KATO, G. J., LEE, W. M., CHEN, L. L. & DANG, C. V. 1992. Max: functional domains and interaction with c-Myc. *Genes & Development,* 6**,** 81-92.
KENNETH, N. S., RAMSBOTTOM, B. A., GOMEZ-ROMAN, N., MARSHALL, L., COLE, P. A. & WHITE, R. J. 2007. TRRAP and GCN5 are used by c-Myc to activate RNA polymerase III transcription. *Proceedings of the National Academy of Sciences USA,* 104**,** 14917-14922.
KHATRI, N., BARADIA, D., VHORA, I., RATHI, M. & MISRA, A. 2014. Development and characterization of siRNA Lipoplexes: effect of different lipids, in vitro evaluation in cancerous cell lines and in vivo toxicity study. *AAPS PharmSciTech,* 15**,** 1630-1643.

KHATTAR, E. & TERGAONKAR, V. 2017. Transcriptional regulation of telomerase reverse transcriptase (TERT) by MYC. *Frontiers in Cell and Developmental Biology,* 5**,** 1-7.
KHVOROVA, A., REYNOLDS, A. & JAYASENA, S. D. 2003. Functional siRNAs and miRNAs exhibit strand bias. *Cell,* 115**,** 209-216.
KIM, D.-H., BEHLKE, M. A., ROSE, S. D., CHANG, M.-S., CHOI, S. & ROSSI, J. J. 2005. Synthetic dsRNA Dicer substrates enhance RNAi potency and efficacy. *Nature Biotechnology,* 23**,** 222-226.
KIM, D., HONG, A., PARK, H. I., SHIN, W. H., YOO, L., JEON, S. J. & CHUNG, K. C. 2017a. Deubiquitinating enzyme USP22 positively regulates c-Myc stability and tumorigenic activity in mammalian and breast cancer cells. *Journal of Cellular Physiology,* 232**,** 3664-3676.
KIM, H.-G., REDDOCH, J. F., MAYFIELD, C., EBBINGHAUS, S., VIGNESWARAN, N., THOMAS, S., JONES, D. E. & MILLER, D. M. 1998. Inhibition of transcription of the human c-myc protooncogene by intermolecular triplex. *Biochemistry,* 37**,** 2299-2304.
KIM, H., SON, Y. J., MAO, W., LEONG, K. W. & YOO, H. S. 2017b. Atom transfer radical polymerization of multi-shelled cationic corona for the systemic delivery of siRNA. *Nano Letters,* 18**,** 314-325.
KIM, J., LEE, J.-H. & IYER, V. R. 2008. Global identification of Myc target genes reveals its direct role in mitochondrial biogenesis and its E-box usage in vivo. *PloS ONE,* 3**,** e1798. DOI:10.1371/journal.pone.0001798
KIM, J. W., ZELLER, K. I., WANG, Y., JEGGA, A. G., ARONOW, B. J., O'DONNELL, K. A. & DANG, C. V. 2004. Evaluation of myc E-box phylogenetic footprints in glycolytic genes by chromatin immunoprecipitation assays. *Molecular and Cellular Biology,* 24**,** 5923-5936.
KNAPP, D. C., MATA, J. E., REDDY, M. T., DEVI, G. R. & IVERSEN, P. L. 2003. Resistance to chemotherapeutic drugs overcome by c-Myc inhibition in a Lewis lung carcinoma murine model. *Anticancer Drugs,* 14**,** 39-47.
KOBAYASHI, H., WATANABE, R. & CHOYKE, P. L. 2014. Improving conventional enhanced permeability and retention (EPR) effects; what is the appropriate target? *Theranostics,* 4**,** 81-89.
KOERNER, M. M., PALACIO, L. A., WRIGHT, J. W., SCHWEITZER, K. S., RAY, B. D. & PETRACHE, H. I. 2011. Electrodynamics of lipid membrane interactions in the presence of zwitterionic buffers. *Biophysical Journal,* 101**,** 362-369.
KUNTSCHE, J., HORST, J. C. & BUNJES, H. 2011. Cryogenic transmission electron microscopy (cryo-TEM) for studying the morphology of colloidal drug delivery systems. *International Journal of Pharmaceutics,* 417**,** 120-137.
KUZYK, A. & MAI, S. 2014. c-MYC-induced genomic instability. *Cold Spring Harbor Perspectives in Medicine,* 4**,** a014373. DOI:10.1101/cshperspect.a014373.
KYO, S., TAKAKURA, M., TAIRA, T., KANAYA, T., ITOH, H., YUTSUDO, M., ARIGA, H. & INOUE, M. 2000. Sp1 cooperates with c-Myc to activate transcription of the human telomerase reverse transcriptase gene (hTERT). *Nucleic Acids Research,* 28**,** 669-677.
LAPPALAINEN, K., JÄÄSKELÄINEN, I., SYRJÄNEN, K., URTTI, A. & SYRJÄNEN, S. 1994. Comparison of cell proliferation and toxicity assays using two cationic liposomes. *Pharmaceutical research,* 11**,** 1127-1131.
LAZEBNIK, M., KESWANI, R. K. & PACK, D. W. 2016. Endocytic Transport of Polyplex and Lipoplex siRNA Vectors in HeLa Cells. *Pharmacetical Research,* 33**,** 2999-3011.
LEDER, A., PATTENGALE, P. K., KUO, A., STEWART, T. A. & LEDER, P. 1986. Consequences of widespread deregulation of the c-myc gene in transgenic mice: multiple neoplasms and normal development. *Cell,* 45**,** 485-495.
LEE, A. V., OESTERREICH, S. & DAVIDSON, N. E. 2015. MCF-7 Cells—Changing the Course of Breast Cancer Research and Care for 45 Years. *Journal of the National Cancer Institute,* 107**,** DOI:10.1093/jnci/djv073.
LEMAITRE, J.-M., BUCKLE, R. S. & MÉCHALI, M. 1996. c-Myc in the Controlm of Cell Proliferation and Embryonic Development. *Advances in Cancer Research,* 70**,** 95-144.

LEONETTI, C., BIROCCIO, A., BENASSI, B., STRINGARO, A., STOPPACCIARO, A., SEMPLE, S. C. & ZUPI, G. 2001. Encapsulation of c-myc antisense oligodeoxynucleotides in lipid particles improves antitumoral efficacy in vivo in a human melanoma line. *Cancer Gene Therapy,* 8**,** 459-468.

LEONETTI, C., BIROCCIO, A., CANDILORO, A., CITRO, G., FORNARI, C., MOTTOLESE, M., DEL BUFALO, D. & ZUPI, G. 1999. Increase of cisplatin sensitivity by c-myc antisense oligodeoxynucleotides in a human metastatic melanoma inherently resistant to cisplatin. *Clinical Cancer Research,* 5**,** 2588-2595.

LEUNG, A., TAM, Y. & CULLIS, P. R. 2014. Lipid nanoparticles for short interfering RNA delivery. *Advances in Genetics,* 88**,** 71-110.

LEVIN, A. A. 1999. A review of the issues in the pharmacokinetics and toxicology of phosphorothioate antisense oligonucleotides. *Biochimica et Biophysica Acta,* 1489**,** 69-84.

LI, B., CAREY, M. & WORKMAN, J. L. 2007. The role of chromatin during transcription. *Cell,* 128**,** 707-719.

LI, B. & SIMON, M. C. 2013. Molecular pathways: targeting MYC-induced metabolic reprogramming and oncogenic stress in cancer. *Clinical Cancer Research,* 19**,** 5835-5841.

LI, L., HU, X., ZHANG, M., MA, S., YU, F., ZHAO, S., LIU, N., WANG, Z., WANG, Y. & GUAN, H. 2017. Dual Tumor-Targeting Nanocarrier System for siRNA Delivery Based on pRNA and Modified Chitosan. *Molecular Therapy-Nucleic Acids,* 8**,** 169-183.

LI, Q. & DANG, C. V. 1999. c-Myc Overexpression Uncouples DNA Replication from Mitosis. *Molecular and Cellular Biology,* 19**,** 5339-5351.

LI, S.-D., CHONO, S. & HUANG, L. 2008. Efficient oncogene silencing and metastasis inhibition via systemic delivery of siRNA. *Molecular Therapy,* 16**,** 942-946.

LI, S., TSENG, W., STOLZ, D. B., WU, S., WATKINS, S. & HUANG, L. 1999. Dynamic changes in the characteristics of cationic lipidic vectors after exposure to mouse serum: implications for intravenous lipofection. *Gene Therapy,* 6**,** 585-594.

LI, X., LIU, X., XU, W., ZHOU, P., GAO, P., JIANG, S., LOBIE, P. E. & ZHU, T. 2013. c-MYC-regulated miR-23a/24-2/27a cluster promotes mammary carcinoma cell invasion and hepatic metastasis by targeting Sprouty2. *Journal of Biological Chemistry,* 288**,** 18121-18133.

LIANG, C.-C., PARK, A. Y. & GUAN, J.-L. 2007. In vitro scratch assay: a convenient and inexpensive method for analysis of cell migration in vitro. *Nature Protocols,* 2**,** 329-333.

LIN, C. Y., LOVÉN, J., RAHL, P. B., PARANAL, R. M., BURGE, C. B., BRADNER, J. E., LEE, T. I. & YOUNG, R. A. 2012. Transcriptional amplification in tumor cells with elevated c-Myc. *Cell,* 151**,** 56-67.

LIN, X., SUN, R., ZHAO, X., ZHU, D., ZHAO, X., GU, Q., DONG, X., ZHANG, D., ZHANG, Y. & LI, Y. 2017. C-myc overexpression drives melanoma metastasis by promoting vasculogenic mimicry via c-myc/snail/Bax signaling. *Journal of Molecular Medicine,* 95**,** 53-67.

LINDSTEN, T., JUNE, C. H. & THOMPSON, C. B. 1988. Multiple mechanisms regulate c-myc gene expression during normal T cell activation. *The EMBO Journal,* 7**,** 2787-2794.

LINGEL, A., SIMON, B., IZAURRALDE, E. & SATTLER, M. 2004. Nucleic acid 3'-end recognition by the Argonaute2 PAZ domain. *Nature Structural & Molecular Biology,* 11**,** 576-577.

LIU, H., ZHOU, M., LUO, X., ZHANG, L., NIU, Z., PENG, C., MA, J., PENG, S., ZHOU, H., XIANG, B., LI, X., LI, S., HE, J., LI, X. & LI, G. 2008a. Transcriptional regulation of BRD7 expression by Sp1 and c-Myc. *BMC Molecular Biology,* 9**,** 1-14.

LIU, Y.-C., LI, F., HANDLER, J., HUANG, C. R. L., XIANG, Y., NERETTI, N., SEDIVY, J. M., ZELLER, K. I. & DANG, C. V. 2008b. Global regulation of nucleotide biosynthetic genes by c-Myc. *PloS ONE,* 3**,** e2722. DOI:10.1371/journal.pone.0002722.

LOKE, S., STEIN, C., ZHANG, X., AVIGAN, M., COHEN, J. & NECKERS, L. 1988. Delivery of c-myc antisense phosphorothioate oligodeoxynucleotides to hematopoietic cells in culture by liposome fusion: specific reduction in c-myc protein expression correlates with inhibition of cell growth and DNA synthesis. *Mechanisms in B-Cell Neoplasia 1988.* Springer.

LORENZIN, F., BENARY, U., BALUAPURI, A., WALZ, S., JUNG, L. A., VON EYSS, B., KISKER, C., WOLF, J., EILERS, M. & WOLF, E. 2016. Different promoter affinities account for specificity in MYC-dependent gene regulation. *Elife,* 5**,** e15161. DOI:10.7554/eLife.15161.
LU, J. J., LANGER, R. & CHEN, J. 2009. A Novel Mechanism Is Involved in Cationic Lipid-Mediated Functional siRNA Delivery. *Molecular Pharmaceutics,* 6**,** 763-771.
LUNAVAT, T., JANG, S., NILSSON, L., PARK, H., REPISKA, G., LÄSSER, C., NILSSON, J., GHO, Y. & LÖTVALL, J. 2016. RNAi delivery by exosome-mimetic nanovesicles-Implications for targeting c-Myc in cancer. *Biomaterials,* 102**,** 231-238.
MA, B., ZHANG, S., JIANG, H., ZHAO, B. & LV, H. 2007. Lipoplex morphologies and their influences on transfection efficiency in gene delivery. *Journal of Controlled Release,* 123**,** 184-194.
MA, S., JIANG, Y.-Y., WU, L.-F., HAO, J.-J., ZHANG, Y., XU, X., CAI, Y. & WANG, M.-R. 2017. Annexin A2 (ANXA2) promotes migration and invasion of esophageal cancer cells via stabilizing c-Myc and promoting HIF-1α transcription. *Proceedings: AACR Annual Meeting 2017,* 77**,** DOI:10.1158/1538-7445.AM2017-891.
MACRAE, I. J., MA, E., ZHOU, M., ROBINSON, C. V. & DOUDNA, J. A. 2008. In vitro reconstitution of the human RISC-loading complex. *Proceesings of the National Academy of Sciences USA,* 105**,** 512-517.
MAIYO, F. C., MOODLEY, R. & SINGH, M. 2016. Cytotoxicity, Antioxidant and Apoptosis Studies of Quercetin-3-O Glucoside and 4-(beta-D-Glucopyranosyl-1-->4-alpha-L-Rhamnopyranosyloxy)-Benzyl Isothiocyanate from Moringa oleifera. *Anticancer Agents in Medicinal Chemistry,* 16**,** 648-656.
MANN, M. J. & DZAU, V. J. 2000. Therapeutic applications of transcription factor decoy oligonucleotides. *Journal of Clinical Investigation,* 106**,** 1071-1075.
MARUYAMA, K. 2011. Intracellular targeting delivery of liposomal drugs to solid tumors based on EPR effects. *Advanced Drug Delivery Reviews,* 63**,** 161-169.
MARUYAMA, K., YUDA, T., OKAMOTO, A., KOJIMA, S., SUGINAKA, A. & IWATSURU, M. 1992. Prolonged circulation time in vivo of large unilamellar liposomes composed of distearoyl phosphatidylcholine and cholesterol containing amphipathic poly (ethylene glycol). *Biochimica et Biophysica Acta (BBA)-Lipids and Lipid Metabolism,* 1128**,** 44-49.
MAZZOCCOLI, G., COLANGELO, T., PANZA, A., RUBINO, R., DE CATA, A., TIBERIO, C., VALVANO, M. R., PAZIENZA, V., MERLA, G. & AUGELLO, B. 2016. Deregulated expression of cryptochrome genes in human colorectal cancer. *Molecular Cancer,* 15**,** DOI:10.1186/s12943-016-0492-8.
MCCULLY, M., HERNANDEZ, Y., CONDE, J., BAPTISTA, P. V., JESUS, M., HURSTHOUSE, A., STIRLING, D. & BERRY, C. C. 2015. Significance of the balance between intracellular glutathione and polyethylene glycol for successful release of small interfering RNA from gold nanoparticles. *Nano Research,* 8**,** 3281-3292.
MCEWAN, I. J., DAHLMAN-WRIGHT, K., FORD, J. & WRIGHT, A. P. 1996. Functional interaction of the c-Myc transactivation domain with the TATA binding protein: evidence for an induced fit model of transactivation domain folding. *Biochemistry,* 35**,** 9584-9593.
MCGUFFIE, E. & CATAPANO, C. 2002. Design of a novel triple helix-forming oligodeoxyribonucleotide directed to the major promoter of the c-myc gene. *Nucleic Acids Research,* 30**,** 2701-2709.
MCGUFFIE, E. M., PACHECO, D., CARBONE, G. M. & CATAPANO, C. V. 2000. Antigene and antiproliferative effects of a c-myc-targeting phosphorothioate triple helix-forming oligonucleotide in human leukemia cells. *Cancer Research,* 60**,** 3790-3799.
MCKEOWN, M. R. & BRADNER, J. E. 2014. Therapeutic strategies to inhibit MYC. *Cold Spring Harbor Perspectives in Medicine,* 4**,** a014266. DOI:10.1101/cshperspect.a014266.
MCMAHON, S. B., VAN BUSKIRK, H. A., DUGAN, K. A., COPELAND, T. D. & COLE, M. D. 1998. The novel ATM-related protein TRRAP is an essential cofactor for the c-Myc and E2F oncoproteins. *Cell,* 94**,** 363-374.

MCMAHON, S. B., WOOD, M. A. & COLE, M. D. 2000. The Essential Cofactor TRRAP Recruits the Histone Acetyltransferase hGCN5 to c-Myc. *Molecular and Cellular Biology,* 20**,** 556-562.
MENSSEN, A. & HERMEKING, H. 2002. Characterization of the c-MYC-regulated transcriptome by SAGE: identification and analysis of c-MYC target genes. *Proceedings of the National Academy of Sciences,* 99**,** 6274-6279.
MERVE, A., ACQUATI, S., HOECK, J., JEYAPALAN, J., BEHRENS, A. & MARINO, S. 2017. Tmod-01. Cmyc Overexpression Induces Choroid Plexus Tumours Through Modulation Of Inflammatory Pathways. *Neuro-oncology,* 19**,** iv48.
MÉVEL, M., KAMALY, N., CARMONA, S., OLIVER, M. H., JORGENSEN, M. R., CROWTHER, C., SALAZAR, F. H., MARION, P. L., FUJINO, M., NATORI, Y., THANOU, M., ARBUTHNOT, P., YAOUANC, J.-J., JAFFRÈS, P. A. & MILLER, A. D. 2010. DODAG; a versatile new cationic lipid that mediates efficient delivery of pDNA and siRNA. *Journal of Controlled Release,* 143**,** 222-232.
MISHRA, S., WEBSTER, P. & DAVIS, M. E. 2004. PEGylation significantly affects cellular uptake and intracellular trafficking of non-viral gene delivery particles. *European Journal of Cell Biology,* 83**,** 97-111.
MISLICK, K. A. & BALDESCHWIELER, J. D. 1996. Evidence for the role of proteoglycans in cation-mediated gene transfer. *Proceedings of the National Academy of Sciences USA,* 93**,** 12349-12354.
MOCHIZUKI, S., KANEGAE, N., NISHINA, K., KAMIKAWA, Y., KOIWAI, K., MASUNAGA, H. & SAKURAI, K. 2013. The role of the helper lipid dioleoylphosphatidylethanolamine (DOPE) for DNA transfection cooperating with a cationic lipid bearing ethylenediamine. *Biochimica et Biophysica Acta (BBA) - Biomembranes,* 1828**,** 412-418.
MORENO, P. M. & PÊGO, A. P. 2014. Therapeutic antisense oligonucleotides against cancer: hurdling to the clinic. *Frontiers in Chemistry,* 2**,** DOI:10.3389/fchem.2014.00087.
MORRIS, K. V., CHAN, S. W.-L., JACOBSEN, S. E. & LOONEY, D. J. 2004. Small interfering RNA-induced transcriptional gene silencing in human cells. *Science,* 305**,** 1289-1292.
MORRISH, F., GIEDT, C. & HOCKENBERY, D. 2003. c-MYC apoptotic function is mediated by NRF-1 target genes. *Genes & Development,* 17**,** 240-255.
MORRISH, F., NOONAN, J., PEREZ-OLSEN, C., GAFKEN, P. R., FITZGIBBON, M., KELLEHER, J., VANGILST, M. & HOCKENBERY, D. 2010. Myc-dependent mitochondrial generation of acetyl-CoA contributes to fatty acid biosynthesis and histone acetylation during cell cycle entry. *Journal of Biological Chemistry,* 285**,** 36267-36274.
MORRISSEY, D. V., LOCKRIDGE, J. A., SHAW, L., BLANCHARD, K., JENSEN, K., BREEN, W., HARTSOUGH, K., MACHEMER, L., RADKA, S. & JADHAV, V. 2005. Potent and persistent in vivo anti-HBV activity of chemically modified siRNAs. *Nature Biotechnology,* 23**,** 1002-1007.
NAICKER, K., ARIATTI, M. & SINGH, M. 2014. PEGylated galactosylated cationic liposomes for hepatocytic gene delivery. *Colloids and Surfaces B: Biointerfaces,* 122**,** 482-490.
NAIDU, R., WAHAB, N. A., YADAV, M. & KUTTY, M. K. 2002. Protein expression and molecular analysis of c-myc gene in primary breast carcinomas using immunohistochemistry and differential polymerase chain reaction. *International Journal of Molecular Medicine,* 9**,** 189-196.
NAIR, S. K. & BURLEY, S. K. 2003. X-ray structures of Myc-Max and Mad-Max recognizing DNA: molecular bases of regulation by proto-oncogenic transcription factors. *Cell,* 112**,** 193-205.
NANBRU, C., PRATS, A.-C., DROOGMANS, L., DEFRANCE, P., HUEZ, G. & KRUYS, V. 2001. Translation of the human c-myc P0 tricistronic mRNA involves two independent internal ribosome entry sites. *Oncogene,* 20**,** 4270-4280.
NAPOLI, C., LEMIEUX, C. & JORGENSEN, R. 1990. Introduction of a chimeric chalcone synthase gene into petunia results in reversible co-suppression of homologous genes in trans. *The Plant Cell,* 2**,** 279-289.
NAPOLI, S., NEGRI, U., ARCAMONE, F., CAPOBIANCO, M. L., CARBONE, G. M. & CATAPANO, C. V. 2006. Growth inhibition and apoptosis induced by daunomycin-conjugated triplex-forming

oligonucleotides targeting the c-myc gene in prostate cancer cells. *Nucleic Acids Research,* 34**,** 734-744.
NAPOLI, S., PASTORI, C., MAGISTRI, M., CARBONE, G. M. & CATAPANO, C. V. 2009. Promoter-specific transcriptional interference and c-myc gene silencing by siRNAs in human cells. *The EMBO journal,* 28**,** 1708-1719.
NAU, M. M., BROOKS, B. J., BATTEY, J., SAUSVILLE, E., GAZDAR, A. F., KIRSCH, I. R., MCBRIDE, O. W., BERTNESS, V., HOLLIS, G. F. & MINNA, J. D. 1985. L-myc, a new myc-related gene amplified and expressed in human small cell lung cancer. *Nature,* 318**,** 69-73.
NAVARRO, G., MOVASSAGHIAN, S. & TORCHILIN, P. 2013. Current Trends in the Use of Cationic Polymer Assemblies for siRNA and Plasmid DNA Delivery. *Pharmaceutical Nanotechnology,* 1**,** 165-183.
NCHINDA, G., ÜBERLA, K. & ZSCHÖRNIG, O. 2002. Characterization of cationic lipid DNA transfection complexes differing in susceptability to serum inhibition. *BMC Biotechnology,* 2**,** DOI:10.1186/1472-6750-2-12.
NEEL, B. G., JHANWAR, S. C., CHAGANTI, R. & HAYWARD, W. S. 1982. Two human c-onc genes are located on the long arm of chromosome 8. *Proceedings of the National Academy of Sciences USA,* 79**,** 7842-7846.
NEIDLE, S. 2016. Quadruplex nucleic acids as novel therapeutic targets. *Journal of medicinal chemistry,* 59**,** 5987-6011.
NGUYEN, J., STEELE, T. W., MERKEL, O., REUL, R. & KISSEL, T. 2008. Fast degrading polyesters as siRNA nano-carriers for pulmonary gene therapy. *Journal of Controlled Release,* 132**,** 243-251.
NIE, Z., HU, G., WEI, G., CUI, K., YAMANE, A., RESCH, W., WANG, R., GREEN, D. R., TESSAROLLO, L. & CASELLAS, R. 2012. c-Myc is a universal amplifier of expressed genes in lymphocytes and embryonic stem cells. *Cell,* 151**,** 68-79.
NOLAND, C. L., MA, E. & DOUDNA, J. A. 2011. siRNA repositioning for guide strand selection by human Dicer complexes. *Molecular Cell,* 43**,** 110-121.
O'BRIEN, J., WILSON, I., ORTON, T. & POGNAN, F. 2000. Investigation of the Alamar Blue (resazurin) fluorescent dye for the assessment of mammalian cell cytotoxicity. *European Journal of Biochemistry,* 267**,** 5421-5426.
OSKARSSON, T. & TRUMPP, A. 2005. The Myc trilogy: lord of RNA polymerases. *Nature Cell Biology,* 7**,** 215-217.
OTT, G., ROSENWALD, A. & CAMPO, E. 2013. Understanding MYC-driven aggressive B-cell lymphomas: pathogenesis and classification. *ASH Education Program Book,* 2013**,** 575-583.
PALACIOS, J. & GAMALLO, C. 1998. Mutations in the β-catenin gene (CTNNB1) in endometrioid ovarian carcinomas. *Cancer Research,* 58**,** 1344-1347.
PAPAHADJOPOULOS, D., ALLEN, T. M., GABIZON, A., MAYHEW, E., MATTHAY, K., HUANG, S. K., LEE, K. D., WOODLE, M. C., LASIC, D. D., REDEMANN, C. & ET AL. 1991. Sterically stabilized liposomes: improvements in pharmacokinetics and antitumor therapeutic efficacy. *Proceedings of the National Academy of Sciences USA,* 88**,** 11460-11464.
PAPOULAS, O., WILLIAMS, N. G. & KINGSTON, R. E. 1992. DNA binding activities of c-Myc purified from eukaryotic cells. *The Journal of Biological Chemistry,* 267**,** 10470-10480.
PASTORINO, F., BRIGNOLE, C., MARIMPIETRI, D., PAGNAN, G., MORANDO, A., RIBATTI, D., SEMPLE, S. C., GAMBINI, C., ALLEN, T. M. & PONZONI, M. 2003. Targeted liposomal c-myc antisense oligodeoxynucleotides induce apoptosis and inhibit tumor growth and metastases in human melanoma models. *Clinical Cancer Research,* 9**,** 4595-4605.
PASTORINO, F., MUMBENGEGWI, D. R., RIBATTI, D., PONZONI, M. & ALLEN, T. M. 2008. Increase of therapeutic effects by treating melanoma with targeted combinations of c-myc antisense and doxorubicin. *Journal of Controlled Release,* 126**,** 85-94.
PASTORINO, F., STUART, D., PONZONI, M. & ALLEN, T. 2001. Targeted delivery of antisense oligonucleotides in cancer. *Journal of Controlled Release,* 74**,** 69-75.

PATEL, H., ZAVERI, A., ZAVERI, D., SHAH, S. & SOLANKI, A. 2013. Comparison of the MTT and alamar blue assay for in vitro anti cancer activity by testing of various chalcone and thiosemicarbazone derivatives. *International Journal of Pharma & Bio Sciences,* 4**,** 707-716.
PAUL, C. D., MISTRIOTIS, P. & KONSTANTOPOULOS, K. 2017. Cancer cell motility: lessons from migration in confined spaces. *Nature Reviews Cancer,* 17**,** 131-140.
PELENGARIS, S., KHAN, M. & EVAN, G. 2002. c-MYC: more than just a matter of life and death. *Nature Reviews Cancer,* 2**,** 764-776.
PENN, L. J., BROOKS, M. W., LAUFER, E. M., LITTLEWOOD, T. D., MORGENSTERN, J. P., EVAN, G. I., LEE, W. M. & LAND, H. 1990. Domains of human c-myc protein required for autosuppression and cooperation with ras oncogenes are overlapping. *Molecular and Cellular Biology,* 10**,** 4961-4966.
PERRY, R. H., BELLOVIN, D. I., SHROFF, E. H., ISMAIL, A. I., ZABUAWALA, T., FELSHER, D. W. & ZARE, R. N. 2013. Characterization of MYC-induced tumorigenesis by in situ lipid profiling. *Analytical Chemistry,* 85**,** 4259-4262.
PETER, M., ROSTY, C., COUTURIER, J., RADVANYI, F., TESHIMA, H. & SASTRE-GARAU, X. 2006. MYC activation associated with the integration of HPV DNA at the MYC locus in genital tumors. *Oncogene,* 25**,** 5985-5993.
PEUKERT, K., STALLER, P., SCHNEIDER, A., CARMICHAEL, G., HANEL, F. & EILERS, M. 1997. An alternative pathway for gene regulation by Myc. *The EMBO Journal,* 16**,** 5672-5686.
PHOTOS, P. J., BACAKOVA, L., DISCHER, B., BATES, F. S. & DISCHER, D. E. 2003. Polymer vesicles in vivo: correlations with PEG molecular weight. *Journal of Controlled Release,* 90**,** 323-334.
POSTEL, E., MANGO, S. E. & FLINT, S. 1989. A nuclease-hypersensitive element of the human c-myc promoter interacts with a transcription initiation factor. *Molecular and Cellular Biology,* 9**,** 5123-5133.
POURDEHNAD, M., TRUITT, M. L., SIDDIQI, I. N., DUCKER, G. S., SHOKAT, K. M. & RUGGERO, D. 2013. Myc and mTOR converge on a common node in protein synthesis control that confers synthetic lethality in Myc-driven cancers. *Proceedings of the National Academy of Sciences USA,* 110**,** 11988-11993.
POZZI, D., MARCHINI, C., CARDARELLI, F., AMENITSCH, H., GARULLI, C., BIFONE, A. & CARACCIOLO, G. 2012. Transfection efficiency boost of cholesterol-containing lipoplexes. *Biochimica et Biophysica Acta (BBA)-Biomembranes,* 1818**,** 2335-2343.
PRATT, A. J. & MACRAE, I. J. 2009. The RNA-induced silencing complex: a versatile gene-silencing machine. *Journal of Biological Chemistry,* 284**,** 17897-17901.
QIN, B. & CHENG, K. 2010. Silencing of the IKKε gene by siRNA inhibits invasiveness and growth of breast cancer cells. *Breast Cancer Research,* 12**,** DOI:10.1186/bcr2644.
RAICHUR, A., NAKAJIMA, Y., NAGAOKA, Y., MATSUMOTO, K., MIZUKI, T., KATO, K., MAEKAWA, T. & KUMAR, D. S. 2015. Strategist PLGA Nano-capsules to Deliver siRNA for Inhibition of Carcinoma and Neuroblastoma Cell Lines by Knockdown of MYC Proto-oncogene using CPPs and PNA. *NanoWorld Journal,* 1**,** 32-45.
RAMPERSAD, S. N. 2012. Multiple applications of Alamar Blue as an indicator of metabolic function and cellular health in cell viability bioassays. *Sensors,* 12**,** 12347-12360.
RAMSAY, G., EVAN, G. I. & BISHOP, J. M. 1984. The protein encoded by the human proto-oncogene c-myc. *Proceedings of the National Academy of Sciences,* 81**,** 7742-7746.
RANA, T. M. 2007. Illuminating the silence: understanding the structure and function of small RNAs. *Nature Reviews Molecular Cell Biology,* 8**,** 23-36.
RAND, T. A., PETERSEN, S., DU, F. & WANG, X. 2005. Argonaute2 cleaves the anti-guide strand of siRNA during RISC activation. *Cell,* 123**,** 621-629.
RAY, S., ATKURI, K. R., DEB-BASU, D., ADLER, A. S., CHANG, H. Y., HERZENBERG, L. A. & FELSHER, D. W. 2006. MYC can induce DNA breaks in vivo and in vitro independent of reactive oxygen species. *Cancer Research,* 66**,** 6598-6005.

REJMAN, J., OBERLE, V., ZUHORN, I. S. & HOEKSTRA, D. 2004a. Size-dependent internalization of particles via the pathways of clathrin-and caveolae-mediated endocytosis. *Biochemical Journal,* 377**,** 159-169.

REJMAN, J., WAGENAAR, A., ENGBERTS, J. B. & HOEKSTRA, D. 2004b. Characterization and transfection properties of lipoplexes stabilized with novel exchangeable polyethylene glycol–lipid conjugates. *Biochimica et Biophysica Acta (BBA)-Biomembranes,* 1660**,** 41-52.

RESINA, S., PREVOT, P. & THIERRY, A. R. 2009. Physico-chemical characteristics of lipoplexes influence cell uptake mechanisms and transfection efficacy. *PLoS ONE,* 4**,** e6058. DOI:10.1371/journal.pone.0006058.

REYES-GONZÁLEZ, J. M., ARMAIZ-PEÑA, G. N., MANGALA, L. S., VALIYEVA, F., IVAN, C., PRADEEP, S., ECHEVARRÍA-VARGAS, I. M., RIVERA-REYES, A., SOOD, A. K. & VIVAS-MEJÍA, P. E. 2015. Targeting c-MYC in platinum-resistant ovarian cancer. *Molecular Cancer Therapeutics,* 14**,** 2260-2269.

RIBBLE, D., GOLDSTEIN, N. B., NORRIS, D. A. & SHELLMAN, Y. G. 2005. A simple technique for quantifying apoptosis in 96-well plates. *BMC Biotechnology,* 5**,** DOI:10.1186/1472-6750-5-12.

RISS, T. L., MORAVEC, R., NILES, A., BENINK, H., WORZELLA, T. & MINOR, L. 2004. Cell viability assays. *In:* SITTAMPALAM, G., COUSSENS, N. & NELSON, H. E. A. (eds.) *Assay Guidance Manual [Internet]*. Bethesda (MD): Eli Lilly & Company and the National Center for Advancing Translational Sciences.

ROBINSON, K., ASAWACHAICHARN, N., GALLOWAY, D. A. & GRANDORI, C. 2009. c-Myc Accelerates S-Phase and Requires WRN to Avoid Replication Stress. *PLoS ONE,* 4**,** e5951. DOI:10.1371/journal.pone.0005951.

ROMANO, N. & MACINO, G. 1992. Quelling: transient inactivation of gene expression in Neurospora crassa by transformation with homologous sequences. *Molecular Microbiology,* 6**,** 3343-3353.

ROSE, S. D., KIM, D.-H., AMARZGUIOUI, M., HEIDEL, J. D., COLLINGWOOD, M. A., DAVIS, M. E., ROSSI, J. J. & BEHLKE, M. A. 2005. Functional polarity is introduced by Dicer processing of short substrate RNAs. *Nucleic Acids Research,* 33**,** 4140-4156.

ROSS, J., LEMM, I. & BERBERET, B. 2001. Overexpression of an mRNA-binding protein in human colorectal cancer. *Oncogene,* 20**,** 6544-6550.

ROUSSET, M. 1986. The human colon carcinoma cell lines HT-29 and Caco-2: two in vitro models for the study of intestinal differentiation. *Biochimie,* 68**,** 1035-1040.

ROWAN, A., LAMLUM, H., ILYAS, M., WHEELER, J., STRAUB, J., PAPADOPOULOU, A., BICKNELL, D., BODMER, W. & TOMLINSON, I. 2000. APC mutations in sporadic colorectal tumors: a mutational "hotspot" and interdependence of the "two hits". *Proceedings of the National Academy of Sciences USA,* 97**,** 3352-3357.

RUMMUKAINEN, J., KYTÖLÄ, S., KARHU, R., FARNEBO, F., LARSSON, C. & ISOLA, J. J. 2001. Aberrations of chromosome 8 in 16 breast cancer cell lines by comparative genomic hybridization, fluorescence in situ hybridization, and spectral karyotyping. *Cancer Genetics and Cytogenetics,* 126**,** 1-7.

SABÒ, A., KRESS, T. R., PELIZZOLA, M., DE PRETIS, S., GORSKI, M. M., TESI, A., MORELLI, M. J., BORA, P., DONI, M. & VERRECCHIA, A. 2014. Selective transcriptional regulation by Myc in cellular growth control and lymphomagenesis. *Nature,* 511**,** 488-492.

SANKAR, N., KADEPPAGARI, R.-K. & THIMMAPAYA, B. 2009. c-Myc-induced aberrant DNA synthesis and activation of DNA damage response in p300 knockdown cells. *Journal of Biological Chemistry,* 284**,** 15193-15205.

SANTEL, A., ALEKU, M., KEIL, O., ENDRUSCHAT, J., ESCHE, V., FISCH, G., DAMES, S., LÖFFLER, K., FECHTNER, M., ARNOLD, W., GIESE, K., KLIPPEL, A. & KAUFMANN, J. 2006. A novel siRNA-lipoplex technology for RNA interference in the mouse vascular endothelium. *Gene Therapy,* 13**,** 1222-1234.

SARDI, I., DAL CANTO, M., BARTOLETTI, R., GUAZZELLI, R., TRAVAGLINI, F. & MONTALI, E. 1998. Molecular genetic alterations of c-myc oncogene in superficial and locally advanced bladder cancer. *European Urology,* 33**,** 424-430.

SATO, Y., HATAKEYAMA, H., SAKURAI, Y., HYODO, M., AKITA, H. & HARASHIMA, H. 2012. A pH-sensitive cationic lipid facilitates the delivery of liposomal siRNA and gene silencing activity in vitro and in vivo. *Journal of Controlled Release,* 163**,** 267-276.

SATOH, K., YACHIDA, S., SUGIMOTO, M., OSHIMA, M., NAKAGAWA, T., AKAMOTO, S., TABATA, S., SAITOH, K., KATO, K. & SATO, S. 2017. Global metabolic reprogramming of colorectal cancer occurs at adenoma stage and is induced by MYC. *Proceedings of the National Academy of Sciences USA,* 114**,** E7697-E7706.

SCHLOSSER, I., HÖLZEL, M., MÜRNSEER, M., BURTSCHER, H., WEIDLE, U. H. & EICK, D. 2003. A role for c-Myc in the regulation of ribosomal RNA processing. *Nucleic Acids Research,* 31**,** 6148-6156.

SCHROEDER, A., LEVINS, C. G., CORTEZ, C., LANGER, R. & ANDERSON, D. G. 2010. Lipid-based nanotherapeutics for siRNA delivery. *Journal of Internal Medicine,* 267**,** 9-21.

SCHUHMACHER, M., STAEGE, M. S., PAJIC, A., POLACK, A., WEIDLE, U. H., BORNKAMM, G. W., EICK, D. & KOHLHUBER, F. 1999. Control of cell growth by c-Myc in the absence of cell division. *Current Biology,* 9**,** 1255-1258.

SCHUIJERS, J., MANTEIGA, J. C., WEINTRAUB, A. S., DAY, D. S., ZAMUDIO, A. V., HNISZ, D., LEE, T. I. & YOUNG, R. A. 2018. Transcriptional Dysregulation of MYC Reveals Common Enhancer-Docking Mechanism. *Cell Reports,* 23**,** 349-360.

SCHWAB, M., ALITALO, K., KLEMPNAUER, K.-H., VARMUS, H. E., BISHOP, J. M., GILBERT, F., BRODEUR, G., GOLDSTEIN, M. & TRENT, J. 1983. Amplified DNA with limited homology to myc cellular oncogene is shared by human neuroblastoma cell lines and a neuroblastoma tumour. *Nature,* 305**,** 245-248.

SEENISAMY, J., REZLER, E. M., POWELL, T. J., TYE, D., GOKHALE, V., JOSHI, C. S., SIDDIQUI-JAIN, A. & HURLEY, L. H. 2004. The dynamic character of the G-quadruplex element in the c-MYC promoter and modification by TMPyP4. *Journal of the American Chemical Society,* 126**,** 8702-8709.

SEKHON, H. S., LONDON, C. A., SEKHON, M., IVERSEN, P. L. & DEVI, G. R. 2008. c-MYC antisense phosphosphorodiamidate morpholino oligomer inhibits lung metastasis in a murine tumor model. *Lung Cancer,* 60**,** 347-354.

SEKI, Y., YAMAMOTO, H., NGAN, C. Y., YASUI, M., TOMITA, N., KITANI, K., TAKEMASA, I., IKEDA, M., SEKIMOTO, M. & MATSUURA, N. 2006. Construction of a novel DNA decoy that inhibits the oncogenic β-catenin/T-cell factor pathway. *Molecular cancer therapeutics,* 5**,** 985-994.

SEMPLE, S. C., CHONN, A. & CULLIS, P. R. 1996. Influence of cholesterol on the association of plasma proteins with liposomes. *Biochemistry,* 35**,** 2521-2525.

SEMPLE, S. C., CHONN, A. & CULLIS, P. R. 1998. Interactions of liposomes and lipid-based carrier systems with blood proteins: relation to clearance behaviour in vivo. *Advanced Drug Delivery Reviews,* 32**,** 3-17.

SEO, A., YANG, J., KIM, H., JHEON, S., KIM, K., LEE, C., JIN, Y., YUN, S., CHUNG, J. & PAIK, J. 2014. Clinicopathologic and prognostic significance of c-MYC copy number gain in lung adenocarcinomas. *British Journal of Cancer,* 110**,** 2688-2699.

SHAAT, H., MOSTAFA, A., MOUSTAFA, M., GAMAL-ELDEEN, A., EMAM, A., EL-HUSSIENY, E. & ELHEFNAWI, M. 2016. Modified gold nanoparticles for intracellular delivery of anti-liver cancer siRNA. *International Journal of Pharmaceutics,* 504**,** 125-133.

SHAKEEL, S., KARIM, S. & ALI, A. 2006. Peptide nucleic acid (PNA)—a review. *Journal of Chemical Technology and Biotechnology,* 81**,** 892-899.

SHCHORS, K., SHCHORS, E., ROSTKER, F., LAWLOR, E. R., BROWN-SWIGART, L. & EVAN, G. I. 2006. The Myc-dependent angiogenic switch in tumors is mediated by interleukin 1β. *Genes & Development,* 20**,** 2527-2538.

SHICHIRI, M., HANSON, K. D. & SEDIVY, J. M. 1993. Effects of c-myc expression on proliferation, quiescence, and the G0 to G1 transition in nontransformed cells. *Cell Growth & Differentiation,* 4**,** 93-104.

SHIM, G., KIM, M.-G., PARK, J. Y. & OH, Y.-K. 2013. Application of cationic liposomes for delivery of nucleic acids. *Asian Journal of Pharmaceutical Sciences,* 8**,** 72-80.

SHIM, H., CHUN, Y. S., LEWIS, B. C. & DANG, C. V. 1998. A unique glucose-dependent apoptotic pathway induced by c-Myc. *Proceedings of the National Academy of Sciences,* 95**,** 1511-1516.

SHOSTAK, A., RUPPERT, B., HA, N., BRUNS, P., TOPRAK, U. H., LAWERENZ, C., LICHTER, P., RADLWIMMER, B., EILS, J. & BRORS, B. 2016. MYC/MIZ1-dependent gene repression inversely coordinates the circadian clock with cell cycle and proliferation. *Nature Communications,* 7**,** DOI:10.1038/ncomms11807.

SI, J., YU, X., ZHANG, Y. & DEWILLE, J. W. 2010. Myc interacts with Max and Miz1 to repress C/EBPδ promoter activity and gene expression. *Molecular Cancer,* 9**,** 92-92.

SIEUWERTS, A. M., KLIJN, J. G., PETERS, H. A. & FOEKENS, J. A. 1995. The MTT Tetrazolium Salt Assay Scrutinized: How to Use this Assay Reliably to Measure Metabolie Activity of Cell Cultures in vitro for the Assessment of Growth Characteristics, IC50-Values and Cell Survival. *Clinical Chemistry and Laboratory Medicine,* 33**,** 813-824.

SILVERMAN, S. K. 2005. In vitro selection, characterization, and application of deoxyribozymes that cleave RNA. *Nucleic Acids Research,* 33**,** 6151-6163.

SIMONSSON, T. & HENRIKSSON, M. 2002. c-myc Suppression in Burkitt's lymphoma cells. *Biochemical and Biophysical Research Communications,* 290**,** 11-15.

SINGH, M. & ARIATTI, M. 2006. A cationic cytofectin with long spacer mediates favourable transfection in transformed human epithelial cells. *International Journal of Pharmaceutics,* 309**,** 189-198.

SINGH, M., ROGERS, C. B. & ARIATTI, M. 2007. Targeting of glycosylated lipoplexes in HepG2 cells: Anomeric and C-4 epimeric preference of the asialoglycoprotein receptor. *South African Journal of Science,* 103**,** 204-210.

SINGH, Y., TOMAR, S., KHAN, S., MEHER, J. G., PAWAR, V. K., RAVAL, K., SHARMA, K., SINGH, P. K., CHAURASIA, M. & REDDY, B. S. 2015. Bridging small interfering RNA with giant therapeutic outcomes using nanometric liposomes. *Journal of Controlled Release,* 220**,** 368-387.

SMITH, A., VERRECCHIA, A., FAGA, G., DONI, M., PERNA, D., MARTINATO, F., GUCCIONE, E. & AMATI, B. 2009. A positive role for Myc in TGFβ-induced Snail transcription and epithelial-to-mesenchymal transition. *Oncogene,* 28**,** 422-430.

SMITH, D., MYINT, T. & GOH, H. 1993. Over-expression of the c-myc proto-oncogene in colorectal carcinoma. *British Journal of Cancer,* 68**,** 407-413.

SONG, E., ZHU, P., LEE, S.-K., CHOWDHURY, D., KUSSMAN, S., DYKXHOORN, D. M., FENG, Y., PALLISER, D., WEINER, D. B. & SHANKAR, P. 2005. Antibody mediated in vivo delivery of small interfering RNAs via cell-surface receptors. *Nature Biotechnology,* 23**,** 709-717.

SONG, L., AHKONG, Q., RONG, Q., WANG, Z., ANSELL, S., HOPE, M. & MUI, B. 2002. Characterization of the inhibitory effect of PEG-lipid conjugates on the intracellular delivery of plasmid and antisense DNA mediated by cationic lipid liposomes. *Biochimica et Biophysica Acta (BBA)-Biomembranes,* 1558**,** 1-13.

SONG, Y., DONG, M. M. & YANG, H. F. 2011. Effects of RNA interference targeting four different genes on the growth and proliferation of nasopharyngeal carcinoma CNE-2Z cells. *Cancer Gene Therapy,* 18**,** 297-304.

SOUCEK, L., LAWLOR, E. R., SOTO, D., SHCHORS, K., SWIGART, L. B. & EVAN, G. I. 2007. Mast cells are required for angiogenesis and macroscopic expansion of Myc-induced pancreatic islet tumors. *Nature Medicine,* 13**,** 1211-1218.

SOUCEK, L., WHITFIELD, J., MARTINS, C. P., FINCH, A. J., MURPHY, D. J., SODIR, N. M., KARNEZIS, A. N., SWIGART, L. B., NASI, S. & EVAN, G. I. 2008. Modelling Myc inhibition as a cancer therapy. *Nature,* 455**,** 679-683.

SOULE, H. D., VAZGUEZ, J., LONG, A., ALBERT, S. & BRENNAN, M. 1973. A human cell line from a pleural effusion derived from a breast carcinoma. *Journal of the National Cancer Institute,* 51**,** 1409-1416.

SOUTSCHEK, J., AKINC, A., BRAMLAGE, B., CHARISSE, K., CONSTIEN, R., DONOGHUE, M., ELBASHIR, S., GEICK, A., HADWIGER, P. & HARBORTH, J. 2004. Therapeutic silencing of an endogenous gene by systemic administration of modified siRNAs. *Nature,* 432**,** 173-178.

SPAGNOU, S., MILLER, A. D. & KELLER, M. 2004. Lipidic carriers of siRNA: differences in the formulation, cellular uptake, and delivery with plasmid DNA. *Biochemistry,* 43**,** 13348-13356.

SPARKS, A. B., MORIN, P. J., VOGELSTEIN, B. & KINZLER, K. W. 1998. Mutational analysis of the APC/β-catenin/Tcf pathway in colorectal cancer. *Cancer Research,* 58**,** 1130-1134.

SPOTTS, G. D., PATEL, S. V., XIAO, Q. & HANN, S. R. 1997. Identification of downstream-initiated c-Myc proteins which are dominant-negative inhibitors of transactivation by full-length c-Myc proteins. *Molecular and Cellular Biology,* 17**,** 1459-1468.

STALLER, P., PEUKERT, K., KIERMAIER, A., SEOANE, J., LUKAS, J., KARSUNKY, H., MOROY, T., BARTEK, J., MASSAGUE, J., HANEL, F. & EILERS, M. 2001. Repression of p15INK4b expression by Myc through association with Miz-1. *Nature Cell Biology,* 3**,** 392-399.

STEPHENS, A. 2004. Technology evaluation: AVI-4126, AVI BioPharma. *Current Opinion in Molecular Therapeutics,* 6**,** 551-558.

STEVENSON, M. 2003. Dissecting HIV-1 through RNA interference. *Nature Reviews Immunology,* 3**,** 851-858.

STEWART, D. A., THOMAS, S. D., MAYFIELD, C. A. & MILLER, D. M. 2001. Psoralen-modified clamp-forming antisense oligonucleotides reduce cellular c-Myc protein expression and B16-F0 proliferation. *Nucleic Acids Research,* 29**,** 4052-4061.

STEWART, D. A., XU, X., THOMAS, S. D. & MILLER, D. M. 2002. Acridine-modified, clamp-forming antisense oligonucleotides synergize with cisplatin to inhibit c-Myc expression and B16-F0 tumor progression. *Nucleic Acids Research,* 30**,** 2565-2574.

STOCKERT, J. C., BLÁZQUEZ-CASTRO, A., CAÑETE, M., HOROBIN, R. W. & VILLANUEVA, Á. 2012. MTT assay for cell viability: Intracellular localization of the formazan product is in lipid droplets. *Acta Histochemica,* 114**,** 785-796.

SUGIYAMA, A., KUME, A., NEMOTO, K., LEE, S., ASAMI, Y., NEMOTO, F., NISHIMURA, S. & KUCHINO, Y. 1989. Isolation and characterization of s-myc, a member of the rat myc gene family. *Proceedings of the National Academy of Sciences USA,* 86**,** 9144-9148.

SUH, M. S., SHIM, G., LEE, H. Y., HAN, S.-E., YU, Y.-H., CHOI, Y., KIM, K., KWON, I. C., WEON, K. Y. & KIM, Y. B. 2009. Anionic amino acid-derived cationic lipid for siRNA delivery. *Journal of Controlled Release,* 140**,** 268-276.

SUK, J. S., XU, Q., KIM, N., HANES, J. & ENSIGN, L. M. 2016. PEGylation as a strategy for improving nanoparticle-based drug and gene delivery. *Advanced Drug Delivery Reviews,* 99**,** 28-51.

SUŁKOWSKI, W. W., PENTAK, D., NOWAK, K. & SUŁKOWSKA, A. 2005. The influence of temperature, cholesterol content and pH on liposome stability. *Journal of Molecular Structure,* 744–747**,** 737-747.

SUN, J., LU, Z., DENG, Y., WANG, W., HE, Q., YAN, W. & WANG, A. 2018. Up-regulation of INSR/IGF1R by C-myc promotes TSCC tumorigenesis and metastasis through the NF-κB pathway. *Biochimica et Biophysica Acta,* 1864**,** 1873-1882.

SUN, L.-Q., CAIRNS, M. J., GERLACH, W. L., WITHERINGTON, C., WANG, L. & KING, A. 1999. Suppression of smooth muscle cell proliferation by a c-myc RNA-cleaving deoxyribozyme. *Journal of Biological Chemistry,* 274**,** 17236-17241.

TACK, F., NOPPE, M., VAN DIJCK, A., DEKEYZER, N., VAN DER LEEDE, B.-J., BAKKER, A., WOUTERS, W., JANICOT, M. & BREWSTER, M. 2008. Delivery of a DNAzyme targeting c-myc to HT29 colon carcinoma cells using a gold nanoparticulate approach. *Die Pharmazie-An International Journal of Pharmaceutical Sciences,* 63**,** 221-225.

TAGALAKIS, A. D., DO HYANG, D. L., BIENEMANN, A. S., ZHOU, H., MUNYE, M. M., SARAIVA, L., MCCARTHY, D., DU, Z., VINK, C. A. & MAESHIMA, R. 2014. Multifunctional, self-assembling anionic peptide-lipid nanocomplexes for targeted siRNA delivery. *Biomaterials,* 35**,** 8406-8415.

TAI, J., WANG, G., LIU, T., WANG, L., LIN, C. & LI, F. 2012. Effects of siRNA targeting c-Myc and VEGF on human colorectal cancer Volo cells. *Journal of Biochemical and Molecular Toxicology,* 26**,** 499-505.

TAKAHASHI, Y., YAMAOKA, K., NISHIKAWA, M. & TAKAKURA, Y. 2009. Quantitative and temporal analysis of gene silencing in tumor cells induced by small interfering RNA or short hairpin RNA expressed from plasmid vectors. *Journal of Pharmaceutical Sciences,* 98**,** 74-80.

TANGUDU, N. K., VERMA, V. K., CLEMONS, T. D., BEEVI, S. S., HAY, T., MAHIDHARA, G., RAJA, M., NAIR, R. A., ALEXANDER, L. E. & PATEL, A. B. 2015. RNA Interference Using c-Myc–Conjugated Nanoparticles Suppresses Breast and Colorectal Cancer Models. *Molecular Cancer Therapeutics,* 14**,** 1259-1269.

TANIGUCHI, K., IWATSUKI, A., SUGITO, N., SHINOHARA, H., KURANAGA, Y., OSHIKAWA, Y., TAJIRIKA, T., FUTAMURA, M., YOSHIDA, K. & UCHIYAMA, K. 2018. Oncogene RNA helicase DDX6 promotes the process of c-Myc expression in gastric cancer cells. *Molecular Carcinogenesis,* 57**,** 579-589.

TANSEY, W. P. 2014. Mammalian MYC Proteins and Cancer. *New Journal of Science,* 2014**,** DOI:10.1155/2014/757534.

TARATULA, O., GARBUZENKO, O. B., KIRKPATRICK, P., PANDYA, I., SAVLA, R., POZHAROV, V. P., HE, H. & MINKO, T. 2009. Surface-engineered targeted PPI dendrimer for efficient intracellular and intratumoral siRNA delivery. *Journal of Controlled Release,* 140**,** 284-293.

TAXMAN, D. J., MOORE, C. B., GUTHRIE, E. H. & HUANG, M. T.-H. 2010. Short hairpin RNA (shRNA): design, delivery, and assessment of gene knockdown. *RNA Therapeutics: Function, Design, and Delivery***,** 139-156.

TEMPLETON, N. 2003. Cationic liposomes as in vivo delivery vehicles. *Current Medicinal Chemistry,* 10**,** 1279-1287.

TEMPLETON, N. S., LASIC, D. D., FREDERIK, P. M., STREY, H. H., ROBERTS, D. D. & PAVLAKIS, G. N. 1997. Improved DNA: liposome complexes for increased systemic delivery and gene expression. *Nature Biotechnology,* 15**,** 647-652.

THOMAS, L. R., FOSHAGE, A. M., WEISSMILLER, A. M., POPAY, T. M., GRIEB, B. C., QUALLS, S. J., NG, V., CARBONEAU, B., LOREY, S. & EISCHEN, C. M. 2016. Interaction of MYC with host cell factor-1 is mediated by the evolutionarily conserved Myc box IV motif. *Oncogene,* 35**,** 3613-3618.

THOMAS, L. R., WANG, Q., GRIEB, B. C., PHAN, J., FOSHAGE, A. M., SUN, Q., OLEJNICZAK, E. T., CLARK, T., DEY, S. & LOREY, S. 2015. Interaction with WDR5 promotes target gene recognition and tumorigenesis by MYC. *Molecular Cell,* 58**,** 440-452.

THOMAS, T., FAALAND, C. A., GALLO, M. A. & THOMAS, T. 1995. Suppression of c-myc oncogene expression by a polyamine-complexed triplex forming oligonucleotide in MCF-7 breast cancer cells. *Nucleic Acids Research,* 23**,** 3594-3599.

TOLCHER, A. W., PAPADOPOULOS, K. P., PATNAIK, A., RASCO, D. W., MARTINEZ, D., WOOD, D. L., FIELMAN, B., SHARMA, M., JANISCH, L. A. & BROWN, B. D. 2015. Safety

and activity of DCR-MYC, a first-in-class Dicer-substrate small interfering RNA (DsiRNA) targeting MYC, in a phase I study in patients with advanced solid tumors. *Journal of Clinical Oncology*, DOI:10.1200/jco.2015.33.15_suppl.11006.

TOMASETTI, L., LIEBL, R., WASTL, D. S. & BREUNIG, M. 2016. Influence of PEGylation on nanoparticle mobility in different models of the extracellular matrix. *European Journal of Pharmaceutics and Biopharmaceutics,* 108**,** 145-155.

TORCHILIN, V. 2011. Tumor delivery of macromolecular drugs based on the EPR effect. *Advanced Drug Delivery Reviews,* 63**,** 131-135.

TORCHILIN, V. P., OMELYANENKO, V. G., PAPISOV, M. I., BOGDANOV, A. A., JR., TRUBETSKOY, V. S., HERRON, J. N. & GENTRY, C. A. 1994. Poly(ethylene glycol) on the liposome surface: on the mechanism of polymer-coated liposome longevity. *Biochimica et Biophysica Acta,* 1195**,** 11-20.

TRESZL, A., ÁDÁNY, R., RÁKOSY, Z., KARDOS, L., BÉGÁNY, Á., GILDE, K. & BALÁZS, M. 2004. Extra copies of c-myc are more pronounced in nodular melanomas than in superficial spreading melanomas as revealed by fluorescence in situ hybridisation. *Cytometry Part B: Clinical Cytometry,* 60**,** 37-46.

UDATSU, Y., KUSAFUKA, T., KURODA, S., MIAO, J. & OKADA, A. 2001. High frequency of β-catenin mutations in hepatoblastoma. *Pediatric Surgery International,* 17**,** 508-512.

URBAN-KLEIN, B., WERTH, S., ABUHARBEID, S., CZUBAYKO, F. & AIGNER, A. 2005. RNAi-mediated gene-targeting through systemic application of polyethylenimine (PEI)-complexed siRNA in vivo. *Gene Therapy,* 12**,** 461-466.

VAFA, O., WADE, M., KERN, S., BEECHE, M., PANDITA, T. K., HAMPTON, G. M. & WAHL, G. M. 2002. c-Myc can induce DNA damage, increase reactive oxygen species, and mitigate p53 function: a mechanism for oncogene-induced genetic instability. *Molecular Cell,* 9**,** 1031-1044.

VAN DE WATER, F. M., BOERMAN, O. C., WOUTERSE, A. C., PETERS, J. G., RUSSEL, F. G. & MASEREEUW, R. 2006. Intravenously administered short interfering RNA accumulates in the kidney and selectively suppresses gene function in renal proximal tubules. *Drug Metabolism and Disposition,* 34**,** 1393-1397.

VAN RIGGELEN, J., YETIL, A. & FELSHER, D. W. 2010. MYC as a regulator of ribosome biogenesis and protein synthesis. *Nature Reviews Cancer,* 10**,** 301-309.

VANDER HEIDEN, M. G., CANTLEY, L. C. & THOMPSON, C. B. 2009. Understanding the Warburg effect: the metabolic requirements of cell proliferation. *Science,* 324**,** 1029-33.

VAUX, D. L., CORY, S. & ADAMS, J. M. 1988. Bcl-2 gene promotes haemopoietic cell survival and cooperates with c-myc to immortalize pre-B cells. *Nature,* 335**,** 440-442.

VENNSTROM, B., SHEINESS, D., ZABIELSKI, J. & BISHOP, J. 1982. Isolation and characterization of c-myc, a cellular homolog of the oncogene (v-myc) of avian myelocytomatosis virus strain 29. *Journal of Virology,* 42**,** 773-779.

VERVOORTS, J., LÜSCHER-FIRZLAFF, J. & LÜSCHER, B. 2006. The ins and outs of MYC regulation by posttranslational mechanisms. *Journal of Biological Chemistry,* 281**,** 34725-34729.

VERVOORTS, J., LÜSCHER-FIRZLAFF, J. M., ROTTMANN, S., LILISCHKIS, R., WALSEMANN, G., DOHMANN, K., AUSTEN, M. & LÜSCHER, B. 2003. Stimulation of c-MYC transcriptional activity and acetylation by recruitment of the cofactor CBP. *EMBO Reports,* 4**,** 484-490.

VITA, M. & HENRIKSSON, M. 2006. The Myc oncoprotein as a therapeutic target for human cancer. *Seminars in Cancer Biology,* 16**,** 318-330.

VIVAS-MEJIA, P. E., GONZALEZ, J. M. R. & SOOD, A. K. 2018. Nanoliposomal c-MYC-siRNA inhibits in vivo tumor growth of cisplatin-resistant ovarian cancer. Google Patents.

WALKER, B., WARDELL, C., BRIOLI, A., BOYLE, E., KAISER, M., BEGUM, D., DAHIR, N., JOHNSON, D., ROSS, F. & DAVIES, F. 2014. Translocations at 8q24 juxtapose MYC with genes that harbor superenhancers resulting in overexpression and poor prognosis in myeloma patients. *Blood Cancer Journal,* 4**,** e191. DOI:10.1038/bcj.2014.13.

WALZ, S., LORENZIN, F., MORTON, J., WIESE, K. E., VON EYSS, B., HEROLD, S., RYCAK, L., DUMAY-ODELOT, H., KARIM, S., BARTKUHN, M., ROELS, F., WUSTEFELD, T., FISCHER, M., TEICHMANN, M., ZENDER, L., WEI, C. L., SANSOM, O., WOLF, E. & EILERS, M. 2014. Activation and repression by oncogenic MYC shape tumour-specific gene expression profiles. *Nature,* 511**,** 483-487.

WANG, C., LISANTI, M. P. & LIAO, D. J. 2011. Reviewing once more the c-myc and Ras collaboration: Converging at the cyclin D1-CDK4 complex and challenging basic concepts of cancer biology. *Cell Cycle,* 10**,** 57-67.

WANG, J., LU, Z., WIENTJES, M. G. & AU, J. L.-S. 2010. Delivery of siRNA therapeutics: barriers and carriers. *The AAPS Journal,* 12**,** 492-503.

WANG, X., YU, B., REN, W., MO, X., ZHOU, C., HE, H., JIA, H., WANG, L., JACOB, S. T. & LEE, R. J. 2013a. Enhanced hepatic delivery of siRNA and microRNA using oleic acid based lipid nanoparticle formulations. *Journal of Controlled Release,* 172**,** 690-698.

WANG, X., ZHAO, X., GAO, P. & WU, M. 2013b. c-Myc modulates microRNA processing via the transcriptional regulation of Drosha. *Scientific Reports,* 3**,** DOI:10.1038/srep01942.

WANG, Y., LIU, S., ZHANG, G., ZHOU, C., ZHU, H., ZHOU, X., QUAN, L., BAI, J. & XU, N. 2005. Knockdown of c-Myc expression by RNAi inhibits MCF-7 breast tumor cells growth in vitro and in vivo. *Breast Cancer Research,* 7**,** R220-R228.

WANG, Y., WU, M. C., SHAM, J. S., ZHANG, W., WU, W. Q. & GUAN, X. Y. 2002. Prognostic significance of c-myc and AIB1 amplification in hepatocellular carcinoma. *Cancer,* 95**,** 2346-2352.

WATERS, C., LITTLEWOOD, T., HANCOCK, D., MOORE, J. & EVAN, G. 1991. c-myc protein expression in untransformed fibroblasts. *Oncogene,* 6**,** 797-805.

WATT, R., NISHIKURA, K., SORRENTINO, J., CROCE, C. M. & ROVERA, G. 1983. The structure and nucleotide sequence of the 5'end of the human c-myc oncogene. *Proceedings of the National Academy of Sciences USA,* 80**,** 6307-6311.

WEBB, M. S., TORTORA, N., CREMESE, M., KOZLOWSKA, H., BLAQUIERE, M., DEVINE, D. V. & KORNBRUST, D. J. 2001. Toxicity and toxicokinetics of a phosphorothioate oligonucleotide against the c-myc oncogene in cynomolgus monkeys. *Antisense and Nucleic Acid Drug Development,* 11**,** 155-163.

WEISMAN, S., HIRSCH-LERNER, D., BARENHOLZ, Y. & TALMON, Y. 2004. Nanostructure of cationic lipid-oligonucleotide complexes. *Biophysical Journal,* 87**,** 609-614.

WHITFIELD, J. R., BEAULIEU, M.-E. & SOUCEK, L. 2017. Strategies to inhibit Myc and their clinical applicability. *Frontiers in Cell and Developmental Biology,* 5**,** DOI:10.3389/fcell.2017.00010.

WICKSTROM, E. L., BACON, T. A., GONZALEZ, A., FREEMAN, D. L., LYMAN, G. H. & WICKSTROM, E. 1988. Human promyelocytic leukemia HL-60 cell proliferation and c-myc protein expression are inhibited by an antisense pentadecadeoxynucleotide targeted against c-myc mRNA. *Proceedings of the National Academy of Sciences,* 85**,** 1028-1032.

WILSON, A., MURPHY, M. J., OSKARSSON, T., KALOULIS, K., BETTESS, M. D., OSER, G. M., PASCHE, A.-C., KNABENHANS, C., MACDONALD, H. R. & TRUMPP, A. 2004. c-Myc controls the balance between hematopoietic stem cell self-renewal and differentiation. *Genes & Development,* 18**,** 2747-2763.

WILSON, D. R. & GREEN, J. J. 2017. Nanoparticle Tracking Analysis for Determination of Hydrodynamic Diameter, Concentration, and Zeta-Potential of Polyplex Nanoparticles. *Methods in Molecular Biology,* 1570**,** 31-46.

WISE, D. R., DEBERARDINIS, R. J., MANCUSO, A., SAYED, N., ZHANG, X.-Y., PFEIFFER, H. K., NISSIM, I., DAIKHIN, E., YUDKOFF, M. & MCMAHON, S. B. 2008. Myc regulates a transcriptional program that stimulates mitochondrial glutaminolysis and leads to glutamine addiction. *Proceedings of the National Academy of Sciences USA,* 105**,** 18782-18787.

WITTRUP, A., AI, A., LIU, X., HAMAR, P., TRIFONOVA, R., CHARISSE, K., MANOHARAN, M., KIRCHHAUSEN, T. & LIEBERMAN, J. 2015. Visualizing lipid-formulated siRNA release from endosomes and target gene knockdown. *Nature Biotechnology,* 33**,** 870-876.
XIA, Y., GUO, M., XU, T., LI, Y., WANG, C., LIN, Z., ZHAO, M. & ZHU, B. 2018. siRNA-loaded selenium nanoparticle modified with hyaluronic acid for enhanced hepatocellular carcinoma therapy. *International Journal of Nanomedicine,* 13**,** 1539-1552.
XIAO, Q., CLAASSEN, G., SHI, J., ADACHI, S., SEDIVY, J. & HANN, S. R. 1998. Transactivation-defective c-MycS retains the ability to regulate proliferation and apoptosis. *Genes & Development,* 12**,** 3803-3808.
XIE, F., YUAN, Y., XIE, L., RAN, P., XIANG, X., HUANG, Q., QI, G., GUO, X., XIAO, C. & ZHENG, S. 2017. miRNA-320a inhibits tumor proliferation and invasion by targeting c-Myc in human hepatocellular carcinoma. *OncoTargets and Therapy,* 10**,** 885-894.
XIE, X., LIN, W., LI, M., YANG, Y., DENG, J., LIU, H., CHEN, Y., FU, X., LIU, H. & YANG, Y. 2016. Efficient siRNA Delivery Using Novel Cell-Penetrating Peptide-siRNA Conjugate-Loaded Nanobubbles and Ultrasound. *Ultrasound in Medicine & Biology,* 42**,** 1362-1374.
XU, C.-F. & WANG, J. 2015. Delivery systems for siRNA drug development in cancer therapy. *Asian Journal of Pharmaceutical Sciences,* 10**,** 1-12.
XU, L. & ANCHORDOQUY, T. J. 2008. Cholesterol domains in cationic lipid/DNA complexes improve transfection. *Biochimica et Biophysica Acta (BBA)-Biomembranes,* 1778**,** 2177-2181.
XU, L. & ANCHORDOQUY, T. J. 2010. Effect of cholesterol nanodomains on the targeting of lipid-based gene delivery in cultured cells. *Molecular Pharmaceutics,* 7**,** 1311-1317.
XU, L., LI, S., ZHOU, W., KANG, Z., ZHANG, Q., KAMRAN, M., XU, J., LIANG, D., WANG, C. & HOU, Z. 2017. p62/SQSTM1 enhances breast cancer stem-like properties by stabilizing MYC mRNA. *Oncogene,* 36**,** 304-317.
XU, Y., HUI, S. W., FREDERIK, P. & SZOKA, F. C. 1999. Physicochemical characterization and purification of cationic lipoplexes. *Biophysical Journal,* 77**,** 341-353.
XUE, H. Y., LIU, S. & WONG, H. L. 2014. Nanotoxicity: a key obstacle to clinical translation of siRNA-based nanomedicine. *Nanomedicine,* 9**,** 295-312.
YADAV, D., SANDEEP, K., PANDEY, D. & DUTTA, R. K. 2017. Liposomes for drug delivery. *Journal of Biotechnology and Biomaterials,* 7**,** DOI:10.4172/2155-952X276.
YAN, K. S., YAN, S., FAROOQ, A., HAN, A., ZENG, L. & ZHOU, M.-M. 2003. Structure and conserved RNA binding of the PAZ domain. *Nature,* 426**,** 469-474.
YAN, S., ZHOU, C., LOU, X., XIAO, Z., ZHU, H., WANG, Q., WANG, Y., LU, N., HE, S., ZHAN, Q., LIU, S. & XU, N. 2009. PTTG overexpression promotes lymph node metastasis in human esophageal squamous cell carcinoma. *Cancer Research,* 69**,** 3283-3290.
YANG, Q., DU, W. W., WU, N., YANG, W., AWAN, F. M., FANG, L., MA, J., LI, X., ZENG, Y. & YANG, Z. 2017. A circular RNA promotes tumorigenesis by inducing c-myc nuclear translocation. *Cell Death and Differentiation,* 24**,** 1609-1620.
YANG, S. Y., ZHENG, Y., CHEN, J. Y., ZHANG, Q. Y., ZHAO, D., HAN, D. E. & CHEN, X. J. 2013. Comprehensive study of cationic liposomes composed of DC-Chol and cholesterol with different mole ratios for gene transfection. *Colloids and Surfaces B: Biointerfaces,* 101**,** 6-13.
YANG, Y., HU, Y., WANG, Y., LI, J., LIU, F. & HUANG, L. 2012. Nanoparticle Delivery of Pooled siRNA for Effective Treatment of Non-Small Cell Lung Caner. *Molecular Pharmaceutics,* 9**,** 2280-2289.
YANG, Y., LI, J., LIU, F. & HUANG, L. 2011. Systemic delivery of siRNA via LCP nanoparticle efficiently inhibits lung metastasis. *Molecular Therapy,* 20**,** 609-615.
YANG, Y., YANG, Y., XIE, X., WANG, Z., GONG, W., ZHANG, H., LI, Y., YU, F., LI, Z. & MEI, X. 2015. Dual-modified liposomes with a two-photon-sensitive cell penetrating peptide and NGR ligand for siRNA targeting delivery. *Biomaterials,* 48**,** 84-96.
YUAN, Y., CAI, H., YANG, X.-J., LI, W., HE, J., GUO, T.-K. & CHEN, Y.-R. 2014. Liposome-mediated induction of apoptosis of human hepatoma cells by c-myc antisense phosphorothioate

oligodeoxynucleotide and 5-fluorouracil. *Asian Pacific Journal of Cancer Prevention,* 15**,** 5529-5533.
ZAKARIA, M., SARKAR, D. & CHATTOPADHYAY, P. 2017. Induction of Transcriptional Gene Silencing by Expression of shRNA Directed to c-Myc P2 Promoter in Hepatocellular Carcinoma by Tissue-Specific Virosomal Delivery. *Methods in Molecular Biology* 1543**,** 245-257.
ZATSEPIN, T. S., KOTELEVTSEV, Y. V. & KOTELIANSKY, V. 2016. Lipid nanoparticles for targeted siRNA delivery–going from bench to bedside. *International Journal of Nanomedicine,* 11**,** 3077-3086.
ZELLER, K. I., ZHAO, X., LEE, C. W. H., CHIU, K. P., YAO, F., YUSTEIN, J. T., OOI, H. S., ORLOV, Y. L., SHAHAB, A., YONG, H. C., FU, Y., WENG, Z., KUZNETSOV, V. A., SUNG, W.-K., RUAN, Y., DANG, C. V. & WEI, C.-L. 2006. Global mapping of c-Myc binding sites and target gene networks in human B cells. *Proceedings of the National Academy of Sciences USA,* 103**,** 17834-17839.
ZELPHATI, O. & SZOKA, F. C. 1996. Mechanism of oligonucleotide release from cationic liposomes. *Proceedings of the National Academy of Sciences USA,* 93**,** 11493-11498.
ZHAI, D., CUI, C., XIE, L., CAI, L. & YU, J. 2018. Sterol regulatory element-binding protein 1 cooperates with c-Myc to promote epithelial-mesenchymal transition in colorectal cancer. *Oncology Letters,* 15**,** 5959-5965.
ZHANG, C., TANG, N., LIU, X., LIANG, W., XU, W. & TORCHILIN, V. P. 2006. siRNA-containing liposomes modified with polyarginine effectively silence the targeted gene. *Journal of Controlled Release,* 112**,** 229-239.
ZHANG, C., XU, B., LU, S., ZHAO, Y. & LIU, P. 2017a. HN1 contributes to migration, invasion, and tumorigenesis of breast cancer by enhancing MYC activity. *Molecular Cancer,* 16**,** DOI:10.1186/s12943-017-0656-1.
ZHANG, H. 2017. Thin-Film Hydration Followed by Extrusion Method for Liposome Preparation. *Methods in Molecular Biology,* 1522**,** 17-22.
ZHANG, J., CHEN, M., ZHAO, X., ZHANG, M., MAO, J., CAO, X. & ZHANG, Z. 2018. Controlled and localized delivery of c-myc AS-ODN to cells by 3-aminopropyl-trimethoxylsilane modified SBA-15 mesoporous silica. *AIP Advances,* 8**,** DOI:10.1063/1.5012535.
ZHANG, Q., WEST-OSTERFIELD, K., SPEARS, E., LI, Z., PANACCIONE, A. & HANN, S. R. 2017b. MB0 and MBI Are Independent and Distinct Transactivation Domains in MYC that Are Essential for Transformation. *Genes,* 8**,** DOI:10.3390/genes8050134.
ZHANG, X., GE, Y.-L. & TIAN, R.-H. 2009. The knockdown of c-myc expression by RNAi inhibits cell proliferation in human colon cancer HT-29 cells in vitro and in vivo. *Cellular & Molecular Biology Letters,* 14**,** 305-318.
ZHANG, X., ZHAO, X., FISKUS, W., LIN, J., LWIN, T., RAO, R., ZHANG, Y., CHAN, J. C., FU, K. & MARQUEZ, V. E. 2012. Coordinated silencing of MYC-mediated miR-29 by HDAC3 and EZH2 as a therapeutic target of histone modification in aggressive B-Cell lymphomas. *Cancer Cell,* 22**,** 506-523.
ZHANG, Y. & ANCHORDOQUY, T. J. 2004. The role of lipid charge density in the serum stability of cationic lipid/DNA complexes. *Biochimica et Biophysica Acta (BBA)-Biomembranes,* 1663**,** 143-157.
ZHANG, Y., LI, H., SUN, J., GAO, J., LIU, W., LI, B., GUO, Y. & CHEN, J. 2010. DC-Chol/DOPE cationic liposomes: a comparative study of the influence factors on plasmid pDNA and siRNA gene delivery. *International Journal of Pharmaceutics,* 390**,** 198-207.
ZHANG, Y., PENG, L., MUMPER, R. J. & HUANG, L. 2013. Combinational delivery of c-myc siRNA and nucleoside analogs in a single, synthetic nanocarrier for targeted cancer therapy. *Biomaterials,* 34**,** 8459-8468.
ZHAO, W. & SONG ZHUANG, X.-R. Q. 2011. Comparative study of the in vitro and in vivo characteristics of cationic and neutral liposomes. *International Journal of Nanomedicine,* 6**,** 3087-3098.

ZHAO, Y., JIAN, W., GAO, W., ZHENG, Y.-X., WANG, Y.-K., ZHOU, Z.-Q., ZHANG, H. & WANG, C.-J. 2013. RNAi silencing of c-Myc inhibits cell migration, invasion, and proliferation in HepG2 human hepatocellular carcinoma cell line: c-Myc silencing in hepatocellular carcinoma cell. *Cancer Cell International,* 13**,** DOI:10.1186/1475-2867-13-23.

ZHENG, Y., GUO, Y., LI, Y., WU, Y., ZHANG, L. & YANG, Z. 2014. A novel gemini-like cationic lipid for the efficient delivery of siRNA. *New Journal of Chemistry,* 38**,** 4952-4962.

ZHOU, J., LI, H., LI, S., ZAIA, J. & ROSSI, J. J. 2008. Novel dual inhibitory function aptamer–siRNA delivery system for HIV-1 therapy. *Molecular Therapy,* 16**,** 1481-1489.

ZHOU, J., RALSTON, J., SEDEV, R. & BEATTIE, D. A. 2009. Functionalized gold nanoparticles: synthesis, structure and colloid stability. *Journal of Colloid and Interface Science,* 331**,** 251-262.

ZINDY, F., EISCHEN, C. M., RANDLE, D. H., KAMIJO, T., CLEVELAND, J. L., SHERR, C. J. & ROUSSEL, M. F. 1998. Myc signaling via the ARF tumor suppressor regulates p53-dependent apoptosis and immortalization. *Genes & Development,* 12**,** 2424-2433.

ZUCKERMAN, J. E. & DAVIS, M. E. 2015. Clinical experiences with systemically administered siRNA-based therapeutics in cancer. *Nature Reviews Drug Discovery,* 14**,** 843-856.

ZURAWEL, R. H., CHIAPPA, S. A., ALLEN, C. & RAFFEL, C. 1998. Sporadic medulloblastomas contain oncogenic β-catenin mutations. *Cancer Research,* 58**,** 896-899.

http://www.thermofisher.com/us/en/home/brands/product-brand/lipofectamine/lipofectamine-3000.html#sup Accessed as at 01/03/2018.

APPENDIX A
Published abstract

J Pharma Care Health Sys 2016, 3:2(Suppl)
http://dx.doi.org/10.4172/2376-0419.C1.012

conferenceseries.com

4th African Pharma Congress

June 20-21, 2016 Cape Town, South Africa

Novel cholesterol based siRNA lipoplexes with and without PEG-modification: Characterization and *in vitro* cytotoxicity studies

Saffiya Habib, Mario Ariatti and **Moganavelli Singh**
University of KwaZulu-Natal, South Africa

Cationic liposomes have potential in carrying small interfering RNA (siRNA) molecules as gene medicines. However, unfavorable liposome-serum interactions often limit their efficacy. In order to address this concern, liposome-stabilizing agents, cholesterol (Chol) and polyethylene glycol (PEG) were incorporated in the design of new liposome-siRNA systems. The helper lipid, Chol, was combined in equimolar quantities with the cytofectin, N,N-dimethylaminopropylamidosuccinyl holesterylformylhydrazide (MS09), to give unilamellar vesicles. For PEG-modification, distearoylphosphatidylethanolamine poly(ethylene glycol) 2000 was added at 2 mol %. Electrostatic association of liposomes with siRNA was followed in band shift and fluorescence quenching assays. Liposome-siRNA complexes (lipoplexes) were observed as globular aggregates by cryo-transmission electron microscopy. Characterization of lipoplexes by Zeta-potential Nanoparticle Tracking Analysis (Z-NTA) showed that lipoplex size and zeta potential were dependent on both liposome composition and the MS09: siRNA (w/w) mixing ratio. siRNA within lipoplexes resisted serum-induced damage at MS09:siRNA (w/w) ratios of 12:1-32:1. The effects of lipoplexes on cell growth were evaluated with a non-targeting siRNA sequence in transformed and non-transformed human cell lines. MTT and alamarBlue® assays showed that MCF-7 and HEK293 cells retained at least 78% viability at final siRNA and lipid concentrations of 57 nM and 29-60 µM, respectively. In general, cell survival profiles of MS09/Chol and MS09/Chol/PEG liposomes compared favorably with that of Lipofectamine™ 3000 and control formulations which contained the conventional helper lipid, dioleoylphosphatidylethanolamine (DOPE). At present, the siRNA delivery capability of liposomes is under assessment and the most promising formulations will be applied to the delivery of oncogene-specific siRNA in gene silencing experiments.

saffiya.habib@gmail.com

Structural and functional study of a novel cathelicidin antimicrobial peptide BuMAP-28 and its analogue (BuMAP-28)18

Varuna P Panicker and **Sisilamma George**
Kerala Veterinary and Animal Sciences University, India

Cathelicidin antimicrobial peptides BuMAP-28 and (BuMAP-28)18 were synthesized and used for the present study. Amino acid sequences of the antimicrobial domain were deduced from the gene sequence of myeloid antimicrobial peptide of buffalo. Peptides are highly cationic, amphipathic showed a net charge of +11 for both BuMAP-28 and its analogue; a predicted hydrophobic ratio of 39% for BuMAP-28 and 33% for (BuMAP-28)18. Ramachandran plot analysis indicating a high structural stability for the peptides. *In silico* structural analysis of the peptides revealed a helix-turn helix which is later confirmed by CD analysis. Biological activity testing of the peptides revealed that the peptide has got a broad spectrum antimicrobial and anti-cancerous activity. Peptides showed wide spectrum of activity against Gram-positive, Gram-negative bacteria, fungi, spirochetes and virus. Peptides are active against even methicillin resistant *S. aureus* with lower MIC values. *In vitro* antibacterial and antifungal activities were later confirmed by morphological testing and SEM. Peptides are also proved to be effective against HeLa cell lines. Cytotoxic studies revealed that the truncation of BuMAP-28 could reduce the hemolytic activity when compared to the parent peptide. Murine models injected with Duck *Pasteurella* (DP1), when treated with the peptides protected 100% of the animals at 12.5 µM doses. Studies revealed that the truncation of the peptide could reduce the hemolytic activity without a considerable change in antimicrobial activity.

drpanickerpvarunavet@gmail.com

APPENDIX B

Supplementary Z-NTA data

1. Number of lipid molecules that constitute liposomal vesicles

Table B1: Estimated number of lipid molecules per liposomal vesicle

Formulation	**Average number of lipid molecules[a] (× 10^5/vesicle)**				
	Total lipid	**MS09**	**DOPE**	**Chol**	**DSPE-PEG_{2000}**
MS09/DOPE	8.56	4.28	4.28	-	-
MS09/Chol (1:1)	11.60	5.80	-	5.80	-
MS09/DOPE/PEG	11.00	5.39	5.39	-	0.22
MS09/Chol/PEG (1:1)	8.75	4.29	-	4.29	0.22

Note:
[a]Estimates were made based on the lipid concentration of liposome stock suspensions and NTA-derived concentration of liposomal vesicles

2. Summarised data

Table B2: Size and size distribution of liposomes and lipoplexes by NTA

Liposome formulation	MS09:siRNA ($^{w}/_{w}$)	Size (nm)					
		Mean[a]	**Mode[a]**	**SD[a,b]**	**D10[a,c]**	**D50[a,c]**	**D90[a,c]**
MS09/DOPE Batch 1	-[d]	164.2 ± 4.7	133.5 ± 15.2	81.1 ± 17.2	95.8 ± 5.5	134.9 ± 5.7	259.3 ± 15.8
	12:1	125.6 ± 12.2	98.4 ± 11.6	43.6 ± 18.8	78.4 ± 5.2	98.1 ± 7.1	163.8 ± 35.1
	16:1	127.6 ± 24.4	92.4 ± 24.5	68.5 ± 25.3	61.9 ± 24.7	103.8 ± 15.7	218.8 ± 63.7
	20:1	156.9 ± 10.6	128.0 ± 17.1	57.6 ± 3.3	101.0 ± 7.1	135.6 ± 9.7	224.5 ± 15.7
	24:1	203.1 ± 11.1	166.9 ± 21.8	72.9 ± 14.6	115.6 ± 13.2	183.1 ± 3.2	290.2 ± 28.0
	28:1	202.4 ± 20.9	195.7 ± 21.0	69.6 ± 15.0	112.9 ± 16.4	191.7 ± 21.2	288.0 ± 38.7
	32:1	222.8 ± 1.5	184.3 ± 28.5	81.0 ± 11.8	136.0 ± 6.1	197.2 ± 4.7	322.5 ± 6.7
MS09/Chol (1:1) Batch 1	-[d]	167.6 ± 3.3	137.5 ± 10.8	69.2 ± 7.7	104.2 ± 3.4	143.6 ±2.2	246.2 ± 6.3
	12:1	130.6 ± 10.0	117.5 ± 12.6	42.0 ± 12.3	79.6 ± 3.6	119.5 ± 7.6	181.8 ± 23.2
	16:1	228.8 ± 11.2	126.8 ± 7.3	147.7 ± 20.3	87.4 ± 29.0	165.7 ± 1.3	322.2 ± 185.4
	20:1	184.4 ± 12.6	140.0 ± 14.2	89.0 ± 15.6	91.0 ± 10.9	146.6 ± 14.0	290.8 ± 27.5
	24:1	145.1 ± 64.5	93.3 ± 2.2	105.4 ± 100.3	62.9 ± 1.2	93.6 ± 12.2	316.9 ± 258.6
	28:1	160.5 ± 9.5	133.1 ± 6.4	71.6 ± 1.9	91.7 ± 3.7	136.6 ± 12.2	252.9 ± 21.8
	32:1	164.9 ± 3.3	142.0 ± 0.8	65.7 ± 4.0	94.4 ± 0.1	141.5 ± 4.1	269.6 ± 13.2
MS09/DOPE/PEG Batch 1	-[d]	149.7 ± 14.7	125.3 ± 4.3	56.5 ± 6.7	95.1 ± 10.1	128.7 ± 16.5	225.6 ± 14.5
	12:1	158.0 ± 10.1	125.3 ± 4.3	51.6 ± 10.2	104.3 ± 5.6	140.0 ± 7.9	215.1 ± 13.5
	16:1	161.2 ± 3.2	133.6 ± 14.3	55.9 ± 7.1	101.0 ± 2.7	139.6 ± 2.6	213.2 ± 7.6
	20:1	166.7 ± 4.1	131.5 ± 4.0	57.2 ± 3.6	104.6 ± 0.2	147.4 ± 4.1	239.9 ± 23.0
	24:1	153.9 ± 2.4	145.3 ± 8.8	54.4 ± 3.5	102.8 ± 1.2	135.0 ± 0.4	211.3 ± 16.9
	28:1	156.9 ± 4.7	127.1 ± 5.0	48.8 ± 3.3	101.9 ± 2.3	140.5 ± 5.8	220.9 ± 7.1
	32:1	155.2 ± 6.4	136.1 ± 14.2	52.7 ± 4.5	97.8 ± 0.3	136.4 ± 2.1	219.2 ± 20.4
MS09/Chol/PEG (1:1) Batch 1	-[d]	174.7 ± 17.8	125.1 ± 5.4	87.0 ± 16.7	95.2 ± 6.3	137.1 ± 7.3	304.9 ± 34.8
	12:1	163.6 ± 12.9	138.6 ± 6.1	61.1 ± 13.4	100.1 ± 13.4	138.1 ± 10.1	251.2 ± 28.3
	16:1	169.2 ± 22.4	115.5 ± 17.6	101.5 ± 40.3	84.0 ± 4.6	131.1 ± 2.8	266.3 ± 54.2
	20:1	187.5 ± 11.6	155.0 ± 14.6	84.9 ± 21.9	101.2 ± 15.4	160.8 ± 7.9	280.7 ± 44.3

Table B2 continued on next page

Table B2 continued

Liposome formulation	MS09:siRNA ($^{w}/_{w}$)	Size (nm)					
		Mean[a]	Mode[a]	SD[a,b]	D10[a,c]	D50[a,c]	D90[a,c]
MS09/Chol/PEG (1:1) Batch 1	24:1	152.3 ± 12.4	122.7 ± 3.7	58.0 ± 19.8	94.4 ± 4.6	128.0 ± 9.1	234.8 ± 59.5
	28:1	166.0 ± 0.9	124.0 ± 24.3	59.2 ± 6.2	102.8 ± 11.3	143.9 ± 1.3	244.4 ± 26.3
	32:1	175.4 ± 7.6	153.9 ± 35.2	65.6 ± 1.2	107.0 ± 4.5	154.6 ± 15.3	280.1 ± 28.6
MS09/Chol (1:2)	-[d]	386.3 ± 10.9	356.5 ± 17.6	90.2 ± 0.2	202.2 ± 3.7	343.6 ± 9.3	502.7 ± 48.2
MS09/Chol (1:3)	-[d]	337.1 ± 4.4	309.0 ± 12.7	81.3 ± 20.1	174.4 ± 1.4	314.7 ± 4.0	389.6 ± 21.3
MS09/Chol/PEG (1:2)	-[d]	423.9 ± 3.7	358.0 ± 12.0	94.0 ± 0.1	127.3 ± 4.6	377.9 ± 6.4	351.1 ± 19.4
MS09/Chol/PEG (1:3)	-[d]	418.5 ± 9.9	357.5 ± 57.3	76.7 ± 18.8	149.3 ± 18.9	360.8 ± 59.1	457.4 ± 78.7
MS09/DOPE Batch 2 t = 0 months	-[d]	169.0 ± 1.0	135.6 ± 6.8	83.8 ± 2.1	97.5 ± 1.8	132.6 ± 1.1	268.6 ± 1.5
MS09/DOPE Batch 3	-[d]	169.5 ± 0.7	132.2 ± 15.0	85.7 ± 2.5	97.7 ± 0.9	132.3 ± 4.5	267.0 ± 1.4
MS09/Chol (1:1) Batch 2 t = 0 months	-[d]	165.1 ± 2.1	139.6 ± 10.6	71.4 ± 9.4	105.7 ± 0.8	141.9 ± 1.5	266.4 ± 13.5
MS09/Chol (1:1) Batch 3	-[d]	171.6 ± 3.3	134.8 ± 10.7	71.8 ± 3.7	105.2 ± 4.7	146.9 ± 1.2	269.5 ± 2.4
MS09/DOPE/PEG Batch 2 t = 0 months	-[d]	144.4 ± 4.9	129.1 ± 5.8	50.0 ± 4.4	84.1 ± 1.9	126.2 ± 5.4	241.5 ± 10.2
MS09/DOPE/PEG Batch 3	-[d]	142.8 ± 9.0	128.9 ± 8.5	60.3 ± 6.3	86.8 ± 4.1	133.2 ± 5.0	227.3 ± 5.4
MS09/Chol/PEG (1:1), Batch 2 t = 0 months	-[d]	167.6 ± 1.2	127.4 ± 4.1	70.4 ± 1.1	106.3 ± 0.9	146.4 ± 4.8	251.5 ± 5.6
MS09/Chol/PEG (1:1), Batch 3	-[d]	170.3 ± 2.0	128.7 ± 5.6	89.6 ± 1.8	93.2 ± 0.9	139.0 ± 1.5	303.5 ± 6.5

Table B2 continued on next page

Table B2 continued

Liposome formulation	MS09:siRNA ($^{w}/_{w}$)	Size (nm)					
		Mean[a]	Mode[a]	SD[a,b]	D10[a,c]	D50[a,c]	D90[a,c]
MS09/DOPE Batch 2 t = 5 months	-[d]	153.8 ± 5.5	141.7 ± 5.9	68.3 ± 8.8	89.2 ± 5.1	145.2 ± 13.0	229.9 ± 10.5
MS09/DOPE Batch 2 t = 10 months	-[d]	167.1 ± 6.4	162.7 ± 3.1	69.3 ± 8.4	92.2 ± 8.1	154.9 ± 5.1	251.2 ± 16.8
MS09/Chol (1:1) Batch 2 t = 5 months	-[d]	159.8 ± 8.7	135.4 ± 4.5	64.5 ± 5.0	95.4 ± 4.4	133.2 ± 3.5	244.1 ± 6.9
MS09/Chol (1:1) Batch 2 t = 10 months	-[d]	159.2 ± 8.4	141.1 ± 5.5	80.7 ± 6.0	93.9 ± 1.6	141.1 ± 8.0	267.2 ± 10.6
MS09/DOPE/PEG Batch 2 t = 5 months	-[d]	148.4 ± 5.8	132.0 ± 2.3	43.3 ± 2.2	86.7 ± 3.9	137.4 ± 2.2	237.3 ± 5.4
MS09/DOPE/PEG Batch 2 t = 10 months	-[d]	144.9 ± 4.3	136.1 ± 7.8	48.9 ± 3.0	95.6 ± 2.3	134.0 ± 2.4	244.9 ± 5.0
MS09/Chol/PEG (1:1), Batch 2 t = 5 months	-[d]	156.9 ± 5.0	128.6 ± 2.5	76.9 ± 2.7	93.3 ± 2.6	132.4 ± 1.5	278.6 ± 0.8
MS09/Chol/PEG (1:1), Batch 2 t = 10 months	-[d]	146.8 ± 8.2	128.6 ± 2.0	77.6 ± 4.9	91.1 ± 1.4	142.6 ± 10.4	278.9 ± 3.0

Notes:
[a]Each value represents the mean ± S.D (n = 3)
[b]The SD value is a measure of the width of the size distribution profile
[c]The D10, D50 and D90 values indicate the percent under-size
[d]The associated values are those of liposomes alone

Table B3: Zeta potential and zeta potential distribution of liposomes and lipoplexes by Z-NTA

Liposome formulation	MS09:siRNA ($^{w}/_{w}$)	ζ potential (mV)					
		Mean[a]	Mode[a]	SD[a,b]	D10[a,c]	D50[a,c]	D90[a,c]
MS09/DOPE Batch 1	-[d]	-26.1 ± 5.4	-27.9 ± 5.4	24.2 ± 1.8	-52.8 ± 5.0	-27.2 ± 5.3	0.0 ± 6.9
	12:1	-30.0 ± 0.4	-28.9 ± 1.0	26.0 ± 0.8	-58.6 ± 0.9	-30.7 ± 0.7	-2.3 ± 0.9
	16:1	-34.1 ± 3.9	-33.6 ± 4.5	28.4 ± 9.4	-62.7 ± 1.3	-35.1 ± 4.4	-5.9 ± 4.4
	20:1	-16.4 ± 4.7	-15.1 ± 3.9	20.9 ± 1.3	-39.8 ± 3.3	-16.6 ± 4.7	-4.4 ± 7.4
	24:1	-21.0 ± 2.5	-18.8 ± 2.7	17.4 ± 0.6	-41.4 ± 3.6	-20.8 ± 2.4	-3.1 ± 2.2
	28:1	-19.8 ± 1.2	-17.2 ± 0.7	16.5 ± 2.3	-38.9 ± 2.0	-19.6 ± 1.2	-3.0 ± 4.1
	32:1	-18.1 ± 0.7	-16.6 ± 1.1	16.1 ± 0.8	-35.9 ± 1.3	-17.9 ± 0.6	-2.5 ± 1.5
MS09/Chol (1:1) Batch 1	-[d]	-27.7 ± 1.6	-30.3 ± 3.8	25.8 ± 1.2	-56.5 ± 2.7	-28.4 ± 1.5	0.2 ± 1.6
	12:1	-30.0 ± 0.8	-33.9 ± 1.6	25.8 ± 2.6	-58.0 ± 2.1	-30.5 ± 0.8	-2.7 ± 3.7
	16:1	-40.4 ± 3.6	-43.9 ± 5.4	24.6 ± 5.1	-64.7 ± 2.4	-42.9 ± 3.2	-13.8 ± 9.4
	20:1	-32.2 ± 0.8	-32.3 ± 1.5	22.1 ± 0.7	-55.2 ± 1.3	-32.9 ± 1.2	-9.4 ± 0.4
	24:1	-32.1 ± 1.7	-35.2 ± 0.8	29.6 ± 2.8	-64.7 ± 3.7	-33.6 ± 1.1	-5.6 ± 1.8
	28:1	-27.7 ± 0.7	-27.7 ± 2.7	21.5 ± 0.3	-50.5 ± 0.6	-28.2 ± 1.2	-5.5 ± 0
	32:1	-29.8 ± 0.1	-27.1 ± 1.4	24.0 ± 0.5	-56.4 ± 0.4	-30.0 ± 0.6	-4.9 ± 0.8
MS09/DOPE/PEG Batch 1	-[d]	-28.5 ± 4.1	-27.5 ± 2.9	24.4 ± 1.1	-56.1 ± 5.9	-28.9 ± 3.7	-2.4 ± 3.6
	12:1	-32.9 ± 6.3	-32.3 ± 6.5	22.3 ± 0.3	-57.3 ± 7.1	-33.3 ± 6.2	-9.3 ± 5.8
	16:1	-36.7 ± 3.0	-35.8 ± 2.8	22.5 ± 0.5	-62.1 ± 3.4	-37.1 ± 3.0	-12.7 ± 2.3
	20:1	-34.3 ± 0.7	-32.9 ± 1.0	20.5 ± 0.5	-57.0 ± 1.0	-34.6 ± 0.6	-13.0 ± 1.0
	24:1	-17.8 ± 0.6	-17.1 ± 0.9	23.5 ± 0.2	-44.5 ± 0.8	-18.3 ± 0.6	7.6 ± 0.3
	28:1	-25.5 ± 2.9	-24.0 ± 3.1	20.8 ± 0.5	-48.5 ± 2.2	-25.9 ± 0.3	-3.8 ± 3.1
	32:1	-30.6 ± 2.1	-30.9 ± 2.1	20.6 ± 0.2	-53.4 ± 1.3	-31.2 ± 2.0	-8.9 ± 2.8
MS09/Chol/PEG (1:1) Batch 1	-[d]	-36.6 ± 1.0	-36.2 ± 4.9	25.0 ± 0.3	-64.5 ± 0.2	-37.4 ± 2.0	-9.0 ± 0.8
	12:1	-23.2 ± 0.3	-21.2 ± 0.7	21.9 ± 1.9	-47.3 ± 4.1	-23.0 ± 0.3	-0.5 ± 2.4
	16:1	-22.1 ± 1.8	-22.6 ± 2.1	25.2 ± 1.4	-50.5 ± 3.9	-22.5 ± 1.7	5.1 ± 1.7
	20:1	-18.8 ± 0.5	-18.0 ± 2.0	21.7 ± 1.7	-42.7 ± 1.6	-19.0 ± 0.9	3.6 ± 1.0
	24:1	-20.1 ± 0.1	-19.9 ± 1.6	21.7 ± 0.4	-43.6 ± 1.3	-20.6 ± 0.2	2.8 ± 0.6
	28:1	-17.2 ± 0.8	-16.0 ± 2.3	21.7 ± 1.3	-41.5 ± 2.3	-17.6 ± 1.0	5.4 ± 1.1
	32:1	-16.0 ± 0.2	-15.6 ± 0.3	21.5 ± 1.5	-39.9 ± 1.9	-16.5 ± 0.3	7.5 ± 1.6

Table B3 continued on next page

Table B3 continued

Liposome formulation	MS09:siRNA ($^{w}/_{w}$)	ζ potential (mV)					
		Mean[a]	Mode[a]	SD[a,b]	D10[a,c]	D50[a,c]	D90[a,c]
MS09/Chol (1:2)	-[d]	-14.4 ± 3.8	-13.7 ± 2.1	22.4 ± 1.8	-39.6 ± 1.6	-15.0 ± 4.0	3.5 ± 5.2
MS09/Chol (1:3)	-[d]	-13.0 ± 6.4	-11.9 ± 6.0	26.8 ± 2.3	-48.6 ± 6.4	-14.2 ± 6.4	5.6 ± 2.8
MS09/Chol/PEG (1:2)	-[d]	-8.9 ± 2.5	-9.2 ± 1.8	18.7 ± 0.8	-30.8 ± 1.8	-9.9 ± 2.5	10.5 ± 3.3
MS09/Chol/PEG (1:3)	-[d]	-6.3 ± 2.6	-6.6 ± 2.4	15.5 ± 5.9	-24.8 ± 10.1	-7.1 ± 2.7	10.1 ± 3.5
MS09/DOPE Batch 2 t = 0 months	-[d]	-32.7 ± 3.4	-30.2 ± 9.9	24.1 ± 2.1	-52.0 ± 1.2	-29.9 ± 1.2	-0.8 ± 1.5
MS09/DOPE Batch 3	-[d]	-29.5 ± 3.1	-27.5 ± 7.2	25.9 ± 0.2	-50.6 ± 1.4	-26.6 ± 0.5	-0.8 ± 1.2
MS09/Chol (1:1) Batch 2 t = 0 months	-[d]	-28.1 ± 0.2	-26.9 ± 4.9	25.5 ± 0.5	-57.3 ± 0.7	-30.7 ± 1.1	1.1 ± 1.7
MS09/Chol (1:1) Batch 3	-[d]	-27.0 ± 1.1	-28.5 ± 11.9	27.5 ± 1.5	-57.6 ± 1.5	-30.6 ± 1.7	0.6 ± 2.1
MS09/DOPE/PEG Batch 2 t = 0 months	-[d]	-31.1 ± 1.8	-27.2 ± 4.4	25.0 ± 1.6	-62.0 ± 1.6	-31.5 ± 0.6	-6.1 ± 1.7
MS09/DOPE/PEG Batch 3	-[d]	-28.6 ± 1.1	-26.6 ± 3.5	25.0 ± 0.9	-59.0 ± 1.2	-30.4 ± 2.0	-3.8 ± 2.1
MS09/Chol/PEG (1:1), Batch 2 t = 0 months	-[d]	-36.8 ± 0.8	-37.5 ± 8.8	25.5 ± 0.6	-64.9 ± 0.1	-37.2 ± 0.6	-5.4 ± 1.1
MS09/Chol/PEG (1:1), Batch 3	-[d]	-30.6 ± 1.1	-37.2 ± 4.4	27.0 ± 0.2	-60.7 ± 0.5	-30.1 ± 1.2	-3.5 ± 1.2
MS09/DOPE t = 5 months	-[d]	-31.3 ± 1.1	-32.5 ± 1.3	25.4 ± 1.8	-56.4 ± 1.0	-30.9 ± 1.7	-2.9 ± 1.8
MS09/DOPE t = 10 months	-[d]	-18.5 ± 3.2	-17.2 ± 0.9	23.3 ± 2.6	-54.0 ± 4.1	-20.0 ± 4.8	-30.0 ± 2.1

Table B3 continued on next page

Table B3 continued

Liposome formulation	MS09:siRNA ($^{w}/_{w}$)	ζ potential (mV)					
		Mean[a]	**Mode[a]**	**SD[a,b]**	**D10[a,c]**	**D50[a,c]**	**D90[a,c]**
MS09/Chol (1:1) Batch 2 t = 5 months	-[d]	-26.9 ± 2.4	-27.6 ± 1.1	25.5 ± 0.8	-56.4 ± 1.0	-27.7 ± 1.4	-0.8 ± 2.3
MS09/Chol (1:1) Batch 2 t = 10 months	-[d]	-28.8 ± 1.6	-26.5 ± 1.2	22.3 ± 1.2	-54.7 ± 5.7	-24.3 ± 0.5	-2.4 ± 1.4
MS09/DOPE/PEG Batch 2 t = 5 months	-[d]	-30.2 ± 1.6	-27.4 ± 3.0	25.8 ± 2.0	-62.2 ± 3.4	-29.3 ± 1.5	-6.0 ± 2.7
MS09/DOPE/PEG Batch 2 t = 10 months	-[d]	-36.8 ± 1.2	-30.4 ± 4.0	19.1 ± 3.2	-48.3 ± 2.1	-36.5 ± 1.6	-5.3 ± 1.1
MS09/Chol/PEG (1:1), Batch 2 t = 5 months	-[d]	-38.9 ± 2.5	-38.5 ± 3.1	23.3 ± 0.9	-64.2 ± 2.3	-38.5 ± 1.9	-0.9 ± 4.7
MS09/Chol/PEG (1:1), Batch 2 t = 10 months	-[d]	-38.9 ± 4.3	-38.3 ± 7.5	25.5 ± 0.7	-70.7 ± 2.0	-55.1 ± 2.6	-8.5 ± 1.2

Notes:
[a]Each value represents the mean ± S.D (n = 3)
[b]The SD value is a measure of the width of the zeta potential distribution profile
[c]The D10, D50 and D90 values indicate the percent of particles under the given zeta potential value
[d]The associated values are those of liposomes alone

3. Additional NTA concentration-derived estimates

Table B4: Estimated number of liposomal vesicles and siRNA molecules per liposome-siRNA nanocomplex

Liposome formulation	MS09:siRNA ($^{w}/_{w}$)	Average number of vesicles/nanocomplex	Average number of siRNA molecules/nanocomplex
MS09/DOPE	12:1[a]	3	n/a
	16:1	3	4500
	20:1	2	1800
	24:1	2	2100
	28:1	3	2400
	32:1	5	4000
MS09/Chol (1:1)	12:1[a]	3	n/a
	16:1	3	3900
	20:1	3	4500
	24:1	3	4000
	28:1	3	2000
	32:1	2	1700
MS09/DOPE/PEG	12:1[a]	3	n/a
	16:1	3	3100
	20:1	3	2400
	24:1	3	1900
	28:1	2	1700
	32:1	2	1700
MS09/Chol/PEG (1:1)	12:1[a,b]	1	n/a
	16:1[b]	1	1700
	20:1	3	3100
	24:1	3	3000
	28:1[b]	1	1000
	32:1	2	1500

Notes:
[a]Complete dye displacement was not achieved at these MS09:siRNA ($^{w}/_{w}$) ratios
[b]siRNA was likely to have been surface-associated in these samples

4. Flow Profiles

4.1 Liposome suspensions

A) MS09/DOPE

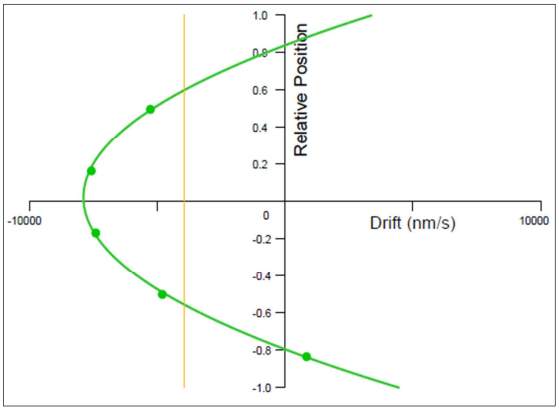

B) MS09/Chol (1:1)

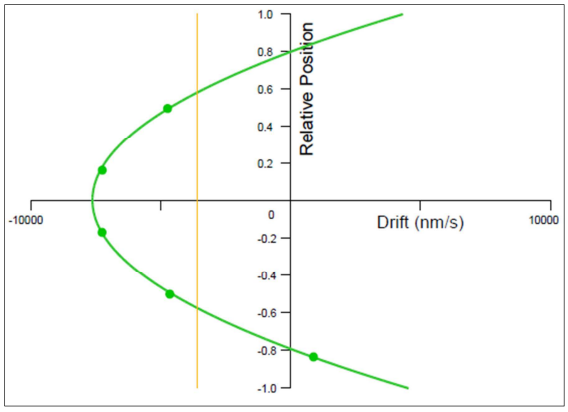

C) MS09/DOPE/PEG

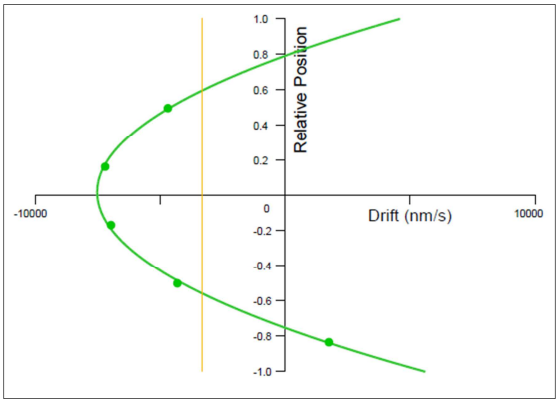

D) MS09/Chol/PEG (1:1)

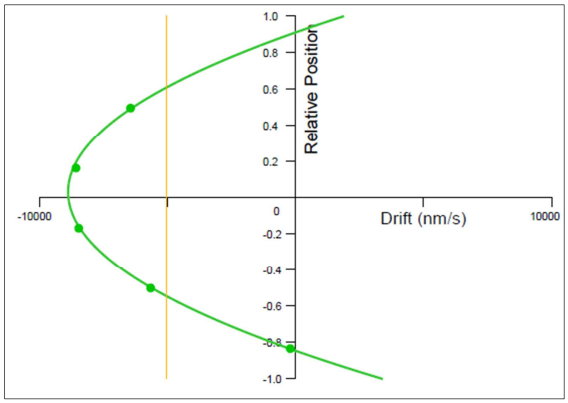

4.2 Lipoplexes

MS09/DOPE LIPOPLEXES

A) MS09:siRNA ($^{w}/_{w}$) = 12:1

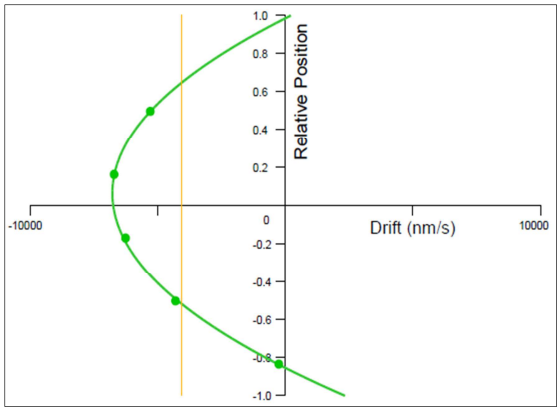

B) MS09:siRNA ($^{w}/_{w}$) = 16:1

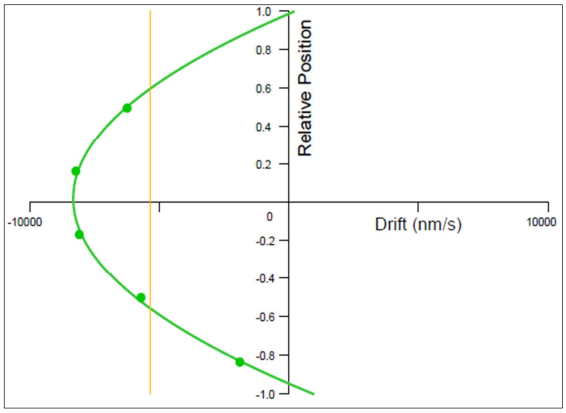

C) MS09:siRNA ($^{w}/_{w}$) = 20:1

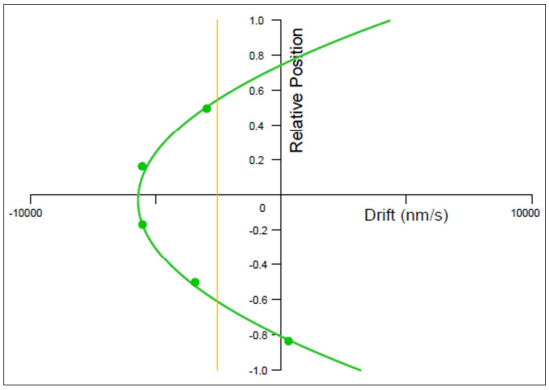

D) MS09:siRNA ($^{w}/_{w}$) = 24:1

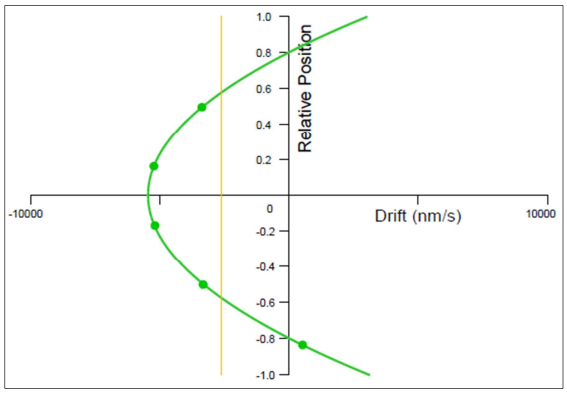

E) MS09:siRNA ($^{w}/_{w}$) = 28:1

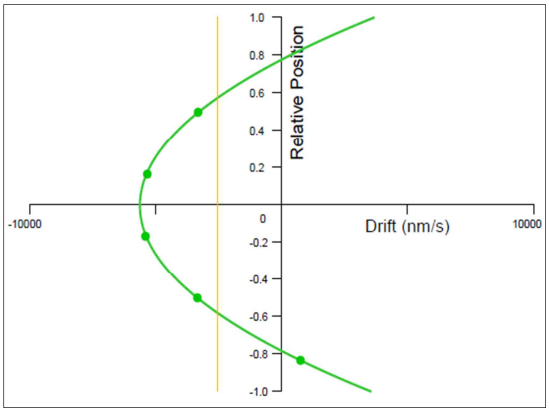

F) MS09:siRNA ($^{w}/_{w}$) = 32:1

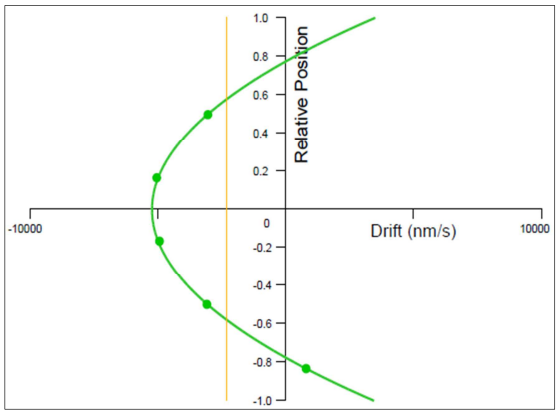

MS09/Chol (1:1) LIPOPLEXES

G) MS09:siRNA ($^{w}/_{w}$) = 12:1

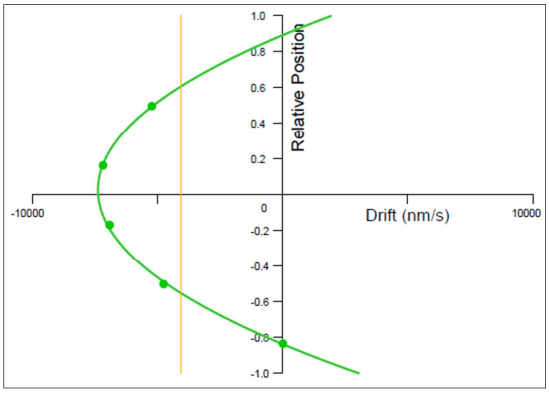

H) MS09:siRNA ($^{w}/_{w}$) = 16:1

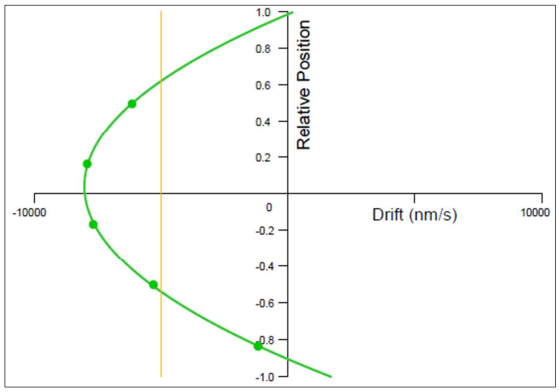

I) MS09:siRNA ($^{w}/_{w}$) = 20:1

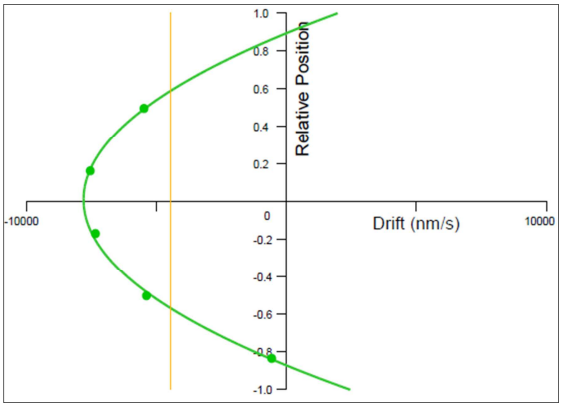

J) MS09:siRNA ($^{w}/_{w}$) = 24:1

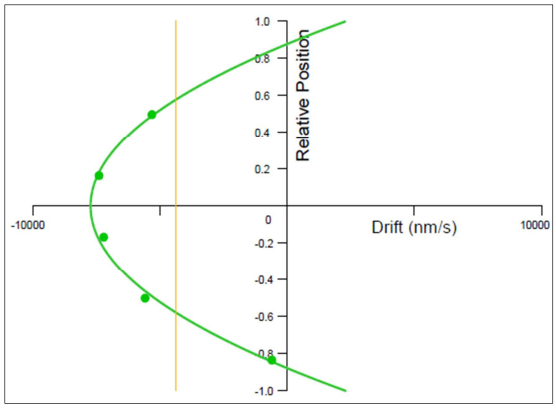

K) MS09:siRNA ($^{w}/_{w}$) = 28:1

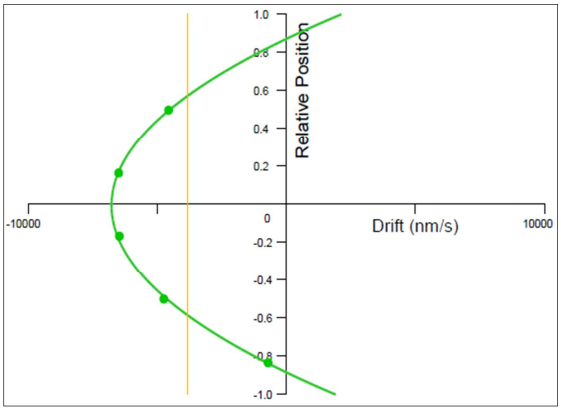

L) MS09:siRNA ($^{w}/_{w}$) = 32:1

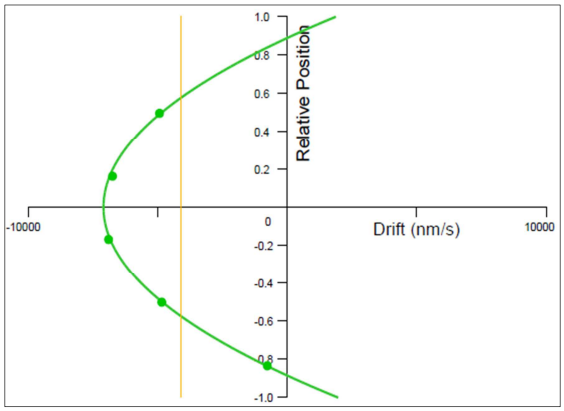

MS09/DOPE/PEG LIPOPLEXES

M) MS09:siRNA ($^{w}/_{w}$) = 12:1

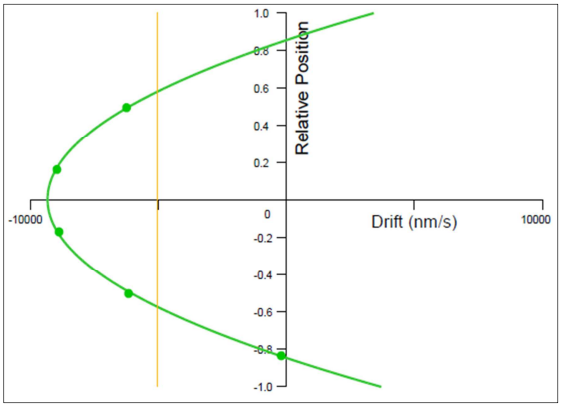

N) MS09:siRNA ($^{w}/_{w}$) = 16:1

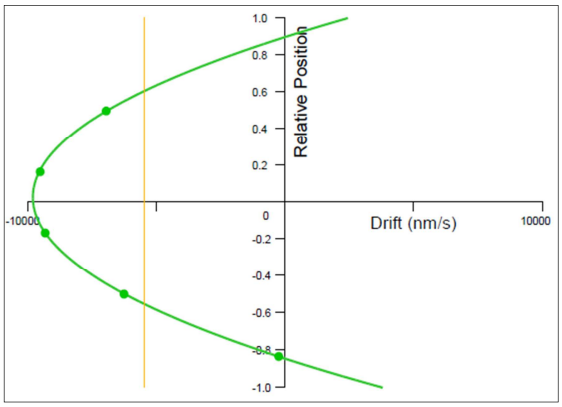

O) MS09:siRNA ($^{w}/_{w}$) = 20:1

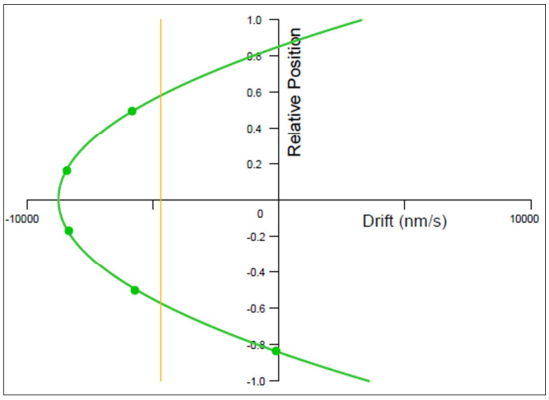

P) MS09:siRNA ($^{w}/_{w}$) = 24:1

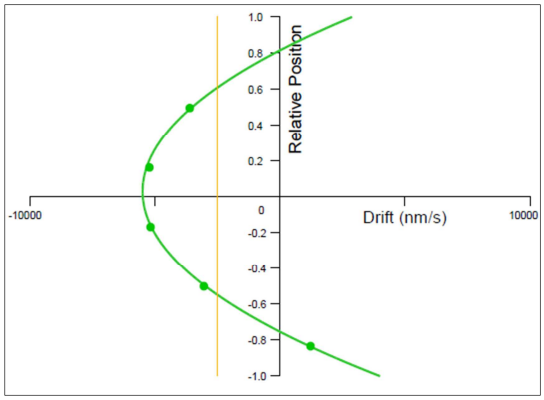

Q) MS09:siRNA ($^{w}/_{w}$) = 28:1

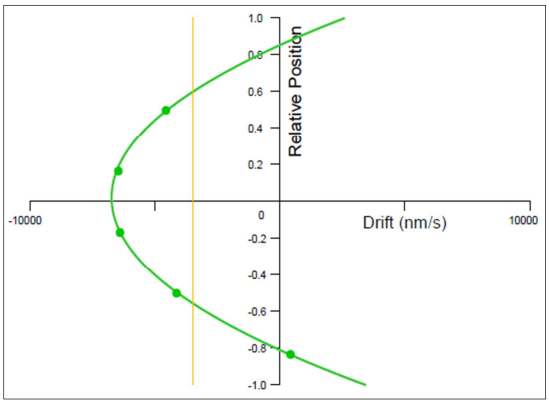

R) MS09:siRNA ($^{w}/_{w}$) = 32:1

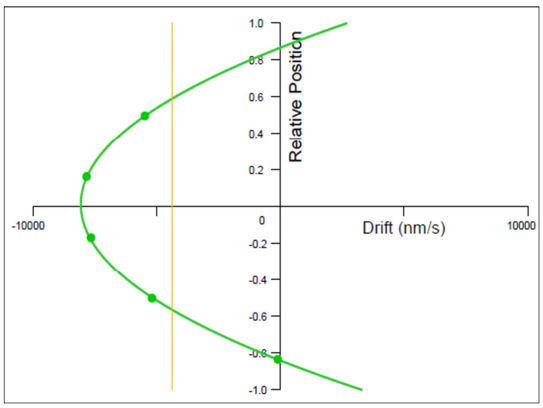

MS09/Chol/PEG (1:1) LIPOPLEXES

S) MS09:siRNA ($^{w}/_{w}$) = 12:1

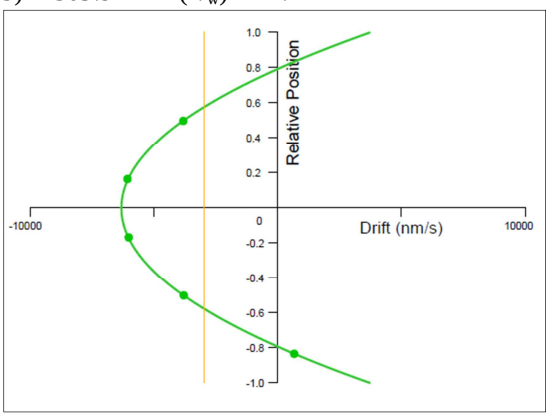

T) MS09:siRNA ($^{w}/_{w}$) = 16:1

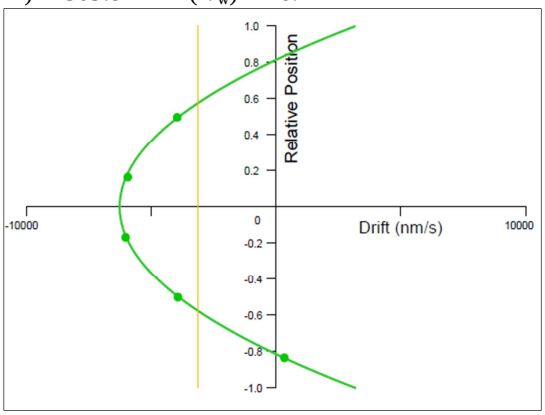

U) MS09:siRNA ($^{w}/_{w}$) = 20:1

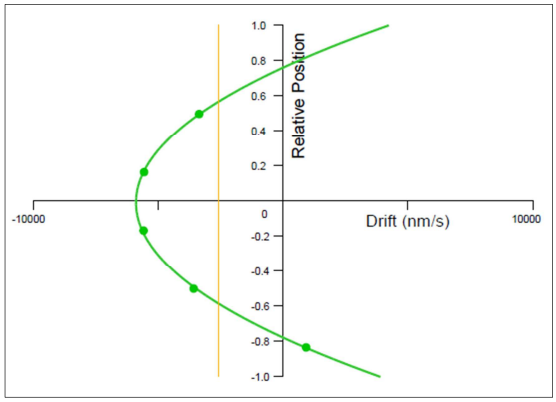

V) MS09:siRNA ($^{w}/_{w}$) = 24:1

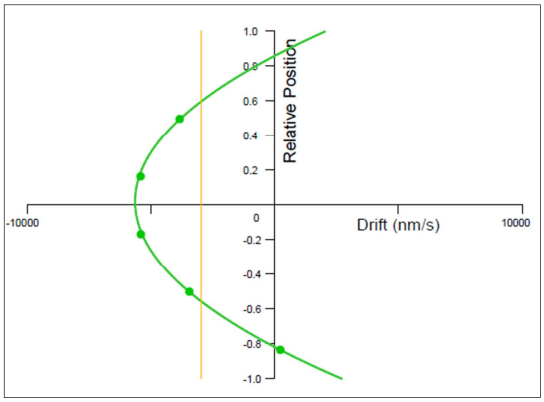

W) MS09:siRNA ($^{w}/_{w}$) = 28:1

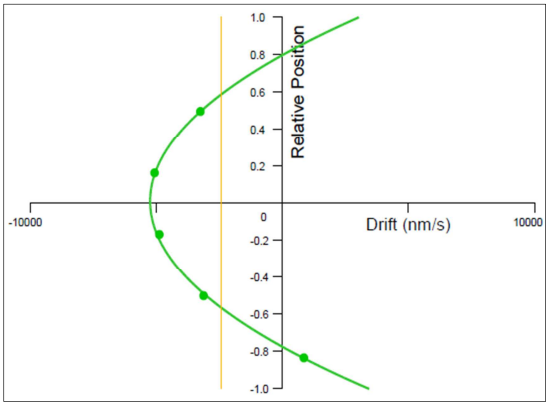

X) MS09:siRNA ($^{w}/_{w}$) = 32:1

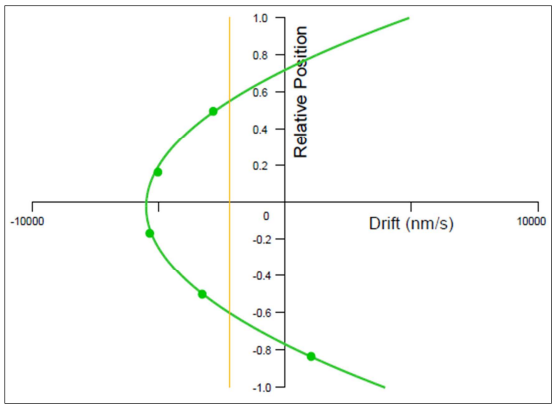

Note the following:

1. One representative flow profile per sample is shown.

5. Zeta potential and size *vs*. concentration graphs

5.1 Liposome suspensions

A) MS09/DOPE

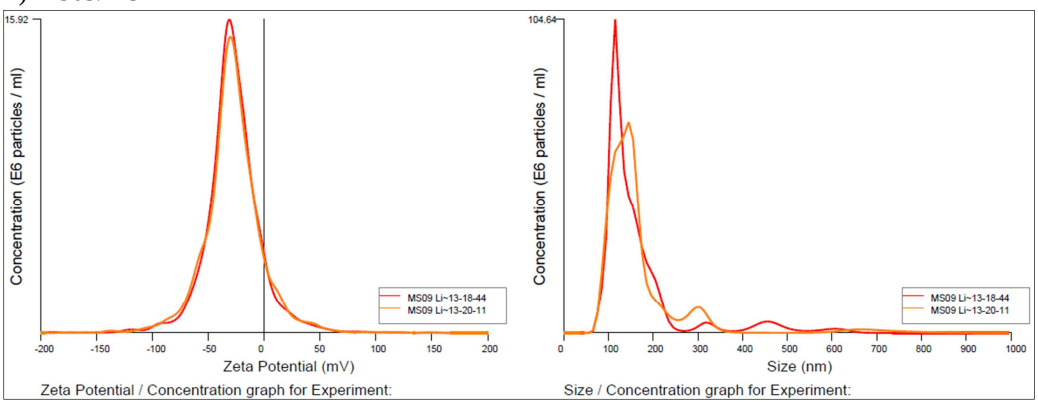

B) MS09/Chol (1:1)

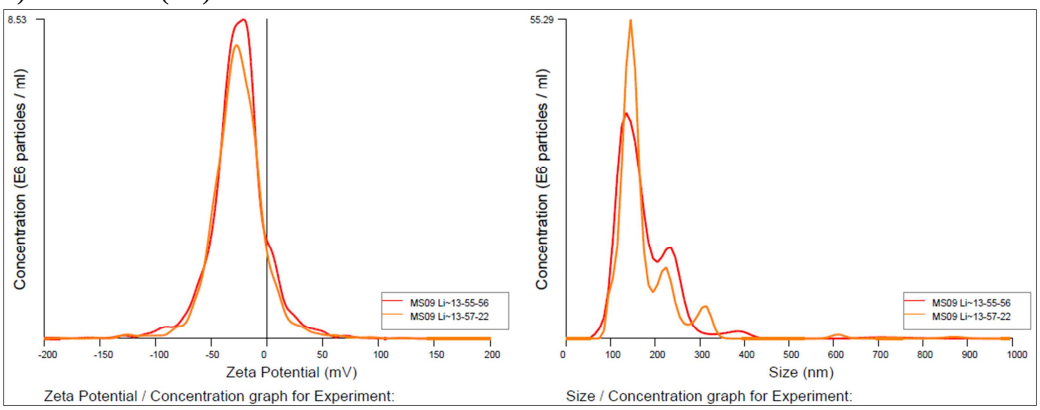

C) MS09/DOPE/PEG

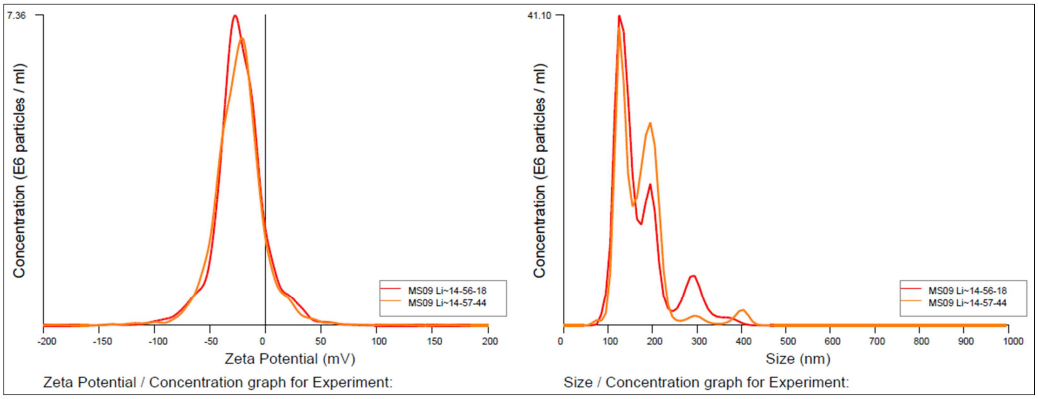

D) MS09/Chol/PEG (1:1)

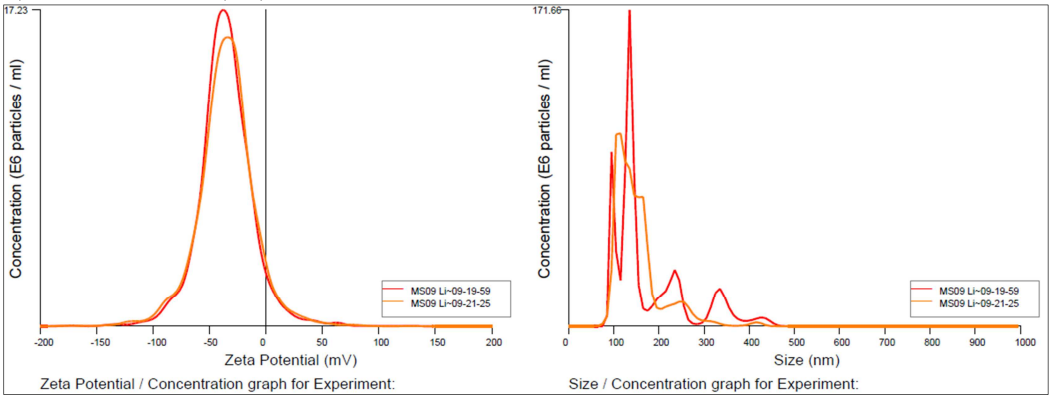

5.2 Lipoplexes

MS09/DOPE LIPOPLEXES

A) MS09:siRNA ($^{w}/_{w}$) = 12:1

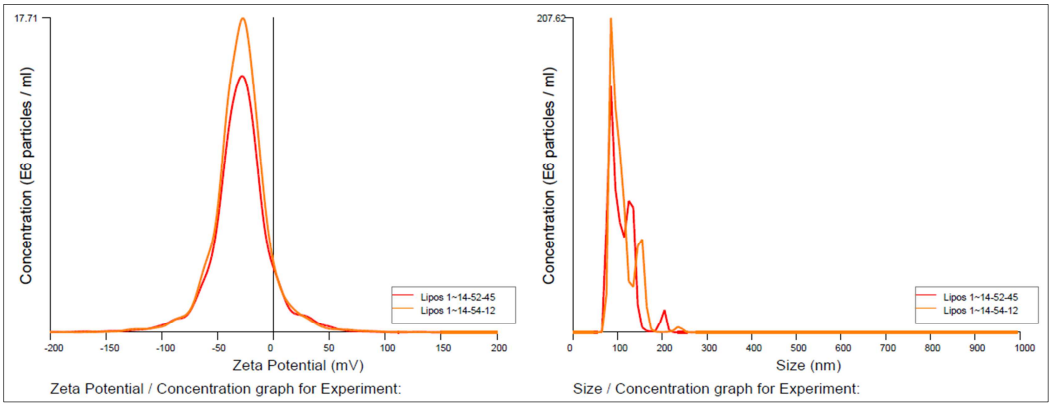

B) MS09:siRNA ($^{w}/_{w}$) = 16:1

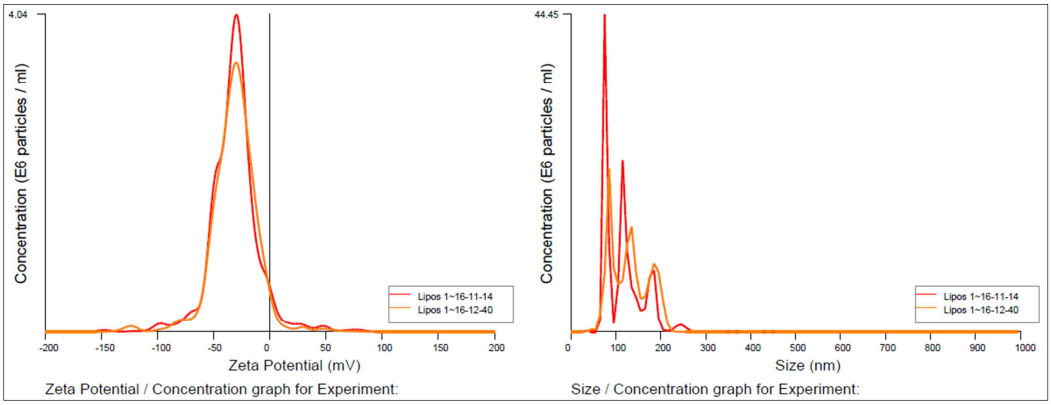

C) MS09:siRNA ($^{w}/_{w}$) = 20:1

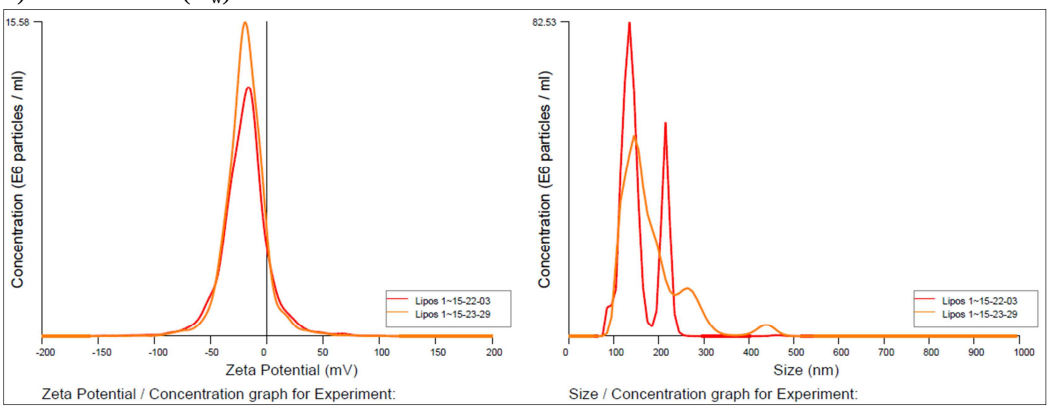

D) MS09:siRNA ($^{w}/_{w}$) = 24:1

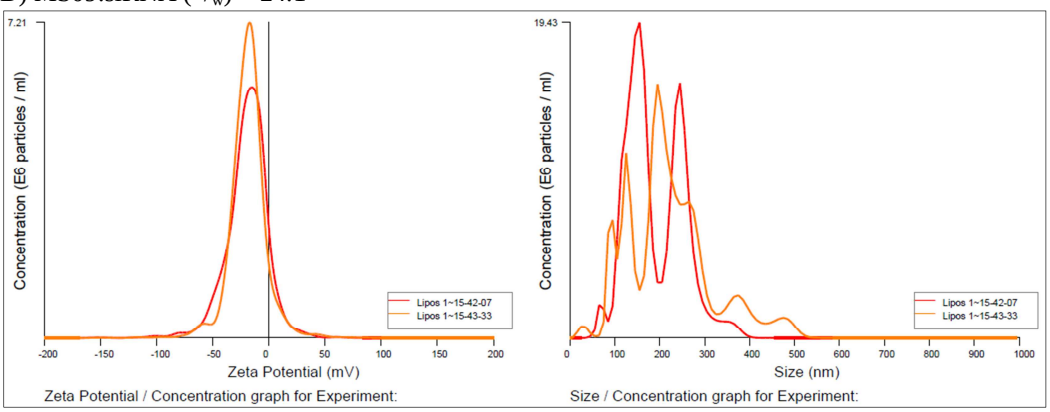

E) MS09:siRNA ($^{w}/_{w}$) = 28:1

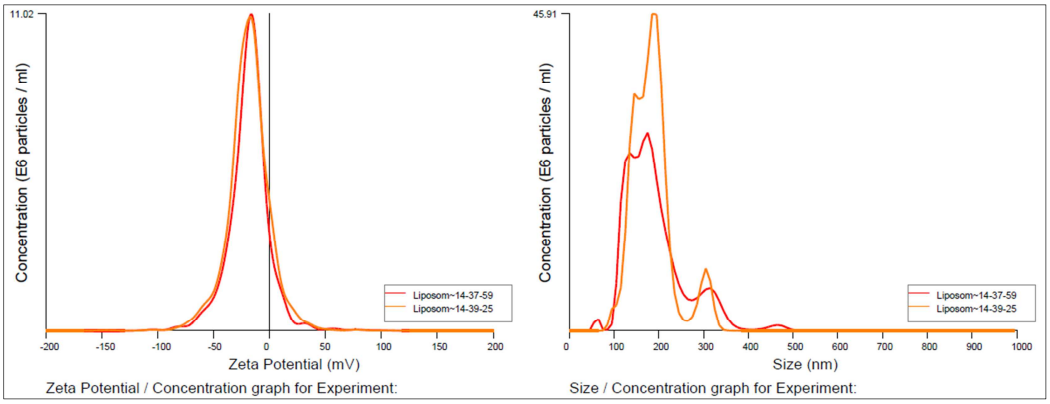

F) MS09:siRNA ($^{w}/_{w}$) = 32:1

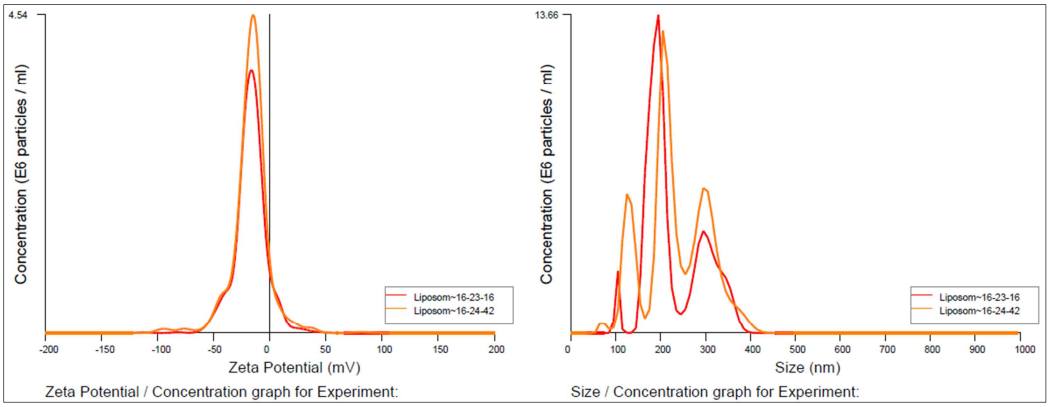

MS09/Chol (1:1) LIPOPLEXES

G) MS09:siRNA ($^{w}/_{w}$) = 12:1

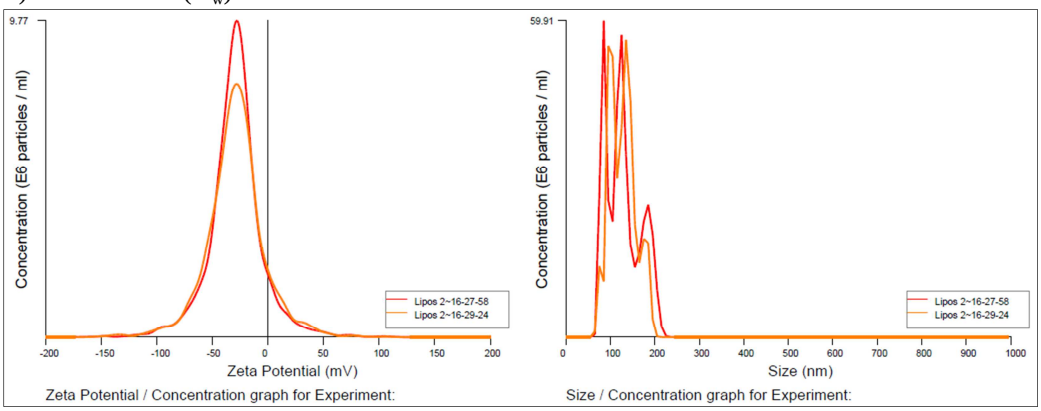

H) MS09:siRNA ($^{w}/_{w}$) = 16:1

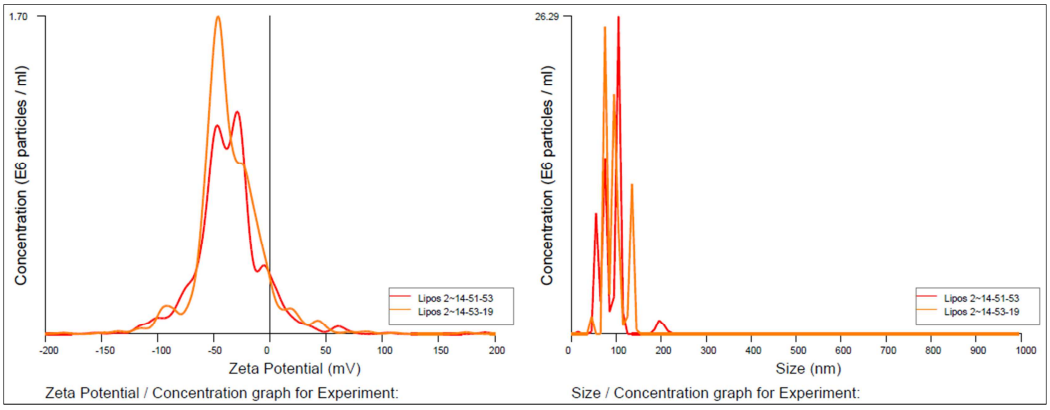

I) MS09:siRNA ($^{w}/_{w}$) = 20:1

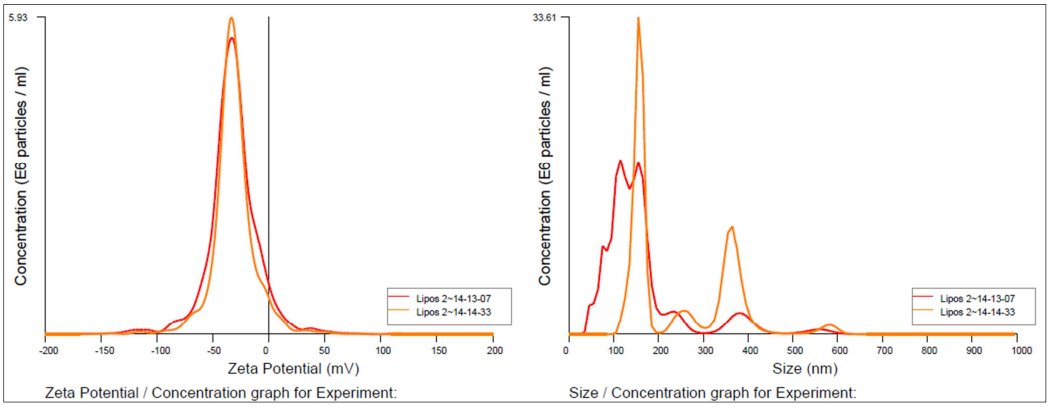

J) MS09:siRNA ($^{w}/_{w}$) = 24:1

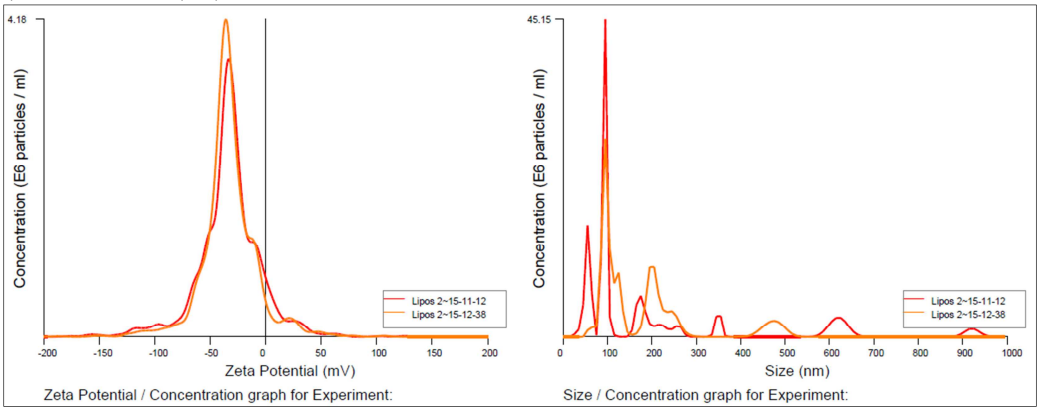

K) MS09:siRNA ($^{w}/_{w}$) = 28:1

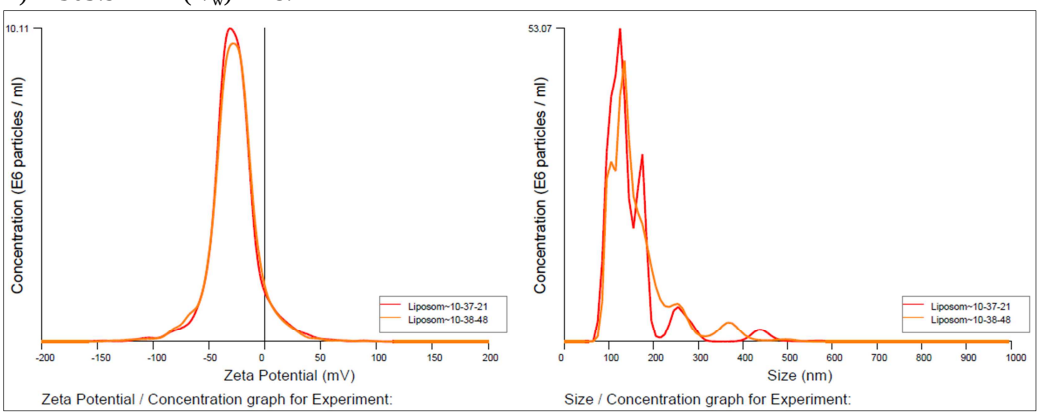

L) MS09:siRNA ($^{w}/_{w}$) = 32:1

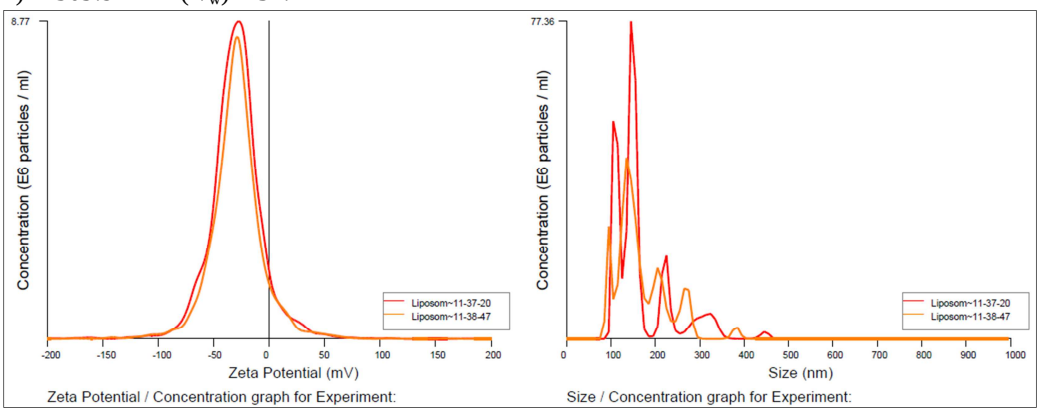

MS09/DOPE/PEG LIPOPLEXES

M) MS09:siRNA ($^{w}/_{w}$) = 12:1

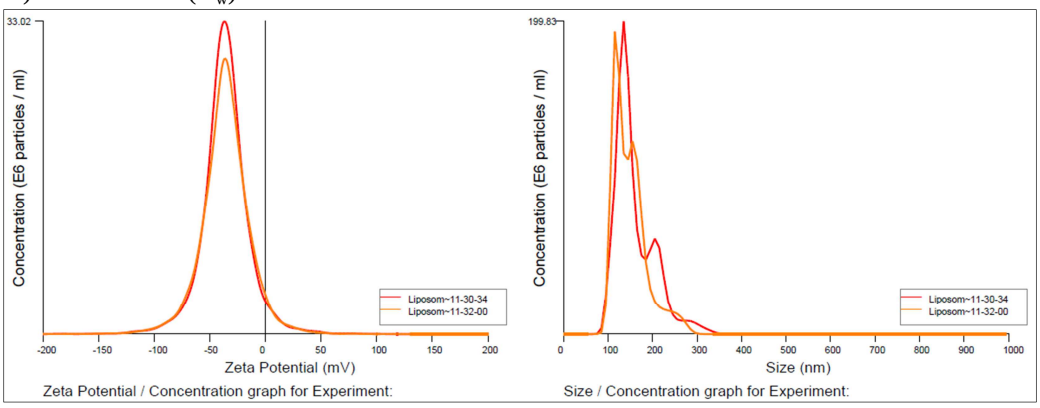

N) MS09:siRNA ($^{w}/_{w}$) = 16:1

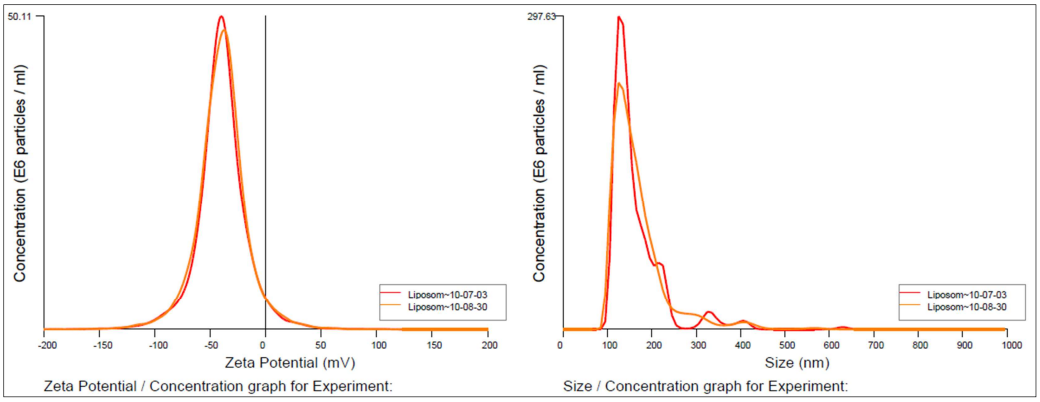

O) MS09:siRNA ($^{w}/_{w}$) = 20:1

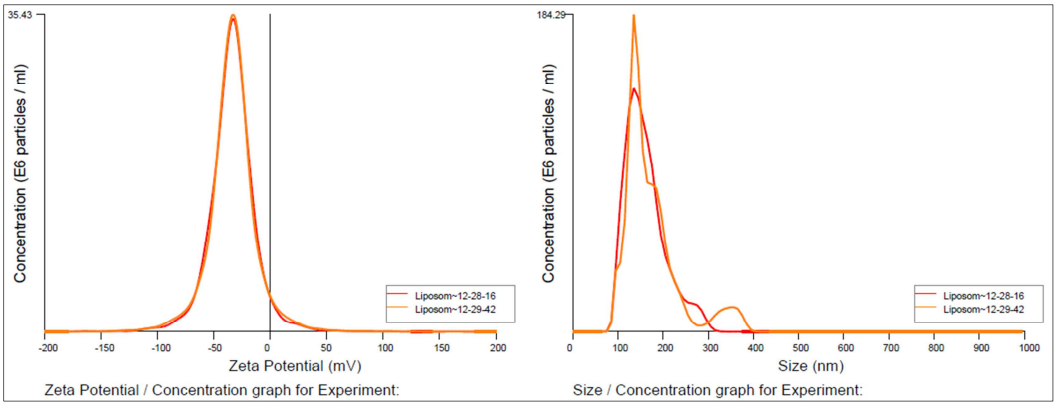

P) MS09:siRNA ($^{w}/_{w}$) = 24:1

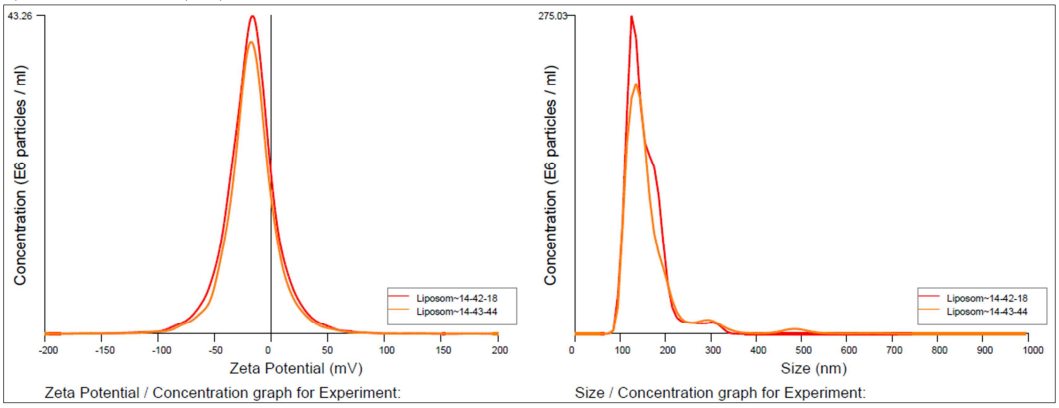

Q) MS09:siRNA ($^{w}/_{w}$) = 28:1

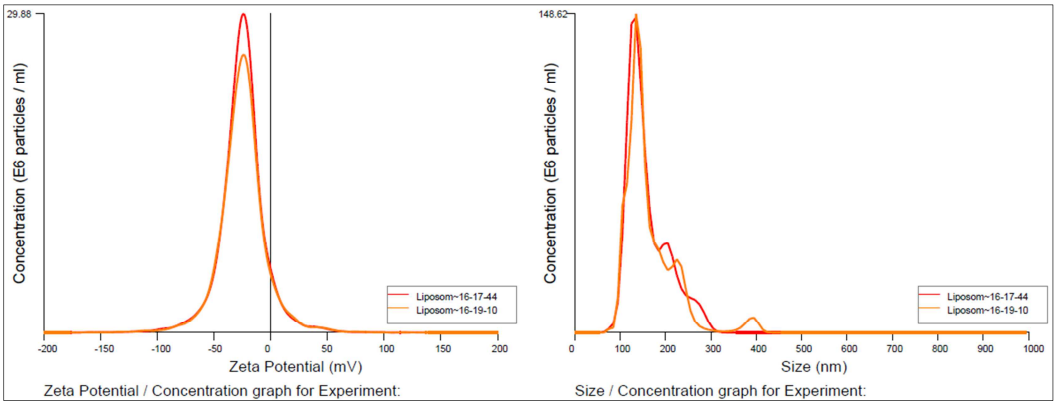

R) MS09:siRNA ($^{w}/_{w}$) = 32:1

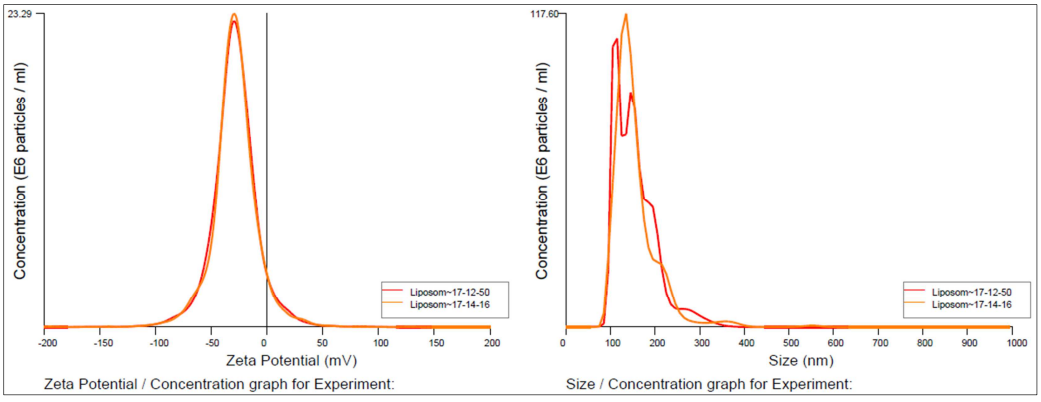

MS09/Chol/PEG (1:1) LIPOPLEXES

S) MS09:siRNA ($^{w}/_{w}$) = 12:1

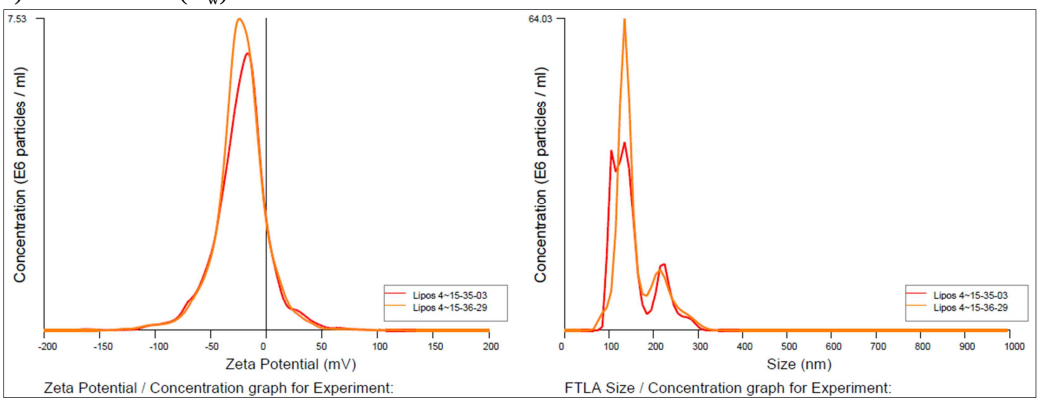

T) MS09:siRNA ($^{w}/_{w}$) = 16:1

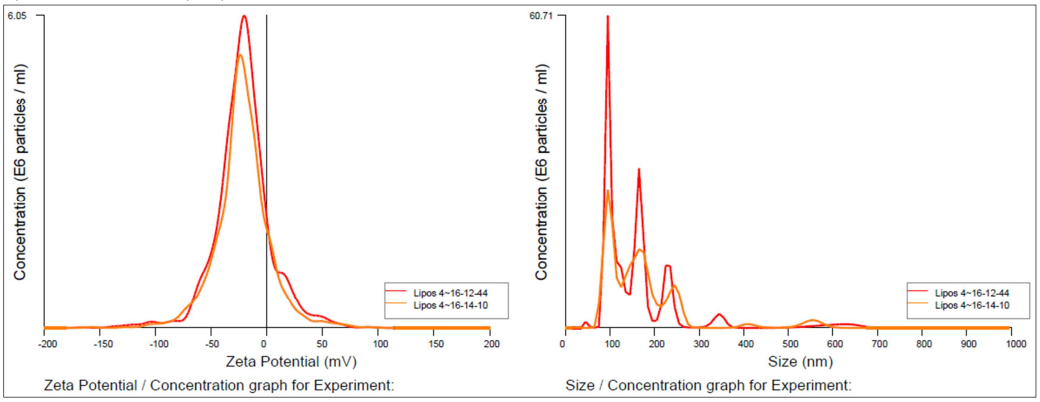

U) MS09:siRNA ($^{w}/_{w}$) = 20:1

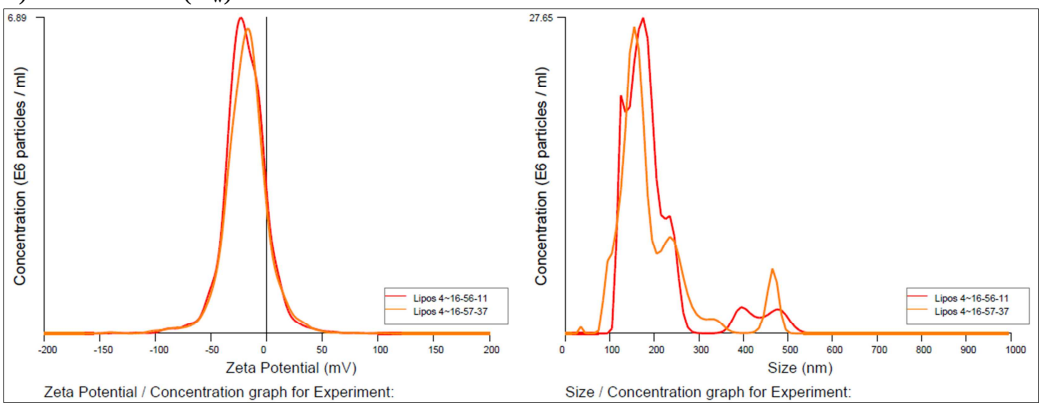

V) MS09:siRNA ($^{w}/_{w}$) = 24:1

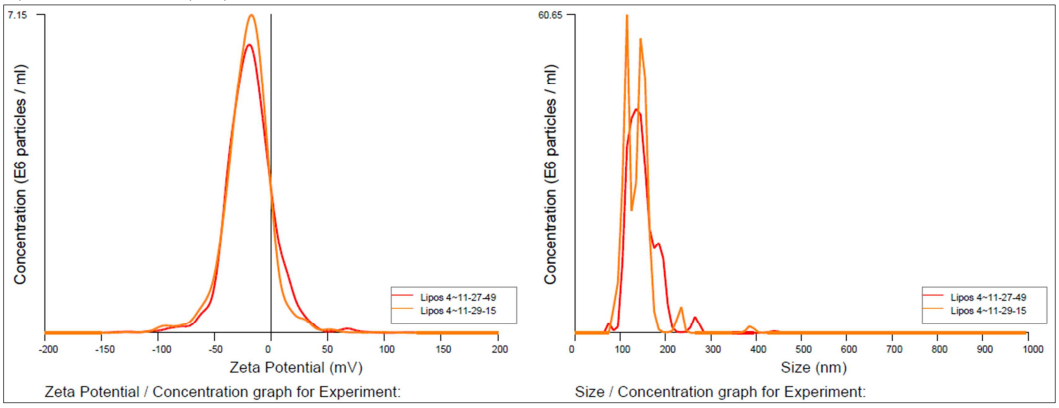

W) MS09:siRNA ($^{w}/_{w}$) = 28:1

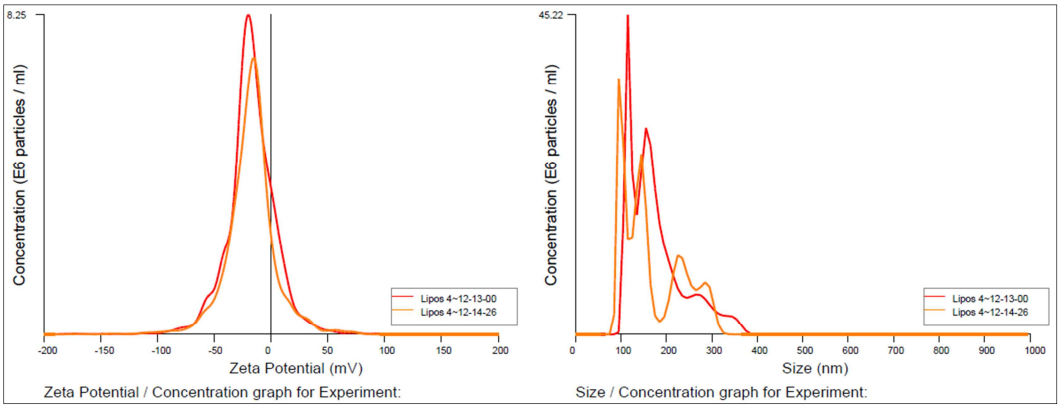

X) MS09:siRNA ($^{w}/_{w}$) = 32:1

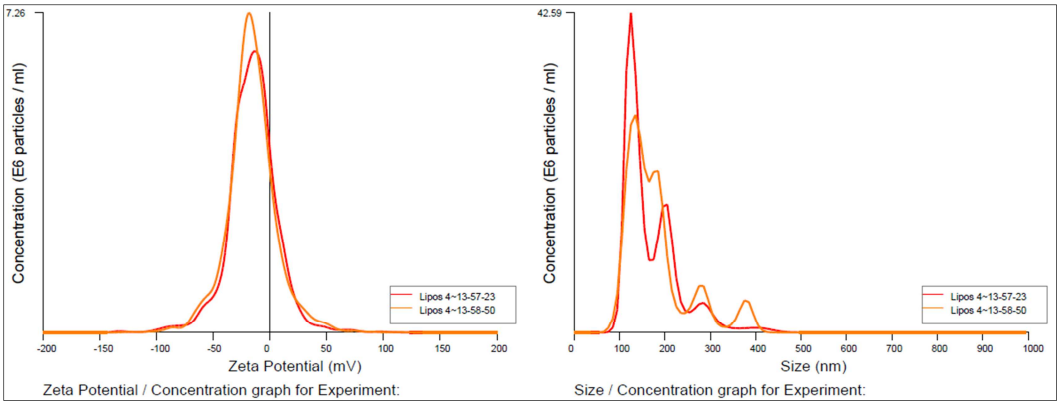

Note the following:
1. Graphs representative of a single experimental run per sample are shown.
2. Each curve on a graph represents the analysis of one video of particle motion recorded for a given experimental run.

APPENDIX C
Miscellaneous calculations

1. Estimation of the average number of lipid molecules per vesicle

Example: MS09/DOPE formulation

- Lipid concentration of liposome suspension = 8 μmol/ml

- 1 mol = 6.022×10^{23} lipid molecules
  1 μmol = 6.022×10^{17} lipid molecules
  8 μmol = $6.022 \times 10^{17} \times 8$ lipid molecules = 4.82×10^{18}
  Therefore, lipid concentration of liposome suspension
  = 4.82×10^{18} lipid molecules/ml

- Average number of liposomal vesicles/ml (value plotted in Figure 4.4c)
  = 4.93×10^{12}

- Average number of lipid molecules/vesicle $= \frac{4.82 \times 10^{18}}{4.93 \times 10^{12}} = 8.56 \times 10^{5}$

- Estimation of the average numbers of individual lipid components per vesicle was made assuming that the ratio at which these were combined in lipid mixtures was maintained in each vesicle of a given formulation.

- Average number of MS09 molecules/vesicle = $0.5 \times 8.56 \times 10^{5} = 4.28 \times 10^{5}$
- Average number of DOPE molecules/vesicle = $0.5 \times 8.56 \times 10^{5} = 4.28 \times 10^{5}$

2. N/P ($^{+}/_{-}$) charge ratio

Example: Lipoplex assembled at MS09:siRNA ($^{w}/_{w}$) ratio of 12:1

Molecular weight of MS09 = 629 g/mol (Singh and Ariatti, 2006)

- Average molecular weight of ribonucleotide = 340 g/mol (Thermo Fisher Scientific, DNA and RNA molecular weights and conversions accessed via https://www.thermofisher.com/us/en/home/references/ambion-tech-support/rna-tools-and-calculators/dna-and-rna-molecular-weights-and-conversions.html as at 4/4/17)

- Assumptions (a) 629 ng MS09 = 1 nano equivalent +ve charge
  (b) 340 ng siRNA = 1 nano equivalent –ve charge

- The complex contained 0.3 g (300 ng) siRNA and 3.6 g (3 600 ng) MS09
- +ve charge in complex $= \frac{3\,600}{629} = 5.723$ nano equivalents
- -ve charge in complex $= \frac{300}{340} = 0.882$ nano equivalents
- N/P $(^{+}/_{-}) = \frac{5.723}{0.882} = 6.5$

3. Final siRNA concentration

- Average molecular weight of siRNA = 13 400 g/mol (Dharmacon, Lafayette, CO, USA)
  Therefore 0.1 µg $= \frac{100\text{ ng}}{13\,400\text{ ng/nmol}} = 7.46 \times 10^{-3}$ nmol $= 7.46$ pmol
  $\backsim 7.5$ pmol

- In a 48-well plate,
  Total volume = 250 µl (growth medium) + 10 µl (transfecting complex) = 260 µl
  Transfecting complexes contained 0.2 µg, 0.1 µg or 0.05 µg siRNA

- When 0.2 µg (14.92 pmol) was introduced:
  siRNA concentration in transfecting complex $= \frac{14.92 \times 10^{-6}\ \mu\text{mol}}{10 \times 10^{-6}\ \text{L}} = 1.49\ \mu\text{M}$
  Final concentration $= \frac{14.92 \times 10^{-3}\ \text{nmol}}{260 \times 10^{-6}\ \text{L}} = 57.38\ \text{nM} \sim 57\ \text{nM}$

- When 0.1 µg (7.46 pmol) was introduced:
  siRNA concentration in transfecting complex $= \frac{7.46 \times 10^{-6}\ \mu\text{mol}}{10 \times 10^{-6}\ \text{L}} = 0.75\ \mu\text{M}$
  Final concentration $= \frac{7.46 \times 10^{-3}\ \text{nmol}}{260 \times 10^{-6}\ \text{L}} = 28.69\ \text{nM} \sim 29\ \text{nM}$

- When 0.05 µg (3.73 pmol) was introduced:
  siRNA concentration in transfecting complex $= \frac{3.73 \times 10^{-6}\ \mu\text{mol}}{10 \times 10^{-6}\ \text{L}} = 0.37\ \mu\text{M}$

$$\text{Final concentration} = \frac{3.73 \times 10^{-3}\ \text{nmol}}{260 \times 10^{-6}\ \text{L}} = 14.35\ \text{nM} \sim 14\ \text{nM}$$

The above calculations are theoretical i.e. assume no loss due to pipetting.

4. Final cytofectin and lipid concentration

This sample calculation applies to the following scenario:

Cells in 48-well plates were transfected with lipoplex suspension (10 µl) assembled from siRNA (0.2 µg) and MS09/DOPE liposome at MS09:siRNA ($^{w}/_{w}$) ratio of 12:1.

Molecular weight of MS09 = 629 g/mol

Lipid concentration of MS09/DOPE formulation = 5.5 µg/µl = 8×10^{-3} µmol/µl

MS09 (i. e. cytofectin) concentration in MS09/DOPE suspension = 2.52 µg/µl

- The lipoplex contained (0.2×12) µg = 2.4 µg MS09

  µmol MS09 $= \frac{2.4\ \mu g}{629\ \mu g/\mu mol} = 3.815 \times 10^{-3}$

  Final MS09 concentration $= \frac{3.815 \times 10^{-3}\ \mu mol}{260 \times 10^{-6}\ L} = 14.7\ \mu M$

- The lipoplex contained $\left(\frac{2.4\ \mu g \times 5.5\ \mu g/\mu l}{2.52\ \mu g/\mu l}\right)$ µg total lipid = 5.238 µg

  µmol lipid $= \left(\frac{5.238\ \mu g \times (8 \times 10^{-3} \mu mol/\mu l)}{5.5\ \mu g/\mu l}\right) = 7.619 \times 10^{-3}$

  Final lipid concentration $= \frac{7.619 \times 10^{-3} \mu mol}{260 \times 10^{-6}\ L} = 29.3\ \mu M$

5. Estimation of average number of vesicles/nanocomplex

This example applies to the MS09/DOPE lipoplex at MS09:siRNA ($^{w}/_{w}$) ratio of 16:1,

The NTA-generated lipoplex concentration reflects the number of nanocomplexes in the diluted sample; hence the concentration of nanocomplexes in the original 10 µl suspension was estimated by multiplying this value with the dilution factor, i.e. 700. The average of three experimental runs was taken, i.e. $1.58 \times 10^{11} \pm 5.44 \times 10^{10}$ particles/ml, and this value was plotted in Figure 4.12c, of section 4.3. This is the equivalent of an average of **1.58×10^{9} particles in 10 µl**.

The average number of liposomal vesicles in the MS09/DOPE stock suspensions was calculated in the same way, i.e. $4.93 \times 10^{12} \pm 4.85 \times 10^{11}$ particles/ml. To prepare lipoplexes 1 µl stock suspension was used. This implies that, for a well-dispersed liposome suspension, an estimated $(4.93 \times 10^{12} \div 1000) =$ **4.93×10^{9}** liposomal vesicles was introduced into 10 µl. Hence, the estimated average number of MS09/DOPE liposomal vesicles involved in the formation of one liposome-siRNA complex at the MS09:siRNA ($^{w}/_{w}$) ratio of 16:1 is:

$$\frac{4.93 \times 10^{9}\text{liposomal vesicles}}{1.58 \times 10^{9}\text{lipoplexes}} = 3.12 \backsim 3$$

6. Estimation of average number of siRNA molecules/nanocomplex

This example pertains to the MS09/DOPE lipoplex at MS09:siRNA ($^{w}/_{w}$) ratio of 16:1,

- The lipoplex suspension was prepared using 1 µl liposome stock suspension i.e. 2.52 µg MS09
- Hence:
  $\left(\frac{2.52}{16}\right)$ µg $=$ 0.1575 µg $=$ 157.5 ng siRNA was added
- Average molecular weight of siRNA = 13 400 ng/nmol
- Therefore

  nmoles siRNA in lipoplex suspension $= \left(\frac{157.5}{13\,400}\right) = 1.175 \times 10^{-2}$
- 6.022×10^{23} molecules in 1 mol siRNA
  $= 6.022 \times 10^{14}$ molecules in 1 nmol siRNA.
- Hence 1.175×10^{-2} nmol contains $(6.022 \times 10^{14}) \times (1.175 \times 10^{-2})$ siRNA molecules
- $= 7.076 \times 10^{12}$

$$\text{number of siRNA molecules per complex} = \frac{\text{number of siRNA molecules in 10 µl}}{\text{average number of nanocomplexes in 10 µl}}$$

$$= \frac{7.076 \times 10^{12}}{1.58 \times 10^{9}} = 4.5 \times 10^{3}$$

APPENDIX D

Set-up for gel retardation and nuclease digestion assays

Table D1: Preparation of MS09/DOPE-siRNA complexes for gel retardation assay

MS09:siRNA ($^{w}/_{w}$)		0	4:1	8:1	12:1	16:1	20:1	24:1	28:1
siRNA	**(µg)**	0.3	0.3	0.3	0.3	0.3	0.3	0.3	0.3
	(µl)[a]	1.12	1.12	1.12	1.12	1.12	1.12	1.12	1.12
MS09	**(µg)**	0	1.2	2.4	3.6	4.8	6.0	7.2	8.4
Liposome	**(µg)**	0	2.62	5.23	7.86	10.48	13.10	15.71	18.33
	(µl)[b]	0	0.95	1.90	2.86	3.81	4.76	5.71	6.67
HBS	**(µl)**	8.88	7.93	6.98	6.02	5.07	4.12	3.17	2.21
Total volume	**(µl)**	10	10	10	10	10	10	10	10

[a]siRNA stock = 0.268 µg/µl
[b]MS09/DOPE stock diluted 1:1 ($^{v}/_{v}$) in HBS = 2.75 µg/µl

Table D2: Preparation of MS09/Chol (1:1)-siRNA complexes for gel retardation assay

MS09:siRNA ($^{w}/_{w}$)		0	8:1	12:1	16:1	20:1	24:1	28:1	32:1
siRNA	**(µg)**	0.3	0.3	0.3	0.3	0.3	0.3	0.3	0.3
	(µl)[a]	1.12	1.12	1.12	1.12	1.12	1.12	1.12	1.12
MS09	**(µg)**	0	2.4	3.6	4.8	6.0	7.2	8.4	9.6
Liposome	**(µg)**	0	3.87	5.80	7.73	9.67	11.60	13.53	15.47
	(µl)[b]	0	1.90	2.86	3.81	4.76	5.71	6.67	7.62
HBS	**(µl)**	8.88	6.98	6.02	5.07	4.12	3.17	2.21	1.26
Total volume	**(µl)**	10	10	10	10	10	10	10	10

[a]siRNA stock = 0.268 µg/µl
[b]MS09/Chol (1:1) stock diluted 1:1 ($^{v}/_{v}$) in HBS = 2.03 µg/µl

Table D3: Preparation of MS09/DOPE/PEG-siRNA complexes for gel retardation assay

MS09:siRNA ($^{w}/_{w}$)		0	8:1	12:1	16:1	20:1	24:1	28:1	32:1
siRNA	**(µg)**	0.3	0.3	0.3	0.3	0.3	0.3	0.3	0.3
	(µl)[a]	1.12	1.12	1.12	1.12	1.12	1.12	1.12	1.12
MS09	**(µg)**	0	2.4	3.6	4.8	6.0	7.2	8.4	9.6
Liposome	**(µg)**	0	5.68	8.52	11.36	14.20	17.03	19.87	22.71
	(µl)[b]	0	1.95	2.93	3.90	4.88	5.85	6.83	7.80
HBS	**(µl)**	8.88	6.93	5.95	4.98	4.0	3.03	2.05	1.08
Total volume	**(µl)**	10	10	10	10	10	10	10	10

[a]siRNA stock = 0.268 µg/µl
[b]MS09/DOPE/PEG stock diluted 1:1 ($^{v}/_{v}$) in HBS = 2.91 µg/µl

Table D4: Preparation of MS09/Chol/PEG (1:1)-siRNA complexes for gel retardation assay

MS09:siRNA ($^{w}/_{w}$)		0	8:1	12:1	16:1	20:1	24:1	28:1	32:1
siRNA	**(µg)**	0.3	0.3	0.3	0.3	0.3	0.3	0.3	0.3
	(µl)[a]	1.12	1.12	1.12	1.12	1.12	1.12	1.12	1.12
MS09	**(µg)**	0	2.4	3.6	4.8	6.0	7.2	8.4	9.6
Liposome	**(µg)**	0	4.31	6.47	8.62	10.78	12.94	15.09	17.25
	(µl)[b]	0	1.95	2.93	3.90	4.88	5.85	6.83	7.80
HBS	**(µl)**	8.88	6.93	5.95	4.98	4.0	3.03	2.05	1.08
Total volume	**(µl)**	10	10	10	10	10	10	10	10

[a]siRNA stock = 0.268 µg/µl
[b]MS09/Chol/PEG (1:1) stock diluted 1:1 ($^{v}/_{v}$) in HBS = 2.21 µg/µl

Table D5: Preparation and treatment of MS09/DOPE-siRNA complexes for nuclease digestion assay

MS09:siRNA ($^{w}/_{w}$)		0	0	12:1	16:1	20:1	24:1	28:1	32:1	
siRNA	**(µl)**[a]	1.12	1.12	1.12	1.12	1.12	1.12	1.12	1.12	
Liposome	**(µl)**[b]	0	0	2.86	3.81	4.76	5.71	6.67	7.62	
HBS	**(µl)**	8.88	8.88	6.02	5.07	4.12	3.17	2.21	1.26	
Total sample	**(µl)**	10	10	10	10	10	10	10	10	*Room temperature, 30 min*
FBS	**(µl)**	0	1.1	1.1	1.1	1.1	1.1	1.1	1.1	*37 ˚C, 4 h*
EDTA	**(µl)**[c]	0	1.15	1.15	1.15	1.15	1.15	1.15	1.15	
SDS	**(µl)**[d]	0	0	1.15	1.15	1.15	1.15	1.15	1.15	*55 ˚C, 25 min*
HBS	**(µl)**	3.4	1.15	0	0	0	0	0	0	
Total volume	**(µl)**	13.4	13.4	13.4	13.4	13.4	13.4	13.4	13.4	

[a]siRNA stock = 0.268 µg/µl
[b]MS09/DOPE stock diluted 1:1 ($^{v}/_{v}$) in HBS = 2.75 µg/µl
[c]EDTA stock = 110 mM in water
[d]SDS stock = 6 % ($^{w}/_{v}$) in water

Table D6: Preparation and treatment of MS09/Chol (1:1)-siRNA complexes for nuclease digestion assay

MS09:siRNA ($^{w}/_{w}$)		0	0	12:1	16:1	20:1	24:1	28:1	32:1	
siRNA	**(µl)**[a]	1.12	1.12	1.12	1.12	1.12	1.12	1.12	1.12	
Liposome	**(µl)**[b]	0	0	2.86	3.81	4.76	5.71	6.67	7.62	
HBS	**(µl)**	8.88	8.88	6.02	5.07	4.12	3.17	2.21	1.26	
Total sample	**(µl)**	10	10	10	10	10	10	10	10	*Room temperature, 30 min*
FBS	**(µl)**	0	1.1	1.1	1.1	1.1	1.1	1.1	1.1	*37 ˚C, 4 h*
EDTA	**(µl)**[c]	0	1.15	1.15	1.15	1.15	1.15	1.15	1.15	
SDS	**(µl)**[d]	0	0	1.15	1.15	1.15	1.15	1.15	1.15	*55 ˚C, 25 min*
HBS	**(µl)**	3.4	1.15	0	0	0	0	0	0	
Total volume	**(µl)**	13.4	13.4	13.4	13.4	13.4	13.4	13.4	13.4	

[a]siRNA stock = 0.268 µg/µl
[b]MS09/Chol (1:1) stock diluted 1:1 ($^{v}/_{v}$) in HBS = 2.03 µg/µl
[c]EDTA stock = 110 mM in water
[d]SDS stock = 6 % ($^{w}/_{v}$) in water

Table D7: Preparation and treatment of MS09/DOPE/PEG-siRNA complexes for nuclease digestion assay

MS09:siRNA ($^{w}/_{w}$)		0	0	12:1	16:1	20:1	24:1	28:1	32:1	
siRNA	**(µl)**[a]	1.12	1.12	1.12	1.12	1.12	1.12	1.12	1.12	
Liposome	**(µl)**[b]	0	0	2.93	3.90	4.88	5.85	6.83	7.80	
HBS	**(µl)**	8.88	8.88	5.95	4.98	4.0	3.03	2.05	1.08	
Total sample	**(µl)**	10	10	10	10	10	10	10	10	*Room temperature, 30 min*
FBS	**(µl)**	0	1.1	1.1	1.1	1.1	1.1	1.1	1.1	*37 ˚C, 4 h*
EDTA	**(µl)**[c]	0	1.15	1.15	1.15	1.15	1.15	1.15	1.15	
SDS	**(µl)**[d]	0	0	1.15	1.15	1.15	1.15	1.15	1.15	*55 ˚C, 25 min*
HBS	**(µl)**	3.4	1.15	0	0	0	0	0	0	
Total volume	**(µl)**	13.4	13.4	13.4	13.4	13.4	13.4	13.4	13.4	

[a]siRNA stock = 0.268 µg/µl
[b]MS09/DOPE/PEG stock diluted 1:1 ($^{v}/_{v}$) in HBS = 2.91 µg/µl
[c]EDTA stock = 110 mM in water
[d]SDS stock = 6 % ($^{w}/_{v}$) in water

Table D8: Preparation and treatment of MS09/Chol/PEG (1:1)-siRNA complexes for nuclease digestion assay

MS09:siRNA ($^{w}/_{w}$)		0	0	12:1	16:1	20:1	24:1	28:1	32:1	
siRNA	**(µl)**[a]	1.12	1.12	1.12	1.12	1.12	1.12	1.12	1.12	
Liposome	**(µl)**[b]	0	0	2.93	3.90	4.88	5.85	6.83	7.80	
HBS	**(µl)**	8.88	8.88	5.95	4.98	4.0	3.03	2.05	1.08	
Total sample	**(µl)**	10	10	10	10	10	10	10	10	*Room temperature, 30 min*
FBS	**(µl)**	0	1.1	1.1	1.1	1.1	1.1	1.1	1.1	*37 ˚C, 4 h*
EDTA	**(µl)**[c]	0	1.15	1.15	1.15	1.15	1.15	1.15	1.15	
SDS	**(µl)**[d]	0	0	1.15	1.15	1.15	1.15	1.15	1.15	*55 ˚C, 25 min*
HBS	**(µl)**	3.4	1.15	0	0	0	0	0	0	
Total volume	**(µl)**	13.4	13.4	13.4	13.4	13.4	13.4	13.4	13.4	

[a]siRNA stock = 0.268 µg/µl
[b]MS09/Chol/PEG (1:1) stock diluted 1:1 ($^{v}/_{v}$) in HBS = 2.21 µg/µl
[c]EDTA stock = 110 mM in water
[d]SDS stock = 6 % ($^{w}/_{v}$) in water

APPENDIX E
MS09/Chol (1:1) *vs.* MS09/DOPE at MS09:siRNA ($^{w}/_{w}$) = 16:1

Table E1: A summary of the properties of MS09/Chol (1:1) and MS09/DOPE lipoplexes at MS09:siRNA ($^{w}/_{w}$) =16:1

Liposome formulation			**MS09/DOPE**	**MS09/Chol (1:1)**
MS09:siRNA ($^{w}/_{w}$)			16:1	16:1
N/P ($^{+}/_{-}$)			8.7:1	8.7:1
Number of liposomal vesicles/nanocomplex[a]			3	3
Number of siRNA molecules/nanocomplex[a]			4500	3900
Number of lipid molecules/nanocomplex[a,b]			25.7×10^5	34.8×10^5
siRNA fully bound at given ratio? (✓/×)	Gel retardation		×	×
	Dye displacement	EtBr	✓	✓
		SYBR Green	✓	✓
Z-NTA[c]	Size (nm)		92.4 ± 24.5	126.8 ± 7.3
	ζ potential (mV)		-33.6 ± 4.5	-43.9 ± 5.4*
Protection of siRNA in serum (10 % $^{v}/_{v}$)	siRNA protected? (✓/×)		✓	✓
	% siRNA protected[c]		75.5 ± 5.01	67.8 ± 0.03**
Dose applied to cells in gene expression studies	siRNA (nM)		12	12
	MS09 (μM)		4.1	4.1
	Total lipid (μM)		8.2	8.2
Cell survival at given dose[c] (%)	MCF-7	AB	99.8 ± 7.7	98.9 ± 8.4
	HT-29	AB	102.1 ± 7.3	100.6 ± 11.5
siRNA uptake at given dose[c] ($\times 10^3$ RFU/mg protein)	MCF-7		29.1 ± 2.7	41.7 ± 3.2**
	HT-29		28.5 ± 1.8	24.8 ± 2.0

Notes:
[a]Reported values are average estimates
[b]This value was estimated based on the estimated average numbers of lipid molecules/vesicle and vesicles/nanocomplex
[c]Data is presented as the mean ± SD (n = 3)
*P < 0.05, **P < 0.01 *vs*. MS09/DOPE (MS09:siRNA $^{w}/_{w}$ = 16:1)

APPENDIX F
Additional cytotoxicity data

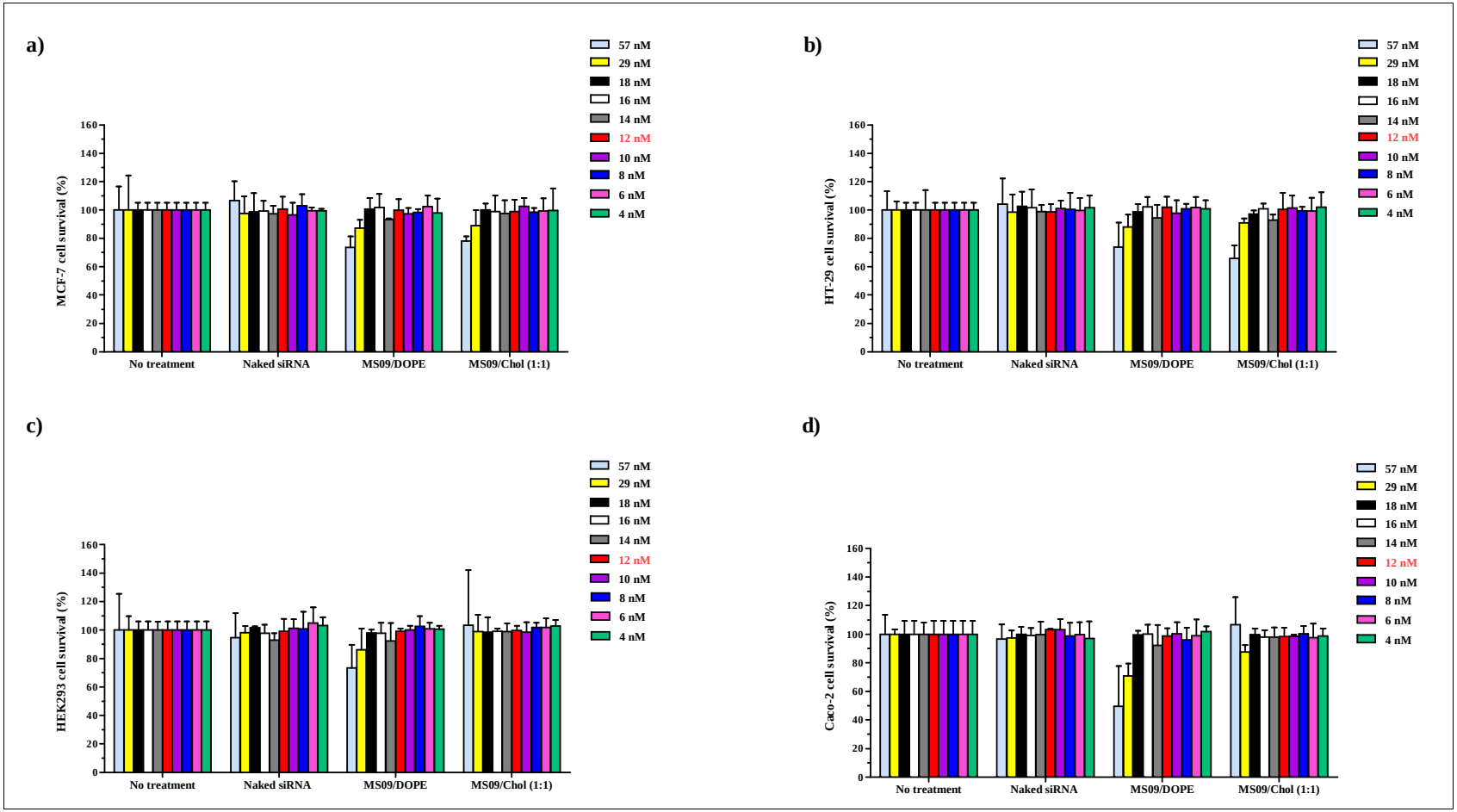

Figure F1: Tolerance of MS09/DOPE and MS09/Chol (1:1) lipoplexes by **a)** MCF-7, **b)** HT-29, **c)** HEK293 and **d)** Caco-2 cells. Lipoplexes were assembled at MS09:siRNA ($^{w}/_{w}$) = 16:1, and introduced to cells at varying final siRNA concentrations. Non-targeting siRNA was used throughout and cell survival was assessed by the AB viability assay 48 h after transfection. Each column represents the mean ± SD (n = 3). $P > 0.05$ *vs*. untreated cells, in all instances.

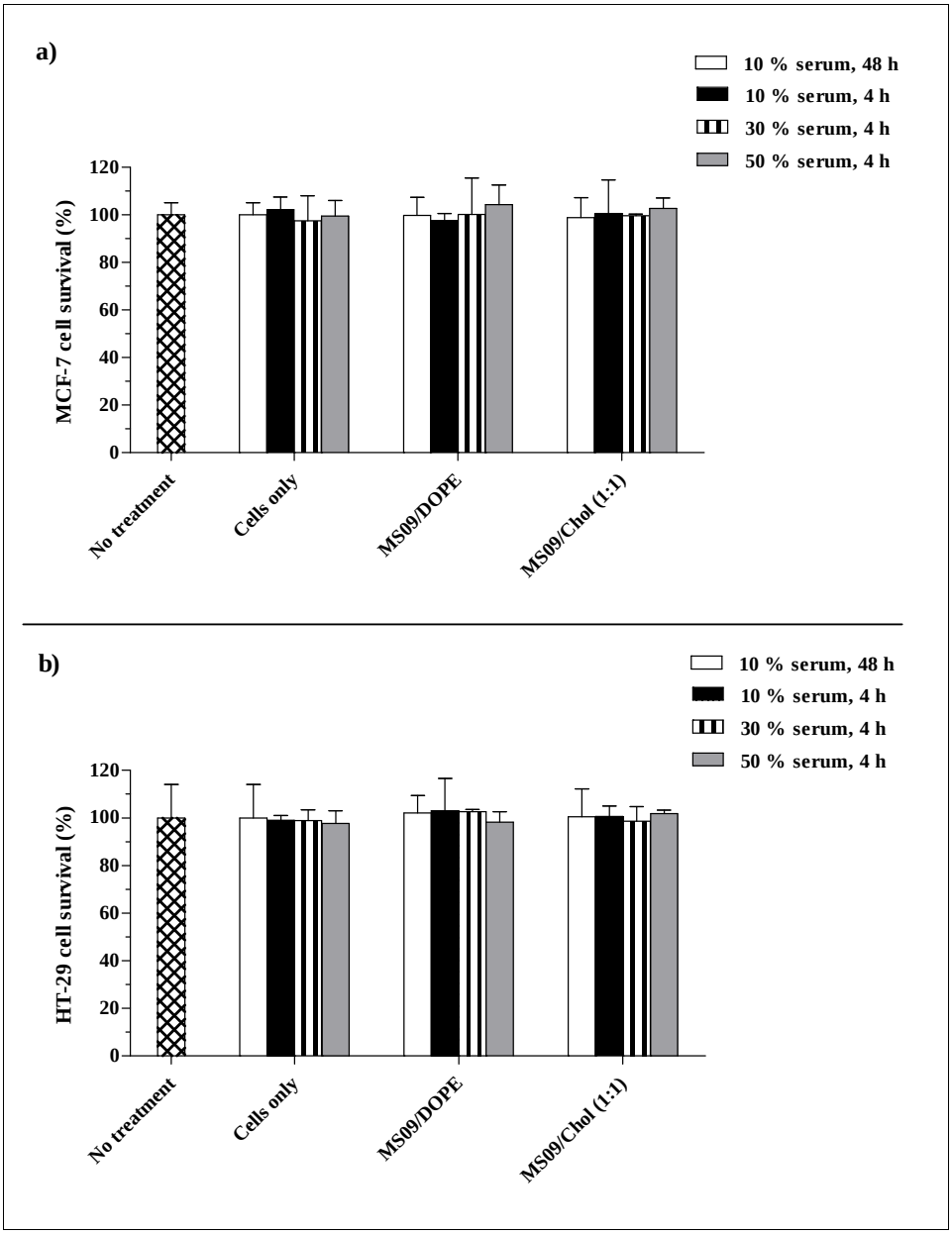

Figure F2: Effect of transfections in high serum concentrations on the growth of **a)** MCF-7 and **b)** HT-29 cells. Cells were subjected to 4 h-long exposure to MS09/DOPE and MS09/Chol (1:1) lipoplexes, assembled at MS09:siRNA ($^{w}/_{w}$) = 16:1, to give final siRNA concentration of 12 nM, in varying serum concentrations. Non-targeting siRNA was used throughout and cell survival was assessed by the AB viability assay at 48 h post-transfection. *No treatment* refers to cells that were grown in 10 % serum for 48 h without transfection. *Cells only* refers to groups exposed to varying serum concentrations without transfection. Each column represents the mean ± SD (n = 3). $P > 0.05$ *vs*. the *No treatment* group, in all instances.

Document Viewer

Turnitin Originality Report

Processed on: 22-Jun-2018 6:39 AM CAT
ID: 977680168
Word Count: 48042
Submitted: 1

Habib S Final Thesis 2018 By Saffiya Habib

Similarity Index	Similarity by Source	
13%	Internet Sources:	8%
	Publications:	8%
	Student Papers:	5%

1% match (Internet from 25-Feb-2014)
http://146.230.128.141

<1% match (Internet from 13-Jun-2018)
https://www.omicsonline.org/2376-0419/2376-0419-African-Pharma-2016-Posters-Accepted-Abstracts.digitalfiles/assets/basic-html/page-20.html

<1% match (student papers from 09-Jan-2018)
Submitted to University of KwaZulu-Natal on 2018-01-09

<1% match (student papers from 28-Jan-2015)
Submitted to University of KwaZulu-Natal on 2015-01-28

<1% match (Internet from 19-Mar-2018)
https://www.dovepress.com/getfile.php?fileID=41038

<1% match (publications)
Domsamy, Shantal, Nicolisha Narainpersad, Moganavelli Singh, and Mario Ariatti. "Novel Targeted Liposomes Deliver siRNA to Hepatocellular Carcinoma Cells in vitro.", Chemical Biology & Drug Design, 2012.

<1% match (Internet from 08-Sep-2017)
https://scholar.sun.ac.za/bitstream/handle/10019.1/96676/oppermann_toxic_2015.pdf?isAllowed=y&sequence=2

<1% match (publications)
Oligodeoxynucleotides, 1989.

<1% match (Internet from 27-Dec-2014)
http://jeff-ref.me

<1% match (publications)
Handbook of Experimental Pharmacology, 2004.

<1% match (publications)
Current Topics in Microbiology and Immunology, 1997.

<1% match (publications)
Li, Ding, Bu Zang, Shang-Tian Yang, Jufang Wang, and Xinping Wang. "Cell-based high-throughput proliferation and cytotoxicity assays for screening traditional Chinese herbal medicines", Process Biochemistry, 2013.

<1% match (Internet from 30-Apr-2016)
https://spandidos-publications.com/ijmm/36/1/130?text=fulltext

<1% match (publications)
Yuan-Yuan Ji, Jun-Tian Liu, Na Liu, Zhi-Dong Wang, Chuan-Hao Liu, "PPARg activator fenofibrate modulates angiotensin II-induced inflammatory responses in vascular smooth muscle cells via the TLR4-dependent signaling pathway", Biochemical Pharmacology, 2009

<1% match (Internet from 28-Jun-2003)
http://www.shellyinc.com

<1% match (publications)
A. M. Struyf, "Preferential radiosensitization in p53-mutated human tumour cell lines by gentoxiflylline-mediated disruption of the G2/M checkpoint control", International Journal of Radiation Biology, 8/1/2002

<1% match (Internet from 20-Oct-2013)
http://www.coursehero.com

<1% match (publications)
Georg Janicki, "Simulation of Methane Recovery from Gas Hydrates Combined with Storing Carbon Dioxide as Hydrates", Journal of Geological Research, 2011

<1% match (student papers from 17-Nov-2014)
Submitted to University of KwaZulu-Natal on 2014-11-17

<1% match (student papers from 06-Dec-2014)
Submitted to University of KwaZulu-Natal on 2014-12-06

<1% match (publications)
Medical Intelligence Unit, 1995.

<1% match (student papers from 28-Dec-2015)
Submitted to University of KwaZulu-Natal on 2015-12-28